Design of a breach retardant dike

Brittle versus ductile failure

ARCADIS

TU Delft

MSc thesis D.D.M.M. Lemmens

2014

MSc thesis: Design of a breach retardant dike

Brittle versus ductile failure

TU Delft, Faculty of Civil Engineering and Geosciences, MSc Hydraulic Engineering
Arcadis, Division Water, Market Group Harbours and Hydraulic Engineering

May 2014

Student
D.D.M.M. Lemmens (1511858)
+31 (0) 6 43920401

dennis@dlemmens.nl
D.D.M.M.Lemmens@student.tudelft.nl
dennis.lemmens@arcadis.nl

Graduation committee

Graduation Professor	Prof. Dr. Ir. C van Rhee	C.vanRhee@tudelft.nl
Supervisor TU Delft	Dr. Ir. P.J. Visser	P.J.Visser@tudelft.nl
Supervisor Arcadis	Ir. F. Bisschop	rik.bisschop@arcadis.nl

Preface

This thesis is the result of my research into retarding the breaching of sand dikes. This research was executed in cooperation with Arcadis. During my research I have had support and help from numerous people, which I would like to thank.

First of all I would like to thank the members of my graduation committee for their feedback and input for my research: prof. dr. ir. C. van Rhee and dr. ir. P.J. Visser from the TU Delft and ir. F. Bisschop from the TU Delft and Arcadis Rotterdam. Their enthusiasm and support during my research kept me motivated and able to finish the thesis.

Furthermore I would like to thank the staff of the Fluid Mechanics Laboratory and the Geotechnical Laboratory of the TU Delft for their help during my laboratory experiments. From the Fluid Mechanics Laboratory my thanks especially go to S. de Vree, A. den Toom and J. van Duin, who helped me with the preparation and setup of the experiments. I would also like to thank the Fluid Mechanics Laboratory for availability to and construction of the tests setups and supplying the necessary materials. Of the Geotechnical Laboratory I would like to thank A. Mulder for providing the means for and helping me with the direct shear tests. I would also like to thank M. Bijleveld from Cebo and G. Hofstra from Finish Beton Groep, for their fast and free of charge supply of the bentonite (Cebo) and the fibres (Finish Beton Groep).

I want to thank my colleagues of Arcadis Rotterdam for their support and interest during my period in their office. For their explanation of and giving me access to VNK2 (‘Veiligheid Nederland in Kaart 2’) results, I would like to thank D. van Hogendorp and J. Leenders (HKV).

Last but not least, I would like to thank my family and friends for their support and interest during my research. Without them it would not have been possible to finish my thesis.

I hope you enjoy reading this thesis as much as I enjoyed working on it.

Dennis Lemmens

Rotterdam, the Netherlands
May 2014

Summary

Dikes constructed from sand have a sand core and a clay layer to protect the core against erosion. It is not unlikely that this clay layer fails due to several failure mechanisms, exposing the sand core to water. This can be catastrophic when water is overtopping the dike. In case the protective cover fails, water can flow over the core and erode the sand, eventually causing the dike to breach. This breaching process is described and modelled for a better understanding of the event. The BRES-model (BReach Erosion in Sand dikes) was specifically created for sand dikes and is used to simulate this process. It determines, among others, the final breach width, flow rate through the breach and duration of the breaching process. These breach parameters are important for determining the rise rates and flow velocities of the water in a polder. By reducing the rise rates and flow velocities, which can be achieved by retarding the breaching process, the number of casualties can be reduced. The safety of the inhabitants depends on the mortality during a flood event, i.e. the fraction of casualties of the inhabitants in a polder. The safety increases when the mortality reduces, i.e. the amount of casualties decreases. To reach a desired ten times higher safety level, the mortality has to decrease by a factor 10.

The breaching process can be retarded in several ways, such as altering the shape of the dike, increasing the cohesion or strength of the sand core, adding components to the dike or influencing the erosion parameters of the sand. Literature research results show that adding a few percent bentonite clay to sand, cementing sand with a biological process or mixing sand with fibres are the most promising options. For these options erosion formulas were determined to implement into the BRES-model.

The most promising options were modelled in the BRES-model using a norm dike. The breaching process of this norm dike was simulated in case it was constructed of sand, mixed with bentonite, biologically cemented or mixed with fibres. The norm dike is the dike which was constructed for the ZWIN'94 experiment. The model simulates the breaching process of these options and the results are compared to each other. From this comparison it is concluded that adding bentonite or polypropylene fibres to sand, or biologically cementing sand lead to similar reductions of the breach parameters. To test the results of the model outcome, laboratory experiments were executed. Sand, sand-bentonite mixtures and sand-fibre mixtures were subjected to direct shear tests, permeability tests and erosion tests. These tests show that sand-fibre mixtures do not significantly influence the measured parameters of the sand. The sand-bentonite mixtures show a significant reduction of the permeability and erosion velocity compared to sand. The erosion velocities of these mixtures can be modelled in the BRES-model with the Van Rijn-Van Rhee formula.

Using the results from the laboratory experiments the effects of bentonite on the breaching process of the norm dike were determined. Even adding a few percent of bentonite reduces the final breach width, maximum breach flow and inundation velocity (rise rate) significantly. For the norm dike it was calculated that 5.4% bentonite would be sufficient to reduce the inundation velocity below the threshold value of 0.5 m/h. This results in a reduction of the mortality of approximately a factor ten. Preliminary research indicates it is possible to mix bentonite with sand in-situ, using a Mixed-In-Place (MIP) technique. A cost indication shows that improving a dike with bentonite using this technique might cost approximately the same as a traditional dike reinforcement.

Based on this research it can be concluded that decreasing the erosion rate of sand with bentonite can lead to a significant reduction of the breach parameters. Depending on the circumstances this may lead to a decrease of mortality and thus an increase in safety, even by a factor 10. This decrease of mortality is already noticeable, in an inundation model, for small variations of the final breach width. Mixing bentonite with sand is possible for new or existing dikes while the costs are of the same magnitude as a traditional dike reinforcement.

Table of contents

Appendices

1 Introduction

All over the world dikes might fail or have failed, this can happen during extreme high river or sea levels. In most cases dikes are protected by a protective cover or revetment, but if these fail a dike can breach catastrophically. This is especially the case for sand dikes, in which a major breach can form within a few hours after failure of the protective cover (Visser, 1998). In such an event water will enter the polder behind the dike fast and the area will be inundated. This flooding causes people to lose their lives and damages land and property. Most casualties of such a flood are caused by relatively large flow velocities and fast rising water levels in the polder. These inundation parameters depend on the speed of the breaching process and the width of the final breach (Rijkswaterstaat, 2006). A possible way to reduce the number of casualties is to reduce these inundation parameters, which can be achieved by slowing down the breaching process.

The breaching process almost always starts with erosion of the inner slope. To prevent this erosion the inner slope has a protective cover of clay and grass. As long as this cover stays intact, the dike will not erode. It is, however, possible that this cover is damaged (e.g. by wave overtopping, piping, macro- or micro-instability) and the sand core of the dike is exposed to water and waves. When that happens the dike core starts to erode. The goal of this thesis is to find a way to retard the erosion of the core of the sand dike and increase the safety in the polder. The definition of this safety is given in the next section.

1.1 Safety behind dikes

In the Netherlands the inundation risk (P_I) used to be determined as the probability of exceedance of a maximum water level in front of the dike (P_E) times the probability of failure of a dike (P_F); $P_I=P_E \cdot P_F$. This risk was used to determine the safety level behind a dike. A drawback of this definition is that it does not include all possible failure mechanisms and it does not take mitigating measures into account. Therefore the definition is changed to the probability of loss of live of a person as a result of a dike failure. This new definition makes it possible to define a more accurate and local level of safety. It includes all relevant failure mechanisms, evacuation, mitigating measures, etc. With the introduction of this new safety definition, also an increase of this safety level by a factor 10 is desired by the Dutch government (Smolders, 2010). The aim of a possible solution is to increase the safety level by this order of magnitude. A formula which is used to derive the safety level is the Localized Individual Risk (LIR) of loss of live due to a flood (Deltares, 2011a):

$$LIR = P_F \cdot (1 - f_{evacuation}) \cdot M_L = P_F \cdot M_A \tag{1.1}$$

in which:

LIR	= Localized Individual Risk of loss of live due to a flood event
P_F	= probability of inundation of the relevant area
$f_{evacuation}$	= fraction of inhabitants evacuated
M_L	= mortality, casualties as fraction of inhabitants left in the flood zone (in the Netherlands estimated to be 0.01)
M_A	= mortality, casualties as fraction of all inhabitants of the flood zone

To increase the safety with a factor 10, the LIR has to be reduced by a factor 10. This can be achieved by decreasing the mortality by a factor 10 as well. The LIR also decreases if extra time for evacuation is won. In that case a larger fraction of the inhabitants can be evacuated. So the risk is influenced in two ways (Deltares, 2011a):

- Reducing the number of inhabitants left in a flood zone (evacuation)
- Reducing the number of casualties of people who stay behind (mortality)

It should be noted that an increase of the evacuation fraction is only relevant in case of a coastal flood. Coastal floods are harder to predict and an unplanned evacuation is more likely, compared to a river flood. An unplanned evacuation starts relatively short before the flood event and any extra time might increase the number of evacuees (Deltares, 2011a). This is not the case for a river flood. River floods can be predicted days before they actually reach the Netherlands. This enables a planned evacuation, with enough time to evacuate a large number of people. However, there are always people who do not want to evacuate. Since probably everyone who can and wants to be evacuated has been evacuated before a river dike breaches, any extra time gained during a river flood will not affect the number of evacuees. Only reducing the number of casualties will reduce the individual risk during a river flood, while during a coastal flood extra time for evacuation might make a differences as well (Deltares, 2011a). The increase in the evacuation fraction is, however, not expected to be significant, although this ultimately depends on the extra available time.

The safety definition and necessary risk reduction are used to determine whether it is technically feasible to increase the safety by retarding the breaching process. This research is focused on coastal dikes because these are usually sand dikes, while river dikes are mainly clay dikes. Also more lives can be saved by retarding the breaching process of a coastal dike than of a river dike, because of the difference in evacuation.

1.2 Feasibility of research

As concluded in section 1.1, the number of expected casualties is important in determining the safety level. This research will try to find a way to reduce the number of casualties due to a dike breach. In the introduction the inundation parameters are mentioned which affect the loss of life due to a dike breach. These parameters are the flow velocities and the rise rates in a polder. Assuming a breach does take place, despite all efforts to prevent this, a reduction of consequences has to be achieved by influencing the inundation parameters. If it is possible to slow down the breaching process, it should be possible to slow down the rise rate in the polder. To show that this is a feasible idea, a small leap into the research is necessary.

The most likely way to reduce the loss of life is to give people more time before the polder floods and when this does happen, at an as slow as possible rate. Research into loss of life due to flood events (Jonkman, 2007) shows that the mortality increases with the inundation speed. This rise rate has an estimated threshold value of 0.5 m/h for the mortality, as is shown in Figure 1.

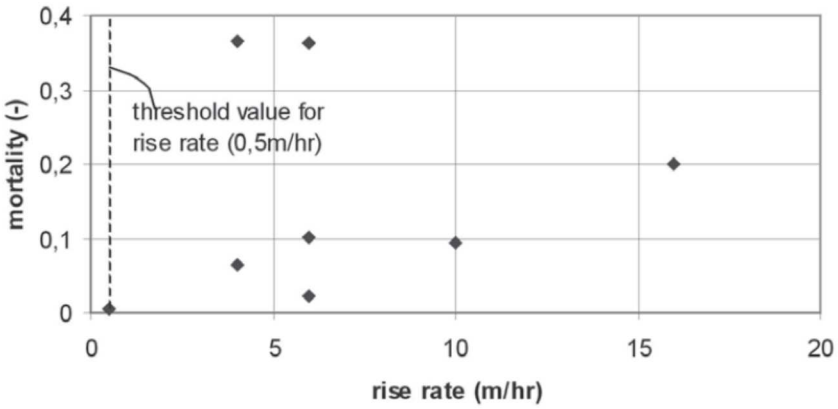

Figure 1 - Mortality due to rise rate (Jonkman, 2007)

Ideas to influence the breaching process are slowing down the erosion process or limiting the maximum breach width. To see the effects of these ideas, the BRES-Visser model (see section 3.1) is run using data from the ZWIN'94 experiment (Louws & Van der Weijde, 1995). The results can be seen in Table 1, in which:

- B_{max} is the final breach width at the breach bottom
- Q_{max} is the maximum flow rate through the breach
- Vi_{max} is the maximum rise rate (inundation velocity) in the polder
- t_6 is the time at which the outside and inside level become equal
- H_p is the final water depth in the polder
- E is the erosion rate

Erosion rate variation	***ZWIN'94***	***E/2***	***%***	***E/4***	***%***	***E/10***	***%***
Width (B_{max}) [m]	38.13	25.51	**66.9**	16.52	**43.3**	8.81	**23.1**
Flow (Q_{max}) [m^3/s]	175.56	108.95	**62.1**	71.03	**40.5**	29.74	**16.9**
Rise rate (Vi_{max}) [m/h]	2.57	1.62	**63.1**	1.10	**42.8**	0.56	**21.7**
Total time (t_6) [s]	2689	3670	**136.5**	4818	**179.2**	9421	**350.4**
Polder water level (H_p) [m]	2.44	2.39	**98.0**	2.27	**93.0**	2.11	**86.5**
Breach width variation	***ZWIN'94***	***B/2***	***%***	***B/4***	***%***	***B/10***	***%***
Width (B_{max}) [m]	38.13	19.07	**50.0**	9.53	**25.0**	3.81	**10.0**
Flow (Q_{max}) [m^3/s]	175.56	124.22	**70.8**	67.18	**38.3**	30.32	**17.3**
Rise rate (Vi_{max}) [m/h]	2.57	2.43	**94.7**	1.73	**67.1**	0.88	**34.1**
Total time (t_6) [s]	2689	3404	**126.6**	4524	**168.2**	9874	**367.2**
Polder water level (H_p) [m]	2.44	2.40	**98.4**	2.30	**94.3**	2.11	**86.5**

Table 1 - Reduction of erosion rate and final breach width

In these simulations, the erosion rate and final breach width were reduced to 50%, 25% and 10% of the ZWIN'94 experiment values. The effect of these reduction on the other parameters are visible. The reduction of the erosion rate leads to a larger reduction of the parameters than restricting the final breach width. The most important parameter is the rise rate (Vi_{max}). A comparison of the reduction of this parameter by reducing the erosion rate (E) or final width (B_{max}) is visible in Figure 2.

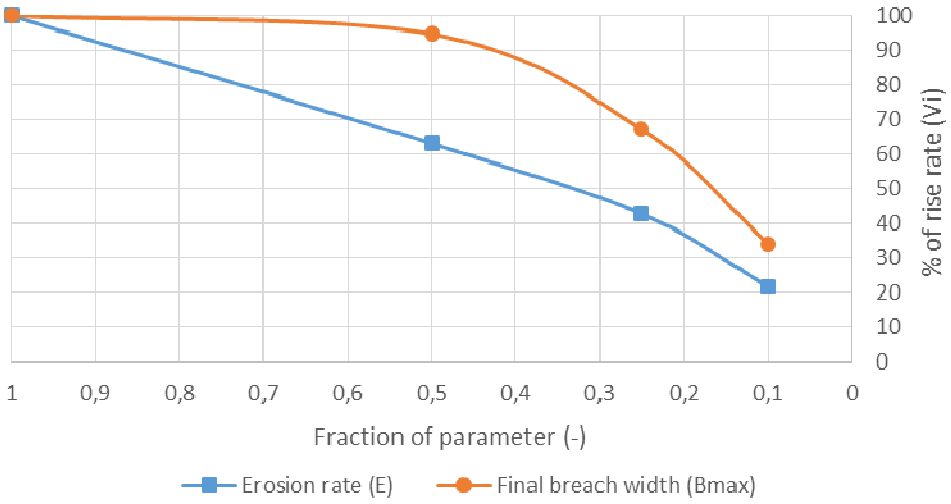

Figure 2 - Effect of erosion rate and final breach width on reduction of rise rate

It is clearly visible that the reduction of the erosion rate, reduces the rise rate in the polder more than a similar reduction of the final breach width. In Table 1 it is shown that a reduction of the erosion rate of 90% can reduce the rise rate sufficiently to be at the threshold value of 0.5 m/h, for the ZWIN'94 experiment. This indicates that it might be possible to increase the safety by a factor 10 by influencing the breach parameters.

1.3 Arrangement of the thesis

In this chapter an introduction into the thesis subject is given. Chapter 2 gives a brief description of the failure mechanisms of dikes and an explanation of the breaching process in detail. This explanation is the bases for the description, adaptations and discussion of the breach model, which is given in chapter 3. Chapter 4 defines the norm dike, which is used to compare options to each other and a normal sand dike. This dike is also used for model testing of the final solution. In chapter 5 several retardant options are presented and discussed and the best options are selected. After this selection, three options remain, which are implemented in the model. In chapter 6 the model results of these options and a comparison of these results are presented. Based on the model results, two options were subjected to tests in the laboratory. The setup, outcome and conclusions of these test are given in chapter 7. Based on the outcome of these experiments, a preferred solution is determined and modelled. The model results and explanation of these results are described in chapter 8. In this chapter also the effect of the solution on the mortality is determined. In chapter 9 a possible execution method is presented and a cost indication is determined. In this chapter also results from a relevant sensitivity study of dike breaches in the Netherlands are presented and discussed. Finally the conclusions and recommendations are given in chapter 10. At the end of the thesis a list of figures and tables can be found, as well as the references, followed by the appendices.

2 Breaching process

In this chapter a description is given of the development of a breach, starting at the initial failure of the protective cover.

2.1 Initial failure

There are multiple ways a dike can fail, which are given in Figure 3. All of these failure modes might (eventually) cause a complete dike breach, but it is also plausible the dike stays partially intact and still retains the water. In such a case it is important the dike will be repaired as soon as possible, as it might not stay intact for long or during a next flood or storm.

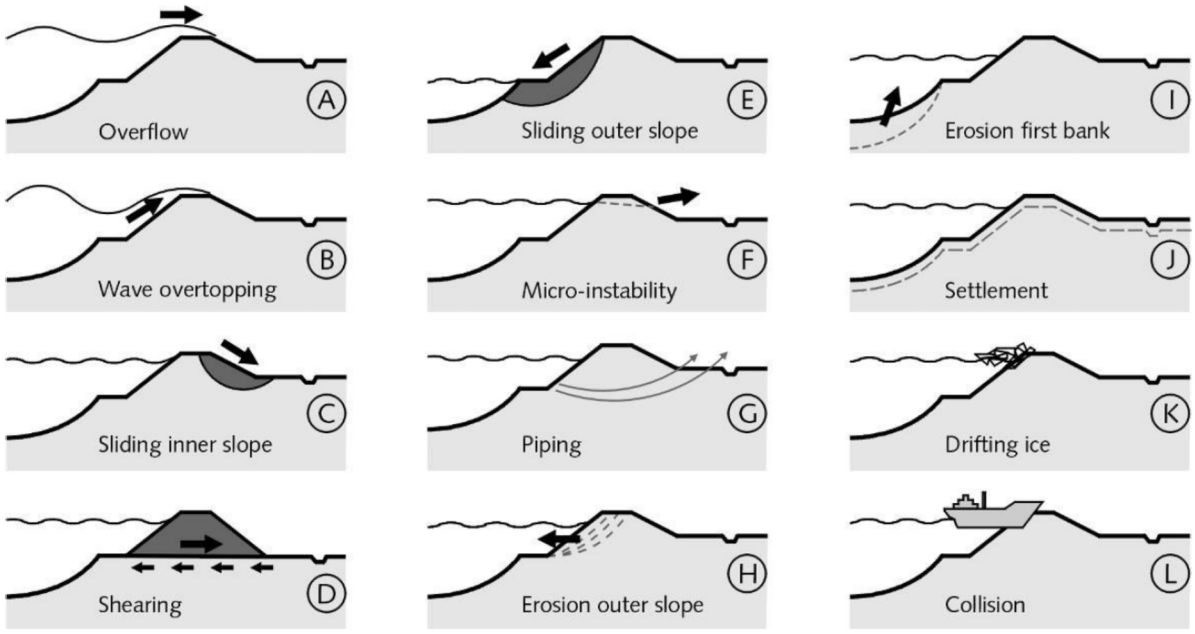

Figure 3 - Failure modes of a dike (Tonneijck & Weijers, 2008)

Normally the core of a sand dike is protected by a clay layer, preventing erosion of the core. However, as the failure modes show, it is possible for this protective layer to be damaged. This could happen due to overflow, wave overtopping, sliding of the inner slope, micro-instability or piping. These events do not cause a sudden dike breach, but allow erosion of the sand core and can eventually lead to a complete dike breach. How this initial failure or damage develops into a full breach, is described in the next section.

2.2 Breach development

The breaching process starts with an initial breach in the crest of the dike (at $t=t_0$) (made on purpose during experiments or representing the damage of the protective cover during a real breach, see section 2.1). Through this initial breach water will start to flow, which initiates the breaching process of the core. In this breaching process five stages can be distinguished (Visser, 1998).

Stage I (t_0-t_1): During this stage the inner slope will erode, increasing the angle of the inner slope from the initial value β_0 to the critical value β_1 (defined as the internal friction angle of sand, but steeper slopes have been observed (Visser, 1998)).

Stage II (t_1-t_2): The water flow will keep cutting into the inner slope, reducing the width of the crest in the process. This continues until the crest width has been reduced to zero.

Stage III (t_2-t_3): During this stage the remainder of the dike core will be eroded down to polder level. In the process the breach is also slightly widened, as the side slopes of the breach maintain a critical angle of γ_1. This stage ends when the breach bottom is equal to the polder level.

Stage IV (t_3-t_4): When the breach bottom is equal to the polder level, the breach will continue to grow vertically and laterally. The vertical erosion depends on the erodibility of the base of the dike and is usually small compared to the lateral erosion. Like during stage III, the side slopes of the breach remain at the critical angle γ_1. Up to now the flow over the dike and through the breach has been supercritical, when the flow becomes subcritical this stage ends.

Stage V (t_4-t_5): In this subcritical flow stage the breach keeps growing laterally, in which the side slope remain at an angle γ_1. During this stage the water level in the polder will continue to rise and the difference between the water level in front of and behind the dike will decrease. This reduces the flow velocity through the breach and eventually the velocity will be too low to induce incipient motion of sand particles, stopping the erosion process and thus the breaching process ($t=t_5$). The breaching process ends when the outside and inside water level are equal ($t=t_6$).

A schematic overview of these five stages is given in Figure 4. A detailed stage by stage description of the breach development process is given in the next sections.

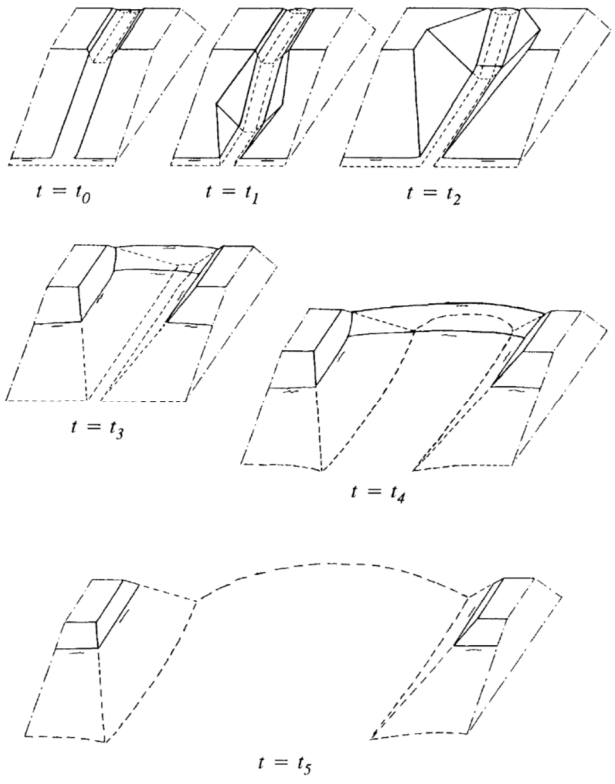

Figure 4 - Schematic overview of the breaching process of a sand dike (Visser, 1998)

Breach development in stage I

During stage I the inner slope steepens due to erosion on the slope. Because of the steepness of the inner slope, the flow on the slope will be supercritical. On the crest the flow will change from subcritical to critical, where the water depth at the top of the inner slope will be equal to the critical water depth. After this point the flow will accelerate along the slope from x to $x=l_n$ (see Figure 5, l_n=adaptation length of the flow). Since erosion of sand depends on the flow velocity, the erosion capacity of the flow will also increase along the slope from x to $x=l_n$, for $x>l_n$ the erosion capacity will remain constant. The flow will continue to erode sand until it the transport capacity is reached, which is at $x=l_a$ (l_a=adaptation length of the sediment transport). Due to this erosion the inner slope will steepen. When no erosion has occurred yet, the slope is at an initial angle β_0 and the erosion will steepen the slope to a critical angle of β_1, defined as the angle of internal friction of sand. When the slope angle is equal to this critical angle, this stage ends (at $t=t_1$).

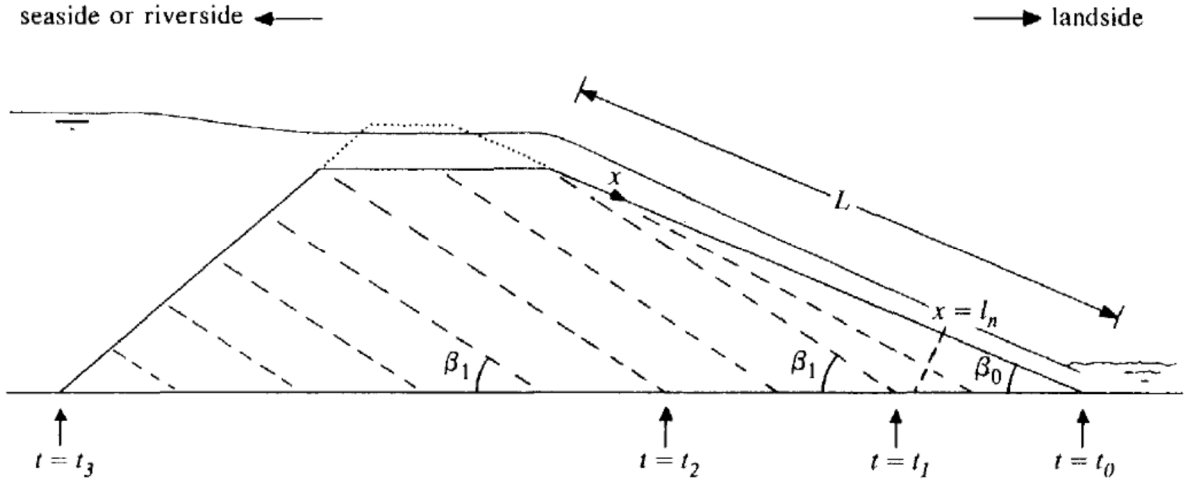

Figure 5 - Breach development during Stages I, II and III (Visser, 1998), the flow is critical on top of the crest and super critical on the inner slope

Breach development in stage II

At this stage the flow remains supercritical and the inner slope is eroded further, at a constant angle β_1. This erosion cuts into the dike, from the inside out, reducing the crest width. This stage continues until the crest width is reduced to zero, as can be seen in Figure 5 (at $t=t_2$).

Breach development in stage III

When the crest width is reduced to zero, the crest height starts to decrease due to the erosion. During this process the flow through the breach increases rapidly, since the size of the breach increases. The flow through the breach is still supercritical. This increased flow also increases erosion. The breach will starts to widen slightly during this process, while the angles of the side slopes of the breach remain at a critical angle γ_1. In Figure 5 it is shown that this stage ends when the crest height is reduced to zero in the breach (at $t=t_3$).

Breach development in stage IV

In this stage the breach will widen and deepen further. The deepening of the breach during this stage depends on a few conditions (Visser, 1998):

- The erosion resistance of the base of the dike.
- The presence or absence of a toe structure on the outer slope, which can protect the slope against further erosion.
- The presence or absence of a relatively high foreland and its erosion resistance.

Depending on which of these conditions is present, the breach can be classified as one of three breach types:

- Type A: The base of the dike has a high resistance against erosion (e.g. a solid clay layer) (A.1), a toe structure is present which protects the outer slope from erosion or a relatively high foreland (A.2) or bottom protection with a high erosion resistance is present (A.2).
- Type B: A relatively high foreland is present, but it does not have a high erosion resistance.
- Type C: There is no high foreland and the base consists of easily erodible material.

The breach type influences the way the breaching process will continue. The conditions in a type A breach will slow down erosion of the dike and hinder the formation of scour holes or reduce its size. In a type B breach a scour hole in front of the dike will be formed, increasing the length of the spillway. Due to this the breach discharge increases compared to a type A breach. A type C breach has the largest scour holes, since there is nothing present to prevent erosion of the base of the dike. This supercritical flow stage ends at $t=t_4$.

Breach development in stage V

In stage V the flow changes from supercritical to subcritical. This is due to the reducing difference between the inside and outside water level. During this stage this difference will reduce to zero and due to this the flow velocity through the breach will decrease. At a certain point the flow velocity is too small to erode sand which stops the breaching process and the breach has reached its final dimensions (at $t=t_5$). It should be noted that stage IV and V might not occur if the polder behind the dike is small. It could be possible that the water level in the polder becomes equal to the outside water level before these stages are reached. If the polder is large enough, the water will continue to flow into the polder until the outside and inside water level are equal (at $t=t_6$).

3 Breach model

The breaching process described in chapter 2 is used to model the breaching of dikes. The computer model that is used to test options to retard the breaching process, is the BRES-model (BReach Erosion in Sand dikes) (Visser, 1998). The model is based on the five stages of the breaching process, describing the physical processes.

3.1 BRES-Visser

An understanding of this model is necessary to use it for modelling and testing of options. In this section a brief description of the model is given, for a more elaborate explanation of the model reference is made to the dissertation of Visser (Visser, 1998).

To understand the BRES-Visser model, first a few definitions are made. In the model several parameters are used, which are presented in Figure 6 and Figure 7. In the model the assumption is made that the breach cross-section always has a trapezoidal shape.

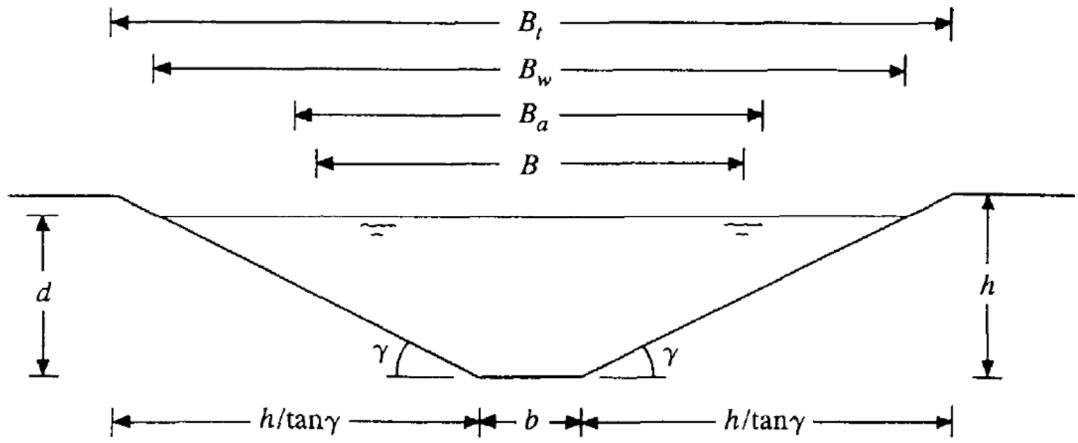

Figure 6 - Cross-section of a breach (Visser, 1998)

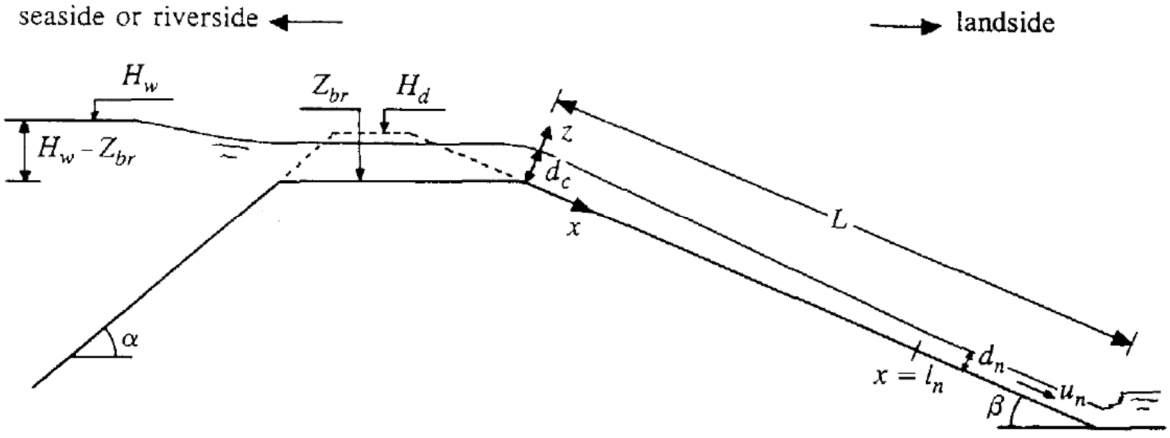

Figure 7 - Longitudinal cross-section of a breach (Visser, 1998)

The variables which are used in the model are defined as follows:

- h is the breach depth from breach bottom (Z_{br}) to crest height (H_d)
$$h = H_d - Z_{br} \tag{3.1}$$
- d is the water depth
- γ is the side-slope angle
- B is the depth-averaged width, averaged over the water depth d
$$B = b + \frac{d}{\tan\gamma} \tag{3.2}$$
- B_a is the depth-averaged width, averaged over the breach depth h
$$B_a = b + \frac{h}{\tan\gamma} \tag{3.3}$$
- B_w is the width at the waterline
$$B_w = b + \frac{2d}{\tan\gamma} \tag{3.4}$$
- B_t is the width at the dike crest
$$B_t = b + \frac{2h}{\tan\gamma} \tag{3.5}$$
- b is the width at the breach bottom
- A is the cross-sectional flow area
$$A = Bd \tag{3.6}$$
- R is the hydraulic radius
$$R = \frac{A}{b + \frac{2d}{\sin\gamma}} \tag{3.7}$$
- C_f is a dimensionless bed friction coefficient
$$C_f = \frac{\kappa^2}{(\ln(12R/k))^2} \tag{3.8}$$
$$k_{(\theta<1)} = 3D_{90} \tag{3.9}$$
$$k_{(\theta\geq1)} = 3\theta D_{90} \tag{3.10}$$
$$\theta = \frac{\tau_b}{\rho\Delta g D} = \frac{u_*^2}{\Delta g D} = \frac{C_f U^2}{\Delta g D} \tag{3.11}$$

- ρ is the water density
- g is the gravitational acceleration
- U is the depth averaged flow velocity
- ß is the angle of the inner slope of the dike
- H_w is the outside water level
- Z_{br} is the height of the bottom of the breach above reference level Z_{br}=0
- L is the length of the inner slope
- x is the coordinate along the inner slope
- z is the coordinate perpendicular to the inner slope

3.1.1 Breach development in stage I, II and III

In the first three stages the flow over the inner slope is supercritical and the discharge through the breach is:

$$Q_{br} = m\left(\frac{2}{3}\right)^{3/2}\sqrt{g}B(H_w - Z_{br})^{3/2} \tag{3.12}$$

where m is the discharge coefficient (m=1.0). This formula is valid for the calculation of the flow during stage I, II, and III, but is also valid during stage IV.

Calculation of water depth and flow velocity for x>ln

The flow on the inner slope accelerates up to $x=l_n$, beyond this point the flow is uniform. The depth-average flow velocity U_n is then calculated with (R_n is the hydraulic radius of the uniform flow):

$$U_n = \frac{(gR_n \sin\beta)^{1/2}}{C_f^{1/2}} \tag{3.13}$$

and the depth of the uniform flow is:

$$d_n = \frac{Q_{br}}{U_n B_n} \tag{3.14}$$

The adaptation point $x=l_n$ can be determined with:

$$l_n = \frac{2.5(Fr_n^2 - 1)d_n}{\tan\beta} \tag{3.15}$$

where:

$$Fr_n^2 \approx Fr^2 = \left(\frac{U}{\sqrt{gd}}\right)^2 = \frac{U^2}{gd\dfrac{B\cos\beta}{B_w}} \tag{3.16}$$

Calculation of water depth at x=0 (critical water depth d_c)

At the top of the inner slope, the water flow is critical and the water depth at x=0 is equal to the critical water depth d_c, which is:

$$d_c^3 = \frac{Q_{br}^2 (B_w)_c}{gB_c^3 \cos\beta} \tag{3.17}$$

When the water flow is critical, the flow velocity is:

$$U_c = \sqrt{gd} = \sqrt{gd_c\frac{B}{B_w}} \tag{3.18}$$

Calculation of water depth and flow velocity for 0<x<l_n

Now the flow velocities and water depths at the top of the inner slope and at the end of the adaptation length are known, the water depth and velocity in between these points can be approximated with:

$$d \approx d_n + (d_c - d_n)e^{-5x/l_n} \tag{3.19}$$

$$U \approx U_n + (U_c - U_n)e^{-5x/l_n} \tag{3.20}$$

Calculation of l_a

Since the water depths and flow velocities at different locations in the breach are known, the sediment transport through the breach can be calculated. Just like the flow has an adaptation length, the sediment transport has one as well. The adaptation length of the sediment transport gives the length after which no erosion takes place anymore, because the maximum sediment transport capacity of the flow is reached. The adaption length l_a is:

$$l_a = \xi \frac{R_w}{B_t} \frac{Ud}{w_s \cos\beta} \tag{3.21}$$

where w_s is the settling velocity of the sediment and ξ is approximately 0.4 in case of uniform flow, in case of accelerating flow on a relatively steep sloping bed ξ is approximately 1. For the breach model, ξ=1 is used during stages I, II and III and ξ=0.4 is used during stages IV and V.

Calculation of sediment transport s(x)

The sediment transport through the breach consists of bed-load (S_{bl}) and suspended load (S_{sl}) transport, determined by:

$$S(x) = S_{bl}(x) + S_{sl}(x) \tag{3.22}$$

During the breaching process the bed-load transport is small compared to the suspended load transport, thus only the suspended load transport is calculated:

$$s(x) = \frac{x}{l_a} S_s \tag{3.23}$$

in which S_s is:

$$S_s = MB_w U^n \tag{3.24}$$

where M is a dimensional coefficient and n is a dimensionless exponent.

Calculation of erosion rate

Using the above formulas, the erosion rate can be calculated. If the length of the inner slope is smaller than the adaptation length of the flow ($L<l_n$), the erosion rate is calculated with:

$$E_{(0<x<l_n)} = \frac{B_w}{B_t}\frac{M}{(1-p)l_a}U^n(1+\mathrm{n}\frac{x}{U}\frac{\delta U}{\delta x}) \tag{3.25}$$

in which p is the bed porosity. When the length of the inner slope is larger than the adaptation length of the flow ($L \geq l_n$), the erosion rate can be calculated with:

$$E_{(l_n \leq x \leq l_a)} = \frac{B_w}{B_t}\frac{M}{(1-p)l_a}(U_n)^n \tag{3.26}$$

Calculation of steepening of inner slope

Due to the erosion process, the inner slope will steepen during stage I. This process is simulated by approximating the erosion rate at $x=x_E=l_n$, for $l_n<L$ or $x=x_E=L$ when $l_n>L$, because the erosion rate at these locations is at its maximum. The process of the steepening of the inner slope can be approximated with:

$$\beta_1 - \beta_0 = \frac{E(\beta_0^+)}{x_E}(t_1 - t_0) \tag{3.27}$$

where:

$$\beta_0^+ = \frac{\beta_1 + \beta_0}{2} \tag{3.28}$$

Using these formulas, the time at which stage I ends, can be calculated with:

$$t_1 = t_0 + \frac{(\beta_1 - \beta_0)x_E}{E(\beta_0^+)} \tag{3.29}$$

Calculation of decrease of crest width

At time t_1, the inner slope has reached the critical angle β_1, the value at which it remains during stages II and III. In stage II the erosion of the inner slope continues until the crest has reached a width (W_d) of zero. The decrease of the crest width can be approximated with:

$$-W_1 = -\frac{B_w}{B_t}\frac{s_s L}{(1-p)l_a \sin\beta_1}(t_2 - t_1) \tag{3.30}$$

where:

$$W_1 = W_d + (H_d - Z_{br})(\frac{1}{\tan\alpha} + \frac{1}{\tan\beta_0}) \tag{3.31}$$

The time at which stage II ends can then be calculated with:

$$t_2 = t_1 + \frac{B_t}{B_w}\frac{W_1(1-p)l_a \sin\beta_1}{s_s L} \tag{3.32}$$

Calculation of decrease of crest height

When the crest width is reduced to zero, the crest height Z_{br} starts decreasing. Due to the lowering of the crest, the flow through the breach will increase and the transport capacity and adaptation length will also increase. The decrease of Z_{br} over a time step can be calculated with:

$$\Delta Z_{br} = -\frac{B_w}{B_t}\frac{\sin\alpha}{\sin(\alpha+\beta_1)}\frac{s_s(L_2)}{(1-p)l_a}\Delta t \tag{3.33}$$

in which L_2 is the length from the top of the inner slope to the toe of the inner slope. During stage III the flow and sediment transport through the breach changes. The flow changes from a Froude number Fr>>1 at the end of stage II to a Froude number slightly above 1 at the end of stage III. For the sediment transport the Shields parameter θ changes from an order of magnitude 10 to 100 at the end of stage II to a θ of an order of magnitude of 1 at the end of stage III.

Calculation of increase of breach width

The increase of the breach width is a result of the above processes. The new width values of the breach can be calculated at any time step using the formulas in the introduction of section 3.1 and the newly calculated water depth and breach depth.

3.1.2 Breach development in stage IV

During stage IV the breach mainly grows laterally. The processes in the breach remain approximately the same. Due to a change in flow regime, the sediment transport adaptation length is changed (ξ=0.4 instead of ξ=1.0), given by:

$$l_a = \xi\frac{d}{h}\frac{Ud}{w_s} \approx \frac{0.15\sqrt{g}h^{3/2}}{w_s} \tag{3.34}$$

Consequently, the ratio between the adaptation length and the breach length is:

$$\frac{l_a}{L_{br}} \approx \frac{0.02\sqrt{gh}}{w_s} \tag{3.35}$$

For the type of sand dikes used in this model $l_a > L_{br}$, so the sediment transport on the slopes of the breach is given by:

$$s(x) = \frac{x}{l_a}s_s \tag{3.36}$$

which causes the vertical erosion of the side slopes over time:

$$\frac{dZ_b}{dt} = -\frac{d}{h}\frac{s_s}{(1-p)l_a} \tag{3.37}$$

Due to the vertical erosion and angle of the side slopes, the side slopes will also erode horizontally, causing the breach width to increase over time, given by:

$$\frac{dB}{dt} = \frac{dB_t}{dt} = 2\frac{d}{h}\frac{s_s}{(1-p)l_a \tan\gamma_1} \tag{3.38}$$

Type A, B and C breaches

When stage IV is reached, there are different types of breaches which can occur, depending on the dike base, the presence of a high foreland or a toe structure on the outer slope. For all types the above formulas hold, but for some types minor adaptations are necessary.

- *Type A.1*
  This type of breach occurs when a dike has a relatively non-erodible base. For this type all previous formulas hold.

- *Type A.2*
  When a toe structure protects the outer slope against erosion, a type A.2 breach occurs. The toe construction acts as a spillway, which causes the flow to accelerate downstream of the toe structure, resulting in the formation of a hydraulic jump. Also for this type of breach, the previous formulas hold. Figure 8 shows a type A.1 or A.2 breach.

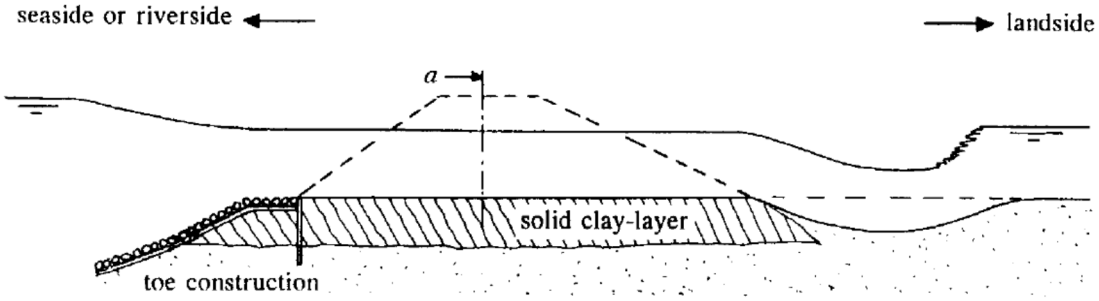

Figure 8 - Type A.1 or A.2 breach (Visser, 1998)

- *Type B*
  A type B breach occurs when a relatively high foreland is present which can be eroded. Retrograde erosion causes the formation of a curved spillway in the foreland. The flow into the breach goes through this spillway and the spillway thus controls the flow discharge through the breach (Figure 9).

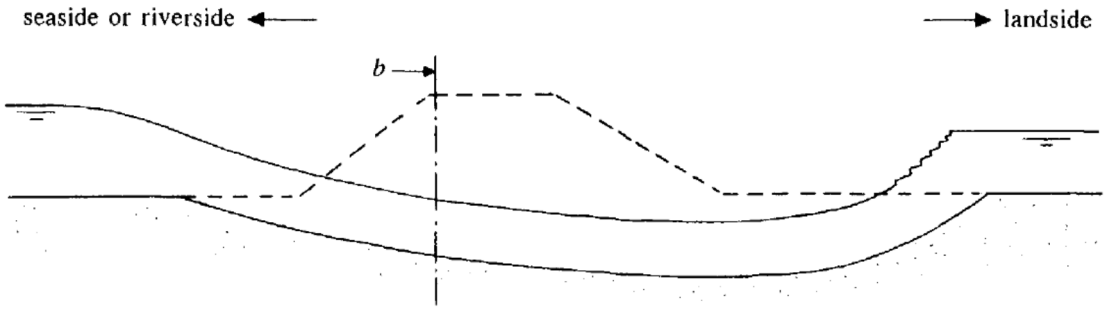

Figure 9 - Type B breach (Visser, 1998)

Due to this effect, the discharge formula (3.12) is slightly adapted (m used to be 1.0, but in this case m is approximated by π/2):

$$Q_{br} = m(\frac{2}{3})^{3/2}\sqrt{g}B(H_w - Z_{br})^{3/2} \tag{3.39}$$

- *Type C*
  When none of the above features are present, the breach is a type C. In this type of breach it is possible for the dike base to erode, which can be calculated with:

$$\frac{dZ_{br}}{dt} = -\frac{d}{h}\frac{s_s}{(1-p)l_a} \tag{3.40}$$

A representation of this type of breach is given in Figure 10.

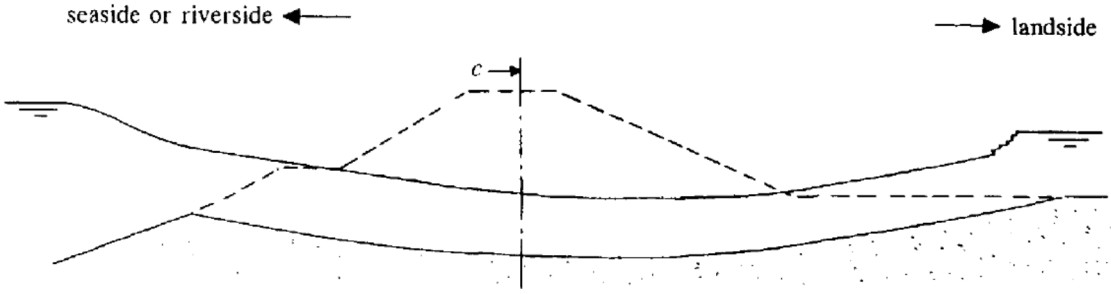

Figure 10 - Type C breach (Visser, 1998)

During stage IV enough water flows through the breach to increase the water level in the polder, which can be calculated with:

$$H_p = d_c + Z_{br} \tag{3.41}$$

$$H_p(t+\Delta t) = H_p(t) + (Q_{br}\cdot\Delta t)/A_p \tag{3.42}$$

in which A_p is the polder area. Due to this increase in polder level, the head difference between the inside and outside water level decreases. This decreases flow velocities in the breach. Stage V is reached when the flow becomes subcritical.

3.1.3 Breach development in stage V

At the start of stage V the flow velocities through the breach have decreased and the flow has become subcritical (Fr<1). This causes the breach growth to slow down, because of reduced erosion at lower flow velocities. Due to the changed flow regime (sub- instead of supercritical) the formulas for calculation of the water depth and flow velocity change into:

$$d = H_p - Z_{br} \tag{3.43}$$

$$U = \sqrt{2g(H_w - H_p)} \tag{3.44}$$

The flow rate through the breach also changes:

$$Q_{br} = mB\sqrt{2g}\sqrt{H_w - H_p}(H_p - Z_{br}) \tag{3.45}$$

where m≈1 for type A and C breaches and m≈π/2 for a type B breach.

In this stage the above formulas and the formulas of stage IV describe the evolution of the breach growth, until the flow velocities have become so low that it is no longer possible to pick up sand. This is determined in the model when the Shields parameter θ has become equal to the critical value θ_{cr}, at that point the breaching process stops. The flow through the breach, however, continues until the water level in the polder H_p is equal to the outside water level H_w.

3.1.4 Sediment formulas in BRES-Visser

Several sand transport or erosion formulas are available in the model to determine the erosion rate (Visser, 1998):

- Bagnold-Visser, BV (1989)

$$s_t = s_b + s_s \tag{3.46}$$

$$s_{b(\beta\le\phi)} = \frac{e_b}{(\tan\phi - \tan\beta)\cos\beta}\frac{C_f U^3}{\Delta g} \le \xi_2(1-p)D_{50}U \tag{3.47}$$

$$s_s = \frac{e_s}{(w_s / U)(\cos\beta)^2}\frac{C_f U^3}{\Delta g} = \frac{e_s C_f U^3}{\Delta g w_s (\cos\beta)^2} \tag{3.48}$$

- Engelund and Hansen, EH (1967)

$$s_t = 0.05 C_f^{-1}(\Delta g D_{50}^3)^{0.5}\theta^{2.5} \tag{3.49}$$

- Van Rijn, VR (1984)

$$s_t = s_b + s_s \tag{3.50}$$

$$s_{b(T<3)} = 0.053(\Delta g D_{50}^3)^{0.5}\frac{T^{2.1}}{(D_*)^{0.3.}} \tag{3.51}$$

$$s_{b(T\ge3)} = 0.1(\Delta g D_{50}^3)^{0.5}\frac{T^{1.5}}{(D_*)^{0.3.}} \tag{3.52}$$

$$s_s = F c_a U d \tag{3.53}$$

- Wilson, WL (1987)

$$s_b = 12.1(\Delta g D^3)^{0.5}(\mu\theta - 0.047)^{1.5} \tag{3.54}$$

The best simulation results are obtained by the model when a combination of these formulas is used. The best and default combination used by the model is Bagnold-Visser (1989) for stage I, II and III and Van Rijn (1984) for stage IV and V. Use of Engelund and Hansen (1967) instead of Van Rijn (1984) also yields good results. A comparison of different combinations can be seen in Figure 11, in which the model results are compared with the Zwin'94 experiment.

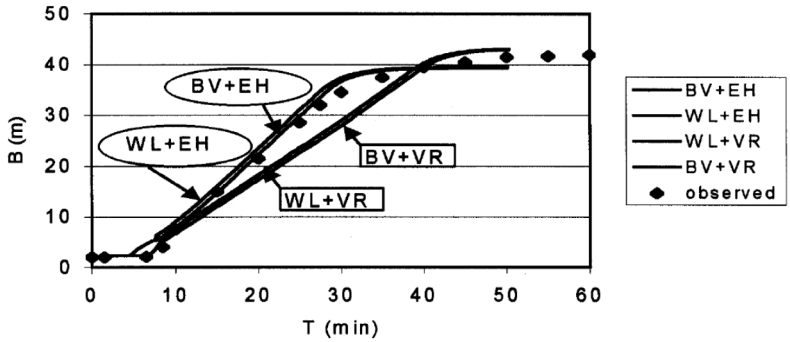

Figure 11 - Comparison of Zwin'94 simulations by BRES-Visser (Ye & Verhagen, 1999)

3.1.5 Discussion of BRES-Visser

A SWOT analysis of the BRES-Visser model was done by (Peeters, et al., 2011), shown in Figure 12.

STRENGTHS	WEAKNESSES
- Hydrodynamic aspects easily adjustable - Model structure easily to extend - Detailed physically-based description of surface erosion, especially breach initiation processes - Validation for real-world case studies, e.g. ZWIN94-test - Stand-alone model - Short simulation time	- Currently unavailable for use in practical cases - Limited number of breach process incorporated (only for homogeneous, sandy dikes) - Not tested during IMPACT & FLOODSITE Hence, performance in practice is unclear. - Erosion at toe determines erosion rate of entire dike (breach initiation) - Breach shape always trapezoidal - No head-cut erosion - Only sediment transport equation - No piping - Model relatively insensitive to water levels on land-side
OPPORTUNITIES	**THREATS**
- Enormous potentials due to detailed physically-based description - Detailed physically-based - Development of a user-friendly interface - Erosion equations can be built-in rather easily	- Model structure not easily adjustable - Limited applicability for inexperienced users - Only for homogeneous, sandy dikes - Some less known model parameters

Figure 12 - SWOT analysis of BRES-Visser (Peeters, et al., 2011) (IMPACT & FLOODSITE are studies about dam and dike breaching (Floodsite, 2009))

In this SWOT analysis one of the weaknesses and threats of the model is that it is only useable for homogenous, sand dikes. Due to the work of (Zhu, 2006) this statement is not entirely true anymore. Zhu developed a BRES-model which is applicable for cohesive soils. This BRES-Zhu model is discussed in the next section.

Robijns (Robijns, 2012) did a sensitivity study of the BRES-Visser model. He concluded that the current model is very sensitive for variations in the internal angle of repose of the side slopes, especially in stage IV and V. Also the difference between erosion of larger and smaller grains was studied. As expected, it is more difficult to erode large grains than small grains, due to the increased resistance of larger grains. The critical shear stress of large grains is higher, making it harder to start erosion. However, the Van Rhee formula (Van Rhee, 2010) predicts that if erosion of large grains has started, the erosion goes faster than for small grains. This is due to the reduced permeability of sand consisting of small grains.

3.2 Adaptations

Since the BRES-Visser model has been developed, is has also been adapted by other researchers. These adaptations are discussed in this section.

Robijns

A phenomenon that is not included in the current model is hindered erosion. Hindered erosion occurs at high flow velocities (U>1.5 m/s), e.g. during the breaching process, and is caused by shear during erosion. During the erosion process the porosity of sand increases. This is caused by the dilation of the sand layer (Figure 13). This increased volume of the pores has to be filled with water.

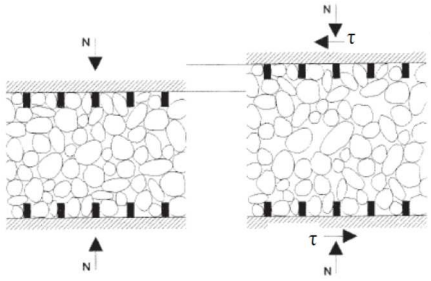

Figure 13 - Increase of porosity during shearing of densely packed sand: dilatant behaviour (Bisschop, et al., 2010)

Because of this dilatant behaviour the pore pressure drops, creating a pressure gradient over the sand layer. The gradient is directed into the sand layer, exerting pressure on the sand layer. This reduces or hinders erosion by increasing the critical shear stress of the sand. Van Rhee uses another approach than the current formulas in the BRES-Visser model to include this phenomenon. Robijns (Robijns, 2012) improved the model by implementing the hindered erosion formula of Van Rhee (Van Rhee, 2010) using a simplified version, Van Rhee-Bisschop (Bisschop, et al., 2010):

$$V_e^5 = \alpha^2 D_*^{0.6} \left(\frac{\theta - \theta_{cr}}{\theta_{cr}} \right)^3 \left(\frac{k}{\delta} \right)^3 \tag{3.55}$$

$$\alpha = 0.00033 \frac{\sqrt{\Delta g D_{50}}}{1 - n_0} \tag{3.56}$$

$$D_* = D_{50} \left(\frac{\Delta g}{\nu^2} \right)^{1/3} \tag{3.57}$$

$$\delta = \frac{n_i - n_0}{1 - n_i} \frac{1}{\Delta(1 - n_0)} \tag{3.58}$$

in which:

V_e	= erosion velocity [m/s]
Δ	= relative density $((\rho_s-\rho)/\rho)$ [-]
D_{50}	= median particle diameter [m]
n_0	= in-situ porosity [-]
n_i	= porosity sheared layer [-]
D_*	= dimensionless particle diameter [-]
v	= kinematic viscosity of water [m^2/s]
θ	= Shields parameter [-]
θ_{cr}	= critical Shields parameter [-]
k	= permeability [m/s]

Implementation of this formula into the model yields better results than the use of the traditional erosion formulas. This formula also simulates the steep angle of the inner slopes better than other formulas. There was a difference between the internal angle of repose of the side slopes entered in the model ($\varphi \approx 32^\circ$) and the observed steepness of the side slopes during the Zwin'94 experiment ($\varphi \approx 60^\circ$). Using Van Rhee-Bisschop in the model yields better results for this steep angle. According to (Robijns, 2012) it seems favourable to use Van Rhee-Bisschop as erosion formula in the model.

Zhu

Zhu (Zhu, 2006) developed a model for the breaching of clay dikes (BRES-Zhu). BRES-Zhu is based on the BRES-Visser model, adapted for the erosion process of cohesive soil. First the differences between the sand and clay breaching process are explained, stage by stage (Zhu, 2006).

Similar to stage I of the breaching process of a sand dike, the breaching process in a clay dike starts with a flow through the initial breach, eroding soil from the inner slope and possibly from the dike crest. Where in a sand dike only shear erosion occurs, in a clay dike also small-scale headcut erosion can occur. This stage continues for both dikes until the critical value of the inner slope angle, β_1, is reached. This angle is steeper for clay dikes (80-90°) than for sand dikes (≈60°).

In stage II this large steepness of the inner slope acts as a headcut in clay dikes. This causes the dike to be eroded by a combination of flow shear erosion, fluidization of the surface, scour of the dike foundation, headcut undermining and discrete headcut mass failure. This is not a continuous erosion process, but it is erosion due to larger lumps of clay detaching from the dike.

In stage III the headcut keeps its critical angle and the same processes keep eroding the dike. Because of the weakness of the remaining dike body, the erosion will go faster. There is also a chance that the remaining dike body in the breach will fail at once, increasing the flow through the breach rapidly.

Stage IV and V are mainly similar for both dike types, albeit that the side slope angle will be a lot steeper than found in sand dikes (80-90°), due to the cohesion of clay.

The erosion process of sand dikes depends mainly on shear erosion. Due to the different erosion mechanisms of clay, it is not possible to calculate the erosion with one formula. For each mechanism, different formula are used to calculate the erosion due to that mechanism. For more insight into these mechanisms and the resulting model is referred to Zhu (Zhu, 2006).

Other erosion formulas

In literature two other erosion formulas were found. To see if these formulas could improve the BRES-model, these two erosion formulas are compared to the ones already used in the BRES-model. Previous improvements of the BRES-model lead to the use of the Van Rhee-Bisschop formula (Bisschop, et al., 2010) as erosion formula. This formula yields results which are in good agreement with the ZWIN'94 data (Visser, 1998). The new erosion formulas are compared to this formula. For a better comparison, also the Van Rijn-Van Rhee formula (Van Rhee, 2010) and the original Van Rijn formula (Bisschop, et al., 2010) are included. These formulas are used for comparison with the Nagakawa-Tsujimoto formula and the Fernandez Luque formula (Van Rijn, 1984). These two formulas have also been adapted in the same way as the Van Rijn-Van Rhee formula, to see the effect of this adaptation on these formulas.

The Van Rijn-Van Rhee formula is an adaptation of the original Van Rijn formula. This adaptation takes the effect of permeability on the erosion rate in to account and is applicable to every erosion formula which uses the critical Shields parameter. Van Rhee adapted the critical Shields parameter to account for the effect of the permeability (Van Rhee, 2010). The Van Rhee adaptation of the critical Shields parameter is:

$$\theta_c^{\,1} = \theta_c \left(\frac{\sin(\phi - \beta)}{\sin(\phi)} + \delta_p \cdot \frac{V_e}{K} \right) \tag{3.59}$$

$$\delta_p = \left(\frac{n_i - p}{1 - n_i} \cdot \frac{1}{\Delta(1-p)} \right) \tag{3.60}$$

The Van Rijn pick-up function is:

$$E = 0.00033 \left(D \left(\frac{\Delta g}{\nu^2} \right)^{1/3} \right)^{0.3} \left(\frac{\theta - \theta_c}{\theta_c} \right)^{1.5} \tag{3.61}$$

The Nagakawa-Tsujimoto pick-up function is:

$$E = \alpha \rho_s (\Delta g D)^{0.5} \left(1 - \frac{\theta_c}{\theta} \right)^3 \theta \tag{3.62}$$

The Fernandez Luque pick-up function is:

$$E = \alpha \rho_s (\Delta g D)^{0.5} (\theta - \theta_c)^{1.5} \tag{3.63}$$

in which:

θ_c = critical Shields parameter (original (θ_c) or adapted (θ_c^1)) [-]
θ = Shields parameter [-]
V_e = erosion velocity [m/s] ($V_e=E/(\rho_s(1-p))$)
K = permeability [m/s]
φ = angle of internal friction [°]
β = angle of bed slope [°]
n_i = maximum porosity of the sand [-]
p = porosity [-]
E = erosion rate [kg/sm^2]
α = 0.02 [-]
ρ_s = density of sand [kg/m^3]
Δ = relative density ($(\rho_s-\rho)/\rho$) [-]
D = grain diameter [m]
v = kinematic viscosity [m^2/s]

Figure 14 shows a plot of the erosion velocities of the different erosion formulas (Van Rijn-Van Rhee, Van Rijn, Van Rhee-Bisschop, Nagakawa-Van Rhee, Nagakawa, Fernandez-Van Rhee, Fernandez) calculated at different flow velocities. As Figure 14 shows, the unadapted formulas (Van Rijn, Nagakawa, Fernandez) overestimate the erosion compared to the Van Rhee-Bisschop formula. Of these three formulas, Van Rijn overestimates the erosion the most. When these formulas use the adapted critical Shields parameter, the calculated erosion velocity goes down. In the figure this is shown with arrows. However, for Nagakawa and Fernandez the differences are small and thus they do not come close to the Van Rhee-Bisschop formula. Since the Van Rhee-Bisschop formula is a simplification of the Van Rijn-Van Rhee formula (original Van Rhee), the results of these two are approximately the same.

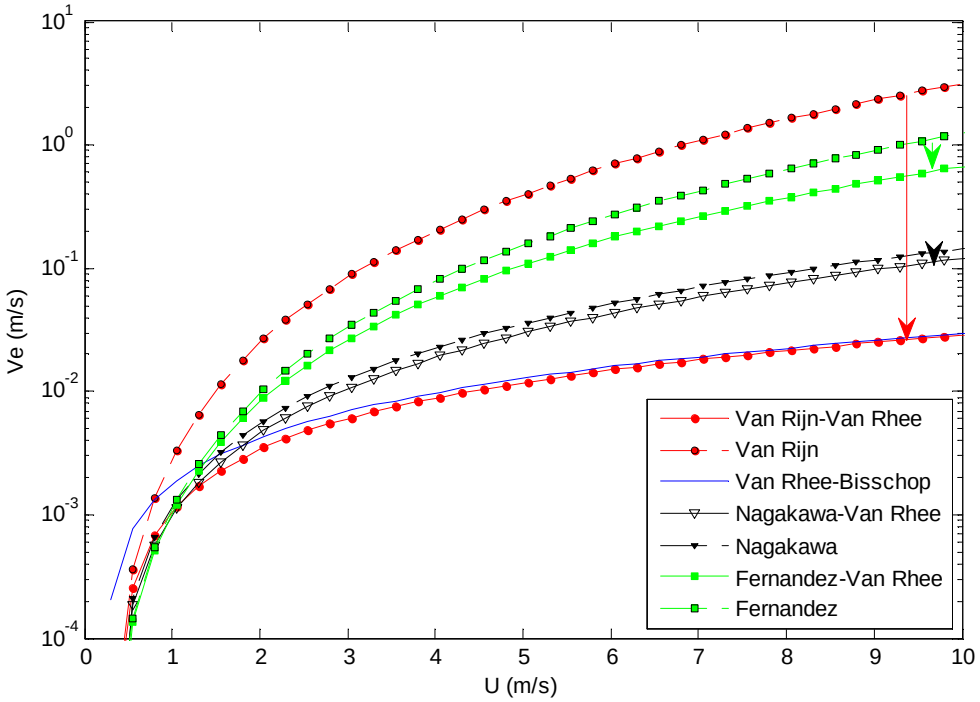

Figure 14 - Comparison of erosion formulas by calculating the erosion velocity (V_e) at several flow velocities (U)

From this it can be concluded that the tested erosion formulas overestimate erosion compared to the Van Rhee formula. The Van Rijn-Van Rhee, or the simplified version the Van Rhee-Bisschop, formula is still the favourable formula as already concluded in section 3.2.

3.3 Discussion

Despite the amount of research on breaching processes and breaching models, still a great deal more can be researched. A better understanding of the breaching processes can increase the accuracy of the breaching models and thus better predict the breaching of dikes. Including more processes and knowledge into the existing models can have the same effect. For instance, not a lot of real-life breaching tests have been executed, executing more of these tests will increase the knowledge of the process and the number of cases to calibrate models with. Also, the effect of clay-layers, revetments and toe-constructions on the breaching process is not very well known. More research into these and other constructions or inhomogeneities in the dike will contribute to a better understanding of their influence. Beside the effect of other materials or constructions, also the effect of overtopping waves is ignored. Waves could have a significant effect on the erosion of the dike, but this needs to be studied and eventually implemented in breaching models.

Beside the BRES-model, there are a lot more breaching models available for sand, clay and composite dikes and dams (Floodsite, 2009). The BRES-model is chosen because of its availability to the author and the studies into the model. Other models might give similar or even better results than the BRES-model, but this is not researched for this thesis. The goal of this research is not to make major improvements to the BRES-model, but to use it to find a way to slow down the breaching process in sand dikes.

4 Norm dike

The retardant options need to be tested and compared with an unimproved sand dike, the norm dike. The BRES-model is validated using the ZWIN'94 experiment (see section 3.1.4) the dike of that experiment is considered the norm dike for this research. The dimensions and parameters of this dike are given, as well as the outcome of the BRES-model for this experiment. In Figure 15 a cross-section of the dike can be seen.

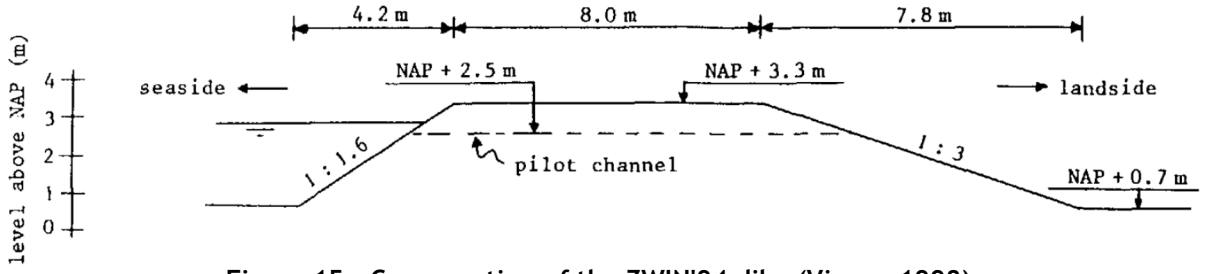

Figure 15 - Cross-section of the ZWIN'94 dike (Visser, 1998)

The dimensions of this cross-section along with other relevant parameters are defined in Table 3. The outside water level is a function of time, since it was influenced by the tide during the experiment. The water level above NAP in time is given by Table 2.

The data from these tables are used in the BRES-model to calculate the final breach width, maximum flow through the breach and duration of the breaching process of the norm dike (using the Van Rhee-Bisschop formula). The result can be seen in Figure 16, in which the blue line represents the model result and the black circles represent the measurements during the ZWIN'94 experiment. Using these calculations, also the duration of the breaching process is determined. This is the time between start of breaching until the inside and outside water levels are equal.

t [s]	*H_w [m]*	*t [s]*	*H_w [m]*	*t [s]*	*H_w [m]*
0	2.70	*2400*	2.45	*4800*	2.27
300	2.72	*2700*	2.44	*5100*	2.23
600	2.71	*3000*	2.42	*5400*	2.19
900	2.68	*3300*	2.41	*5700*	2.14
1200	2.63	*3600*	2.39	*6000*	2.11
1500	2.56	*3900*	2.37	*120000*	2.08
1800	2.51	*4200*	2.34		
2100	2.46	*4500*	2.30		

Table 2 - Outside water level (above NAP) ZWIN'94 experiment (Visser, 1998)

Parameter	*Value*
Bottom level outside water, Z_w [m]	NAP + 0.7
Bottom level polder, Z_p [m]	NAP + 0.7
Water level polder (at $t=t_0$), H_p [m]	NAP + 1.3
Dike height, H_d [m]	NAP + 3.3
Breach bottom (at $t=t_0$), Z_{br} [m]	NAP + 2.5
Width of breach bottom (at $t=t_0$), b [m]	1
Crest width, W_d [m]	8
Outer dike slope, a [-]	1:1.6
Inner dike slope, B [-]	1:3
Side slope angle, γ [°]	60
Water density, ρ_w [kg/m3]	1025
Water temperature, T [°C]	17
Sand density, ρ_s [kg/m3]	2650
Initial porosity, p [-]	0.40
Sheared porosity, n_i [-]	0.48
10% particle size, D_{10} [μm]	180
50% particle size, D_{50} [μm]	220
90% particle size, D_{90} [μm]	350
Angle of repose, φ [°]	32

Table 3 - Parameters ZWIN'94 dike (Visser, 1998)

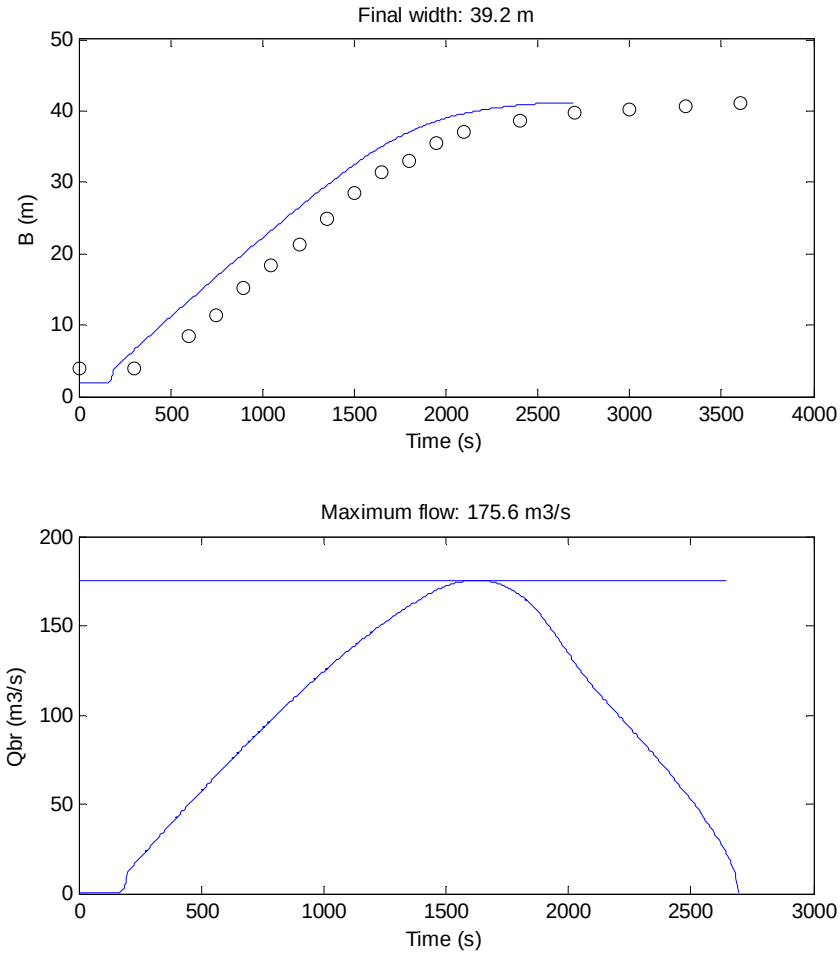

Figure 16 - Breach width (B) and flow rate (Q_{br}) as function of time (t≈2700 s.)

5 Retardant options

In this chapter possible options for retarding breach growth are presented and discussed. First all possible options derived from literature are described. From these options a few are selected for more research. The outcome of this research is used to select the most promising options.

5.1 Listing of options

This section gives an overview of all options derived from literature.

5.1.1 Alter the dike shape

One of the more evident options to retard the breaching process is to alter the shape of the dike. If the dike is wider, it takes more time to erode through the dike and if the flow velocity over the dike can be decreased, the erosion rate goes down. Two possibilities are discussed in this section, reducing the inner slope angle and increasing the crest width.

Reduce the angle of the inner slope

The breaching process starts with an initial breach in the crest of the dike and subsequently flow over the crest and inner slope. The flow over the inner slope erodes the sand and steepens the inner slope angle in stage I. If the flow velocity is higher, so is the erosion capacity of the flow. The flow velocity is higher when the steepness of the inner slope increases. From this it follows that the erosion rate is higher when the inner slope is steeper and thus the duration of stage I decreases. This has been analysed by (Smolders, 2010), the results are presented in Figure 17. It shows that changing the slope from 1/3 to 1/50 increases the duration of stage I approximately by a factor 15. Another consequence of a decrease of the inner slope is that the dike gets wider and thus takes up more space in the polder. For the described test the width of the base of the dike increases with approximately a factor 17 when increasing the slope from 1/3 to 1/50, which is a large increase of the width.

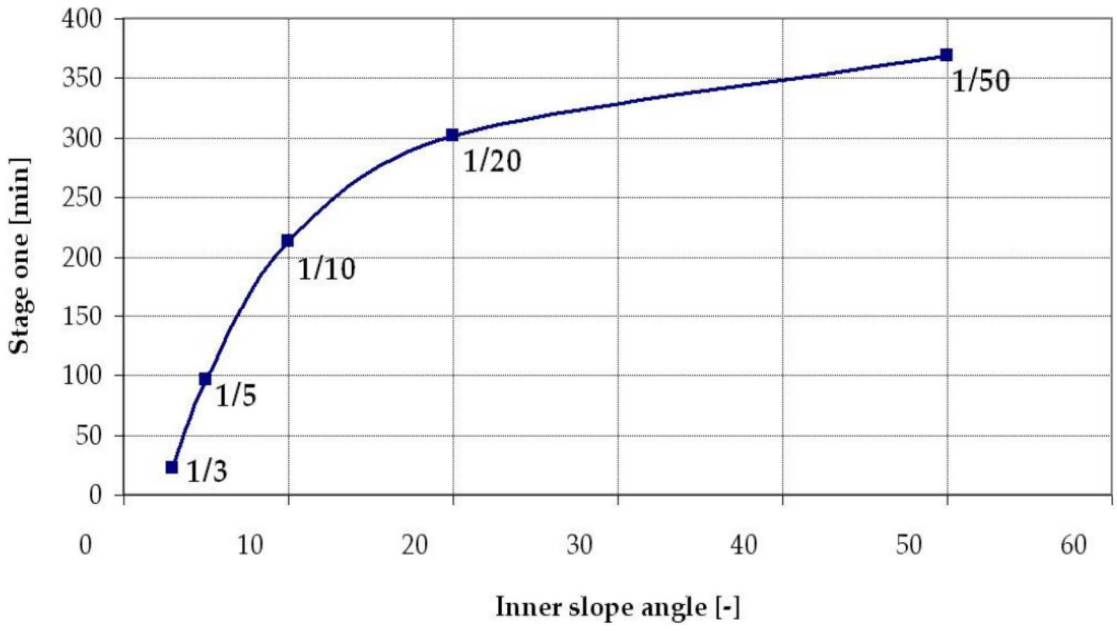

Figure 17 - Relation inner slope angle and duration of stage I (Smolders, 2010)

Increase the crest width

When the inner slope angle is reduced to the critical slope angle, the erosion cuts into the dike towards the outer slope. The erosion rate during this process is the same and thus an increase of the crest width, lengthens the duration of stage II. Again the effect is analysed (Smolders, 2010) and the results are presented in Figure 18. As can be seen, there is a linear relation between the dike width and the duration of stage II, an increase of the width by a factor 5 increases the duration of stage II approximately by a factor 4. This option has the same drawback as decreasing the slope angle, it takes up a lot of space inside the polder.

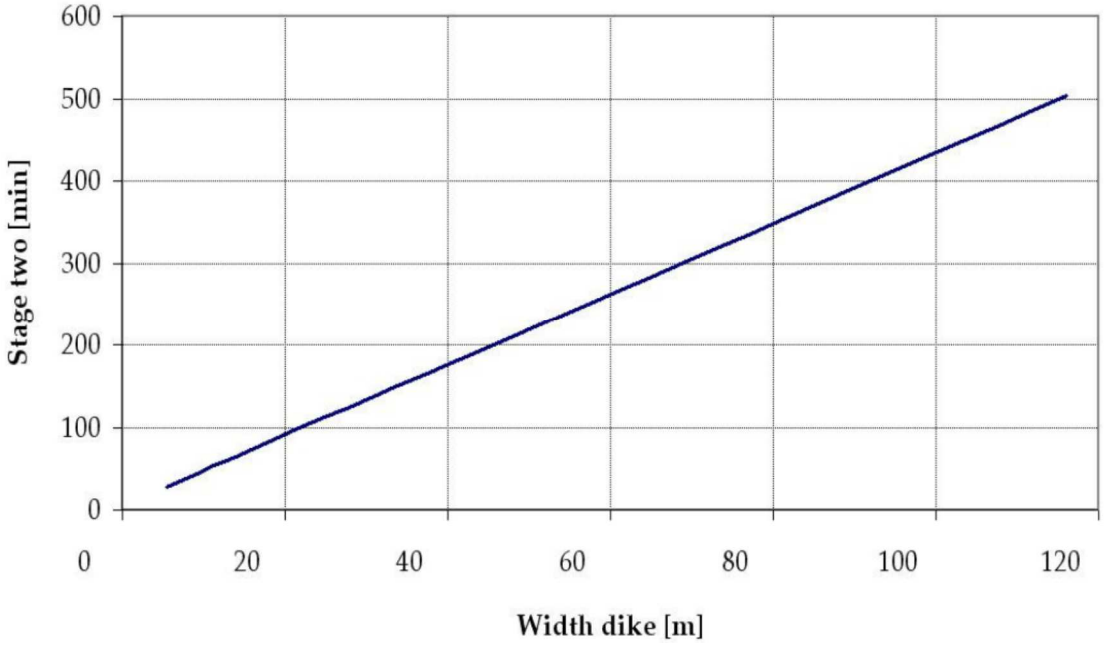

Figure 18 - Relation width of dike and duration of stage II (Smolders, 2010)

5.1.2 Increase the cohesion of the dike

Another possibility to increase the duration of the breaching process is to increase the cohesion of the dike. This effect was shown by (Zhu, 2006) during experiments for verification of the BRES-Zhu model. For comparison a test with a sand dike was included in the experiment. The profile development of the sand and clay dike experiment are shown in Figure 19. This experiment was executed using the same dike dimensions and similar hydraulic conditions. It clearly shows the influence of cohesion on the breaching process. The sand dike was breached in a little less than 3 minutes, while this took almost 3 hours for the clay dike. This large difference in duration of the breaching process makes this an interesting option.

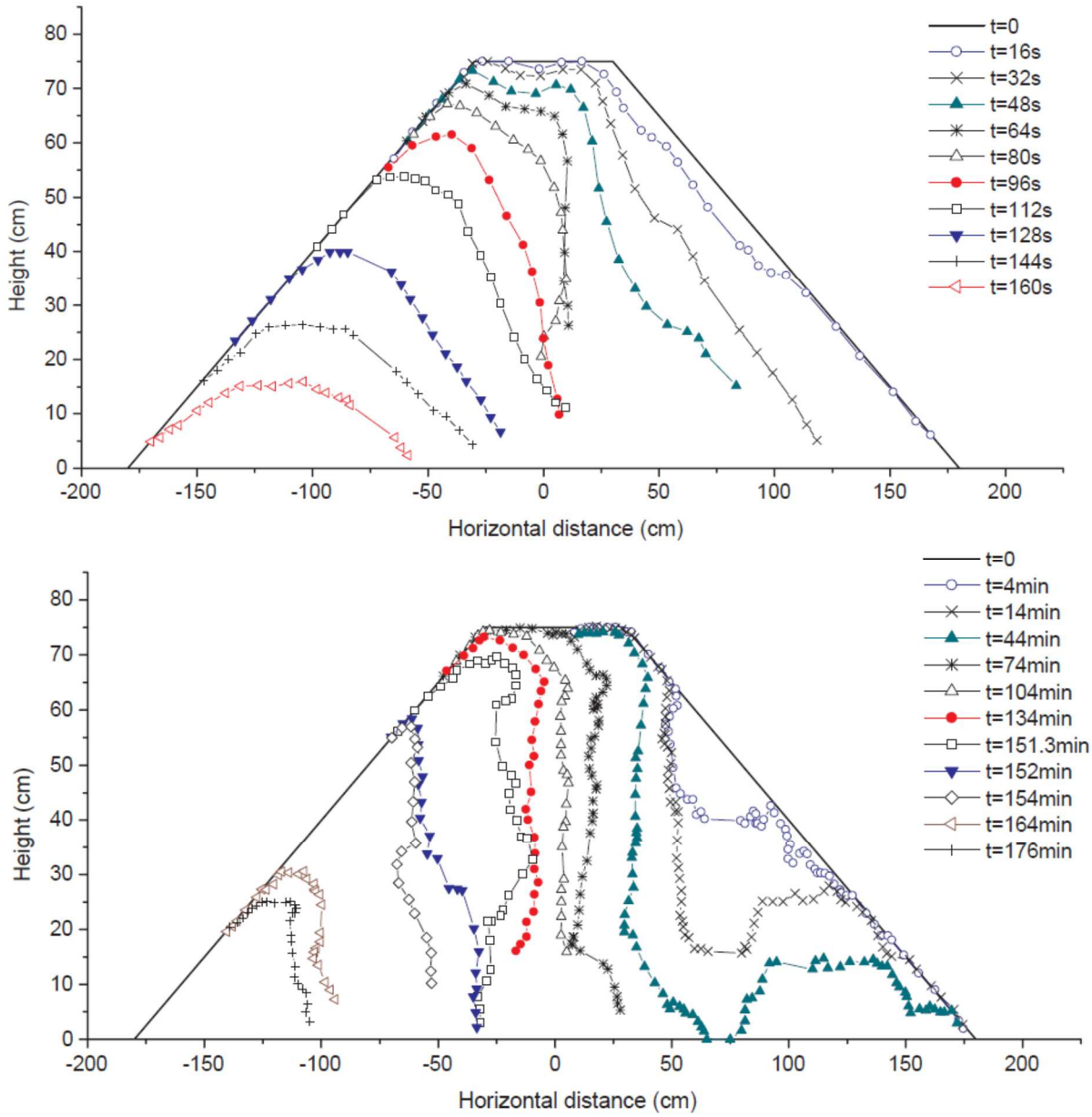

Figure 19 - Profile development of a sand dike (top) and a clay dike (bottom) (Zhu, 2006)

Bentonite clay and sand mixture

A way to retard the erosion of sand is to add bentonite clay to sand (Gailani, 2001). Bentonite is an impure clay material consisting mainly out of montmorillonite, which has highly absorbent properties. Bentonite should be a good additive because it chemically bonds more water than other clays. This increases the volume of the bentonite, which fills the pores in the sand. Due to this it should have the most effect on the erosion rate. During experiments the effect of bentonite clay on the erosion rate of sand was determined (Gailani, 2001). The effects depended on the percentage of bentonite added, shear stress, depth, and consolidation time. The results of these experiments are summarized in Figure 20. This figures shows that even adding a small amount of bentonite to sand has a significant effect on the erosion rates.

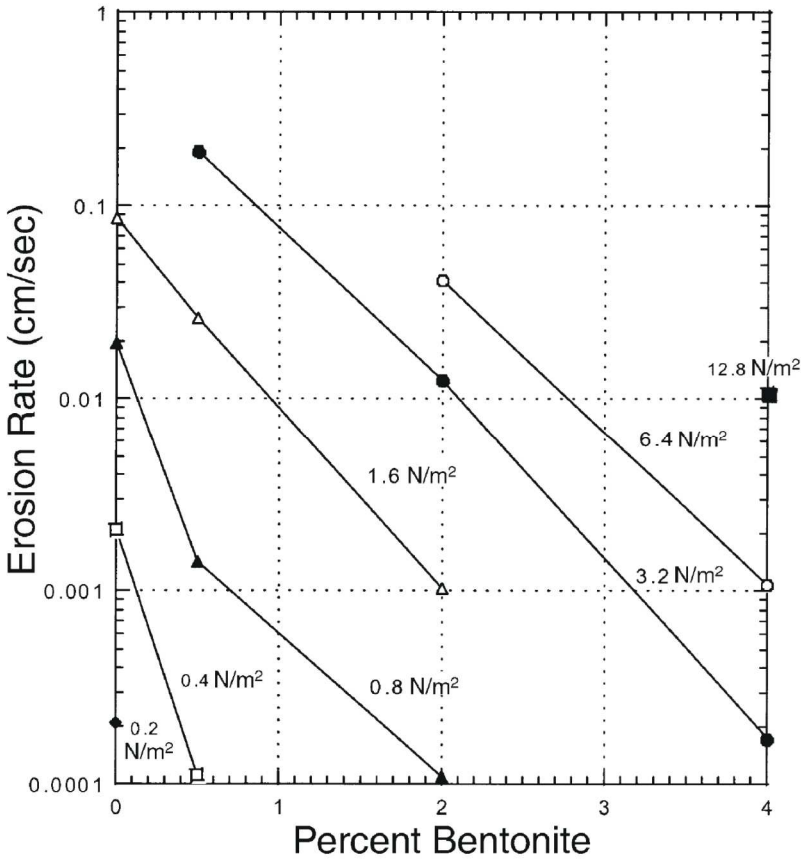

Figure 20 - Erosion rates of sand-bentonite mixtures, depending on bentonite content and shear stress (Gailani, 2001)

5.1.3 Increase strength of the sand

Instead of only increasing the cohesion of the dike, the sand in the dike can also be reinforced. There are several known methods to increase the strength of sand, which are described in this section.

Fibres and sand mixture

An option to increase the strength of sand is to reinforce the sand with fibres (Gray, et al., 1983). They researched the effect of fibres on the shear strength of sand. As an example, in Figure 21 the increase of shear strength of sand, when using reed fibres, is plotted for different percentages of the fibre.

The different lines in Figure 21 stand for different vertical confinement stresses, which have a threshold value to prevent fibres from being pulled out of the sand. When this stress is high enough the fibres are not pulled out, increasing the peak shear strength of the sand. The A_R/A ratio is the ratio between the area of the fibres (A_R) and the area of the sample (A), which is a way to determine the fibre content in a mixture.

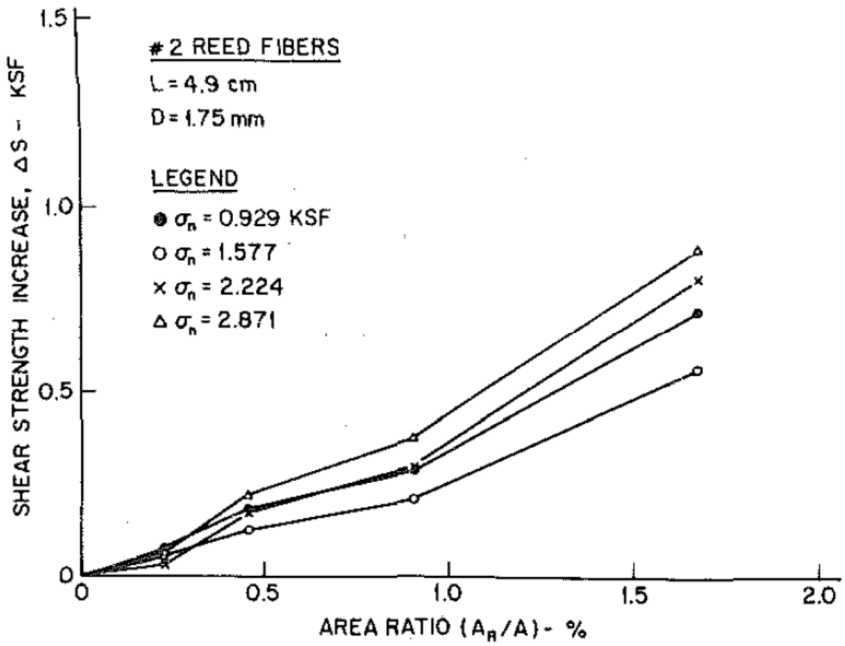

Figure 21 - Increase of shear strength of sand using reed fibres (Gray, et al., 1983)

Another way to prevent fibres from being pulled out, when the vertical confinement stress is too low, is to increase the length of the fibres, as can be seen in Figure 22. This also shows that there is limit to the shear stress increase which can be reached by lengthening the fibres.

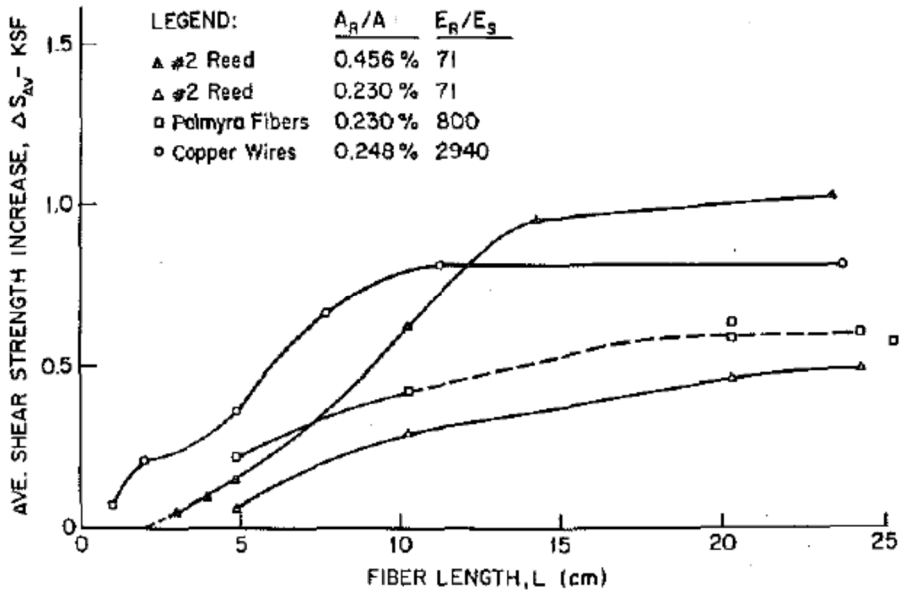

Figure 22 - Influence of the fibre length on the increase of shear strength (Gray, et al., 1983)

This reinforcing of sand could be used to increase the erosion resistance of sand. However, there is no research available about the erosion behaviour of fibre reinforced soil. In order to use this technique to slow down the breaching process, the effects of fibres on the erosion rate of sand were further investigated.

Reinforcement of sand by injection of grout

A proven method of soil improvement and reinforcement is grouting. Grouting is a technique in which a cement- or chemical-water mixture is injected into the soil to mix it with the soil. When this mixture sets, the soil properties have changed. Usually the soil hardens and becomes a concrete-like material with increased cohesion and strength. Grouting can be classified based on the materials used; there are cement suspensions and chemical solutions (Anagnostopoulos, et al., 2011).

When granular soils with large voids or rock with wide cracks has to be grouted, cement grouts are commonly used. They are successful in these type of soils because:

- Easy penetration into the pores
- Large propagation distance under low pressure
- Complete fill of the voids
- Properties do not change once hardened
- Low costs

They are only effective in soils with a permeability of 10^{-5} m/s or higher, otherwise there is no good penetration into the soil. For soils with a permeability below 10^{-5} m/s, chemical grouts can be used. There are a lot of different chemicals which can be used for grouting, which all affect the soil in their own manner, but these will not be elaborated on.

Both type of grouts create a material with different compressive strength and elastic modulus compared to the original soil (Anagnostopoulos, 2005), (Anagnostopoulos, et al., 2011). It also changes the permeability and thus the erodibility of the soil. In Figure 23 the permeability as function of the mixture ratio (in this case epoxy resin and water) is given. It can be seen that the permeability decreases as the mixture ratio (ER/W) increases.

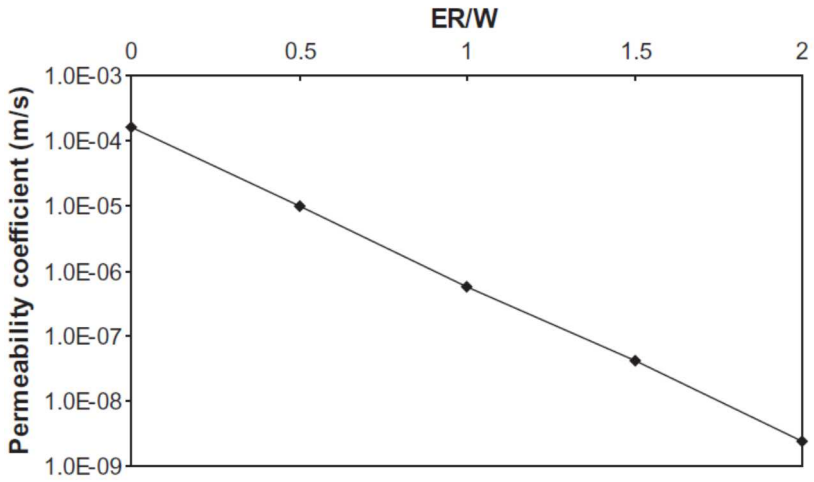

Figure 23 - Permeability as function of the mixture ratio (Anagnostopoulos, et al., 2011)

When the grout is injected, it can only penetrate a limited distance into the soil. Because of this, the effect on the permeability of the soil decreases with the distance from the grouting location (Anagnostopoulos, 2005). This also shows the effect of the grout concentration on the permeability of the soil. The diminishing effect on the permeability as function of the distance from the grouting location, for different grout mixtures can be seen in Figure 24. This again shows that grouting can be an effective measure to decrease the permeability of the soil.

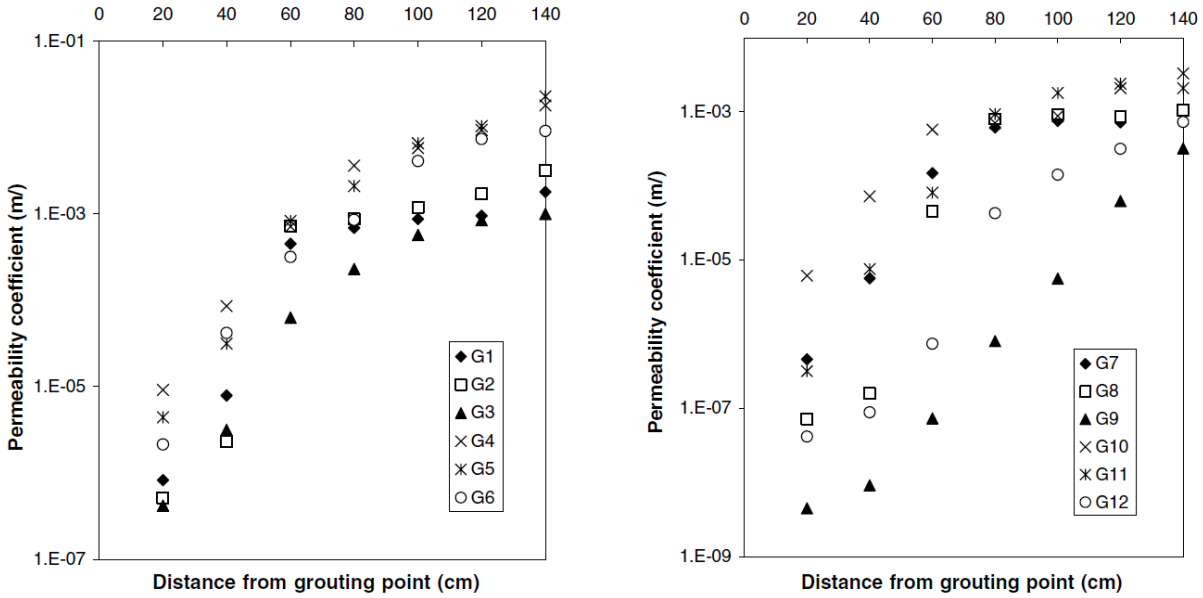

Figure 24 - Permeability at several distances from the grouting location for different grout mixtures (Anagnostopoulos, 2005)

It is, however, necessary to conduct more research into the effects of grouting on all soil properties to be able to assess its effectiveness as a possible option.

Biological reinforcement of sand

Grouting is one technique to harden the soil, but there is another method to achieve approximately the same effect, this is cementation of sand using biological processes (DeJong, et al., 2006). At various locations on earth naturally cemented sands exist. This process is the result of a chemical reaction in the soil, which can be induced and catalysed by an enzyme. The soil changes from sand to a sandstone type of rock. This process changes the properties of the soil, increasing its strength and decreasing its permeability. The effect of the cementation on the permeability is studied by (Ferris, et al., 1997) and can be seen in Figure 25. A reduction of the permeability compared to uncemented sand is visible, which reduces the erodibility of the soil. This is still a relatively new technique and further research into the effects on the soil properties and erodibility is necessary.

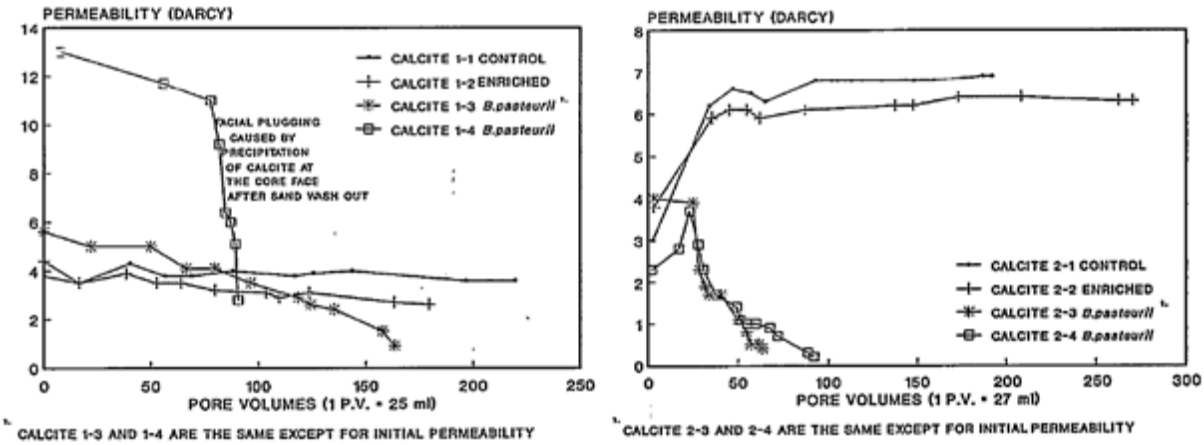

Figure 25 - Permeability of cemented sand (Ferris, et al., 1997)

Reinforce the sand using vegetation

Instead of adding fibres to sand, plant roots have the same reinforcing effect. A study (Verhagen, et al., 2008) shows the effect of roots of vetiver grass on the erodibility of non-cohesive soil. That study stated that the erosion of non-cohesive soil is reduced drastically due to the presence of the roots. In Figure 26 the results of the experiments can be seen. The red lines display the erosion of cohesive soil-vetiver combinations (Soil C with Vetiver), the blue line non-cohesive soil-vetiver combinations (Soil MX with Vetiver) and the green lines bare cohesive soil (Soil C, fallow). The figure shows that the total erosion of the non-cohesive soil with vetiver grass was less than the total erosion of the cohesive soil without vetiver grass. For cohesive soil with vetiver grass the erosion process even stopped.

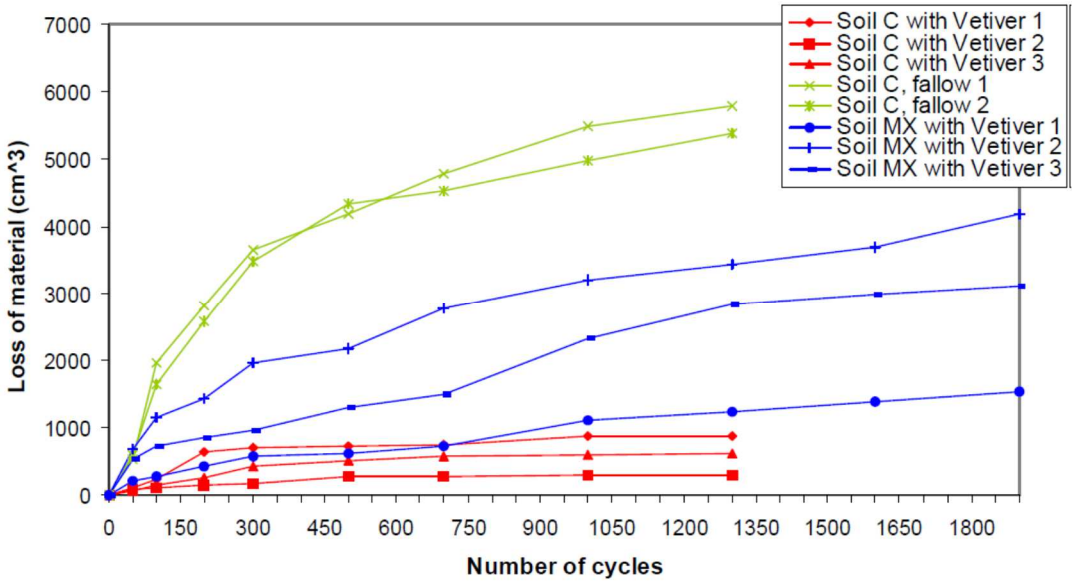

Figure 26 - Cumulative erosion of different soil-vetiver combinations (Verhagen, et al., 2008)

Another point of interest is the penetration depth of the roots into the soil. If, at least, a large volume of the dike needs to be reinforced, the roots should have a large penetration depth into the dike. It is found that the erosion reducing effect of a fibrous root system (grass roots) reduces as the sand content of the soil increases

(De Baets & Poesen, 2010), due to weaker soil-root bonds in sandy soil. This is an unfavourable effect for the reinforcement of sand dikes.

5.1.4 Adding components to the dike

Instead of changing the soil properties of sand, components can be added to the dike to slow down breach growth. Several possibilities are described in this section.

Compartmentation of the dike

When the breach has reached the base of the dike it mainly grows lateral. The inflow into the polder depends on the maximum breach width. A way to decrease this width is to build barriers into the dike, creating compartments. This option is already mentioned by (Visser, 1998). He proposed to create plugs in the cross-section of the dike, e.g. every 100 metres, to prevent further horizontal erosion. When the flow through the breach reaches such a plug or barrier, the breach growth in horizontal direction stops. When these plugs are constructed with regular intervals in the dike, the maximum breach width is pre-determined. If the breach width can be reduced, the inflow through the breach is less and thus the water rises less rapidly in the polder. These barriers can be constructed from different types of material:

- *Sheet piling*
  This is a secure method to limit the erosion, since sheet piling is not erodible. A disadvantage of this type of barrier are the costs, as sheet piling is relatively expensive.
- *Vertical clay layers or cores*
  This type of barrier will not stop erosion completely, but reduces the erosion considerably. The layers or cores will have to be of sufficient width to slow down the erosion for a longer period of time.
- *Geo-textile*
  This option has the same effect as sheet piling, but is cheaper than sheet piling. However, a way to anchor the geo-textile has to be thought of.

Construction of a highly erosion resistant core

Instead of decreasing the width of the breach, it is also possible to prevent vertical erosion of the dike by creating an erosion resistant core. This core should have a relatively high erosion resistance, because if the core fails the breaching processes will continue in the same way as if the core was never present. There exist dikes and dams which have a different core material than the rest of the dike, but little is known about the breaching process of such embankments. Such a core can, for example, be constructed out of:

- *Clay*
  Zhu already showed that the erosion rate of clay is much lower than of sand (Zhu, 2006), making clay a good material to construct such a core.
- *Sheet piling*
  A rather expensive option is putting sheet piles into the centre of the dike along its length.
- *Concrete*
  Another expensive option is constructing a concrete core.

Besides these materials there might be other materials or ways to construct a core. Further research into this is necessary. Something that has to be taken into account is the stability of such a core and the whole dike, if the inner slope is eroded away. It would be of no use to construct such a core if the dike collapses due to instability of the core.

5.1.5 Other options

Besides the above described possible options, there are other options to slow down the breaching process, which do not belong in the above categories. These options are described in this section.

Increase of the erosion resistance of sand without aggregates

It would be interesting if it is possible to increase the erosion resistance of sand by exploiting the properties of sand. Research has shown that seepage into the bed exerts pressure onto the sand grains, increasing their resistance to erosion (Jacobsen & Magda, 1988) and increases the stability of a slope (Van Rhee & Bezuijen, 1992). This stabilizing effect of seepage into a slope (inflow) can be seen in Figure 27.

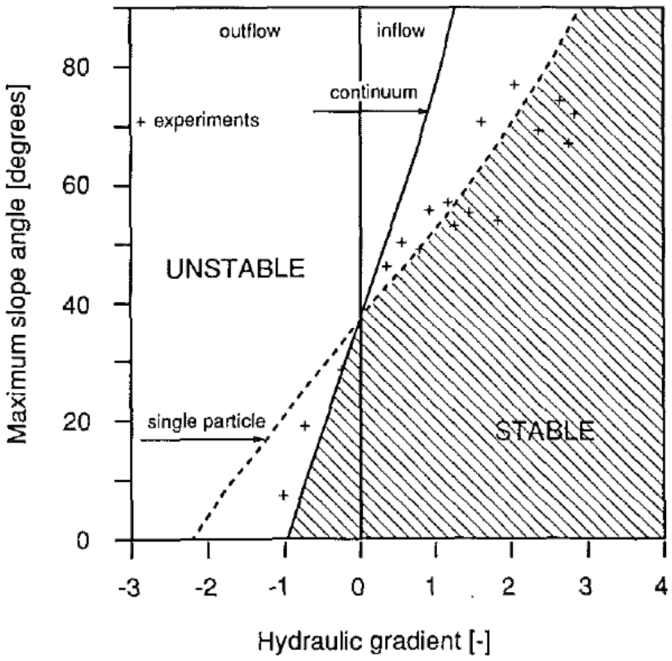

Figure 27 - Effect of inflow on the maximum slope angle (Van Rhee & Bezuijen, 1992)

This figure shows that without inflow the slope is only stable at or less than the internal friction angle (37° in this case) and can become increasingly steeper as the inflow increases. This inflow only occurs when the pressure in the bed is lower than the outside pressure. If water flows into the bed it will probably stop after a while as the pressure inside the bed equals the outside pressure. If it is possible to continuously create an under pressure in the bed, then there would be a continuous inflow. To be able to use this phenomenon to decrease the erosion rate during the breaching process, some kind of drainage system should be present in the dike body. In order to assess the feasibility of this option more research is needed. It is also necessary to find out if this phenomenon increases the erosion resistance enough to really slow down the erosion process.

Another way to increase the pressure on the sand grains is to decrease the permeability of the sand (Bisschop, et al., 2010), which might be achieved by changing the composition of the sand in such a way the voids between the grains become smaller. A possible way is adding bentonite to sand, which has already been explained in section 5.1.2.

Reduction of flow into the breach by a sill

Instead of altering the soil properties or shape of a dike, another option is to reduce the flow through the breach. A reduced flow has a reduced erosion capacity and less water enters the polder, thus slowing down the inundation of the polder. The flow into the breach can be reduced by reducing the area of inflow. This can be achieved by constructing some kind of an erosion resistant barrier or sill (e.g. a toe structure) in front of the dike (Van Gerven, 2004). This reduces the depth of the breach bottom relative to the water level. The dike behind this barrier of sill can still be eroded away, but not the complete breach depth is available for the water to flow through. This reduces the final breach width and inundation velocity, which can be seen in Figure 28 and Figure 29. These figures show the reduction in width and inundation velocity with increasing heights of the sill.

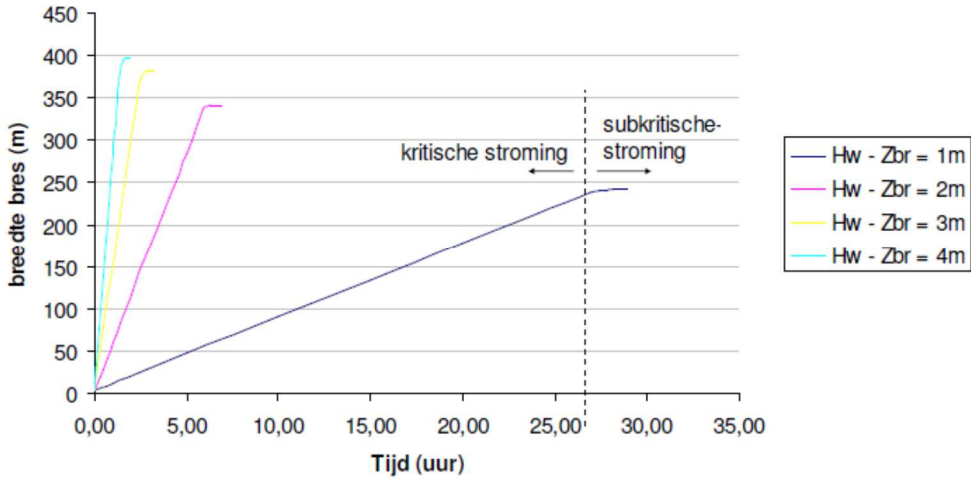

Figure 28 - Development of breach width in time, for different sill heights (Van Gerven, 2004)

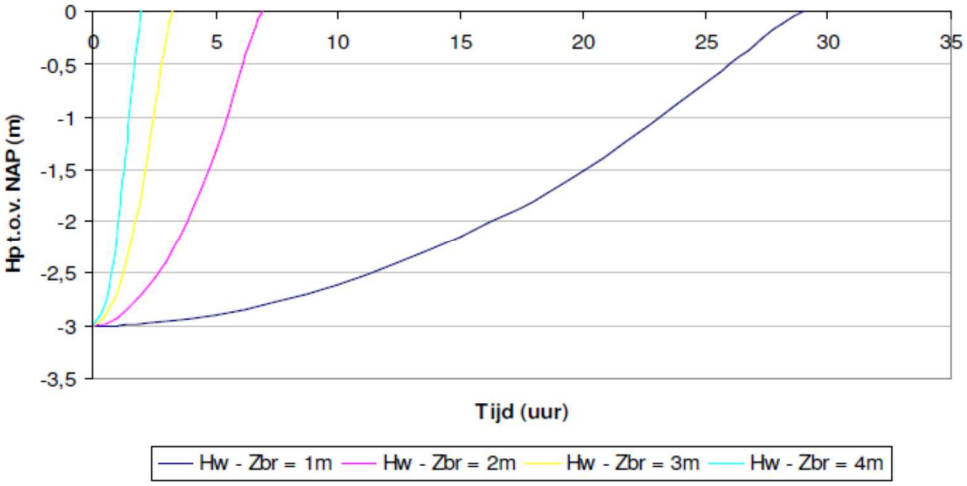

Figure 29 - Rise of polder water level in time, for different sill heights (Van Gerven, 2004)

5.1.6 Discussion

In this section the described options are discussed. All the options are judged based on their possible effectiveness. Of some it is quite certain they are effective and some might be effective, but need more research to be more certain. There are also some options which are already deemed not effective, too expensive or too invasive according to the available research. The possible options described in this section are not all usable for existing dikes. For each option it is argued whether it is usable in an existing dike. For new dikes all options are usable, implemented during or after construction of a dike.

Reduce angle of the inner slope

By reducing the steepness of the inner slope, several ways of slowing down the breaching process are introduced. The flow velocity on the inner slope is lower, reducing the erosion of the top layer and sand core and there is more material to erode, so the breaching process takes longer. This is an effective option, but will take up more and more space in the polder as the steepness of the inner slope decreases. This is because the width of the base of the dike increases, as the inner slope becomes less steep. It is possible to use this option for existing dikes, although this might be difficult due to space limitations.

Increase crest width

When a dike is wider, e.g. by increasing the crest width, more material has to be eroded before a full breach is developed, thus slowing down the breaching process. The exact effect of this option depends on the extra width of the dike. However, this extra width also takes up more space of the polder. For existing dikes it is not always possible to increase the crest width, because the space might be limited.

Bentonite clay and sand mixture

The experiments which were executed to determine the erosion of a bentonite-sand mixture shows promising results. A significant reduction of the erosion rate can be achieved. To be able to truly determine the effectiveness of the option, more research into the effect on the erosion rate (low and high flow velocity) and soil parameters is necessary. To implement this option, sand and bentonite clay will have to be mixed, which is no problem when building a new dike. It might be possible, with an appropriate execution technique, to execute this in existing dikes.

Fibres and sand mixture

Research into this option shows an increase of the shear strength of soil. There is however no knowledge about the effect on the erosion rate of fibre reinforced soil. Until this effect is analysed, it is difficult to judge the effectiveness of this option. For implementation of this option the same arguments as for the bentonite clay and sand mixture hold.

Reinforcement of sand by injection of grout

Grout injection is used frequently to reinforce soil, e.g. for foundation purposes or reduction of water seepage. This indicates that grouting could be an effective option. More research is necessary in order to assess the erosion rate of grout reinforced soil and the stability of such a dike. Since this is an in-situ technique it can be used in existing dikes.

Biological reinforcement of sand

Research of this method is in an early state, but shows promising results. It induces a similar effect in sand as grouting does. The research necessary for that option also has to be executed for this option. Besides that, research into the exact effects on the soil parameters is necessary. It also needs to be tested if the bacteria are effective when applied in a real sand dike. The bacteria can only be used when the dike is already in place, so it is suitable for existing dikes and new dikes after construction.

Reinforce the sand using vegetation

Vegetation is used to reinforce coastlines, dunes, dikes etc., which makes it a proven method of soil reinforcement. However, this reinforcement only applies to the upper layers (e.g. first meter) of the soil and is thus unsuitable for reinforcement of the core of a dike. Since the vegetation has to be planted on top of the dike, it can be used in existing dikes.

Compartmentation of the dike

This is an option which is effective because of the characteristics of the breaching process. However, this option will probably be too invasive on dikes, due to the presumable necessary small size of the compartments (e.g. every 100 metres), almost requiring a dike to be rebuild. This makes this option only practical for new dikes.

Construction of a highly erosion resistant core

It is possible to construct a core which will likely stop the breaching process once the inner part of the dike has been eroded away. For this option a suitable core material has to be determined and research into the stability of the core and dike during the breaching process is necessary. A core can be constructed more easily when constructing a new dike, but some of the materials are also suitable for use in an existing dike.

Increase of the erosion resistance of sand without aggregates

This option seems interesting, but needs further research to determine the effectiveness and feasibility. Since it is not known how to implement this option into a dike, it could be used for new or existing dikes, depending on the available technique.

Reduction of flow velocities in the breach by a sill

The effectiveness of this option was determined with a computer model. More research into the influence on the flow through the breach and the design of such a sill can be executed. This option, however, takes up a lot of space on the outer slope of the dike. The structure necessary for this option can be constructed in front of an existing dike.

The judgement for each option is given in Table 4 and further actions are determined.

Option	*Judgement*	*Further action*
Reduce angle of the inner slope	*Promising, but too space consuming*	*None*
Increase crest width	*Promising, but too space consuming*	*None*
Bentonite clay and sand mixture	Promising, most likely for new dikes	More research
Fibres and sand mixture	Could work, most likely for new dikes	More research
Reinforcement of sand by injection of grout	Could work, but invasive and expensive	More research
Biological reinforcement of sand	Could work, research in early stage	More research
Reinforce the sand using vegetation	*Probably will not work*	*None*
Compartmentation of the dike	*Could work, but to invasive*	*None*
Construction of a highly erosion resistant core	Could work, but invasive and expensive	More research
Increase of the erosion resistance of sand without aggregates	Interesting, but difficult	More research
Reduction of flow velocities in the breach by a sill	*Will work, but too space consuming*	*None*

Table 4 - Judgement of options

5.2 Further research

The analysis in section 5.1 identified a few interesting options, which are subjected to more research. This research increases the knowledge about these options, which is used for selection of three feasible options. This section is a summary of this research, the complete study can be found in appendix A.

Bentonite clay and sand mixture

Experimental results of this option do show that it is an effective option. The reduction of the erosion rate of sand is significant. However, the experiments were only scale model tests and were not executed at high flow velocities. In literature several formulas for calculating the erosion rate are available. However, these formulas have to be compared to each other as well as to experimental results to determine which one yields the best results. A possible execution method for this option is found, in-situ mixing, which should make practical implementation in existing dikes possible.

Fibre and sand mixture

This option is usually used to reinforce soil in case of instable slopes or to increase its resistance against deformations. It increases the shear strength of sand. In literature there are some accounts of reduction of piping due to fibres and increase of cohesion, which show that fibres can also have an erosion reducing effect. No research was executed into this phenomena and thus there are no formulas available for the erosion rate. However, a sand-fibre mixture can be compared to a root system. There is some research available on the erosion rate of soil-root systems. This was used to get an indication of the effect on the erosion rate of this option. Further study is necessary regarding this effect and assumed resemblance. The fibres will have to be mixed into the sand for them to have effect. There are techniques which can execute this in-situ. This option could work, but more research is needed to fully understand the effects. However, since there is an indication that a little amount of fibres (<1% fibre content) is needed to reduce erosion, it is an interesting option.

Reinforcement of sand by grout injection

Grout injection, more specifically permeation grouting, is a well-known technique, which is used often in practice. This technique reduces the permeability and porosity of the sand, which is favourable for reduction of the erosion rates. Grouting also increases the shear strength. There are, however, no known formulas for predicting the erosion rate of grouted sand. A formula will have to be deduced based on the soil properties of grouted sand. Since this is a well-known technique, practical implementation should not be too difficult. However, grouted sand is a kind of concrete, it has a high strength. This poses a problem for the use of grout in dikes. Since dikes are built on soil that tends to settle, the dike has to follow those settlements. Due to the strength of grouted sand, the dike can no longer follow the settlements and cracks can appear in the reinforced dike. The cracks can grow and water can flow through them, decreasing the strength and stability of the dike. This makes grouting an unfavourable option for retarding the breaching process.

Biological reinforcement of sand

This is the most innovative option. It could be seen as a form of the concept 'building with nature'. The effects on sand are somewhat similar to grouting. The expected strength increase of sand probably will be less than it would be with grouting. Based on what is known about the soil parameters and by making some assumptions, it is possible to come up with an erosion formula. This is a crude estimate, so experiments are necessary to come to a more exact formula and prediction of the erosion rate. For the execution of this option, there are two techniques available, which probably need to be combined to get the desired effect. These techniques have never been used in-situ or on such a scale, so it is hard to say whether they will work as desired in a sand dike. Despite the uncertainties, it is an interesting and ecological option.

Increase of erosion resistance of sand without aggregates

This is the most fundamental option with regard to the relevant processes. In principle this option does work, as experiments show. However, these experiments were on a small scale, which makes it easy to adjust the hydraulic gradient. There is no experience with changing the hydraulic gradient on a large scale, making it difficult to estimate the effect of this option on a sand dike. The system to be thought necessary to achieve this, is probably complex and sensitive to failure, especially compared to the other options. This is due to the fact this system has to be operated during a flood event, while the other options are already in place and functional. It will contain moving parts, which will also need maintenance. Besides the difficulties at system level, the principle itself is complicated as well. By introducing a hydraulic gradient into the bed it is also possible to increase the erosion, depending on several parameters. Regulating the hydraulic gradient in such a way it reduces erosion is complicated. Because of these problems, it is difficult to determine the effect and it is doubtful if the necessary systems are reliable enough.

Construction of a highly erosion resistant core

This option is a design option, not focussed on changing the erodibility of sand, but on stopping the breaching process while developing. As long as a good design is made, this option will work, but it is difficult to implement such a design into an existing dike.

5.3 Selection

After the more elaborate research into the options, the options which are implemented into the model for testing are selected. Based on the summary of the research, each option is scored on several aspects, given in Table 5. Each aspect is assigned a multiplication factor to differentiate between the importance of the aspects. The final score of each option is a weighted average of the sub scores.

	Execution	*Experience*	*Effect*	*Knowledge*	*Maintenance*	*Long term effects*	*Final score*
Multiplication factor	4.5	2.0	5.5	1.0	3.5	4.5	
Bentonite clay and sand mixture	4	3	4	3	5	4	**4.0**
Fibres and sand mixture	4	3	4	4	5	4	**4.1**
Reinforcement of sand by grout injection	4	4	3	4	3	1	**2.9**
Biological reinforcement of sand	3	2	3	2	4	4	**3.2**
Increase of erosion resistance of sand without aggregates	1	1	2	2	1	3	**1.7**
Construction of a highly erosion resistant core	2	2	4	3	3	3	**2.9**

Table 5 - Scoring of options (minimum-maximum score: 1-5)

Based on this table and the arguments given in the research summary three options are selected for comparison:

- Bentonite clay and sand mixture
- Fibres and sand mixture
- Biological reinforcement of sand

These most promising options are compared to each other, for which the BRES-model is used. For this, first the options were made fit for modelling, after which the model is adjusted and the options were compared. This is described in chapter 6.

6 Comparison of options

In this chapter the three most promising options are compared to each other. This is achieved by implementing the erosion formulas of the different solutions into the BRES-model, using the norm dike. In the next sections the erosion formulas are given. The model results of the options can be found in these sections as well.

The model results give the flow through the breach and breach width as function of time, as well as the maximum flow, final breach width and duration. For all the options these results are given in figures in appendix C. In these figures the measurements of the ZWIN'94 experiment are also plotted for comparison (the black circle in the figures). The horizontal line in the flow rate plot gives the maximum flow rate. In the last section of this chapter these results are compared to each other. Based on this comparison the results are discussed and the best option is determined.

6.1 Sand and bentonite dike

The erosion formula for a sand-bentonite mixture is determined in appendix B, which is given by formulas (6.1) and (6.2). This formula is the Van Rijn formula with an adapted critical shear stress and an inclusion for the bentonite percentage.

$$V_e = \frac{0.00033}{10B_{\%}} \cdot (\Delta g D_{50})^{0.5} \cdot D_*^{0.3} \cdot \left(\frac{\tau - \tau_c}{\tau_c} \right)^{1.5} \cdot \frac{1}{1-n_0} \tag{6.1}$$

$$\tau_c = \left(1 + \frac{a \exp(b\rho_b)}{D_{50}^{\,2}} + \frac{c_5}{\frac{1}{6}\pi g(\rho_s - \rho_w)} \right) 0.414 D_{50} \tag{6.2}$$

in which:

V_e	= erosion velocity [m/s]
$B_{\%}$	= bentonite volume percentage [%]
Δ	= relative density [-]
D_{50}	= median particle diameter [m]
D_*	= dimensionless particle diameter [-]
τ	= shear stress [N/m^2]
τ_c	= critical shear stress [N/m^2]
n_0	= in-situ porosity [-]
ρ_b	= bulk density of sediment [kg/m^3]
ρ_s	= density of solids [kg/m^3]
ρ_w	= density of water [kg/m^3]
n, a, b, c_5	= parameters determined using appendix B, Table 25

Model results

The erosion formula for a sand-bentonite mixture is implemented in the BRES-model. The model was run for 2% and 4% added bentonite of which the results can be seen in appendix C.

Remarks

The erosion formula for sand-bentonite mixtures is based on measurements of the erosion rate of these mixtures. The used erosion formula is based on these measurements, but there is no data of the erosion rate at high flow velocities. The formula is therefore an estimation of the erosion rate and more research is needed to increase the accuracy of the formula. The model results are therefore no accurate representation but an indication of the physical process.

6.2 Sand and fibres dike

The erosion rate of sand mixed with fibres is determined by applying a reduction factor on the erosion velocity of sand. This reduction factor is determined in appendix B, based on the erosion of soil-root systems. The formula used to calculate the erosion velocity of a sand and fibre mixture is given by:

$$V_{e\_sand-fibres} = V_{e\_sand} \cdot RSD \tag{6.3}$$

$$RSD = \exp(-1.14RD) \tag{6.4}$$

$$RD = \frac{f_{\%} \cdot \rho_f \cdot V_{soil}}{V_{soil}} \tag{6.5}$$

in which:

$V_{e\_sand-fibres}$ = erosion velocity of sand-fibre mixture [m/s]
V_{e_sand} = erosion velocity of sand [m/s]
RSD = relative soil detachment rate [-]
RD = fibre density in the sand [kg/m^3]
$f_{\%}$ = mass percentage of fibres [-]
ρ_f = fibre density [kg/m^3]
V_{soil} = soil volume [m^3]

To reduce the erosion rate with a factor 10, 0.22% polypropylene (PP) fibre should be sufficient, thus this fibre type and percentage is used in the BRES-model.

Model results

The erosion reduction factor is implemented in the BRES-model. The breaching process of a sand dike mixed with fibres was simulated. To achieve this, the reduction factor was applied to the erosion rates calculated with the Van Rhee-Bisschop formula. The result of the simulation are given in appendix C.

Remarks

The erosion reduction factor formula is based on empirical research and the similarity between randomly distributed fibres and a fibrous grass root system. Since these researches were not executed for synthetic, in this case polypropylene, fibres, it is uncertain whether this reduction factor is correct. To be able to determine a better formula, laboratory test should be executed. Using what can be found in the available literature, this is one of the better formulas and thus is used to model the breaching process of a sand dike mixed with fibres. It is possible that this formula

gives significantly higher or lower outcomes than measurements, but only laboratory tests can determine this.

6.3 Biologically improved dike

The erosion formula for biologically cemented sand is determined in appendix B, and given by formulas (6.6) and (6.7). This formula takes the effect of the biological cementation on the shear strength and critical shear stress into account.

$$V_e = \frac{c_v}{10 D_{50} \omega} \cdot \frac{\tau_c}{\tau_s - \tau_c} \cdot \frac{\tau - \tau_c}{\tau_c} \cdot \frac{1}{\rho_d} \tag{6.6}$$

$$\tau_c = \beta \tau_s \tag{6.7}$$

in which:

V_e = erosion velocity [m/s]
c_v = consolidation coefficient [m/s]
D_{50} = median particle diameter [m]
ω = water content [-]
τ_s = soil shear strength [N/m^2]
β = constant [-] (=2.60·10^{-4})
τ_c = critical shear stress [N/m^2]
ρ_d = dry bulk density cemented sand [kg/m^3]

Model results

The erosion formula for biologically improved sand is implemented in the BRES-model, the model results can be found in appendix C.

Remarks

The erosion formula used to model the breaching process of a biologically improved dike gives an approximation of the erosion rates. The formula is derived using the material parameters and deterministic relations. Since no data on the erosion rate of this material is available, this is the only way to approximate it. To check if this formula is correct, the erosion rate should be measured. The chosen erosion formula is, in this situation, a conservative one, since this formula gives the highest erosion velocity of the tested formulas (see appendix B). Other formulas give lower erosion velocities and therefore lead to better retarding of the breaching process. The model results are therefore no accurate presentation but a crude approximation of the real process.

6.4 Comparison

The most promising options are modelled and compared to the result of the norm dike. In Figure 30 and Table 6 the results of the different options (2% & 4% Bentonite, Cemented sand and 0.22% PP-fibre) and the norm dike (Sand) are presented. Figure 30 gives the breach width and flow rate as function of time. Table 6 gives the duration, final breach width and maximum flow rate of the different options and norm dike. Besides the values for these parameters, the factor between the options and norm dike is calculated, to give an impression of the differences between the options.

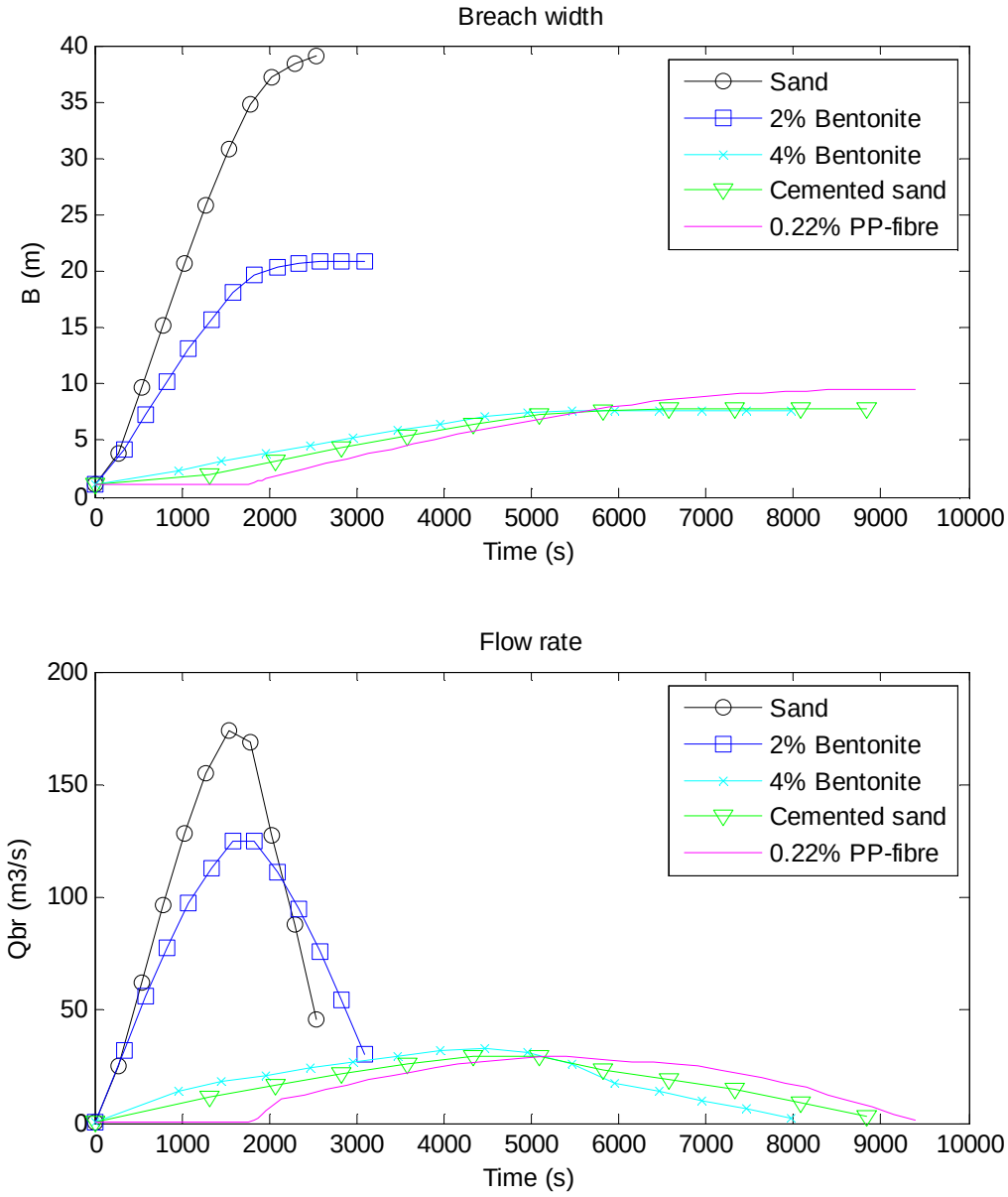

Figure 30 - Breach width (B) and flow rate (Q_{br}) as function of time for the original norm dike and adapted with the given options

	Duration [s]	*Breach width [m]*	*Maximum flow [m³/s]*
Sand (norm dike)	2700	39.2	176
2% Bentonite	3300 *(1.2x)*	20.9 *(0.5x)*	126 *(0.7x)*
4% Bentonite	8200 *(3.0x)*	7.7 *(0.2x)*	33 *(0.2x)*
Cemented sand	9200 *(3.4x)*	7.5 *(0.2x)*	30 *(0.2x)*
0.22% PP-fibre	9400 *(3.5x)*	9.6 *(0.3x)*	30 *(0.2x)*

Table 6 - Model results of original (sand) and adapted norm dike, including factor between adaptation and original dike values

As Figure 30 and Table 6 show, all options increase the duration of the breaching process (thus slowing it down) and decrease the final breach width and flow through the breach. With the current erosion formulas for the options, adding 4% bentonite to sand, biologically cementing sand and adding 0.22% polypropylene fibre to sand give similar results. They all slow down the breaching process significantly and also decrease the final breach width and flow through the breach significantly. It should be noted that the erosion formula for cemented sand is the most uncertain formula of the options. Besides this uncertainty, the strength increase of the dike is not taken into account in this comparison. Due to this it is possible that cemented sand gives significant better or worse results than it does with the current erosion formula. The erosion reduction due to the polypropylene fibres is also uncertain, as explained in section 6.2. Due to these uncertainties, the bentonite option is preferred. To be able to determine whether this comparison is correct, experiments were conducted (see chapter 7).

7 Experiments

In chapter 6 options to retard the breaching process are compared to each other using the BRES-model. Experiments were executed to test the outcome of this comparison. Not all modelled options could be tested using the available materials and facilities. It was feasible to test sand, sand-bentonite mixtures and sand-fibres mixtures (at higher percentages). The goal and type of the experiments are described in this chapter.

Goal of experiments

The experiments have a main and a sub goal:

- The main goal is to determine if there is a difference in erosion velocities between sand and different sand-bentonite and sand-fibre mixtures.
- The sub goal of the experiments is to determine if the additives influence relevant soil parameters, like shear strength and permeability.

Type of experiments

To achieve these goals, several tests were conducted:

- Direct shear tests
- Permeability tests
- Erosion tests

The erosion tests serve the main goal of the experiments. These tests are performed in a small flow flume in the Fluid Mechanics Laboratory of the TU Delft. By determining the erosion velocity of each mixture and comparing the results, the difference between the mixtures is determined. In this flume a bed of sand or mixture was prepared. After compaction and saturation of the bed, the tests were executed at a fixed flow rate. This flow rate, together with the geometry of the flume, is used to determine the flow velocity. The tests were recorded with a video camera. The video of each test was used to determine the water and bed levels as a function of time. These were used to calculate flow velocity and erosion velocity. The procedure and test setup are further explained in section 7.4.

The direct shear and permeability tests serve the sub goal of the experiment. The results of the direct shear tests are used to determine the angle of internal friction and the (apparent) cohesion of the mixtures. These tests were executed in the Laboratory of Geotechnology of the TU Delft. This experiment is further explained in section 7.2.

The hydraulic conductivity of the mixtures is determined with permeability tests. The permeability test is executed as a falling head test. In case of a falling head test, the subsidence rate of the water level on top of the mixture sample is measured. This rate is a measure for the permeability. The falling head tests were executed using a custom setup, build by the staff of the Fluid Mechanics Laboratory of the TU Delft. The setup and test procedure can be found in section 7.3.

7.1 Mixtures

The tests were executed for different mixtures: clean sand, sand with bentonite and sand with fibres. The mixture ratios and type of sand, bentonite and fibres are described in this chapter. The specifications of the used bentonite and fibres can be found in appendix G.

Sand

The sand used for the tests and for mixing is a pure quartz sand. The gradation curve is given in Figure 31 and the different fraction sizes are given in Table 7. In this table also the coefficient of uniformity (C_u) and coefficient of curvature (C_c) are given.

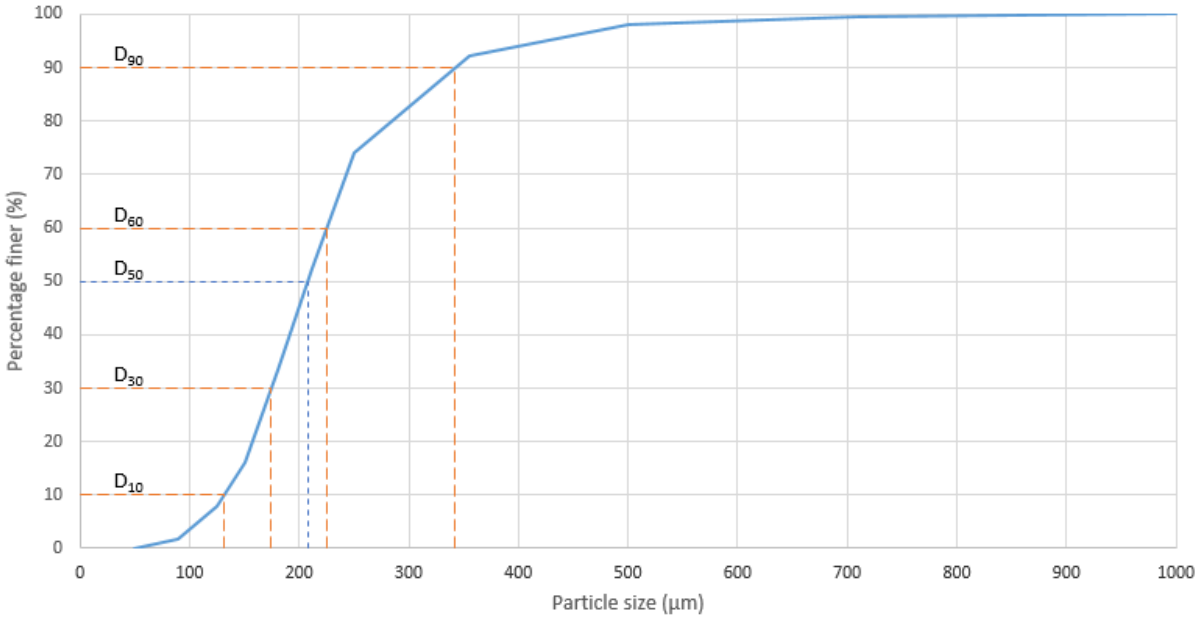

Figure 31 - Gradation curve of the sand used for the experiments

Fraction	*Size [µm]*	*Coefficients*
D_{10}	132	C_u = 1.7
D_{15}	147	C_c = 1.0
D_{30}	174	
D_{50}	**208**	
D_{60}	225	
D_{85}	313	
D_{90}	342	

Table 7 - Fraction sizes and uniformity (C_u) and curvature (C_c) coefficient

These coefficients are calculated using:

$$C_u = \frac{D_{60}}{D_{10}} \tag{7.1}$$

$$C_c = \frac{D_{30}{}^2}{D_{10} \cdot D_{60}} \tag{7.2}$$

These coefficients are criteria for classifying the sand gradation. If $C_u \geq 6$ and $1 < C_c < 3$ the sand is well graded, otherwise it is poorly graded. When these criteria are applied to the used sand, this sand is classified as poorly graded sand (SP) (Holtz & Kovacs, 1981).

Sand-bentonite mixture

The sand-bentonite mixtures were prepared by mixing sand and bentonite using a concrete mixer. The materials were dry mixed in batches of approximately 25 kg (weight of one bag of sand and additive). For mixing Cebogel Sealfix bentonite (Cebo Holland B.V., 2014) was used (appendix G). This bentonite is already used in practice to create sand-bentonite seals. It is a powder of activated sodium bentonite, which has a high swell capacity (approximately 840%).

Two mixtures were tested in the experiments, a 2% and a 4% mixture. These percentages are the dry volume percentages, calculated with an estimated porosity of the powder of 0.63, giving a dry bulk density of 951 kg/m^3. The volume and weight percentages and the mixture ratio for each mixture:

- 2% mixture
    - Dry volume percentage: 2%
    - Dry weight percentage: 1.2%
    - Mixture ratio: 12 g/kg
- 4% mixture
    - Dry volume percentage: 4%
    - Dry weight percentage: 2.4%
    - Mixture ratio: 24 g/kg

Sand-fibre mixture

The sand-fibre mixtures were prepared using the same mixing method as the sand-bentonite mixtures. The type of fibres used are polypropylene (PP) fibres (S200) (Finish Beton Groep, 2014), which are randomly orientated in the sand. These fibres are strips of material with a length of 45 mm, a width of 1.4 mm and a thickness of 180-200 µm (appendix G). Again, two different mixtures were prepared, the dry volume percentage was determined using the density of polypropylene, 920 kg/m^3:

- 0.44% mixture
    - Dry volume percentage: 0.44%
    - Dry weight percentage: 0.25%
    - Mixture ratio: 2.55 g/kg
- 0.88% mixture
    - Dry volume percentage: 0.88%
    - Dry weight percentage: 0.50%
    - Mixture ratio: 5.10 g/kg

These dry volume percentages are higher than determined in the theoretical derivation. This is because initial tests indicated that a fibre content of 0.44% has little effect. It was therefore assumed that a fibre content of 0.22% would have almost no effect. To see if a significant effect could be achieved with fibres, a mixture with a fibre content of 0.88% was included for testing.

7.2 Direct shear experiment

A direct shear test determines the shear stress at different normal stresses. These measurements can be used to calculate the friction angle and (apparent) cohesion. In this section the test setup, conditions and results are explained.

Setup and conditions

The test setup for direct shear tests is shown in Figure 32. The sample box contains two square rings on top of each other, which contain the sample. In these rings the sample was compacted to a desired density. The sample is placed between two drainage plates to allow saturation of the sample and outflow of water during tests. The sample box was filled with water to allow the samples to saturate. On top of the sample different weights can be placed to increase the normal stress.

During the test the bottom ring moves, while the top one stays in place. The sample box, in which the bottom ring is clamped, is pushed by the engine at a rate of 0.5 mm/min. The horizontal and vertical displacement and horizontal (or shear) force are registered during the test. These measurements and the parameters given in Table 8 are used to calculate the shear and normal stresses. The parameters in Table 8 and appendix D give the dry bulk density and porosity of the sand without additives. These are calculated using just the weight of the sand, which is calculated by subtracting the weight of the additive from the total sample weight.

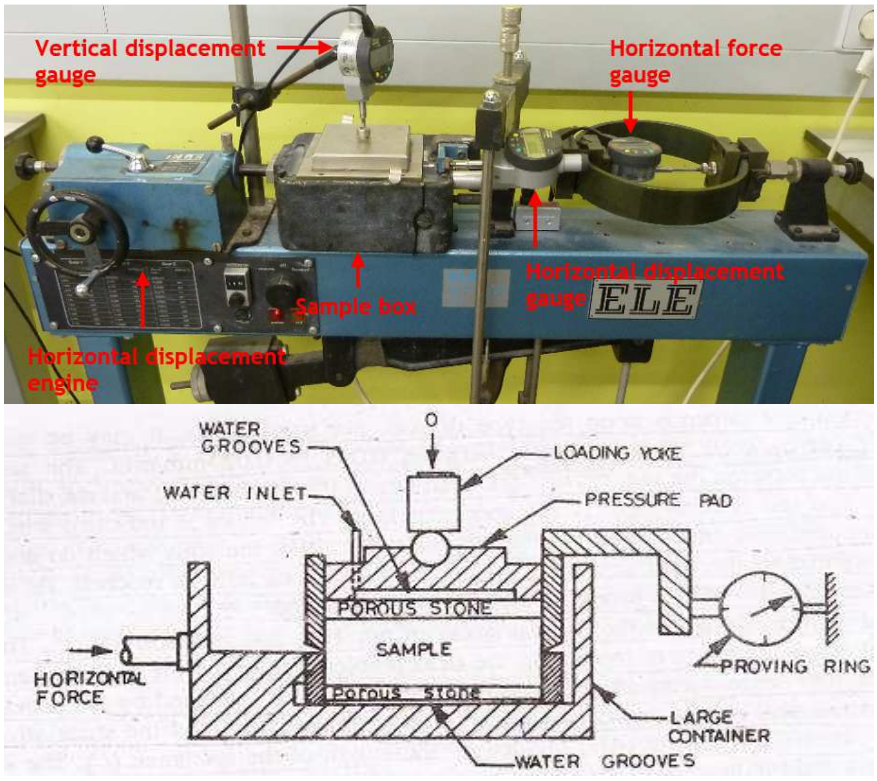

Figure 32 - Test setup direct shear tests (including sketch of sample box (The Constructor, 2012))

Each mixture was tested at three different normal stresses. The results of these tests can be found in appendix D. A summary and comparison of these test results is given in the next section.

Parameter	*Value*
Width sample box [mm]	100
Height sample box [mm]	31
Shear strain rate [mm/min]	0.5
Normal weight 1 [kg]	1.675
Normal weight 2 [kg]	16.175
Normal weight 3 [kg]	30.175
Area samples [mm²]	10000
Height samples [mm]	27
Volume samples [m³]	2.7E-04
Weight samples [kg]	0.400
Dry bulk density sand [kg/m³]	1446-1481
Porosity sand [-]	0.44-0.45

Table 8 - Test conditions direct shear tests

Results

In Figure 33 the maximum shear stresses are plotted against the normal stresses for all tests of the mixtures. These were determined using the measurements and calculation method described in appendix D. Through these points a trendline is plotted for each mixture. Using these trendlines the friction angle and (apparent) cohesion are determined, which are given in Table 9.

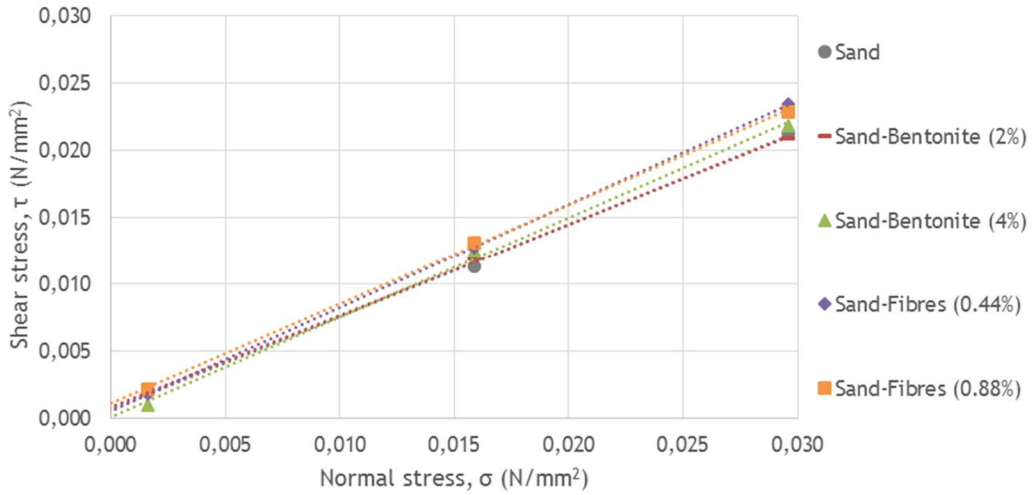

Figure 33 - Results direct shear tests (τ-σ graph)

	φ [°]	*c [kPa]*
Sand	34.6	0.70
Sand-bentonite (2%)	34.3	0.80
Sand-bentonite (4%)	36.7	0.03
Sand-fibres (0.44%)	37.8	0.05
Sand-fibres (0.88%)	36.5	1.10

Table 9 – Friction angle (φ) and (apparent) cohesion (c) of the mixtures

The results show the differences and similarities between the mixtures. As can be seen, adding bentonite to sand does not increase or decrease the friction angle, nor does it increase the cohesion. The sand-fibre mixtures show a very slight increase in maximum shear stress at equal normal stresses compared to sand. This difference increases as the normal stress increases. This results in a steeper angle of friction, but no significant increase in cohesion. For all the mixtures the cohesion is insignificant and negligible.

The increasing difference between the maximum shear stresses of sand-fibre mixtures and the other mixtures can be explained. As the normal stress increases, the fibres and sand are confined with more pressure, increasing the friction between the two materials. This increased friction makes it possible for the fibres to keep the sand grains together under higher forces than only sand grains. This means it requires more force to get a sand-fibre mixture to fail and thus the maximum shear stress is higher. Since this is only noticeable at higher normal stresses, it implicates that there is a threshold for this effect.

There is no clay-like behaviour noticeable (i.e. no significant cohesion) for any mixture, only an increase of the friction angle. Therefore the general conclusion of these tests is that all mixtures behave like sand and can thus be modelled like sand.

7.3 Permeability experiment

A permeability experiment determines the permeability of each mixture using a falling head test. The setup, conditions and results of this experiment are explained in this section.

Setup and conditions

The test setup consist of a hollow rectangular column with a fine mesh as a bottom, a container to place the column on and a bobber to measure the water level. On the bottom of the column a mixture sample is prepared with a desired density. After this, the water level in the container is raised until it overflows and the sample is given time to get saturated (at least a night). To start the test, the column is filled with water until it overflows. After the column is filled, the measurement of the water level in the column over time, is started. Since the container overflows, the ‘outside’ water level remains constant. A picture and sketch of the setup are given in Figure 34. In Table 10 the test parameters and sample conditions are given. These, together with the water level measurements (in appendix E), are used to calculate the hydraulic conductivity coefficients. The results are given in the next section.

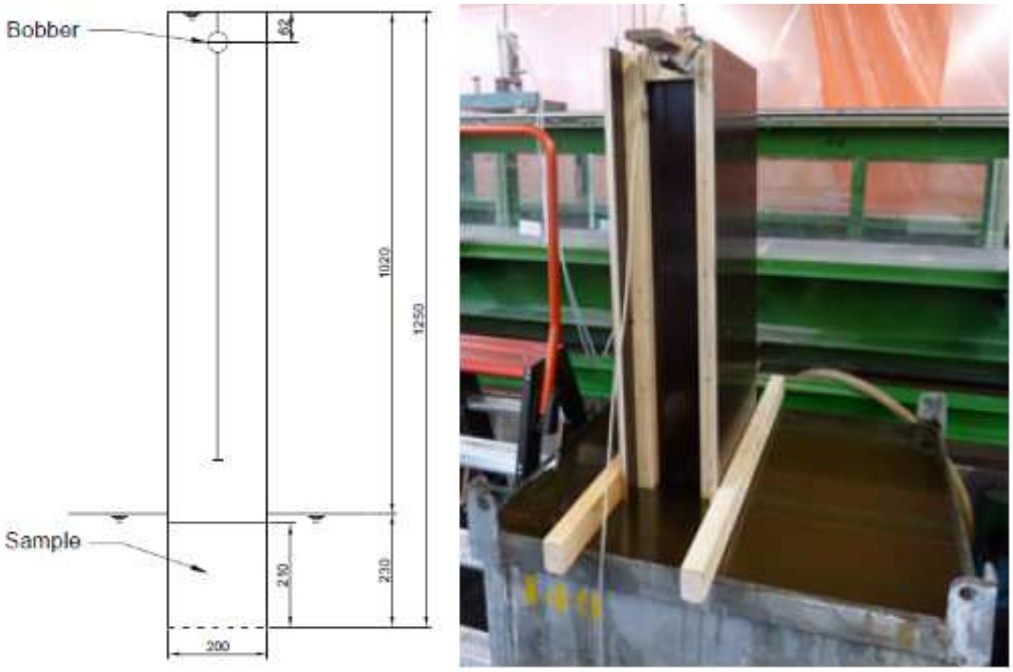

Figure 34 - Test setup permeability tests (measurements in mm)

Parameter	*Value*
Width column [m]	0.201/0.202
Height column [m]	1.25
Initial ΔH [m]	1.02
Distance bobber from top [m]	0.062
Area samples, a, A [m^2]	0.040602
Height samples, L [m]	0.21
Volume samples [m^3]	8.53E-03
Weight samples [kg]	12.9
Dry bulk density sand [kg/m^3]	1477-1512
Porosity sand [-]	0.43-0.44

Table 10 - Test conditions permeability tests

Results

The measurements from the falling head tests are used to calculate the hydraulic conductivity coefficients of the mixtures. This calculation is explained in appendix E. The calculated coefficients are presented in Table 11 and Figure 35, as well as the reduction factor between the mixtures and the sand.

	K [m/s]	*K/K_{sand} [-]*
Sand	1.91E-04	1.00
Sand-fibres (0.44%)	1.22E-04	0.64
Sand-fibres (0.88%)	1.63E-04	0.85
Sand-bentonite (2%)	7.07E-05	0.37
Sand-bentonite (4%)	3.08E-05	0.16

Table 11 - Permeability coefficients and fraction of K_{sand}

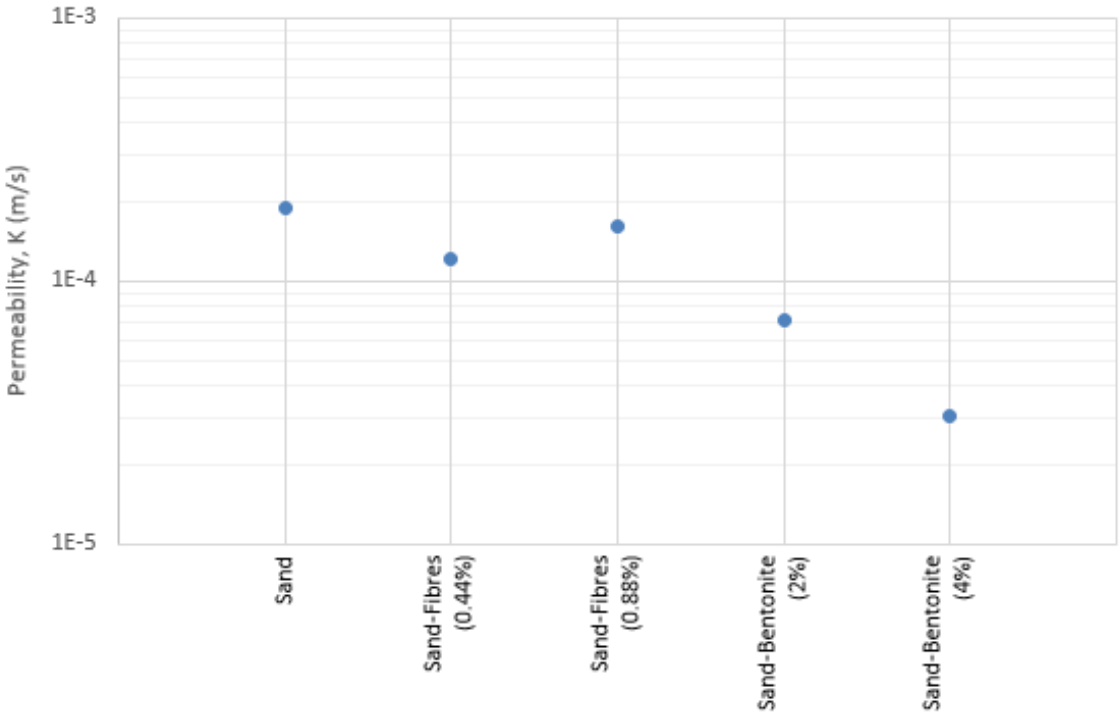

Figure 35 - Comparison of permeability coefficients

As the results show, adding bentonite to sand decreases the permeability significantly. For the 2% mixture the permeability is approximately a factor 2.5-3 less, for the 4% mixture this is approximately a factor 6-6.5. The sand-fibre mixtures also show a small decrease in permeability, but not significant. It also shows no decrease with increasing fibre content. The values found for sand and sand-fibre mixtures are in accordance with generally known values (Geotechdata.info, 2013). When plotting the reduction of permeability (K/K_{sand}) as function of the weight percentage of bentonite, an empirical formula for this reduction can be given (Figure 36). The reduced permeability of the sand-bentonite mixtures is expected to decrease erosion velocities, which is tested in the erosion experiment (section 7.4).

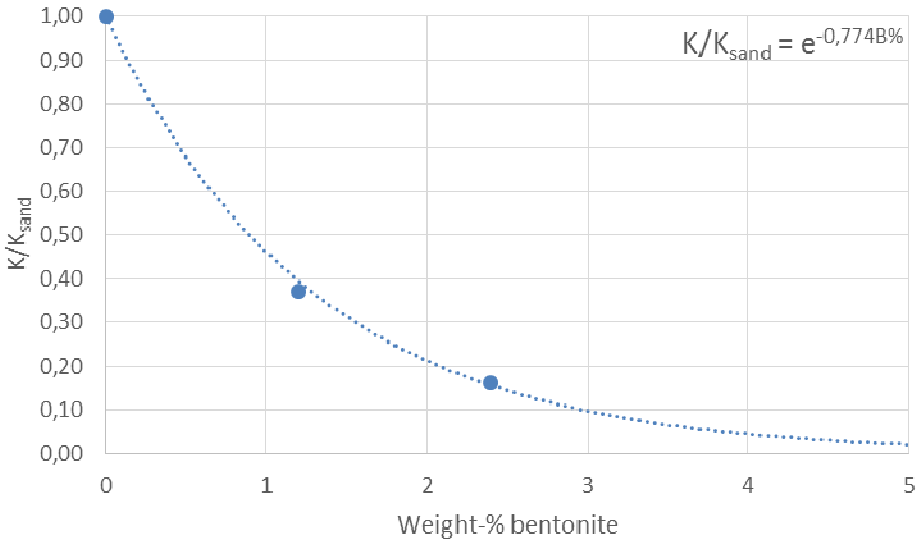

Figure 36 - Reduction of permeability as function of the weight percentage of bentonite

7.4 Erosion experiment

Tests to determine the erosion velocities of the mixtures were performed in a small flume (known as the short practical flume). In this flume a bed of sand or one of the mixtures was prepared and a current was run over the bed to erode it. During a test the flow rate and flume dimensions were constant. The water level and bed level were recorded using a video camera, aimed at a designated measurement area of the flume. In this section the test setup and conditions are explained and the results are discussed.

Setup and conditions

The flow flume has an overall length of 4.4 metres, a width of 0.2 metres and a height of 0.4 metres. In order to increase the maximum attainable flow velocity, the width of the flume was decreased to 0.105 metres and it was possible to slightly increase the water head which drives the flow. This was achieved with a small vertical slide at the beginning of the flow flume. The test setup can be seen in Figure 37. The flow into the flume is driven by gravity, flowing from a tank at a higher level in the laboratory, through a pipe into the flume. A magnetic flow meter was used to measure the flow rate in the pipe, which is equal to the flow rate through the flume.

Figure 37 – Overview of the test setup: narrowing of the flow flume (top left), slide to increase water head (top right), overview of the beginning of the flume (bottom left) and valve for regulating the flow rate (bottom right)

The sides of the flume were made from glass panels, through which the tests were recorded. One of these panels was designated as the measurement area and is shown in Figure 38, on which a grid was drawn. For calculation of the results, a Matlab script was used to interpret the recordings more accurately. Nine vertical lines of the grid were used as a measurement locations in the Matlab script. Due to inaccurate measurements of points 1, 2 and 3 (e.g. due to turbulence), these points are not used to determine flow velocities and erosion velocities. In appendix F it is explained why these points were discarded.

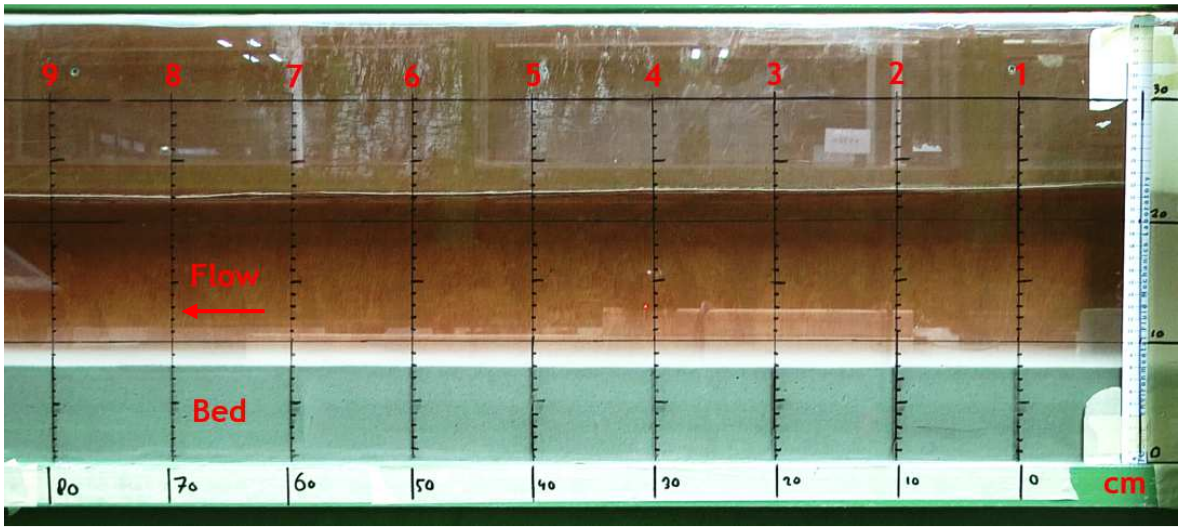

Figure 38 – Measurement area and measurement points, flow direction from point 1 towards 9

In this adapted flow flume a bed of sand or mixture was prepared. A dry bulk density of 1588 kg/m^3 (resulting in a porosity of 0.40) was desired for each test. This could be achieved by dispersing two bags of sand or mixture (approximately 50 kg) in the flume and compact the loose material to a bed height of approximately 8.5 cm. The bed was compacted by hand and by means of a wooden tool and hammer. Due to inconsistency in the compaction method, a small spread in dry bulk densities and therefore porosities has occurred over the tests.

For each test the conditions, like dry bulk density and porosity of the sand in the mixtures, can be found in appendix F. After preparation of the bed, water was put on top of the bed for an extended period of time to allow it to saturate. For the sand-bentonite mixtures this was particularly important, since the bentonite needs time to swell to its full capacity. The saturation times are also noted in appendix F. In Table 12 a summary is given of the conditions of all tests.

Parameter	*Value*
Flow rates, Q [L/s]	10.1-20.2
Width of flume [m]	0.2
Length of flume [m]	4.4
Height of flume [m]	0.4
Length of bed, L_b [m]	3.37
Length of bed slope, L_{bs} [m]	0.4
Width of bed/flow, W_f [m]	0.105
Dry bulk densities sand, $\rho_{db\text{-}sand}$ [kg/m^3]	1482-1667
Porosities sand, p_{sand} [-]	0.37-0.44

Table 12 - Summary of test conditions erosion tests

The tests were executed at two different flow rates for each mixture. In appendix F is explained how these flow rates were used to calculate the flow velocities. In Figure 39 an overview is given of the flow velocities during each test. In this figure lines are plotted through the average flow velocity per measurement point per test.

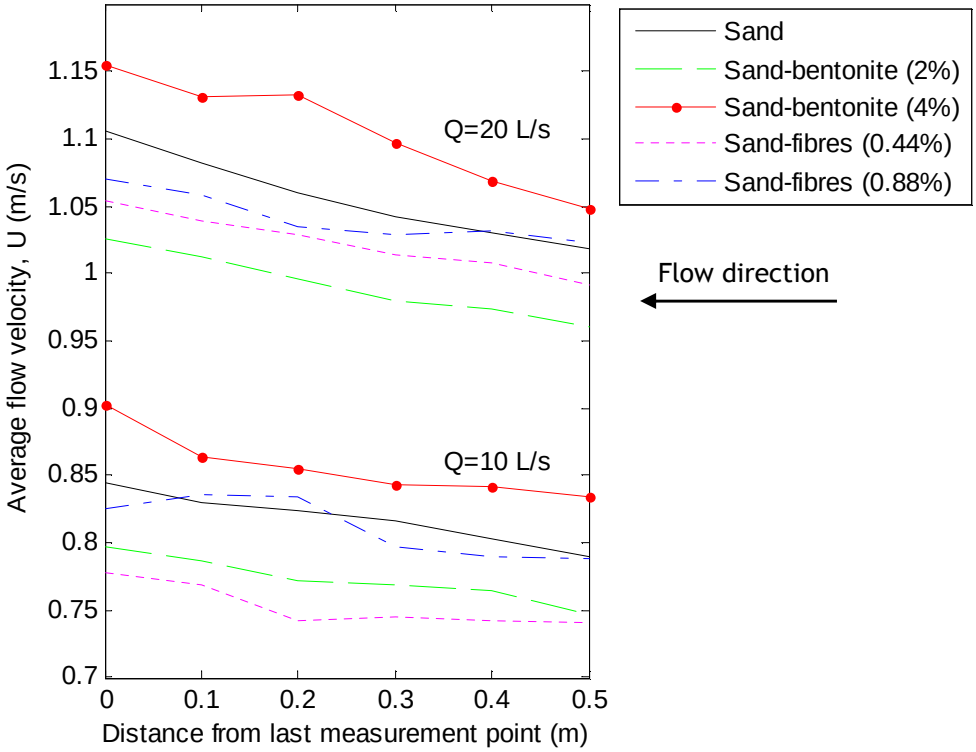

Figure 39 - Average flow velocities per test (measurement point 4 at 0.5 m, to 9 at 0 m)

The flow velocities during all tests increase over the bed in the direction of the flow. This means there are no steady flow conditions during the tests and the flow is accelerating. The lines are also somewhat fickle, which is most likely caused by turbulence in the flow. This turbulence is partly caused by the erosion of the bed itself and partly by the water depth reduction due to the presence of the bed at the beginning of the flume. This last effect was particularly noticeable during the Q=20

L/s tests. A part of the spread in the results can be explained due to this turbulence. The results of the erosion tests are discussed in the next section.

Results

In this section the results of the erosion tests are presented and discussed. Using the water and bed level measurements, the flow velocities and erosion velocities were derived. These were used to create linear fit lines, which are used to calculate the erosion velocity as function of the flow velocity for each mixture. In appendix F the calculation procedure is explained. Figure 40 shows these linear fit lines for all tests, including the average erosion velocity at the average flow velocity of each test.

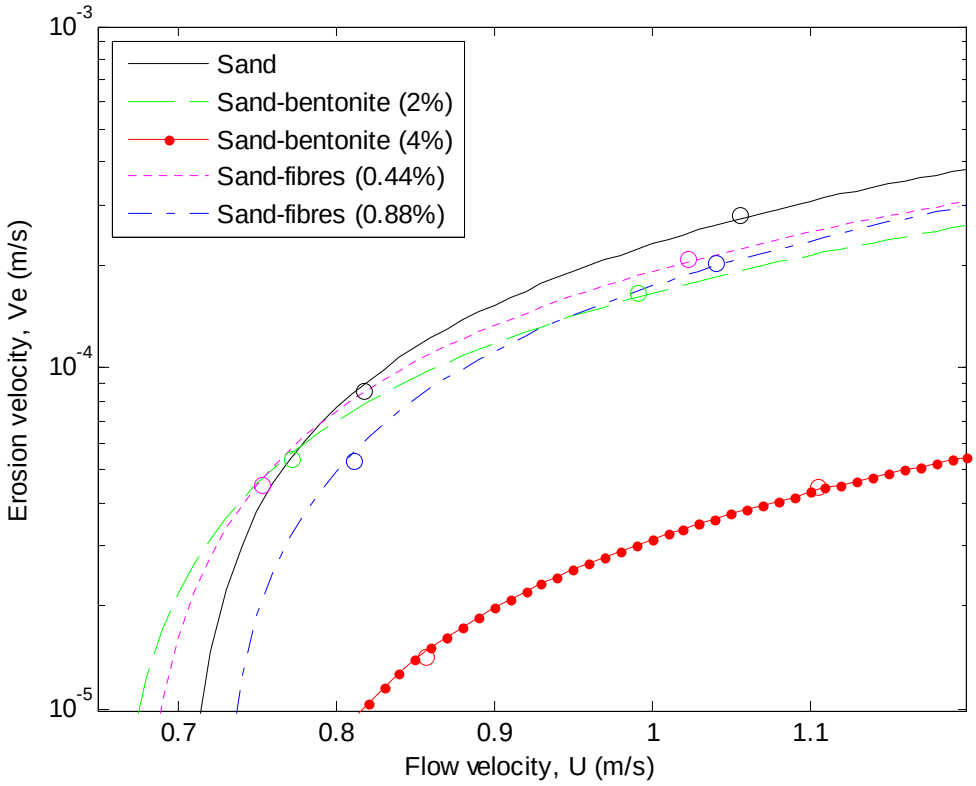

Figure 40 - Linear fit lines and mean values (circles) of erosion tests

The results show the effect of different additives on the erosion velocity. As can be seen, adding fibres or a small amount of bentonite (2%) to sand does not have a significant influence on the erosion velocity. The erosion velocities of these mixtures are relatively close to the erosion velocity of sand. Sand-bentonite (4%) shows a significantly lower erosion velocity than the other mixtures and sand. The figure shows the lines of sand-fibres (0.44%) and sand-bentonite (2%) crossing the line of sand. This is because the lines are linear fit lines, which can have a deviation from actual data. It does not necessarily indicate that the erosion velocities of the mixtures at lower flow velocities are higher than those of sand.

To quantify the differences in erosion velocities, they are compared to the erosion velocity of sand. For each mixture the fraction of erosion velocity of sand, as well as the reduction factors were calculated at two different flow velocities, which can be seen in Table 13. These velocities are approximately the same as the flow velocities during the tests. As this table shows, the erosion velocities are about 1 to 1.5 times

smaller than the erosion velocity of sand, except for sand-bentonite (4%), which shows a reduction of a factor 7 to 9.

	Sand-bentonite (2%)	*Sand-bentonite (4%)*	*Sand-fibres (0.44%)*	*Sand-fibres (0.88%)*
F (U≈0.8 m/s)	0.88	0.11	0.95	0.67
F (U≈1.1 m/s)	0.70	0.14	0.82	0.77
1/F (U≈0.8 m/s)	1.13	8.97	1.05	1.49
1/F (U≈1.1 m/s)	1.43	7.14	1.22	1.30

Table 13 - Fraction of erosion velocity (top two rows) and reduction factor (1/fraction) of mixtures compared to sand

Since the linear fit lines for each mixture are known, it is possible to extent these lines until they cross the U-axis at V_e=0 m/s. This is shown in Figure 41.

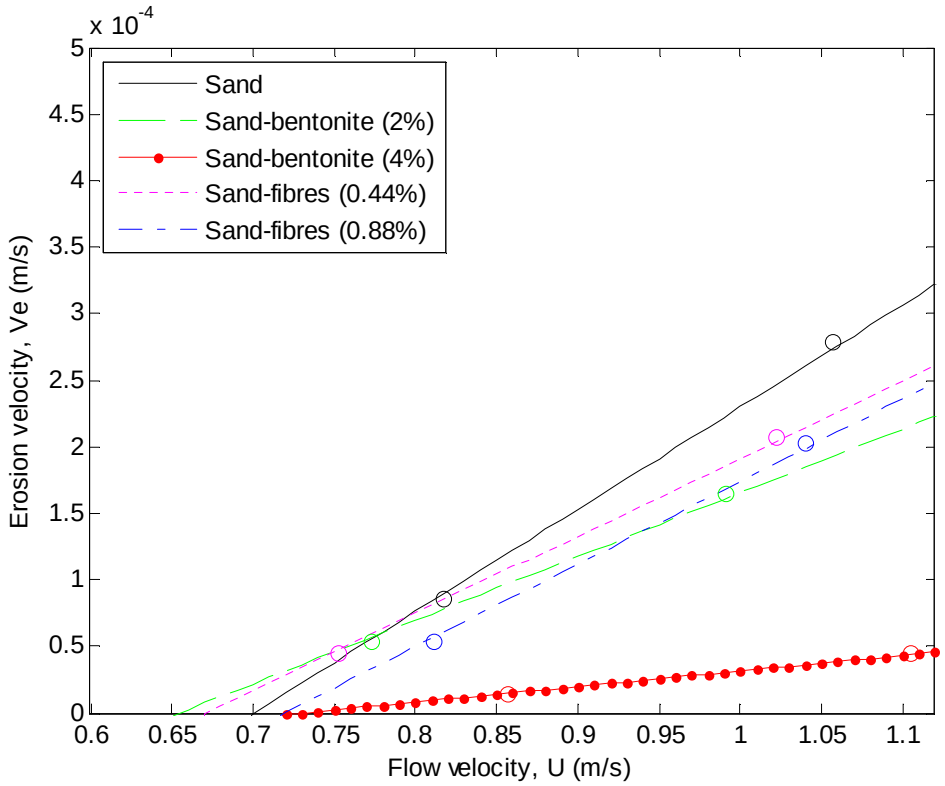

Figure 41 - Crossing of the U-axis at V_e=0 m/s of the linear fit lines (circles are mean test values)

This is to get an indication of the accuracy of the test results and of the critical flow velocity. It can be seen that the lines cross the U-axis relatively close to each other, indicating the test results were fairly accurate. This also means that the critical flow velocities of the mixtures are similar. For all tests also linear fit lines for the erosion velocity as function of U^2 are determined. The U^2-axis crossings at V_e=0 m/s are also calculated, as shown in Figure 42. These U^2 values are proportional to the critical shear stress and an indication of the critical shear velocity. For both U and U^2 the critical values are presented in Table 14.

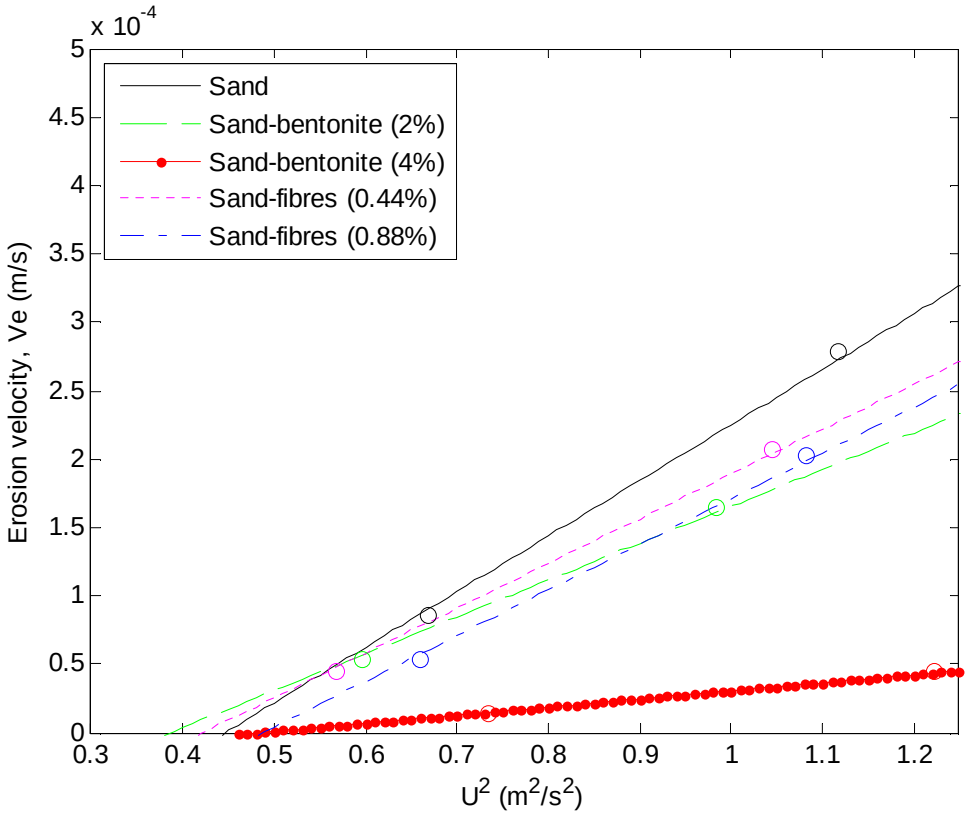

Figure 42 - Crossing of U^2-axis at V_e=0 m/s of the linear fit lines (circles are mean test values)

	Sand	*Sand-bentonite (2%)*	*Sand-bentonite (4%)*	*Sand-fibres (0.44%)*	*Sand-fibres (0.88%)*
U_c *[m/s]*	0.70	0.65	0.73	0.76	0.72
U_c^2 *[m²/s²]*	0.45	0.39	0.48	0.50	0.49

Table 14 - Values of critical U and U^2 (at V_e=0 m/s) for all mixtures

Since both the critical U and U^2 values are similar, it can be concluded that the erosion processes of the mixtures are generally the same as the erosion process of sand. If this was not the case, large deviations in the critical velocities should be visible, e.g. caused by significant cohesion of a mixture.

These results indicate that reducing the erosion velocity of sand is feasible. During these tests the best results were achieved with a sand-bentonite (4%) mixture.

In addition to the above comparisons, Figure 43 shows the V_e/K value at different flow velocities (K is the permeability). If $V_e/K>3$ the high-velocity erosion regime prevails (Van Rhee, 2010), which is not the case for these tests.

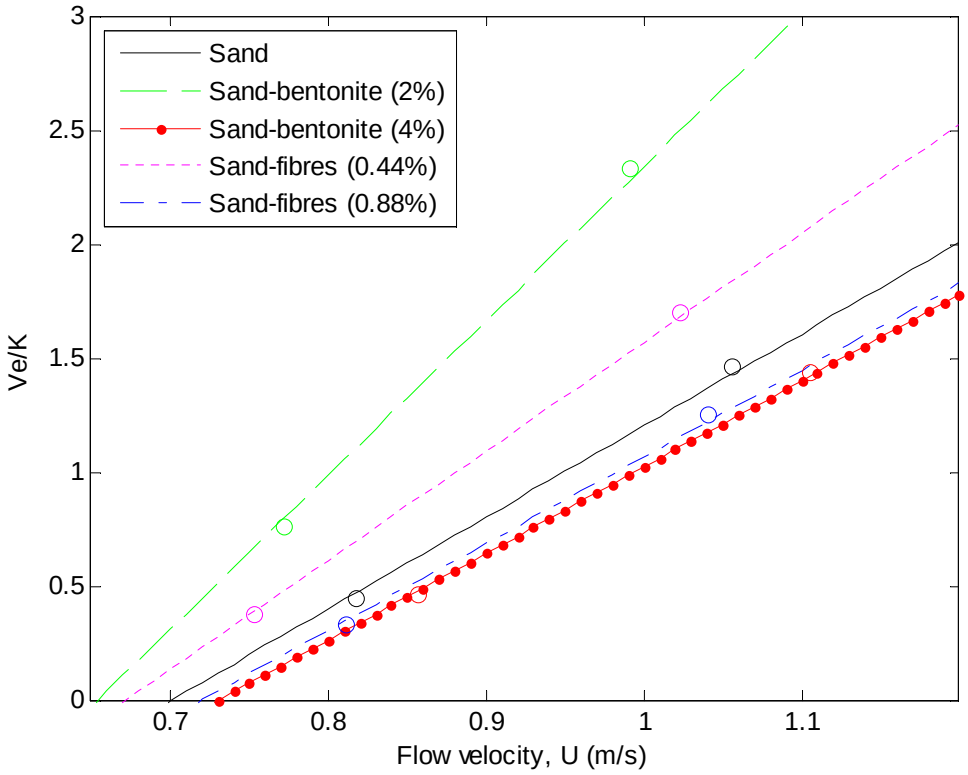

Figure 43 - Erosion velocity (V_e) divided by permeability (K) of the mixtures (circles are mean test values)

Calculation of bed shear stress

In this section the method for calculating the bed shear stresses of the tests is explained. These bed shear stresses are used to compare the test results to erosion theories which use the bed shear stress as input parameter. From the measurements the total pressure and energy loss for each erosion and clear water test are determined. The clear water tests are the same tests as the erosion test, but no bed was present during these tests. The energy loss is used to calculate the bed shear stresses. The measurements needed for these calculations and the results of these calculations are presented in appendix F.

For each test the water depth at six different points was measured (measurement points 4-9). As explained in appendix F these water depths were used to calculate the flow velocities during each test. For each measurement point the average flow velocity and average water depth is known, which are used to calculate the hydraulic radius (R), energy height (H) and pressure (p) using:

$$R = \frac{hw}{2h + w} \tag{7.3}$$

$$H = h + \frac{U^2}{2g} \tag{7.4}$$

$$p = \rho g h \tag{7.5}$$

in which:

R	= hydraulic radius of the total flow area [m]
h	= water depth [m]
w	= flow width [m] (=0.105 m)
H	= energy height [m]
U	= flow velocity [m/s]
p	= pressure [Pa]
ρ	= water density [kg/m^3]

For each test, the average of these parameters are calculated as well. To determine the loss over the measurement section, the gradients of h, U, U^2, H and p are calculated:

$$\frac{dn}{dx} = \frac{n_9 - n_4}{x_9 - x_4} \tag{7.6}$$

in which:

n	= parameter for calculation (h, U, U^2, H or p)
dn/dx	= gradient of h, U, U^2, H or p over measurement section [unit of n/m]
n_4, n_9	= value of n-parameter at measurement point 4 or 9
x_4, x_9	= value of x at measurement point 4 or 9

From the pressure gradient (dp/dx) the total shear stress of each test can be calculated. For the clear water tests, this is only the shear stress as a result of the wall and bottom friction. For the erosion tests, this is the combined shear stress as a result of the wall friction and the bed friction. These shear stresses are calculated using the method described in (Van Rhee & Talmon, 2010). The pressure gradient can also be calculated with (τ_a=total shear stress [Pa]):

$$\frac{dp}{dx} = -\tau_a \frac{1}{R} - \frac{d}{dx}(\rho U^2) = -\tau_a - U^2 \frac{d\rho}{dx} - \rho \frac{dU^2}{dx} \tag{7.7}$$

In this formula also a term for the density gradient is present (dρ/dx), which is assumed to be zero for the executed tests. The density of the flow is assumed to be equal to the density of clear water. By rewriting this formula, an expression for the total shear stress (τ_a) is found:

$$\tau_a = -R\left(\frac{d\tilde{p}}{dx}\right) \tag{7.8}$$

$$\frac{d\tilde{p}}{dx} = \frac{dp}{dx} - \rho \frac{dU^2}{dx} \tag{7.9}$$

The total shear stress is determined based on the pressure gradient corrected for the acceleration of the flow; the corrected pressure gradient (dp/dx-ρdU^2/dx). Since there is no bed present during the clear water tests, the total shear stress is equal to the wall shear stress (τ_w [Pa]) for these tests. The total shear stress of each erosion

test minus the wall shear stress of the clear water tests gives an indication of the bed shear stresses (τ_{a-w} [Pa]) during the tests:

$$\tau_{a-w} = \tau_a - \tau_w \tag{7.10}$$

However, the flow velocities of the tests are not equal to each other. To correct for this a deterministic relation between the wall shear stress and the average U^2 is determined (Figure 101, appendix F), using the values from the clear water tests. It should be noted that the wall shear stress also depends on the hydraulic radius, but in this relation that is neglected. This relation is used to calculate indicative bed shear stresses during the tests:

$$\tau_w = 10.493\bar{U}^2 \tag{7.11}$$

$$\tau_{a-w} = \tau_a - 10.493\bar{U}^2 \tag{7.12}$$

The average flow velocities, average U^2, total and wall shear stresses, and the indicative bed shear stresses are given in Table 15. A more accurate way of calculating the bed shear stresses of the tests, is the Vanoni & Brooks formula (Cheng & Chua, 2005). This formula calculates the wall friction factor and the bed friction factor, which are used to calculate the bed shear stress:

$$\tau_b = \frac{w}{w+2h} \cdot \frac{f_b}{f} \cdot \frac{1}{\rho g h S} \tag{7.13}$$

$$f = \frac{8gRS}{\bar{U}^2} \tag{7.14}$$

$$f_b = f + \frac{2h(f - f_w)}{w} \tag{7.15}$$

$$f_w = \left(20\left(\frac{4\bar{U}R/\nu}{f} \right)^{0.1} - 39 \right)^{-1} \tag{7.16}$$

in which:

τ_b	= bed shear stress [Pa]
S	= energy slope [m/m] (=dH/dx)
R	= hydraulic radius of the total flow area [m]
f_b	= bed friction factor [-]
f_w	= wall friction factor (curve fitting function) [-]
v	= kinematic viscosity of water [m^2/s]

The results of this formula are also given in Table 15. For both methods the bed shear stresses are converted to a Shields parameter (θ) (Visser, 1998). The θ-value is calculated with ($\tau=\tau_a-\tau_w$ or τ_b):

$$\theta = \frac{\tau}{\rho g \Delta D_{50}} \tag{7.17}$$

The results of the Vanoni & Brooks formula and the indicative bed shear stresses are approximately the same, since differences between the two methods are small. This can be seen in Figure 44. For further comparison of the mixtures, the θ-value determined from τ_b is used. This value is used, since the Vanoni & Brooks formula is a better substantiated method for determining the bed shear stress. Based on the θ-values and V_e/K-values (Figure 43) it can concluded that the dominant erosion process is sheet flow erosion, but it is not yet in the high erosion velocity regime. Sheet flow erosion means that layers of particles instead of individual particles are eroded at once.

	U [m/s]	*τ_a [Pa]*	*τ_w [Pa]*	*τ_a-τ_w [Pa]*	*τ_b [Pa]*	*θ [-] (τ_a-τ_w)*	*θ [-] (τ_b)*
Q=10 L/s							
Water	0.74	5.55	5.55				
Sand	0.82	12.10	7.02	5.08	4.15	1.51	1.23
Sand-bentonite (2%)	0.77	11.90	6.27	5.63	6.68	1.67	1.98
Sand-bentonite (4%)	0.86	14.21	7.70	6.51	1.67	1.93	0.50
Sand-fibres (0.44%)	0.75	8.77	5.95	2.82	5.11	0.84	1.52
Sand-fibres (0.88%)	0.81	8.59	6.91	1.68	3.19	0.50	0.95
Q=20 L/s							
Water	0.91	8.78	8.78				
Sand	1.06	27.50	11.72	15.78	12.38	4.69	3.68
Sand-bentonite (2%)	0.99	21.37	10.32	11.05	15.84	3.28	4.71
Sand-bentonite (4%)	1.11	32.09	12.82	19.28	7.50	5.73	2.23
Sand-fibres (0.44%)	1.02	19.46	10.97	8.49	9.52	2.52	2.83
Sand-fibres (0.88%)	1.04	14.86	11.37	3.50	4.28	1.04	1.27

Table 15 - Results calculation bed shear stress

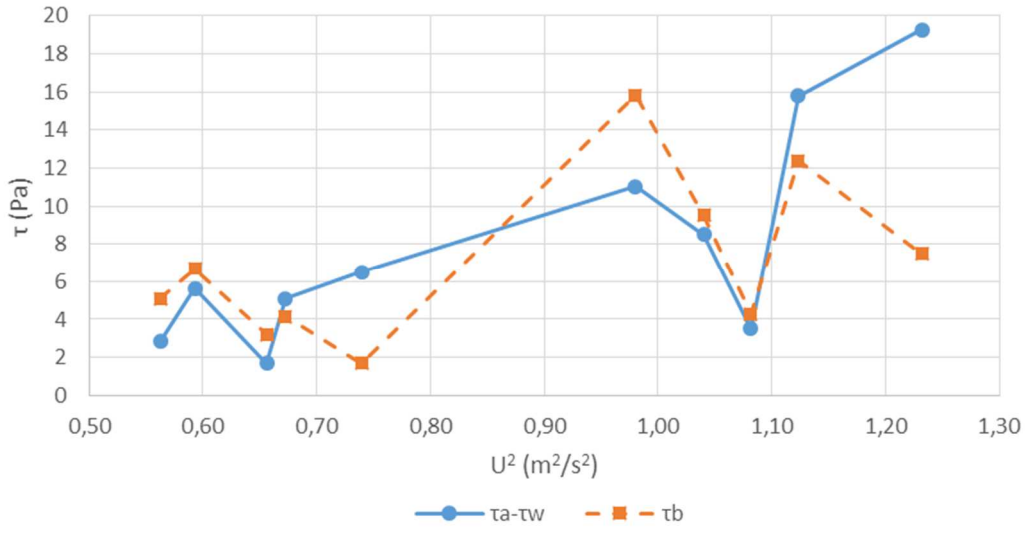

Figure 44 - Bed shear stress (τ_a-τ_w or τ_b) versus U^2

7.5 Erosion formula

To get more insight in the meaning of the test results, these are compared with theory about the critical Shields parameter and the erosion formula of Van Rhee.

Critical Shields parameter

For sand with a known diameter, the critical Shields parameter can be determined using (Visser, 1998):

$$D_* = D_{50}\left(\frac{\Delta g}{\nu^2}\right)^{1/3} \tag{7.18}$$

$$\text{for } D_* \le 4: \quad \theta_c = 0.24 D_*^{-1} \tag{7.19}$$

$$\text{for } 4 < D_* \le 10: \quad \theta_c = 0.14 D_*^{-0.64} \tag{7.20}$$

$$\text{for } 10 < D_* \le 20: \quad \theta_c = 0.04 D_*^{-0.1} \tag{7.21}$$

$$\text{for } 20 < D_* \le 150: \quad \theta_c = 0.013 D_*^{0.29} \tag{7.22}$$

$$\text{for } D_* < 150: \quad \theta_c = 0.055 \tag{7.23}$$

in which:

D_*	= particle parameter [-]
Δ	= relative density [-] (=1.65)
v	= kinematic viscosity [m^2/s] (=$1 \cdot 10^{-6}$ m^2/s)
D_{50}	= particle diameter [m]
θ_c	= critical Shields parameter [-]

Using these formulas and the particle diameter of the sand used for the tests, the critical Shields parameter for this sand is 0.0484. For all tests the θ-value was calculated, which is used to determine the critical θ-value for each mixture. These values are determined by calculating the value at which the linear fit lines crosses the θ-axis at V_e=0 m/s. These linear fit lines can be seen in Figure 45. The values of the critical Shields parameters can be seen in Table 16.

	Sand	*Sand-bentonite (2%)*	*Sand-bentonite (4%)*	*Sand-fibres (0.44%)*	*Sand-fibres (0.88%)*	*Shields*
θ_c	0.156	0.665	-0.314	1.155	0.834	0.048

Table 16 - Critical Shields parameter tests and theory

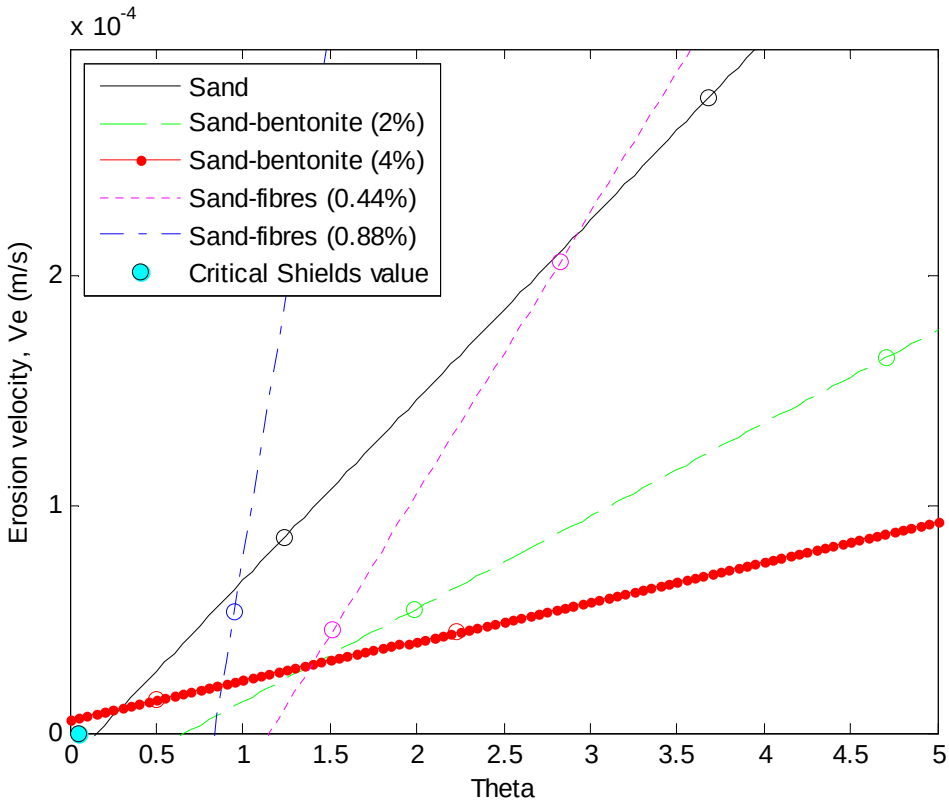

Figure 45 - Crossing of the θ-axis at V_e=0 m/s of the linear fit lines (circles are mean test values) and presentation of the theoretical critical Shields parameter

As these results show, the test values of θ_c vary considerably. This could be because only the mean values of the tests are taken into account. There is a spread in the measurements, which is not accounted for in the methods for determining the bed shear stress. This influences the determination of the linear fit lines, e.g. in such a way the θ_c-value is negative for the sand-bentonite (4%) tests. An improvement could be made by gathering more measurements of the erosion velocities at different bed shear stresses. Another (partial) explanation is the fact that the net erosion velocity was measured, so including sedimentation during the tests. This is contrary to the theoretical calculation of the critical Shields parameter, which does not take sedimentation into account. However, due to the low flow velocities during the tests their most likely was very little or no sedimentation.

Erosion formula

It is necessary to determine whether the experimental results and results from an erosion function are similar. For the used sand, the erosion velocity can be calculated using the Van Rijn-Van Rhee erosion formula, given by (Van Rhee, 2010):

$$V_e = \frac{1}{1-p-c_b}\left(\phi_p \sqrt{g\Delta D_{50}} - c_b w_s\right) \tag{7.24}$$

$$\phi_p = 0.00033 D_*^{0.3}\left(\frac{\theta-\theta_c^1}{\theta_c^1}\right)^{1.5} \tag{7.25}$$

$$\theta_c^{\,1} = \theta_c \left(\frac{\sin(\phi - \beta)}{\sin(\phi)} + \delta_p \cdot \frac{V_e}{K} \right) \tag{7.26}$$

$$\delta_p = \left(\frac{n_i - p}{1 - n_i} \cdot \frac{1}{\Delta(1-p)} \right) \tag{7.27}$$

in which:

V_e	= erosion velocity [m/s]
p	= porosity [-] (during sand tests approximately 0.38)
c_b	= near bed concentration [-]
φ	= angle of internal friction [°] (=34°, see section 7.2)
ß	= angle of bed slope [°] (=0°)
K	= permeability [m/s] (=$1.91 \cdot 10^{-4}$ m/s for sand, see section 7.3)
n_i	= maximum porosity of the sand [-] (=0.48)
w_s	= hindered settling velocity of sand [m/s]

Using this formula, the erosion velocities are calculated for the same conditions as during the tests with clean sand. First this was calculated for clear water erosion, which means assuming a near bed concentration of zero (c_b=0). The result can be seen in Figure 46. The result of the function does not match the result of the sand tests. This is because the near bed concentration was not zero during the tests. By adapting the near bed concentration ($c_b \approx 0.03$) and dividing the permeability by 20 (K=K/20) the calculated and experimental results match quite well, as Figure 46 shows. The reduction in permeability is necessary to fit the formula to the results and does not give the real value for the permeability.

Now the function is fitted to the data of the sand tests, it can be adapted for the sand-bentonite tests. This is achieved by changing the permeability to the value of the sand-bentonite mixtures (2% or 4%), which is $7.07 \cdot 10^{-5}$ or $3.08 \cdot 10^{-5}$ m/s respectively (section 7.3). By only adapting the permeability of the fitted formula, the calculated erosion velocities show a similar reduction as the test results (see Figure 47). This makes the function suitable for modelling the erosion during the breaching process of a sand-bentonite dike.

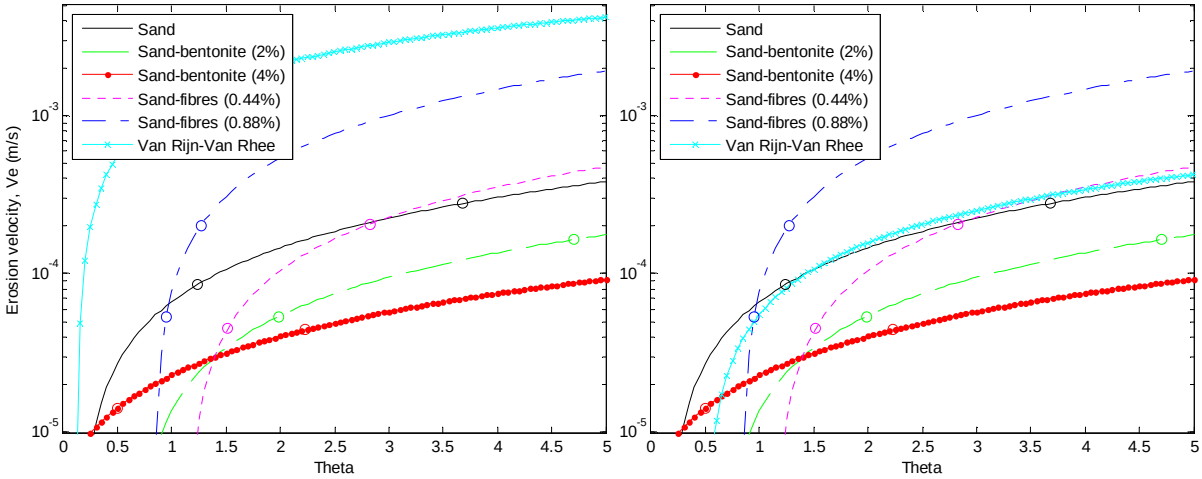

Figure 46 - Comparison of test results with Van Rijn-Van Rhee (circles are mean test values): left for c_b=0 and K=K, right for c_b≈0.03 and K=K/20

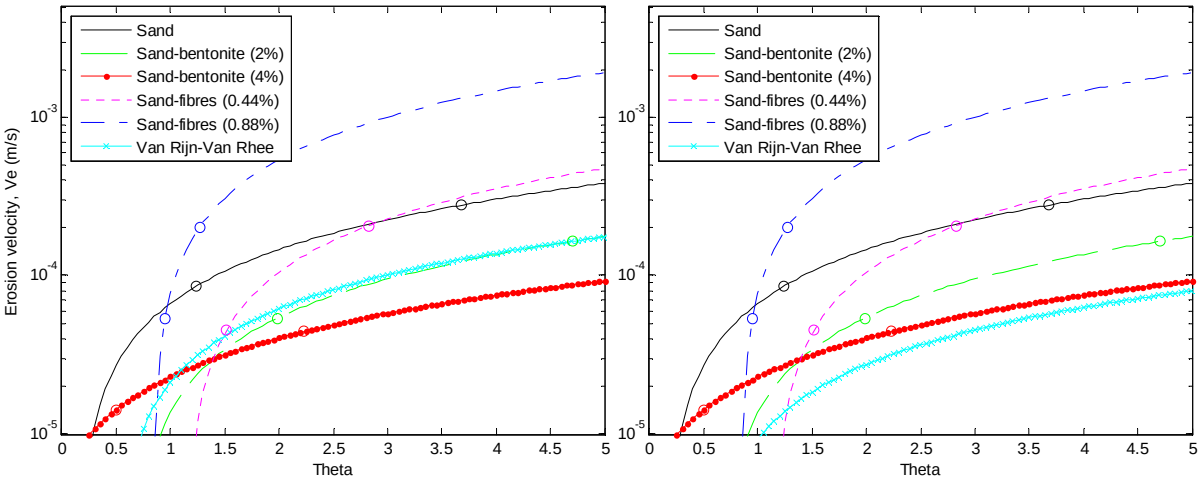

Figure 47 - Fitting of Van Rijn-Van Rhee (for c_b≈0.03 and K=K/20) to the results of the sand-bentonite (2% and 4%) tests, by using the permeability of that mixture and adapting it the same as the sand value (K=K/20) (circles are mean test values)

7.6 Conclusions

Given the results of the experiments it can be concluded that it is possible to reduce the erosion velocity of sand, without in- or decreasing the strength of sand. The direct shear tests and erosion tests indicate that all mixtures still show sand-like behaviour. This is favourable as the mixtures can be assumed to behave as sand, for example in stability calculations of dikes.

The results of the erosion tests are reasonably accurate and the sand-bentonite (4%) mixture shows a significant reduction in erosion velocity. This is a promising result and might be used to slow down the breaching process of a sand dike. However, the tests were executed at relatively low flow velocities and the mixture needs to be tested at higher flow velocities to determine whether the effect is still present then. During these tests only two mixture ratios were tested. Better results could be achieved with other mixture ratios. Increasing the bentonite percentage in the mixture might lead to creating a clay-like material instead of sand with reduced erosion velocities. When determining the most effective ratio, this should be taken into account.

From the permeability tests it is evident that the permeability of sand decreases with increasing bentonite content. Due to this decreasing permeability the erosion velocity decreases. Because of the lower permeability it is more difficult for water to enter the sand bed. This is necessary for the erosion of sand, which needs to dilate before it erodes. When it dilates, water has to flow between the grains to fill the voids. Since this is more difficult if the permeability is lower, a higher pressure gradient over the grains is present. This pressure gradient pushes the grains into the bed, making it harder to erode the sand.

The test results show almost no erosion reducing effect of fibres added to sand, only a small increase of the friction angle. Adding more fibres to sand might result in to a significant reduction of the erosion velocity. However, practice has shown that there is an upper limit to the mixture ratio of sand-fibre mixtures. When the mixture ratio gets too high, the fibres start balling (i.e. clumping together) during mixing. For the used fibres this is at a fibre weight content of approximately 3% (Hejazi, et al., 2012). This might make it practically impossible to achieve the necessary higher mixture ratios than the ones used in these experiments to reduce erosion significantly, making this an ineffective method. However, it could be that a different type of fibre yields better results. For example, fibres with a ribbed surface might work better, because these fibres could have a better ‘grip’ on the sand grains. Based on this it is also concluded that the derived erosion formula for fibres (section 6.2) is not correct and thus the assumptions made for this formula do not hold.

According to these tests, adding bentonite to sand is the best method for reducing the erosion velocity of sand. In this case the best results were achieved with a volume percentage of 4% bentonite (or 2.4% dry weight percentage). This was consistent with the outcome of the model results of the options (chapter 6). The erosion behaviour of a sand-bentonite mixture can be modelled using the Van Rijn-Van Rhee formula, by adapting the permeability. This is a less complicated formula to model the erosion velocity than the formula determined in section 6.1 and is used to model this solution in chapter 8.

8 Modelling of solution

The preferred solution is adding bentonite to sand to decrease the erosion rate. This solution is modelled using the BRES-model. From this chapter onward, the bentonite percentage is given as weight percentage of added bentonite.

8.1 Results experiment

As concluded in section 7.5, it is possible to model a sand-bentonite mixture by adapting the permeability used in the Van Rijn-Van Rhee erosion formula. In section 7.3 an empirical formula for the reduction of permeability as function of the weight percentage of bentonite was determined. This formula calculates the permeability of sand-bentonite mixtures by adapting the unaltered permeability of sand:

$$K_{sb} = K_{sand} \cdot e^{-0.774 \cdot B_{\%}} \tag{8.1}$$

in which:

K_{sb} = permeability of sand-bentonite mixture [m/s]
K_{sand} = permeability of sand [m/s] (calculated in the BRES-model)
$B_{\%}$ = weight percentage of added bentonite [%]

By implementing this formula in the BRES-model, the model can simulate the breaching process for different weight percentages of added bentonite. This was simulated for the norm dike (chapter 4) for sand, 1.2% and 2.4% added bentonite, which can be found in appendix H. A comparison of the results of the different percentages can be seen in Figure 48. For each percentage of added bentonite also the inundation velocity (or rise rate) is calculated, which can be seen in Figure 49.

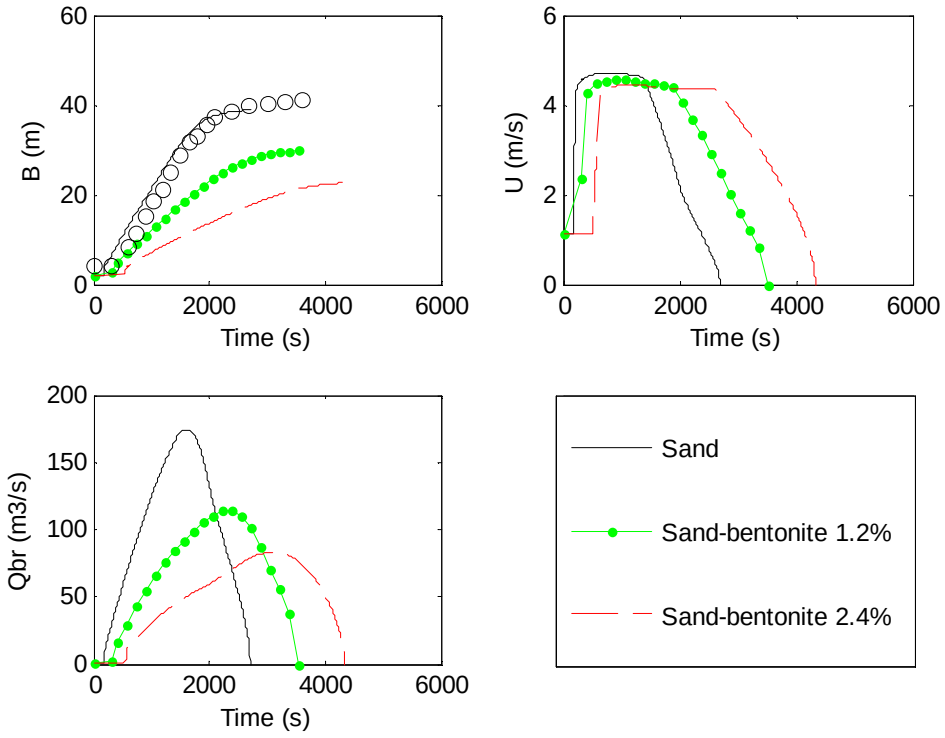

Figure 48 - Comparison of results BRES-model for the norm dike for different added weight percentages of bentonite

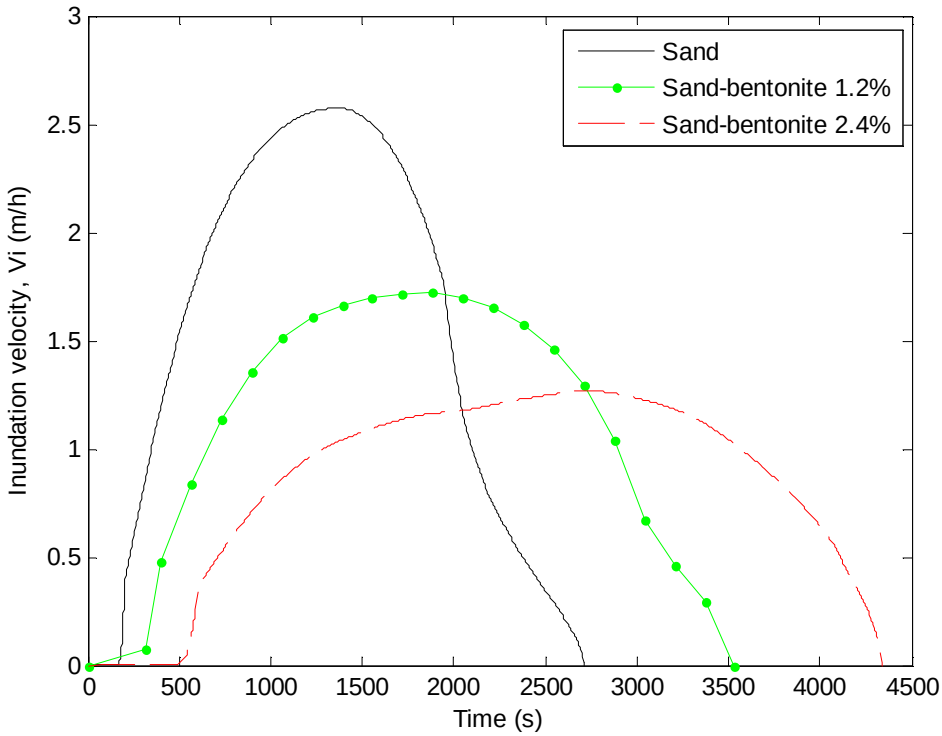

Figure 49 - Comparison of inundation velocities in the ZWIN'94 polder for different added weight percentages of bentonite

The maximum values of these results are given in Table 17.

	Duration [s]	*B_{max} [m]*	*Q_{max} [m^3/s]*	*Vi_{max} [m/h]*
Sand	2707	36.7	174.5	2.57
Sand-bentonite 1.2%	3530 *(1.3x)*	27.8 *(0.8x)*	114.4 *(0.7x)*	1.72 *(0.7x)*
Sand-bentonite 2.4%	4337 *(1.6x)*	20.5 *(0.6x)*	83.1 *(0.5x)*	1.27 *(0.5x)*

Table 17 - Maximum values of the model results and the factor between the results of sand and the mixtures (B=breach width, Q=flow rate, Vi=inundation velocity)

The model results show that adding 2.4 weight percent of bentonite to sand already decreases the maximum values for the norm dike by half. This is however not sufficient to lower the inundation velocity below the threshold value of 0.5 m/h (see section 1.2). Based on the model and experiment results it is possible to determine what weight percentage of bentonite lowers the inundation velocity below this threshold value, which is explained in the next section.

8.2 Necessary mixture

To find the bentonite percentage that lowers the inundation velocity sufficiently, a relation between the reduction factor of this velocity and the bentonite percentage is determined. This is achieved by plotting this reduction factor versus the bentonite percentage, shown in Figure 50. Using this graph an exponential formula is determined, also given in this figure. This is the same type of relation as between the reduction factor of the permeability and the bentonite percentage, which is also plotted in this figure.

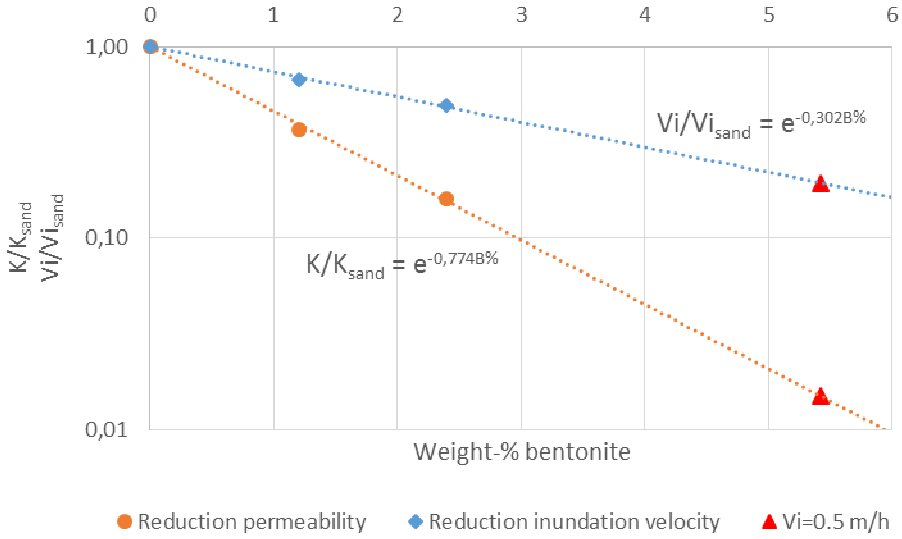

Figure 50 - Determination of necessary reduction factors

To achieve an inundation velocity equal to the threshold value, a reduction of the original inundation velocity of more than 80% is necessary, based on an extrapolation. This gives a reduction factor of 0.195, which corresponds with a bentonite percentage of 5.42%. Using this bentonite percentage also the reduction of permeability is calculated, which needs to be 1.5% of the permeability of sand. An overview of these calculations is given in Table 18.

	Bentonite [weight-%]	***Vi_{max} [m/h]***	***Vi/Vi_{sand} [-]***	***K [m/s]***	***K/K_{sand} [-]***
Sand	0	2.57	1	1.91E-04	1
Sand-bentonite 1.2%	1.20	1.72	0.669	7.07E-05	0.370
Sand-bentonite 2.4%	2.40	1.27	0.494	3.08E-05	0.161
Necessary for Vi=0.5 m/h	5.42	0.50	0.195	2.88E-06	0.015

Table 18 - Determination of necessary bentonite percentage

To show that a sand-bentonite (5.4%) mixture actually leads to an inundation velocity below the threshold value, the breaching process for this mixture was also simulated in the BRES-model. When using the exact same circumstances as during the ZWIN'94 experiment, the model produced no results. A more detailed examination revealed that the outside water level dropped faster than the bottom of the breach. This eventually stopped the flow through the breach, stopping the breaching process. The breaching processes stopped after fase II and never initiated fase III since the outside water level was too low at that time step. For the norm dike it means it is possible to prevent a catastrophic breach in the dike by adding enough bentonite to the sand. This might be possible for other dikes as well, but will depend on the case specific circumstances. For each dike a bentonite percentage could be determined at which the breaching process would not pass stage II.

To be able to show that the determined bentonite percentage could reduce the inundation velocity sufficiently, a second simulation was run. This time the outside water level was programmed to remain at a higher level for a longer period of time,

to ensure a full breach would develop. The result of this simulation is given in appendix H and a comparison with the results of the other mixtures is shown in Figure 51. The inundation velocities of all mixtures are shown in Figure 52.

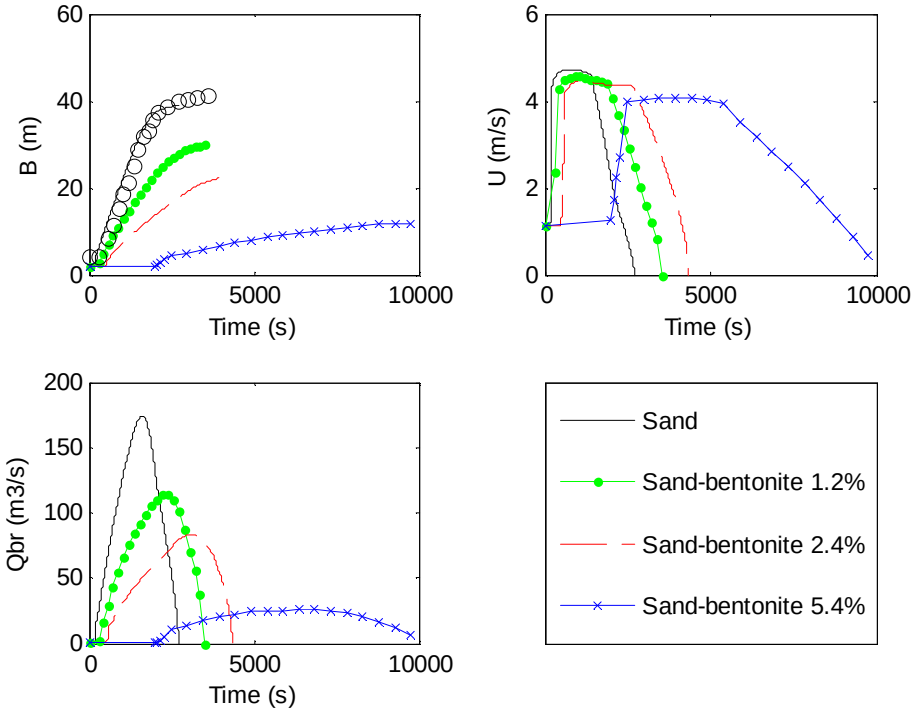

Figure 51 - Comparison of results BRES-model for the norm dike for different added weight percentages of bentonite, including minimum percentage (5.4%)

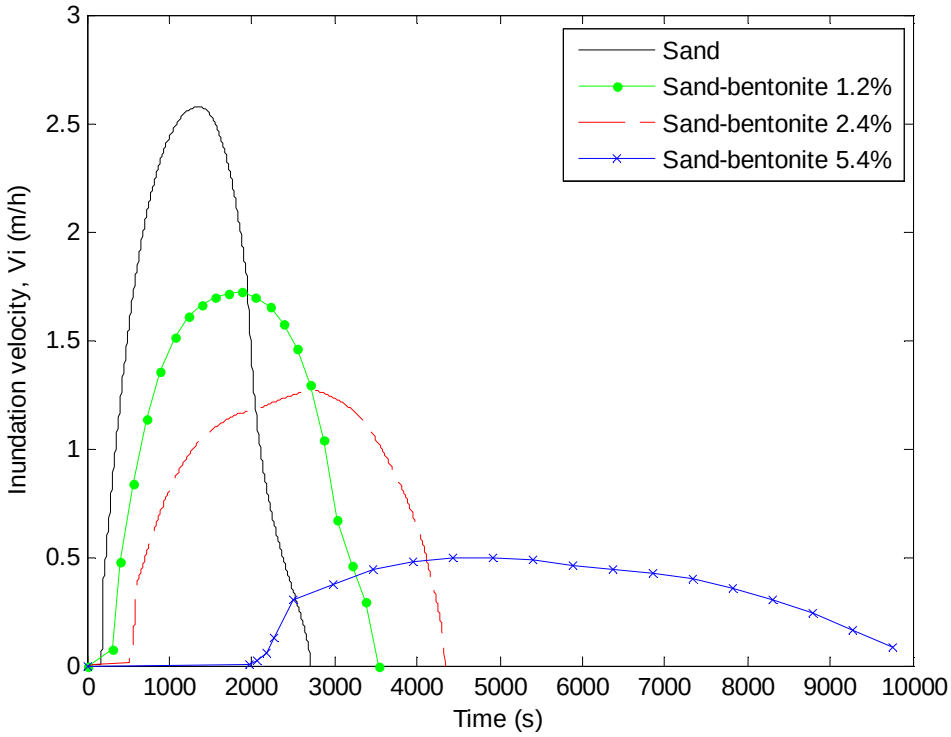

Figure 52 - Comparison of inundation velocities in the ZWIN'94 polder for different added weight percentages of bentonite, including minimum percentage (5.4%)

The maximum values of the results of all mixtures are given in Table 19.

	Duration [s]	*B_{max} [m]*	*Q_{max} [m^3/s]*	*Vi_{max} [m/h]*
Sand	2707	36.7	174.5	2.57
Sand-bentonite 1.2%	3530 *(1.3x)*	27.8 *(0.8x)*	114.4 *(0.7x)*	1.72 *(0.7x)*
Sand-bentonite 2.4%	4337 *(1.6x)*	20.5 *(0.6x)*	83.1 *(0.5x)*	1.27 *(0.5x)*
Sand-bentonite 5.4%	10230 *(3.8x)*	9.4 *(0.3x)*	26.0 *(0.2x)*	0.50 *(0.2x)*

Table 19 - Maximum values of model results for different bentonite weight percentages, including minimum percentage, and the factor between the results of sand and mixtures (5.4%) (B=breach width, Q=flow rate, Vi=inundation velocity)

As the results show a sand-bentonite mixture with a bentonite weight percentage of 5.4% reduces the inundation velocity below the threshold value of 0.5 m/h. It should be noted that this result is only applicable for the dike, polder and circumstances of the ZWIN'94 experiment. In the next section the effect on the mortality is determined.

8.3 Mortality

The mortality is defined as the number of casualties as fraction of the number of people present in a flooding polder. In the Netherlands the mortality during a flood can be calculated using (Jonkman, 2004):

For Vi≥0.5 m/h & h<1.5 m or Vi<0.5 m/h & h>0 m:

$$M = 1.34 \cdot 10^{-3} \cdot e^{0.59 \cdot h} \quad (8.2)$$

For Vi≥0.5 m/h & 1.5≤h≤4.7 m:

$$M = 1.45 \cdot 10^{-3} \cdot e^{1.39 \cdot h} \quad (8.3)$$

For Vi≥0.5 m/h & h>4.7 m:

$$M = 1 \quad (8.4)$$

in which:

M = mortality [-]
Vi = inundation velocity or rise rate of the water in the polder [m/h]
h = water depth in the polder [m]

These empirical formulas are based on research of historical and international floods. There are three different formulas for three situations, but all are a function of the water depth. The first formula (8.2) applies when there is a small water depth (h<1.5 m) or an inundation velocity below the threshold value (Vi<0.5 m/h). The second formula (8.3) gives the mortality for fast inundation velocities (Vi>0.5 m/h) and deeper water (1.5≤h≤4.7 m). The third formula (8.4) is applicable for fast inundation velocities (Vi>0.5 m/h) and deep water (h>4.7 m). In the last case it is assumed everyone in an area with those circumstances drowns. Which formula needs to be used varies over time during the flooding of an area. The inundation velocity changes over time and the water depth increases with time. For the ZWIN'94 experiment and the different bentonite percentages, the mortality over time is calculated using these formulas. The result of this calculation can be seen in Figure 53.

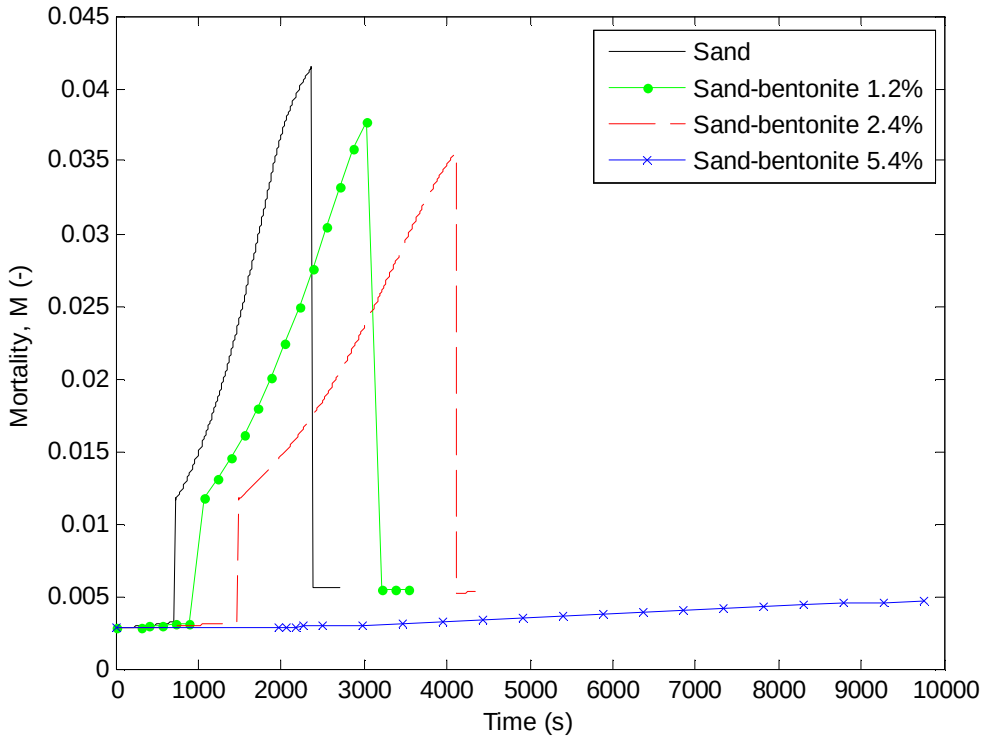

Figure 53 - Mortality over time in the ZWIN'94 polder for different added weight percentages of bentonite

Since the ZWIN'94 polder was (part of) an estuary and thus uninhabited, the calculated mortality is fictitious. It is only used to demonstrate the effect of the bentonite on the mortality. As the results of the calculation show, the mortality for sand and the two lower percentage mixtures show distinct peaks. In contrast to those peaks, the mortality of the minimum necessary bentonite percentage shows no peak. Those peaks are because the inundation velocity and water depth dictate the use of the second formula. For the 5.4% mixture the inundation velocity does not get higher than 0.5 m/h and thus only the first formula (8.2) is used. As long as there is water in the polder, even if it rises very slowly, there is always a risk people lose their live. The first formula calculates the mortality due to this risk. As soon as the inundation velocity exceeds the threshold value, the mortality increases significantly, this is represented by the second formula.

By reducing the inundation velocity below the threshold value a significant decrease of the maximum mortality can be achieved. For each mixture the maximum mortality and the reduction of the mortality compared to the sand dike is given in Table 20.

	Maximum mortality [-]	***Fraction [-]***
Sand	0.0415	1
Sand-bentonite 1.2%	0.0388	0.93
Sand-bentonite 2.4%	0.0356	0.86
Sand-bentonite 5.4%	0.0046	0.11

Table 20 - Maximum mortality and fraction of mortality compared to sand

As these results show, lowering the inundation velocity below the threshold value decreases the maximum mortality almost by a factor 10. Since there will actually not be a catastrophic dike breach, the mortality will be reduced by more than a factor 10. The ZWIN'94 polder was an estuary and thus always contained water, the minimum water depth in the polder was 1.3 metres. At this water depth the mortality is 0.0029 (calculated with (8.2)). The maximum mortality for the 5.4% mixture when no breach occurs is equal to that value (0.0029) and thus a reduction of more than a factor 10 can be achieved.

9 Solution in practice

The presented solution is based on results from laboratory tests and the model results for the ZWIN'94 dike, which show it can lower the mortality. There are, however, some practical aspects which need to be addressed. In this chapter a possible in-situ execution method is described, a cost indication for improving the norm dike using the presented solution is given and cases from a sensitivity study of dike breaches in the Netherlands are discussed.

9.1 Execution

In appendix A a method for in-situ mixing is mentioned, Shallow or Deep Soil Mixing (SSM or DSM), which is a form of Mixed-In-Place (MIP). This technique is used to mix an additive with soil, without removing the soil, i.e. in-situ. The additive can be added to the soil as a slurry or in dry form. The soil is mixed with the additive using a triple auger, which drills into the soil and simultaneously mixes the soil (Bauer, 2014). Figure 54 gives an impression of the technique and equipment.

Figure 54 - Mixed-In-Place (MIP) technique (left) and triple auger drill (right) (Bauer, 2014)

With this technique a limited amount of soil is mixed with one pass of the augers. By repeating the process, an entire dike can be mixed with an additive. Since it is possible to mix the soil with an additive in dry form, it is possible to mix sand with bentonite using MIP.

9.2 Costs

In this section an indication of the costs for mixing bentonite with sand using MIP is given, which are compared with the costs of a standard dike reinforcement.

Costs in-situ mixing of sand-bentonite

Using bentonite to improve sand dikes is a new method, which means no information about the costs of this solution is available. By using characteristic prices an indication for the costs can be given. These are the price for bentonite and the price for MIP. The price for bentonite used in the laboratory experiments was provided by the supplier of the bentonite (Cebo Holland B.V., 2014) and is €211 per 1000 kg or 0.211 €/kg. This is assumed to be a representative price.

The price for MIP is estimated to be between $50 and $100 per cubic metre (Bruce, et al., 1998). To be able to compare to the costs of a standard dike reinforcement (calculated in 2011), it is corrected for inflation and converted to euros. The inflation correction is based on the inflation between 1998 and 2011, which is 38% (US Inflation Calculator, 2014). The exchange rate between the US Dollar and the Euro on the first of January 2011 was 0.75 €/USD (XE, 2014). After correction and conversion, the price for MIP is between €52 and €103 per cubic metre ($€_{'11}=\$_{'98}\cdot 1.38\cdot 0.75$).

Using these prices, the indicative costs are calculated. As an example, these are calculated for the ZWIN'94 dike with the bentonite percentages used for modelling. This is calculated for the dike with original and twice the crest height. The increase in crest height is to get an indication for the costs of a larger dike than the ZWIN'94 dike. Due to the increased crest height, also the inner and outer slope lengthen, which is taken into account in the calculation. The results of these calculations and the costs range per kilometre of dike are given in Table 21 and Table 22.

Bentonite [%]	*Dike [m^3/m]*	*Bentonite [kg/m]*	*Bentonite [€/m]*	*MIP [€/m]*	*Costs range [million €/km]*
1.2	36.3	694	146	1873 - 3746	**2.0 - 3.9**
2.4	36.3	1387	293	1873 - 3746	**2.2 - 4.0**
5.4	36.3	3132	661	1873 - 3746	**2.5 - 4.4**

Table 21 - Indication of costs per kilometre of ZWIN'94 dike

Bentonite [%]	*Dike [m^3/m]*	*Bentonite [kg/m]*	*Bentonite [€/m]*	*MIP [€/m]*	*Costs range [million €/km]*
1.2	103.8	1980	481	5348 - 10697	**5.8 - 11.1**
2.4	103.8	3961	836	5348 - 10697	**6.2 - 11.5**
5.4	103.8	8945	1887	5348 - 10697	**7.2 - 12.6**

Table 22 - Indication of costs per kilometre of ZWIN'94 dike (2x crest height)

Based on these calculations a first indication of the costs is given. The costs for improving the dike with bentonite are between 2.5 and 12.6 million euros per kilometre of dike. This range applies to the ZWIN'94 dike with original and twice the crest height and the determined necessary minimum percentage of bentonite. These calculations also show that the largest part of the costs is determined by the execution method. This is because the costs of MIP per cubic metre are approximately three times the costs of bentonite per cubic metre, or even higher.

Costs standard reinforcement

A standard dike reinforcement uses the normal design philosophy, e.g. heightening, widening or strengthening of the dike. The standard reinforcement does not reduce the mortality rate but reduces the probability of inundation (P_f). This has the same effect on the safety, as the LIR formula (1.1) in section 1.1 shows.

The standard dike reinforcement has already been studied for dikes in the Netherlands. This research looked into, among others, the costs for increasing the

safety by a factor 10 in 2050 with a normal dike reinforcement (Deltares, 2012), (Deltares, 2011a). These studies are part of a flood risk project in the Netherlands called 'Waterveiligheid 21e Eeuw' (Deltares, 2011c). This research includes new insights into the piping mechanism and length effects on the failure chance of dikes, for a better costs determination (Deltares, 2011b). For each dike section in the Netherlands the costs, risk, casualties and economic damage were determined (Deltares, 2012). The necessary dike reinforcement to meet the new safety level is expressed as a fictional height on top of the dike crest. This height is a translation of widening and heightening of the dike, adding a berm against piping or structural solutions. These dike reinforcement methods are shown in Figure 55. A cost formula is formulated to express the costs as function of this fictional height, which gives the costs of the necessary dike reinforcement (Deltares, 2011b). For a few dike sections in the Netherlands these costs are given in Table 23, to give an indication of the order of magnitude and costs range.

Dike section	*Location*	*Length [km]*	*Total costs [million €]*	*Costs [million €/km]*
5-1-1	Texel	1	3	3.0
5-1-2	Texel	25	115	4.6
13-1-1	N-Holland-N	12	84	7.0
13-1-2	N-Holland-N	3	44	14.7
13-1-3	N-Holland-N	6	32	5.3
13-1-4	N-Holland-N	6	88	14.7

Table 23 - Costs reinforcement of dike sections (Deltares, 2012)

Comparison of costs

The costs of a bentonite improved dike and a standard reinforced dike are compared to each other. The range of costs of the standard reinforced dikes is between 3.0 and 14.7 million euros per kilometre of dike. The indicative costs of the bentonite improved dike range from 2.5 to 12.6 million euros per kilometre of dike. These cost ranges are of the same order of magnitude and similar to each other. Based on this crude cost comparison it can be concluded that improving the dike with bentonite is not more expensive than a standard dike reinforcement.

In the Netherlands a full scale test of MIP for dike reinforcement was executed. For this test the inner slope of the 'Lekdijk' was reinforced with cement using MIP (Ceelen, 2008). This test was also used to estimate the costs of such a reinforcement. According to this estimation, the costs were between €2500 and €4500 per metre or 2.5 to 4.5 million euros per kilometre of dike. This estimation is within the same order of magnitude as the cost indication of the bentonite improved dike. The range of this estimation is smaller than the calculated costs, which might be because the technique was only tested in one dike.

However, some remarks about this cost comparison need to be made. The cost calculation of the sand-bentonite dike is very crude and needs refining. In this calculation it is assumed that the determined minimum percentage of bentonite for the ZWIN'94 dike applies for all dikes. This is most likely not true, since this percentage depends on a lot of variables, which are different for each dike.

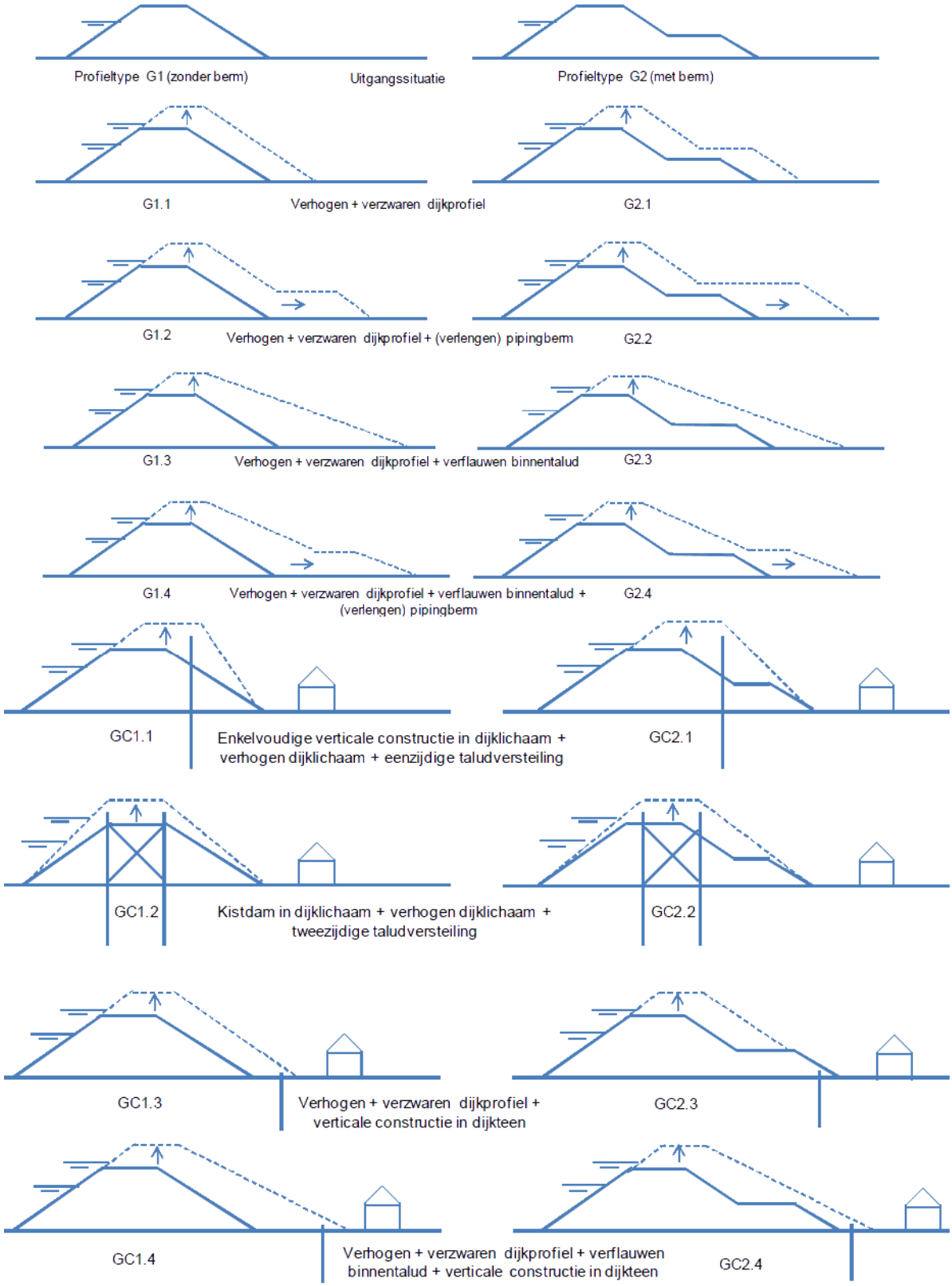

Figure 55 - Standard dike reinforcement methods (in Dutch) (Deltares, 2011b)

9.3 Cases

To see what the effects of retarding the breaching process are in practice, a few cases are discussed. As mentioned in section 9.2, a flood risk project is being executed in the Netherlands. For this project an inundation model (Sobek 1D/2D) is used to determine the consequences of a flood due to a dike breach; this project part is called 'Veiligheid Nederland in Kaart 2' (VNK2), which means 'Flood Risk in the Netherlands' (FLORIS). The safety is determined for all dike sections and multiple breach locations in such a section. For some of these breach locations a sensitivity study was executed, to determine the effect of a slightly larger final breach width. In the model this was simulated by increasing the final breach width by 5%. The results of this sensitivity study is used to show the difference in consequences between a normal and an increased final breach width. Due to limited access to data, the used cases are for dike ring 5 and 13, Texel and North-Holland (same as the cost calculation). The cases which are used are given in appendix I (VNK2, 2014), containing the following information:

- Case and dike ring number
- Outside water body and breach location
- Name of scenarios for normal width (B) and increased with (B+5%)
- Exceedance frequency of outside water level used in the model
- Inhabitants of the flooded area for both scenarios
- Number of casualties for both scenarios (without evacuation)
- Mortality for both scenarios (=casualties/people in flooded area)
- Total damage in million euros for both scenarios
- Ratio of casualties, mortality and damage between both scenarios

Using these cases and scenarios, a first comparison between a flood with a normal (B) and increased (B+5%) breach width is made. For each case the number of casualties for both scenarios is presented in Figure 56. As this figure shows, the number of casualties for an increased breach width is (almost) always higher than for a smaller breach width. Partially this is because in some cases a larger breach width increases the number of people which are affected (i.e. the inundated area increases), increasing the number of casualties. However, this does not explain the total increase in casualties.

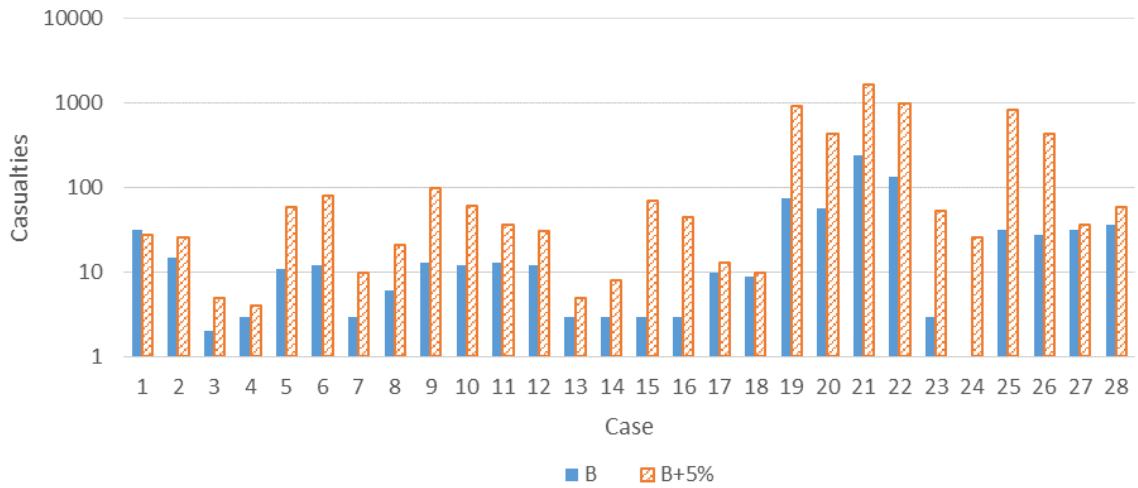

Figure 56 – Casualties of each case for scenario B (solid columns) and B+5% (dashed columns)

For a better comparison of the scenarios the difference in mortality is determined. In Figure 57 the mortalities for the scenarios of each case and the differences in mortality between the scenarios (ΔM=M(B)-M(B+5%)) is given.

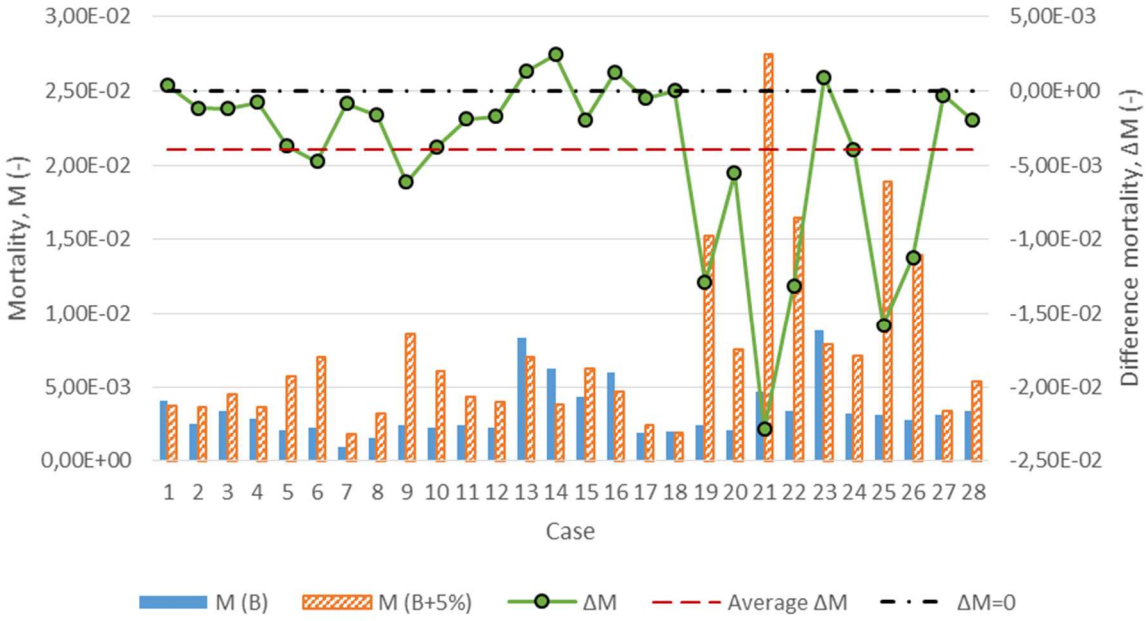

Figure 57 - Comparison of mortality between B and B+5%; columns give mortality per case for scenario B and B+5% (left axis); solid line is difference between scenario B and B+5% per case, dashed-dotted line is difference of zero and dashed line is average of this difference (right axis)

As can be determined from this figure, the mortality of the B+5% scenarios is almost always higher than the mortality of the B scenarios. This results in a negative difference in cases where M(B)<M(B+5%) and a positive difference in the other cases. A positive difference can be caused by a disproportional increase of the number of casualties compared to the number of people in the flooded area, between the two scenarios. Which means more people lose their lives, while the number of affected people does not increase as much. Because it is almost always a negative difference (ΔM<0), the average difference in mortality of all cases is smaller than zero. This means that a reduction of the breach width reduces mortality in case of a flood.

To visualize the reduction of casualties and therefore mortality, three randomly selected cases are presented in more detail. For these three cases the number of casualties per grid cell of the model is given for both scenarios. This is presented for case 9, 21 and 25 in Figure 58, Figure 59 and Figure 60. In these figures differently coloured squares are visible, each colour corresponds to a number of casualties in a square. The yellow dot in the figures is the location of the breach. For each case the total number of casualties for each scenarios is:

- Case 9: Casualties scenario B is 13 and casualties scenario B+5% is 98
- Case 21: Casualties scenario B is 239 and casualties scenario B+5% is 1666
- Case 25: Casualties scenario B is 32 and casualties scenario B+5% is 842

As these cases illustrate, the effect of a decreased final breach width can be really significant. Since the final breach width can be decreased by adding bentonite to a dike, this can be an effective solution for decreasing the mortality.

Figure 58 – Comparison of casualties per grid cell of case 9, scenario B (left) and B+5% (right)

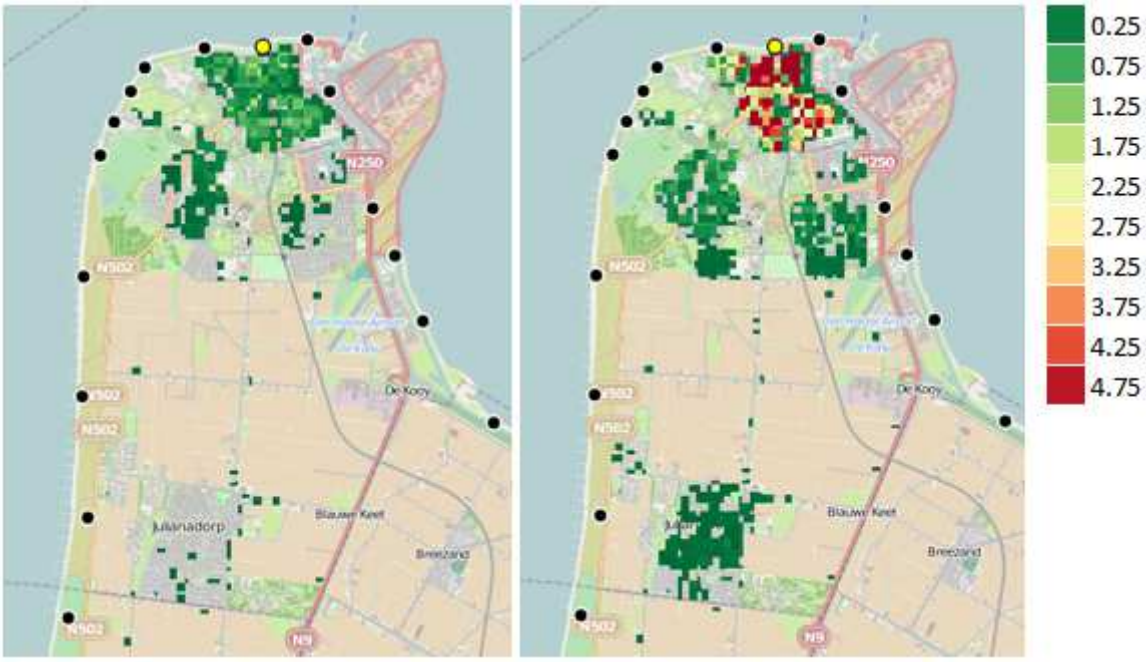

Figure 59 - Comparison of casualties per grid cell of case 21, scenario B (left) and B+5% (right)

Figure 60 - Comparison of casualties per grid cell of case 25, scenario B (left) and B+5% (right)

10 Conclusions and recommendations

In this chapter the conclusions of this thesis are given, as well as recommendations for further research.

10.1 Conclusions

The literature research, experimental results and model results in this thesis can be summarised in a main conclusion:

> **Decreasing the erosion rate of sand with bentonite can lead to significant reductions in breach width, breach flow and inundation velocity. Depending on the circumstances this may result in a decrease of mortality and thus an increase in safety, even with a factor 10.**

The solution presented in this thesis to decrease the erosion rate of sand and thus retard the breaching process is adding bentonite to sand (Figure 40). Since the permeability of the sand is reduced, this solution can also retard or stop piping underneath a sand dike. Only a few percent added bentonite achieves a significant decrease of important breach parameters (Figure 51) and might even stop the breaching process completely. This retarding of the breaching process can have a significant reducing effect on the inundation velocity in a polder (Figure 52). Depending on the dike and polder this decrease of inundation velocity can result in a decreased mortality. Since the mortality is used to calculate the localized individual risk, this risk can be reduced. The reduction of this risk means an increase in safety for inhabitants of a polder. The necessary percentage of added bentonite to increase the safety to a desired level (increase of a factor 10), is different for each case. For the ZWIN'94 experiment this would be a weight percentage of 5.4% (Figure 53). This low percentage does not negatively affect the strength of sand, which means that the dike keeps its original stability and bearing capacity.

A sensitivity study of an inundation model in the Netherlands shows that the mortality can be decreased significantly by decreasing the final breach width (Figure 57), thus increasing the safety. As the results of this thesis show, this can be achieved by adding bentonite to a dike. The retarding of the breaching process with bentonite is achieved without altering the shape, width or height of the dike. With the Mixed-In-Place method existing dikes can be made safer without the drawbacks of traditional dike reinforcement (like increased space consumption). This makes the solution especially interesting for dike improvements for which there is limited space or if there are buildings close to the dike. New dikes with added bentonite can have a higher safety level compared to a traditional dike with the same dimensions. This can be achieved by pre-mixing sand with bentonite, which is relatively simple. The indication of the costs for bentonite improvement of existing dikes shows that these could be of the same order of magnitude as traditional dike reinforcement.

Besides adding bentonite to a dike, it can also be concluded that sand with an initial small percentage of clay can have a similar effect. Due to this it is not necessary to use clean sand for dike construction, but slightly 'polluted' sand might actually be a better option. This only applies when the clay content in the sand does not affect the strength or stability of the dike. The retarding effect of clay in sand probably varies, depending on the type of clay and clay content.

10.2 Recommendations

In this thesis a lot of research results are presented, which lead to several conclusions. Apart from these conclusions, also some recommendations for further research are made.

A lot of options derived from literature are presented and some of those were discarded due to insufficient available research. However, these options might be promising and should be subjected to more experimental research, e.g. biological improvement of sand. In this thesis bentonite is marked as the preferred clay due to its large swelling capacity. Research with other clay types might find a comparable effect while using cheaper or better available clay, although this depends on the location of the dike.

Besides more research of discarded options, the presented solution needs more research as well. This is necessary to improve calculations of the erosion rates and predictions of the retarded breaching process. Which is also necessary to explain the difference between the erosion measurements and the outcome of the Van Rhee formula (Figure 46). The experiments were only executed for two percentages and one approximate density. To learn about the effects at higher percentages and other densities, more tests should be executed. This could lead to determination of an optimum bentonite percentage, resulting in a higher erosion reduction. Besides variation of the mixture parameters, the mixtures should also be tested at higher flow velocities. The current calculations are based on the effect on the erosion rate, but are not validated with breach tests. To see the effect of bentonite on the breaching process, also scale model and full scale breach tests of dikes should be executed.

This research shows that adding bentonite is a technical feasible option to increase the safety level. However, it is also necessary to determine if it is a practical feasible option and if it is economically attractive to use this solution. It should be researched in what cases this would be a more practical and economical option than traditional dike improvement. A possible execution technique is described in this thesis. Before this technique can be applied, it is necessary to research the drawbacks and limitations of this technique. The technique should also be tested for mixing bentonite with sand to find and address unexpected issues which may arise. For example, it needs to be determined if mixing bentonite into saturated sand is possible or it is necessary to dewater the dike before mixing. It is also necessary to determine whether the density of the sand after mixing is as desired or that additional measures are necessary to achieve this.

The cost calculation presented in this thesis is just an indication. For a comprehensive overview of the costs for mixing bentonite with sand in a dike, more research into these costs is necessary. Besides more research into the costs, more research is necessary into the effects of a bentonite improved dike on a flood. In this thesis this is only shown by means of a sensitivity study, but could be more elaborate if all the effects of bentonite on the breaching process are taken into account in an inundation model.

List of figures

Cover image - Breach in an unknown dike during the flood of 1953, adapted from: http://www.isgeschiedenis.nl/nieuws/watersnoodramp-van-1953/ [Accessed December 2013].

List of tables

References

Akbulut, S. & Saglamer, A., 2002. Estimating the groutability of granular soils; a new approach. *Tunneling and underground space technology,* Issue 17, pp. 371-380.

Akbulut, S. & Saglamer, A., 2004. Modification of hydraulic conductivity in granular soils using waste materials. *Waste Management,* Issue 24, pp. 491-499.

Anagnostopoulos, A., 2005. Laboratory study of an injected granular soil with polymer grouts. *Tunnelling and Underground Space Technology,* Issue 20, pp. 525-533.

Anagnostopoulos, A., Papaliangas, T., Manolopoulou, S. & Dimopoulos, T., 2011. Physical and mechanical properties of chemically grouted sand. *Tunnelling and Underground Space Technology,* Issue 26, pp. 718-724.

Bauer, 2014. [Online]
Available at:
http://www.bauerfoundations.com/shared/_content/bst/competences/construction_method/en/Mixed_in_Place_details.html
[Accessed April 2014].

Bauer, 2014. *Bauer Dam Rehabilitation.* [Online]
Available at:
http://www.bauerdamrehabilitation.com/export/sites/www.bauerdamrehabilitation.com/en/documents/MIP_en.pdf
[Accessed April 2014].

Bisschop, F., Visser, P., Van Rhee, C. & Verhagen, H., 2010. *Erosion due to high flow velocities: A description of relevant processes,* Delft, The Netherlands: s.n.

Bos, R., Van den Berg, F., De Kant, M. & Looij, R., 2010. Mixed-in-Place: Leren van Praktijkproef Lekdijk. *Land+Water,* November, Issue 11.

Bruce, D., Bruce, M. & DiMillio, A., 1998. *Geosystems, L.P.*. [Online]
Available at:
http://www.geosystemsbruce.com/v20/biblio/z140%20Deep%20Mixing%20Method%20-%20A%20Global%20Perspective.pdf
[Accessed March 2014].

Carter, M. & Bentley, S., 1991. *Correlations of soil properties.* London, UK: Pentech Press.

Cebo Holland B.V., 2014. *Cebo Holland.* [Online]
Available at: http://www.cebo.com/nederland/
[Accessed 03 2014].

Cebo Holland B.V., 2014. *Cebogel Sealfix.* [Online]
Available at: http://www.cebo.com/nederland/nl/bentoniet/cebogel-sealfix.html
[Accessed 27 February 2014].

Ceelen, T., 2008. *Smet-Keller*. [Online]
Available at: http://www.smet-keller.nl/wp-content/downloads/137.Pubicatie.Otar.MIP_33-36_DEF.pdf
[Accessed April 2014].

Chapuis, R. & Aubertin, M., 2003. On the use of the Kozeny-Carman equation to predict the hydraulic conductivity of soils. *Canadian Geotechnical Journal,* Issue 40, pp. 616-628.

Cheng, L. & Cord-Ruwisch, R., 2012. In situ soil cementation with ureolytic bacteria by surface percolation. *Ecological engineering,* Issue 42, pp. 64-72.

Cheng, N. & Chua, L., 2005. Comparison of sidewall correction of bed shear stress in open-channel flow. *Journal of Hydraulic Engineering.*

Cornell University, 1990. *Manual on estimating soil properties for foundation design*. Ithaca, New York, USA: s.n.

Dano, C., Hicher, P. & Tailliez, S., 2004. *Engineering Properties of Grouted Sands.* s.l.:s.n.

De Baets, S. & Poesen, J., 2010. Empirical models for predicting the erosion-reducing effects of plant roots during. *Geomorphology,* Issue 118, pp. 425-432.

De Baets, S., Poesen, J., Gyssels, G. & Knapen, A., 2005. Effects of grass roots on the erodibility of topsoils during concentrated flow. *Geomorphology,* Issue 76, pp. 54-67.

De Boer, G., 2002. *On the consolidation and erosion of cohesive sediments,* Delft, The Netherlands: TU Delft.

DeJong, J., Fritzges, M. & Nüsslein, K., 2006. Microbially Induced Cementation to Control Sand Response. *Journal of Geotechnical and Geoenvironmental Engineering,* 132(11).

Deltares, 2011a. *Analyse van Slachtofferrisico's Waterveiligheid 21e Eeuw,* Delft, the Netherlands: s.n.

Deltares, 2011b. *Kosten van Maatregelen Waterveiligheid 21e Eeuw,* Delft, The Netherlands: s.n.

Deltares, 2011c. *Maatschappelijke kosten-batenanalyse Waterveiligheid 21e Eeuw,* Delft, The Netherlands: s.n.

Deltares, 2012. *Factsheets Basisinformatie Waterveiligheid 21e Eeuw,* Delft, The Netherlands: s.n.

Ferris, F., Stehmeier, L., Kantzas, A. & Mourits, F., 1997. Bacteriogenic mineral plugging. *The Journal of Canadian Petroleum Technology,* 35(8).

Finish Beton Groep, 2014. *Confiber Construction Fibre*. [Online]
Available at: http://www.betongroep.nl/index-en.html
[Accessed 27 February 2014].

Finish Beton Groep, 2014. *Finish Beton Groep.* [Online]
Available at: http://www.betongroep.nl/
[Accessed March 2014].

Floodsite, 2009. *Breaching Process: A state of the art review,* s.l.: s.n.

Gailani, J., 2001. Effects of Bentonite clay on sediment erosion rates. *DOER.*

Geotechdata.info, 2013. *Falling head permeability test.* [Online]
Available at: http://www.geotechdata.info/geotest/falling-head-permeability-test.html
[Accessed 27 February 2014].

Geotechdata.info, 2013. *Soil permeability coefficient.* [Online]
Available at: http://www.geotechdata.info/parameter/permeability.html
[Accessed 27 February 2014].

Gray, D., ASCE, A. & Ohasi, H., 1983. *Mechanics of fiber reinforcement in sand,* s.l.: s.n.

Harkes, M. et al., 2010b. *Adapting Soil Properties by Pore Space Engineering.* Delft: Deltares.

Hejazi, S., Sheikhzadeh, M., Abtahi, S. & Zadhoush, A., 2012. A simple review of soil reinforcement by using natural and synthetic fibers. *Construction and building materials,* Issue 30, pp. 100-116.

Hoek, E., 1990. Estimatin Mohr-Coulomb friction and cohesion values from the Hoek-Brown failure criterion. *International Journal of Rock Mechanics and Mining Sciences,* 27(3), pp. 227-229.

Holtz, R. & Kovacs, W., 1981. *An Introduction to Geotechnical Engineering.* s.l.:Prentice-Hall.

Jacobsen, H. & Magda, W., 1988. *Erosion and pore pressure gradients.* s.l.:s.n.

Jasperse, B., 2012. *Geo-Con Inc..* [Online]
Available at: http://www.geocon.net/pdf/paper03.pdf
[Accessed March 2014].

Jonkman, B., 2004. *Methode voor de bepaling van het aantal slachtoffers ten gevolge van een grootschalige overstroming,* Delft: Dienst Weg- en Waterbouwkunde.

Jonkman, B., 2007. *Loss of life estimation in flood risk assessment,* Delft, The Netherlands: TU Delft.

Le Hir, P. et al., 2008. *Erodibility of natural sediments: experiments on sand-mud mixtures from laboratory and field erosion tests,* s.l.: Sediment and Ecohydraulics.

Léonard, J. & Richard, G., 2004. Estimation of runoff critical shear stress for soil erosion from soil shear strength. *Catena,* Issue 57, pp. 233-249.

Lick, W., Lick, J., Jin, L. & Gailani, J., 2007. Approximate equations for sediment erosion rates. *Estuarin and coastal fine sediments dynamics.*

Liu, X. & Chiew, Y., 2012. Effect of Seepage on Initiation of Cohesionless Sediment Transport. *Act geophysica,* 60(6), pp. 1778-1796.

Louws, D. & Van der Weijde, P., 1995. *Meetverslag bresgroeiproeven Zwin 6 en 7 oktober 1994,* Vlissingen, The Netherlands: Rijkswaterstaat.

Maalej, Y., Dormieux, L., Canou, J. & Dupla, J., 2007. Strength of a granular medium reinforced by cement grouting. *C. R. Mecanique,* Issue 335, pp. 87-92.

Martin, C., 1970. Effect of a Porous Sand Bed on Incipient Sediment Motion. *Water resources research,* 6(4).

Mollins, L., Stewart, D. & Cousens, T., 1996. Predicting the properties of bentonite-sand mixtures. *Clay Minerals,* Issue 31, pp. 243-252.

Moust-Jacobsen, H. & Magda, W., 1988. *Erosion and Pore Pressure gradients.* Aalborg: s.n.

Peeters, P., Van Hoestenberghe, T., Vincke, L. & Visser, P., 2011. *SWOT Analysis of breach models for common dike failure mechanisms.* Brisbane, Australia, s.n.

Rao, A. & Sitaram, N., 1999. Stability and Mobility of Sand-Bed Channels Affected by Seepage. *Journal of irrigation and drainage engineering,* Issue 125, pp. 370-379.

Rijkswaterstaat, 2006. *Veiligheid Nederland in Kaart - Inschatting van het aantal slachtoffers ten gevolge van overstroming,* s.l.: s.n.

Robijns, T., 2012. *Gevoeligheidsstudie van het BRES-model,* Delft, The Netherlands: s.n.

Sallfors, G. & Oberg-Hogsta, A., 2002. Determination of hydraulic conductivity of sand-bentonite mixtures for engineering purposes. *Geotechnical and Geological Engineering,* Issue 20, pp. 65-80.

Schnaid, F., Prietto, P. & Consoli, N., 2001. Characterization of cemented sand in triaxial compression. *Journal of Geotechnica and Geoenvironmental Engineering,* 127(10).

Segetin, M., Jayaraman, K. & Xu, X., 2007. Harakeke reinforcement of soil–cement building materials: Manufacturability and properties. *Building and environment,* Issue 42, pp. 3066-3079.

Smolders, L., 2010. *Feasibility study of a Climate Dike,* Delft, The Netherlands: TU Delft.

Substruck Ltd., n.d. *Pressure Grouting.* [Online]
Available at: http://www.substruck.ie/wp-content/themes/substruck/images/Grout-Model.jpg
[Accessed 2013].

The Constructor, 2012. *Shear strength of soil by direct shear test.* [Online]
Available at: http://theconstructor.org/geotechnical/shear-strength-of-soil-by-direct-shear-test/3112/
[Accessed 27 February 2014].

Tonneijck, M. & Weijers, J., 2008. *Lecture Notes CT5314 Flood Defences.* Delft, The Netherlands: TU Delft.

US Inflation Calculator, 2014. *US Inflation Calculator.* [Online]
Available at: http://www.usinflationcalculator.com/
[Accessed March 2014].

Van Gerven, K., 2004. *Dijkdoorbraken in Nederland - Ontstaan, voorkomen en bestrijden,* Rotterdam, The Netherlands: TU Delft.

Van Paassen, L. et al., 2010. Quantifying biomediated ground improvement by ureolysis: Large-scale biogrout experiment. *Journal of Geotechnical and Geoenvironmental Engineering,* 136(12).

Van Rhee, C., 2010. Sediment Entrainment at High Flow Velocity. *Journal of Hydraulic Engineering,* September.

Van Rhee, C. & Bezuijen, A., 1992. Influence of seepage on stability of sandy slope. *Journal of Geotechnical Engineering,* 118(8).

Van Rhee, C. & Talmon, A., 2010. Sedimentation and erosion of sediment at high solids concentrations. *BHR Group.*

Van Rijn, L., 1984. Sediment pick-up functions. *Journal of Hydraulic Engineering,* 110(10).

Verhagen, H., Fooks, J., Algera, A. & Vu, M., 2008. *The use of vetivers in coastal engineering,* Dubai, UAE: s.n.

Visser, P., 1998. *Breach growth in sand-dikes,* Dordrecht, The Netherlands: TU Delft.

VNK2, 2014. *Lizard Flooding.* [Online]
Available at: http://flooding.lizard.net/ (restricted, access granted for this thesis by VNK2)
[Accessed April 2014].

VNK2, 2014. *Lizard Flooding,* s.l.: VNK2.

XE, 2014. *XE.* [Online]
Available at: http://www.xe.com/currencytables/?from=USD&date=2011-01-01
[Accessed March 2014].

Yasuhara, H., Neupane, D., Hayashi, K. & Okamura, M., 2012. Experiments and predictions of physical properties of sand cemented by enzymatically-induced carbonate precipitation. *Soils and foundations,* Issue 52(3), pp. 539-549.

Ye, S. & Verhagen, H., 1999. *Comparison and validation of two Dutch models of breach growth in sandy dikes.* Beijing, China, s.n.

Zhu, Y., 2006. *Breach growth in clay-dikes,* Delft, The Netherlands: s.n.

Appendices

A Further research of options

In this appendix the result of further research into the options is presented.

Bentonite clay and sand mixture

As already discussed in section 5.1.2 mixing bentonite with sand reduces the erodibility of sand. Even a small percentage of bentonite has a significant effect on the erosion rates. In this section a more detailed description of this option is given.

Principle

The erosion rate of soil is affected by several soil parameters like bulk density, particle size, mineralogy, organic content, trapped gas volume, salinity of pore waters, chemical reactions, and time after deposition. The addition of small amounts of clay minerals has a significant effect on erosion rates (Gailani, 2001). Of the known clay types, bentonite chemically bonds more water than most clay types. This increases the volume of the bentonite, which fills the pores in the sand. The reduction of the pore volume leads to a reduced permeability. This reduced permeability lowers the erosion rate of sand.

The effect of bentonite on the erosion rates of sand can be seen in Figure 61. The calculations of averages and determinations of the trendlines is explained in appendix B.

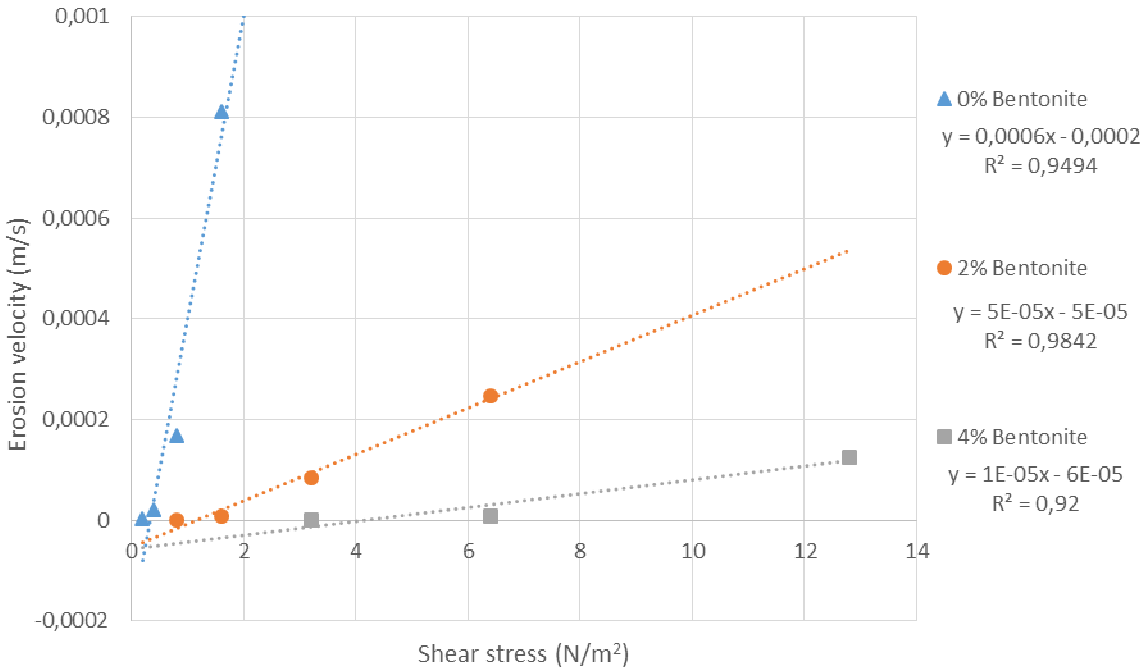

Figure 61 - Erosion velocities for different bentonite-sand mixtures (added bentonite percentage), measured at different shear stresses (composed using (Gailani, 2001))

This figure shows that to attain the same erosion velocity at higher added percentages of bentonite, the shear stress has to increase. Or to put it otherwise, for the same shear stress the erosion velocity decreases when the added percentage of bentonite is higher.

Change of soil parameters

The different erosion behaviour of sand-bentonite mixtures compared to sand is due to changes of the soil parameters. Bentonite affects the permeability of sand. Bentonite clay has great swelling potential when saturated. The volume increase for an unconfined bentonite powder is in the range of 200-1200% relative to a dry sample (Mollins, et al., 1996). Because of this high swelling capacity the pores in the sand get clogged, which reduces the permeability (or hydraulic conductivity) of the soil. This effect was studied (Sallfors & Oberg-Hogsta, 2002) and can be seen in Figure 62.

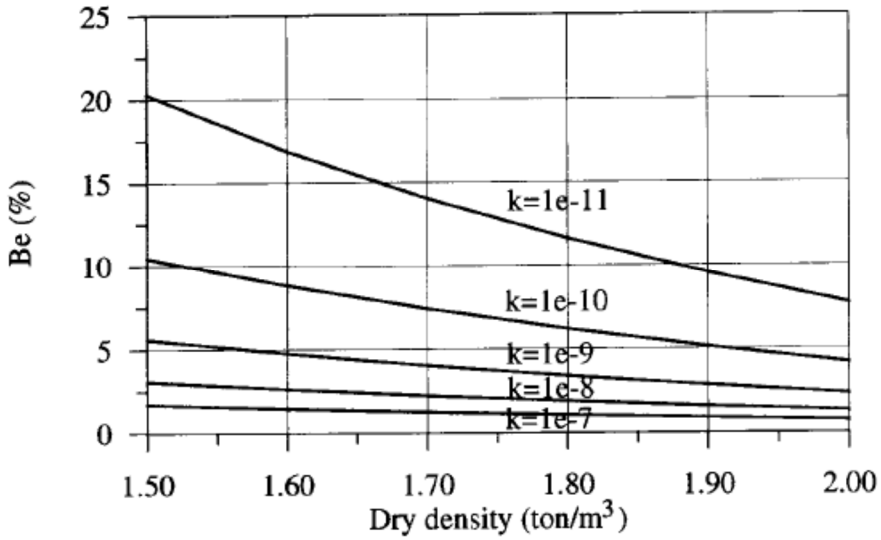

Figure 62 - Hydraulic conductivity (k in m/s) of a homogeneous sand-bentonite mixture as a function of percentage of bentonite versus dry density (Sallfors & Oberg-Hogsta, 2002)

Erosion formula

In literature several formulas for determining the erosion rate of a sediment mixture can be found. Formulas determined using the erosion of natural sediments, often a mixture of mud and sand, are given first. Adding mud to a sand bed increases the erosion threshold significantly, while the sand grains in the mud increase the shear strength. This shear strength increase is maximum at a weight fraction of the sand between 30% and 50%. Based on this phenomena, the critical shear stress depends on a power relationship with the dry bulk density of a sand-mud mixture (Le Hir, et al., 2008):

$$\tau_c = 0.015(\rho_{bulk} - 1000)^{0.73} \qquad \text{(A.1)}$$

in which:

τ_c = critical shear stress [N/m^2]
ρ_{bulk} = the bulk density of the sediment [kg/m^3]

This critical shear stress can be used in an erosion formula, determined from laboratory tests (Le Hir, et al., 2008):

$$E = E_1 \exp(-\kappa \tau_c^{\chi})(\tau - \tau_c) \qquad \text{(A.2)}$$

in which:
E = erosion rate [kg/m^2/s] (for ρ_{bulk}=1.85 kg/m^3)
E_1, κ, x = constants [-] (E_1=0.25, κ=8, x=0.5)

Another formula for determining the erosion rate is based on field measurements in salt- and freshwater (Le Hir, et al., 2008):

$$E = \rho_{dry}\beta(\tau - \tau_c) \tag{A.3}$$

$$\beta = 0.001\exp(-0.113S_c) \quad \text{(salt water)} \tag{A.4}$$

$$\beta = 0.003\exp(-0.063S_c) \quad \text{(fresh water)} \tag{A.5}$$

in which:
τ = applied shear stress [N/m^2]
ρ_{dry} = the dry density of the sediment [kg/m^3]
S_c = sand content [%]

These are basic formulas, based on only a few experiments or observations. Another study (Lick, et al., 2007) determined a set of formulas for a range of sediments, based on literature and experiments. These formulas are valid for particle sizes from 0.0057-1.35 mm and cohesive and non-cohesive sediments.

The general formula, for all particle diameters is:

$$E = 10^{-4}\left(\frac{\tau - \tau_{cn}}{\tau_c - \tau_{cn}}\right)^n \tag{A.6}$$

For small particle sizes (d≤0.125 mm), (A.6) becomes:

$$E = 10^{-4}\left(\frac{\tau}{\tau_c}\right)^n \tag{A.7}$$

For larger particle sizes (d≥0.222 mm), (A.6) becomes:

$$E = A(\tau - \tau_c)^n \tag{A.8}$$

In these formula, τ_c and τ_{cn} are determined using:

$$\tau_c = \left(1 + \frac{a\exp(b\rho_s)}{d^2}\right)\tau_{cn} \tag{A.9}$$

$$\tau_{cn} = 0.414 \cdot d \tag{A.10}$$

$$\tau_c - \tau_{cn} = \frac{0.414 \cdot a\exp(b\rho_s)}{d} \tag{A.11}$$

in which:

τ	= applied shear stress [N/m^2]
τ_{cn}	= critical shear stress for the erosion of non-cohesive particles [N/m^2]
n	= parameter determined using table 2 or 3 of (Lick, et al., 2007) [-]
A	= parameter determined using table 2 of (Lick, et al., 2007) [-]
a	= parameter determined using table 3 of (Lick, et al., 2007) [N/mm^2]
b	= parameter determined using table 3 of (Lick, et al., 2007) [cm^3/g]
d	= particle diameter [mm]
ρ_s	= density of the sediment [g/cm^3]

These formulas can also be used to calculate the erosion rate of a bentonite-sand mixture. For this the critical shear stress is calculated a bit differently, using:

$$\tau_c = \left(1 + \frac{a\exp(b\rho)}{d^2} + \frac{c_5}{c_3 d}\right)\tau_{cn} \quad \text{(A.12)}$$

$$c_3 = \frac{\pi(\rho_s - \rho_w)g}{6} \quad \text{(A.13)}$$

in which:

c_5	= parameter determined using table 4 or 5 of (Lick, et al., 2007)

Practical implementation

In order to benefit from the effects of bentonite on sand, the sand of needs to be mixed with bentonite. When building a new dike, this is no problem, since the sand and bentonite can be mixed before construction. However, for improvement of an existing sand dike, this becomes more difficult, since the sand and bentonite needs to be mixed in-situ. It is possible to use Shallow or Deep Soil Mixing (SSM or DSM) to mix the bentonite and the sand in-situ (Jasperse, 2012), (Bos, et al., 2010).

Fibres and sand mixture

The reinforcement of sand with fibres is described in section 5.1.3. In this section the result of further researched is given.

Principle

The main purpose of soil reinforcement is improvement of the stability, improvement of the bearing capacity, reduction of settlement, and reduction of deformation of a soil mass. This can be achieved by adding fibres to soil. A fibre reinforced soil mass contains randomly distributed fibres, which improve the mechanical behaviour of the soil mass (Hejazi, et al., 2012). These fibres can be divided into two categories, natural and synthetic fibres (Hejazi, et al., 2012). The most interesting fibres for application in a dike are the synthetic fibres: polyester (PET), polypropylene (PP), and glass fibres. Synthetic fibres, unlike natural fibres, do not deteriorate over time and maintain their strength. The PET fibre is interesting because short PET fibre reinforced soil shows a high resistance to piping. The glass fibre is able to increase the cohesion of cohesionless soil. PP fibres are already used for improvement of other

materials and might be interesting for improvement of sand. The principle of fibre reinforcement is shown in Figure 63.

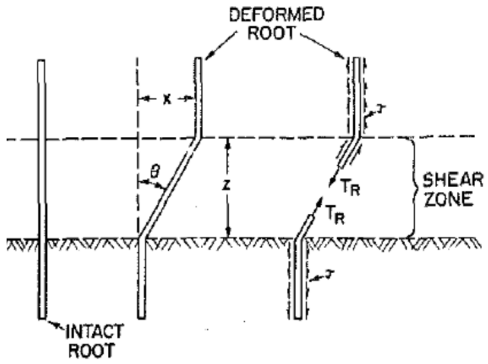

Figure 63 - Principle of fibre reinforcement (Gray, et al., 1983)

The fibres in the soil are randomly distributed, i.e. these have multiple orientations in the soil. These fibres mainly reinforce the soil by increasing its shear strength. In principle the fibres connect different layers in the soil, e.g. a shearing layer to a stable sub-layer, preventing shearing of that layer. The strength of this reinforcement depends on the fibre strength, elasticity, content, and length and the friction or cohesion between the fibres and the soil. Another factor influencing the shear strength is the confinement stress of the soil, which determines the friction between soil and fibres. This friction increases the resistance of fibres against being pulled out of the soil. Figure 64 is a sketch of fibre-soil interaction.

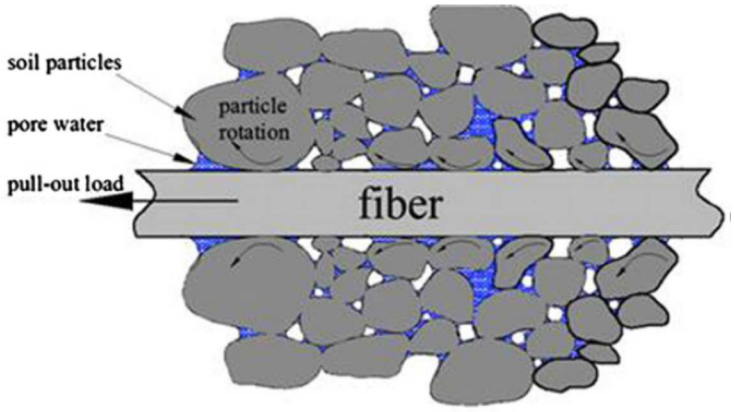

Figure 64 - Fibre-soil interaction (Hejazi, et al., 2012)

Change of soil parameters

As already mentioned, fibre reinforcement increases the cohesion and shear strength of the soil. For soil with randomly distributed fibres the shear strength (ΔS) increase can be calculated with (Hejazi, et al., 2012):

$$\Delta S = N_s(\pi \mathrm{d}_f{}^2/4)\cdot((2(\sigma_n \tan\delta)\cdot(\mathrm{L}_f/d_f))\cdot(\sin\theta+\cos\theta\tan\phi)(\xi) \quad \text{(A.14)}$$

$$N_s = (2\nu_f)/(\pi d_f{}^2) \quad \text{(A.15)}$$

in which:

v_f = volumetric fibre content

d_f = fibre diameter
σ_s = confining stress acting on the fibres
δ = angle of skin frictional resistance [°]
L_f = length of fibre
θ = angle of shear distortion [°]
φ = friction angle of sand [°]
ξ = empirical coefficient (to determine with experiments)

This model is only valid for extensible fibres with a frictional surface.

Erosion formula

For calculation of the erosion velocity of a fibre and sand mixture there are no formulas in literature. However, a fibre and sand mixture has a resemblance to a fibrous root system (e.g. the root system of grass). It is therefore assumed that erosion formulas for a soil-root system can be used to describe the erosion of a fibre-sand mixture. A deterministic formula for determining the erosion reduction of roots is given by (De Baets & Poesen, 2010):

$$RSD = \frac{V_e}{V_{e-bare}} = e^{-2.45RD+0.03RD\cdot sand\%} \tag{A.16}$$

in which:
RSD = Relative Soil Detachment [-]
V_e = erosion velocity of the soil-root system [m/s]
$V_{e\text{-}bare}$ = erosion velocity of bare soil [m/s]
RD = mass of fibres/volume of soil body [kg/m^3]
sand% = sand content of the soil [-]

RSD gives the fraction of the erosion velocity of a bare soil for a reinforced soil. A different formula based on the same parameter (RD) is (De Baets & Poesen, 2010):

$$RSD = \frac{V_e}{V_{e-bare}} = \frac{\left(RD^{-1.76}\right)}{\left(1.59 + RD^{-1.76}\right)} \tag{A.17}$$

This formula gives higher fractions of the erosion velocity, i.e. a smaller reduction, compared to (A.16). It should be noted that the above formulas are both determined for the erosion of topsoil on a hill slope during precipitation and thus for low flow velocities. Also the formulas are not calibrated for high sand contents (close to 100% in a dike). For fibres with a different behaviour than grass roots, it is not known if the formulas are accurate.

Practical implementation

Just as described for bentonite, the fibres need to be mixed into the sand. This is feasible when constructing a new dike, because the mixture can be made beforehand (Segetin, et al., 2007). For an existing dike, it needs to be mixed in-situ using the same techniques as the sand-bentonite option. Another execution problem is the prevention of clumping and balling of fibres (Hejazi, et al., 2012). When not mixed

properly the fibres can clump together or get folded (form balls) and the mixture will not be homogenous. Because of these problems it was found that fibres longer than 51 millimetres do not improve the soil properties significantly.

Reinforcement of sand by injection of grout

Grout injection is a frequently used technique for soil improvement, also known as permeation grouting. It is used to improve soil underneath a foundation, decrease the permeability of soil, create a connection between the soil and a structure, etc. The principle of grouting and its effect on the soil are discussed in this section.

Principle

Injection of grout, or grouting, is the injection of a cement-, chemical- or other additive-water mixture into the soil, to change the properties of the soil. The way soil is affected depends on the mixture ratio and the type of additive. Most common is the use of a cement-water mixture, but chemical-water mixtures (more often chemical-cement-water mixtures) are used as well. There is even research into the use of waste material as a grouting additive (Akbulut & Saglamer, 2004). For grouting of a sand dike the use of chemical additives is not preferred, since those could harm the environment or spoil the ground water. The use of cement-based grouts, possibly with natural additives, is preferred.

The injection grouting technique which is most relevant for the application in sand dikes is permeation grouting. This technique fills the accessible pores of a granular soil with grout, increasing its strength and reducing its permeability. The principle is shown in Figure 65.

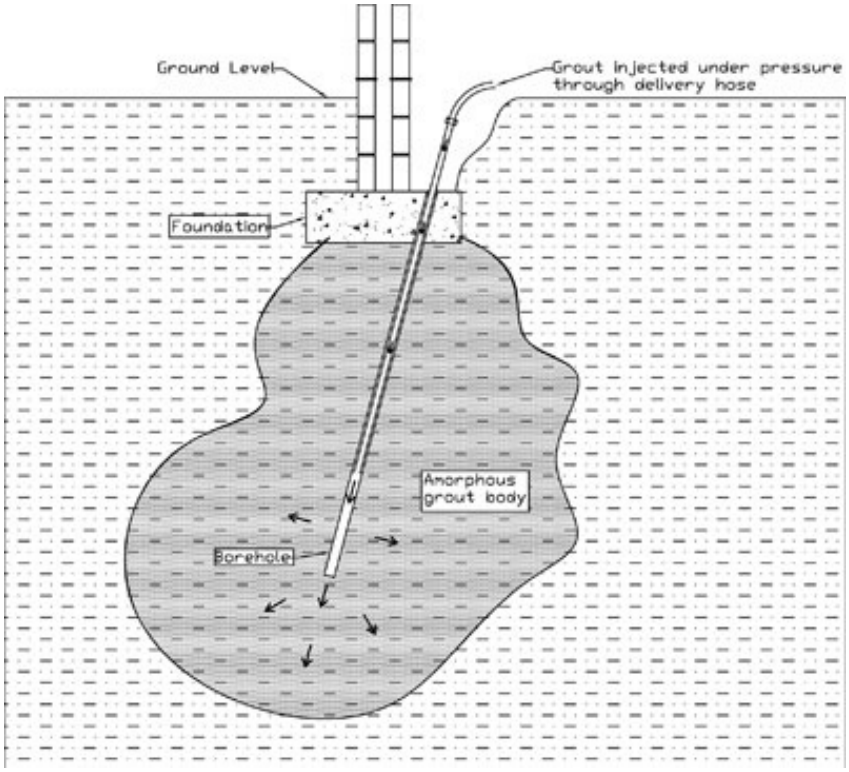

Figure 65 – Impression permeation grouting (Substruck Ltd., sd)

One of the main reasons grouting is used in practice, is to increase the compressive strength and elastic modulus of the original soil. Another reason is to decrease the permeability of soil, e.g. to prevent seepage of contaminated water. The effects of grouting on the soil properties are explained in the next section.

Change of soil parameters

Grouting changes the shear strength, compressive strength, cohesion, and permeability of soil. The increase in compressive strength depends on the cement-to-water (C/W) ratio of the grout material, as can be seen in Figure 66. If this ratio is higher, the grout contains more cement and therefore increases the compressive strength of the ungrouted soil.

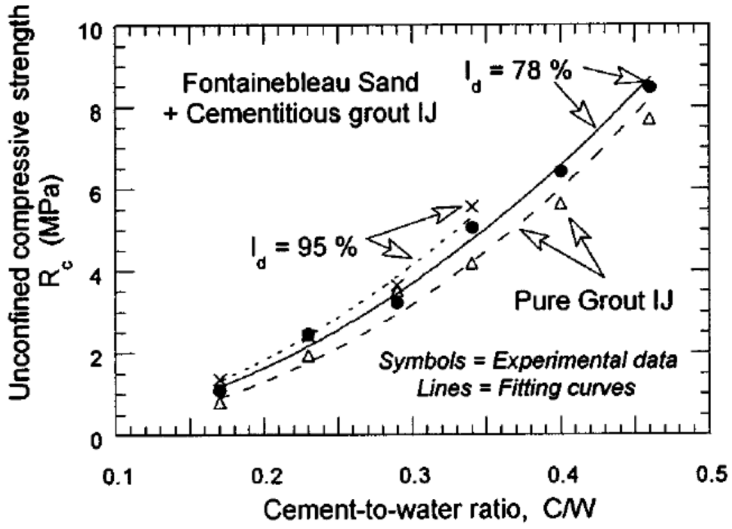

Figure 66 - Compressive strength as function of C/W ratio (Dano, et al., 2004)

Another relevant parameter is the cohesion of the soil, which is also increased by grouting. The cohesion depends on the cement-to-water ratio (C/E) and the cement fraction (percentage of cement in the soil, Φ_c), as is shown in Figure 67.

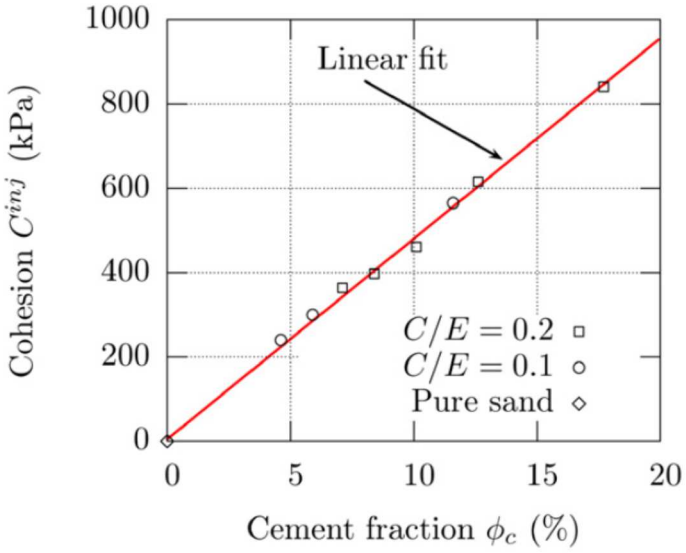

Figure 67 - Cohesion as function of the cement fraction (Maalej, et al., 2007)

A formula to calculate the cohesion of grouted soil is (Dano, et al., 2004):

$$c' = \frac{1-\sin\varphi'}{2\cos\varphi'} A_{soil}(D_r)^{1-n_1 \cdot D_r} \left(C/W\right)^{N(1-n_1 \cdot D_r)} \quad \text{(A.18)}$$

in which:

c'	= cohesion [MPa]
φ'	= internal angle of friction [°]
$A_{soil}(D_r)$	= depends on soil parameters (to be determined)
A_0, N	= experimental parameters (Table 2 (Dano, et al., 2004))
n_1	= constant [-]
D_r	= relative density [-]
C/W	= cement-to-water ratio [-]

Another relevant parameter is the permeability or hydraulic conductivity of the soil. Grouting reduces the permeability of soil. The effect of cement grout with different additives (clay, silica fume and fly ash) on the hydraulic conductivity of sand is studied (Akbulut & Saglamer, 2004). Adding clay to grout proved to be the most effective additive in reducing the hydraulic conductivity. With increasing clay content (CL%, percentage of clay in the grout), the hydraulic conductivity (K) decreases, as Figure 68 shows. Besides the clay content in the grout also the water-to-solid ratio (W/S) determines the effect on the hydraulic conductivity, which can be seen in Figure 69. If the ratio is smaller, thus a higher solid content in the mixture, the hydraulic conductivity is smaller as well.

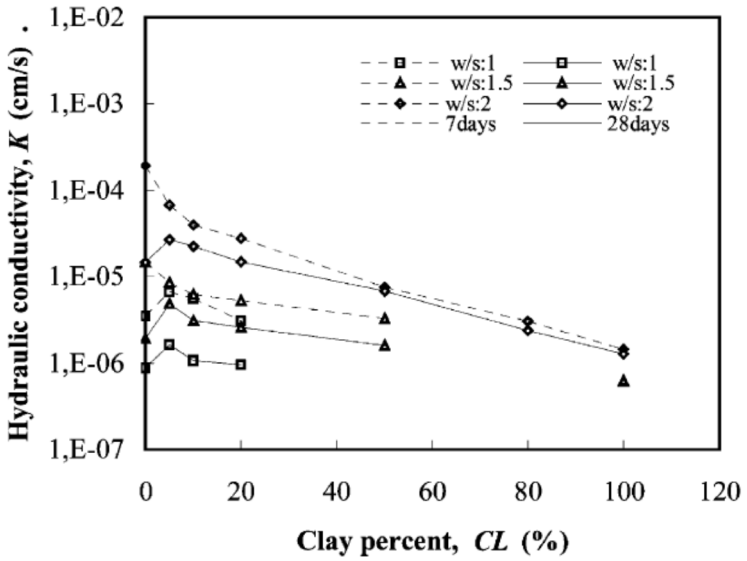

Figure 68 - K as function of CL% for different W/S ratios (Akbulut & Saglamer, 2004)

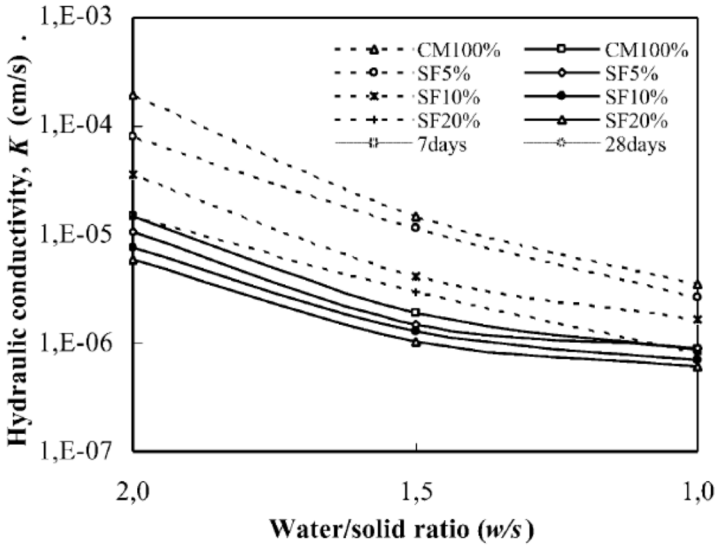

Figure 69 - Influence of the W/S ratio on K (Akbulut & Saglamer, 2004)

Erosion formula

Based on the influence of grouting on the soil parameters the erosion rate for grouted sand will have to be derived, since there are no known formulas for erosion of grouted sand.

Practical implementation

Permeation grouting is a known and frequently used technique, so the execution method for this option is well known. There are some effects which need to be taken into account when grouting sand. The volume of sand that is influenced by one injection is limited, since at some distance from the injection point the pressure is too low to push the grout further into the sand, as can be seen in Figure 70.

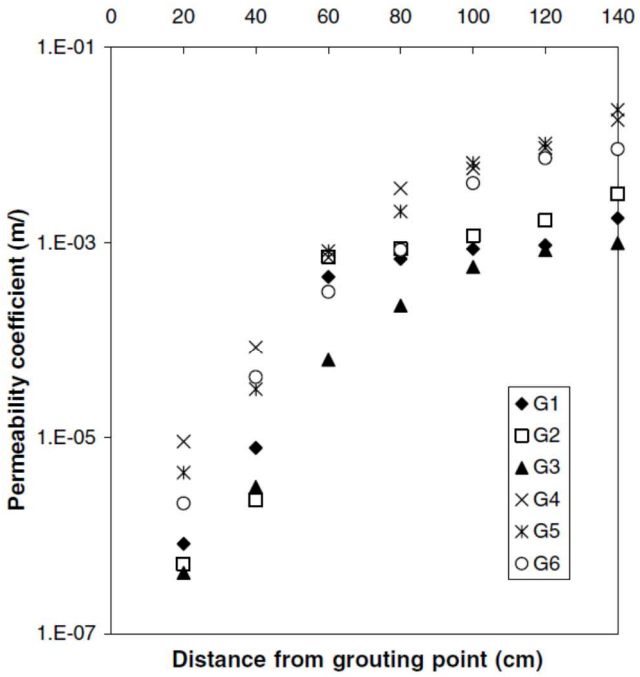

Figure 70 - Permeability as function of distance from the injection location (Anagnostopoulos, 2005)

The groutability (how well the soil can be grouted) of soil depends on the soil and grout properties. By means of a literature study and experiments, a formula for determining the groutability is (Akbulut & Saglamer, 2002):

$$N = \frac{D_{10(soil)}}{d_{90(grout)}} + k_1 \frac{\mathrm{W/C}}{FC} + k_2 \frac{P}{D_r} \qquad \text{(A.19)}$$

in which:

N	= groutability [-]
$D_{10(soil)}$	= soil particle size [mm]
$d_{90(grout)}$	= grout particle size [mm]
W/C	= water-to-cement ratio [-]
FC	= fine content of the soil [-]
P	= grouting pressure [kPa]
D_r	= relative density [-]
k_1	= 0.5 [-]
k_2	= 0.01 [kPa^{-1}]

It is possible to grout soil with a specific grout when N>28. If N<28 the soil cannot be sufficiently grouted. The formula holds for 0<FC<6%, 0.8<W/C<2:1 and 50<P<200. If FC is larger than 6% the soil is not sufficiently grouted. When the W/C ratio increases above 2:1 filtration occurs.

As explained in this section, the effect of grouting on sand depends on several variables, making it hard to accurately predict the properties of grouted sand. It also shows that grouting increases the strength of sand significantly, which poses a problem for dikes constructed on soft soils. These soils tend to settle, which a sand or clay dike can follow. If the grouted dike becomes too rigid due to the increased strength, it can crack due to settlements. These cracks are weak point in the dike, through which water can seep. This seepage can damage the dike even more in case of high water and during a freeze-thaw period. This could make the dike worse than it was before grouting.

Biological reinforcement of sand

Rock or rocklike material erodes slowly, making it interesting to change sand into a rocklike material to slow down erosion. There is a way to turn sand in to a kind of soft rock (a sort of beachrock), by using a certain enzyme. How this is achieved and what the effects on sand are, is explained in this section.

Principle

Sand can turn into beachrock naturally, which takes a long time and requires the right minerals to be present in the sand and/or pore water. There is a way to catalyse this process using an enzyme. This enzyme catalyses ureases, which is hydrolysis of urea ($CO(NH_2)_2$). This chemical reaction is necessary to form calcite ($CaCO_3$) in the voids and on the surfaces of the sand grains, which cements the sand grains. For the enzyme to work, it is necessary to precipitate or inject calcium carbonate ($CaCl_2$) into the sand, after the urea has been precipitated or injected. The chemical reaction goes as follows (Yasuhara, et al., 2012):

1) $CO(NH_2)_2 + 2H_2O \rightarrow 2NH_4^+ + CO_3^{2-}$
2) $CaCl_2 \rightarrow Ca^{2+} + 2Cl^-$
3) $Ca^{2+} + CO_3^{2-} \rightarrow CaCO_3$

A schematic overview of this process is given in Figure 71.

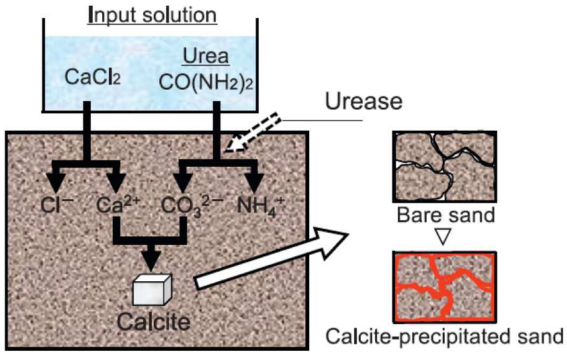

Figure 71 - Schematic overview of the formation of cemented sand (Yasuhara, et al., 2012)

There are multiple ways to harvest the urease enzyme:

- Plants, such as sword beans (Yasuhara, et al., 2012)
- The bacteria *Sporosarcina pasteurii* (Harkes, et al., 2010b)
- The bacteria *Bacillus sphaericus* (Cheng & Cord-Ruwisch, 2012)
- The bacteria *Bacillus pasteurii* (Ferris, et al., 1997), (DeJong, et al., 2006)

There is a difference between getting the enzyme from plants or use bacteria to generate the enzyme. Bacteria have to be cultivated and fixated in the sand before the formation of calcite can start, while using the enzyme extracted from plants can be directly injected into the sand.

Change of soil parameters

By turning sand into beachrock the properties of the soil change. The voids between the grains get clogged, reducing the porosity and permeability. Based on empirical relations, a numerical model for the prediction of the porosity and hydraulic conductivity of cemented sand was formulated (Yasuhara, et al., 2012). The porosity as function of time is calculated with:

$$\phi(t+\Delta t) = (1 + R_n \cdot V_m \cdot \Delta t) \cdot \phi(t) \qquad \text{(A.20)}$$

$$R_n = -k_n A_n \rho_w \left|1 - \Omega_n^{\ \theta}\right|^{\eta} \qquad \text{(A.21)}$$

$$k_n = k_{25} \exp\left[\frac{-E_a}{R}\left(\frac{1}{T} - \frac{1}{298.15}\right)\right] \qquad \text{(A.22)}$$

in which:

Φ = porosity [-]
t = time [s]

V_m = molar volume [m^3/mol] ($3.69x10^{-5}$ for calcite)
A_n = specific surface area [m^2/kg]
ρ_w = water density [kg/m^3]
Ω_n = kinetic mineral saturation ratio [-]
θ, η = constants constrained from dissolution experiments
k_{25} = rate constant at 25°C
E_a = activation energie [J/mol]
R = gas constant [J/K/mol]
T = absolute temperature [K]

The permeability (K) and hydraulic conductivity (k) can be calculated with:

$$K(t) = K_0 \frac{(1-\phi_0)^2}{(1-\phi(t))^2} \cdot \left(\frac{\phi(t)}{\phi_0} \right)^3 \quad \text{(A.23)}$$

$$k(t) = K(t) \frac{\rho_w g}{\mu} \quad \text{(A.24)}$$

This hydraulic conductivity can be converted to an effective hydraulic conductivity in vertical direction, for comparison with a constant or falling head test, using:

$$\bar{k}_v(t) = \frac{h}{\Sigma(h_i / k_i(t))} \quad \text{(A.25)}$$

in which:
K = permeability [m^2]
K_0 = initial permeability [m^2]
Φ_0 = initial porosity [-]
k = hydraulic conductivity [m/s]
μ = dynamic viscosity of water [Pa s]
h = sample height [m]
h_i = height of element i [m]
k_i = hydraulic conductivity of element i [m/s]

This numerical model was build using the above formulas. To test the model, it was compared to the results of experiments. The used model input is given in Table 24.

Parameter	***Value***
Grain diameter, d [µm]	210
Particle density, ρ_s [g/cm^3]	2.64
Temperature, T [°C]	20
Initial porosity, Φ_0 [-]	0.44
Specific surface area , A_n [m^2/kg]	0.98
Initial hydraulic conductivity, K_0 [cm/s]	$4.4x10^{-2}$
Precipitation rate constant, k_{25} [mol/m^2/s]	$1.0x10^{-8}$
Activation energy, E_a [kJ/mol]	62.8

Table 24 - Model parameters, table 5 of (Yasuhara, et al., 2012)

In Figure 72 the modelling and experimental results for the hydraulic conductivity are plotted together, to show the difference between both. The decrease of hydraulic conductivity depends on the elapsed time after the injection and the number of injections. A longer time after injection and/or a higher injection number results in a greater decrease, due to an increased amount of precipitated calcite. As is shown, the difference between the prediction and experiment is quite significant, so the model does not predict the hydraulic conductivity very well.

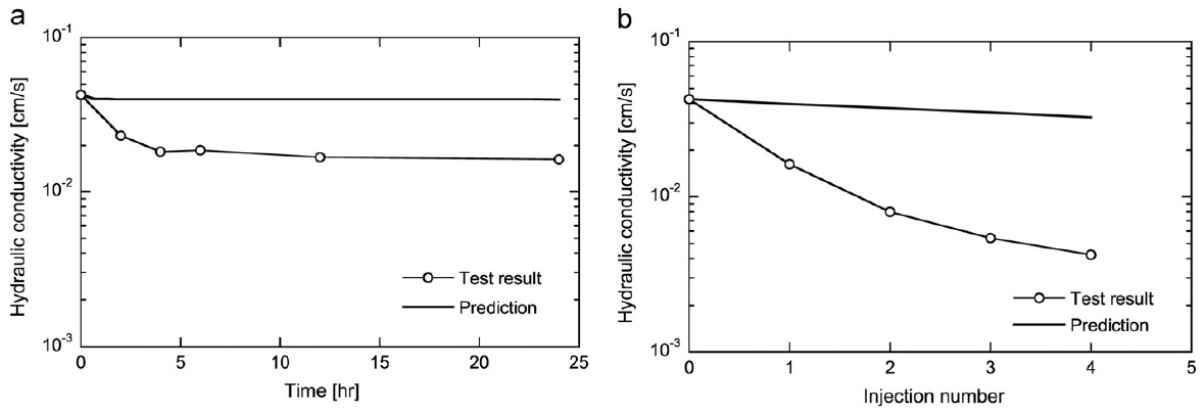

Figure 72 – Model versus experimental results of the hydraulic conductivity for different durations after injection or more injections (Yasuhara, et al., 2012)

The prediction and experimental results of the porosity (Φ) are plotted in Figure 73, which show good agreement. The model can therefore be used to predict the porosity of biological reinforced soil.

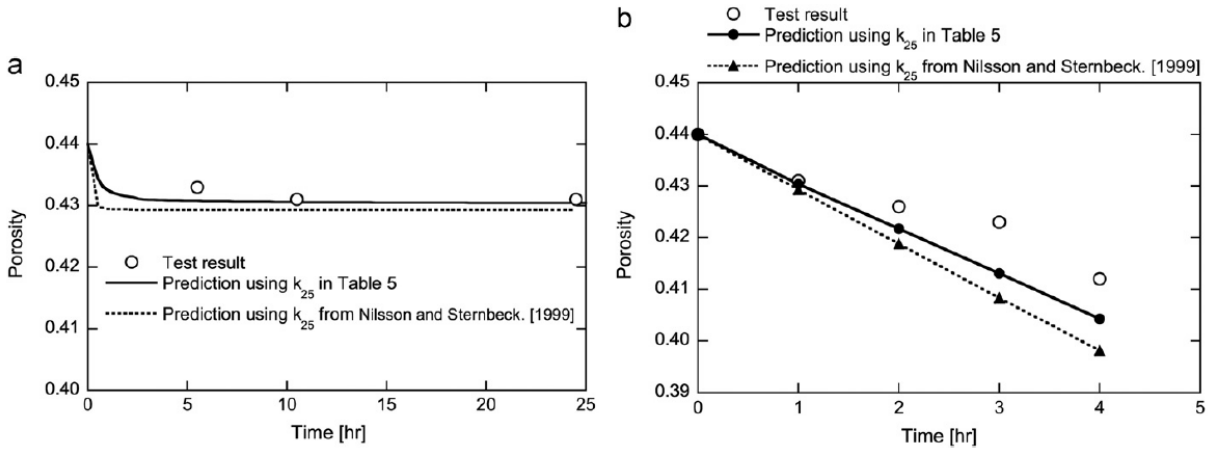

Figure 73 - Model versus experimental results for Φ (Yasuhara, et al., 2012)

Erosion formula

The influence of biological reinforcement on the soil parameters can be used to derive the erosion rate, which is necessary since no erosion formulas are known for this material.

Practical implementation

To induce biological reinforcement of sand, a certain procedure has to be followed. First the suspension with bacteria needs to be inserted into the sand, followed by the calcium carbonate solution. There are two ways of executing this (Cheng & Cord-Ruwisch, 2012):

- Submerged flow or injection
- Surface percolation

The first method is to inject both solutions into the sand, in sequel, to induce the cementation of sand. This method works well in saturated sands in which the flow can be sufficiently controlled, but was not studied for non-saturated sands. The second method is intended for use in non-saturated sand, which uses percolation to insert both solutions in the sand. Test results show that the second method is more effective in non-saturated sands than the first method (Cheng & Cord-Ruwisch, 2012). However, these test were conducted on a sand column of 1 meter and only in non-saturated sand. The effectiveness in saturated sand is not known.

In a sand dike, both saturated and non-saturated sand can be present, depending on the water level in the dike. To fully reinforce the sand in the dike, probably a combination of both methods in necessary. Injection for the saturated sand and percolation for the non-saturated sand. The first method is a well-known one, since it resembles permeation grouting and is therefore probably more reliable. The second method requires almost no equipment, but is new and should be tested more thoroughly before it can be used.

A drawback of this option is the by-product of the chemical reaction, ammonia (NH_3). This will have to be flushed out or neutralized, to prevent harm to the environment and ground water.

Increase of the erosion resistance of sand without aggregates

All the described options require an additive to be added to sand in order to reduce erosion. It is also possible to increase the erosion resistance of sand by exploiting natural phenomena during the erosion process. This is explained in this section.

Principle

The main principle behind increasing the erosion resistance using this method, is increasing the hydraulic gradient over the sand. The effect of the hydraulic gradient on the stability of a sand grain and slope is explained, which is used to explain the effect on the stability of sand beds, incipient motion and erosion rates.

On a sand grain of an underwater slope, several forces are exerted. Gravity has a component parallel to the slope, which tries to pull the grain down, and a component perpendicular to the slope, which keeps the grain into position. The magnitude of these components depend on the slope angle. The second force is a drag force due to seepage in or out of the slope. This seepage exerts a drag force onto the grain, trying to push it in or pull it out of the slope. If the seepage is directed into the slope, this helps to keep the grain in position. In case there is a flow parallel to the slope also a drag force parallel to the slope is exerted on the grain, which tries to

pull it out of its position. The resulting friction and/or drag of these forces determine if the grain starts to move or is stable.

This concept can be applied to the whole slope. As long as all the grains are stable, the slope is stable as well. If a majority of the grains start to move, the slope becomes unstable and starts to collapse. Research has shown that with increasing inflow into the slope, the angle at which this slope is stable increases as well (Van Rhee & Bezuijen, 1992), which can be seen in Figure 74. As this relation shows the slope is stable at steeper angles, if the hydraulic gradient into the slope increases.

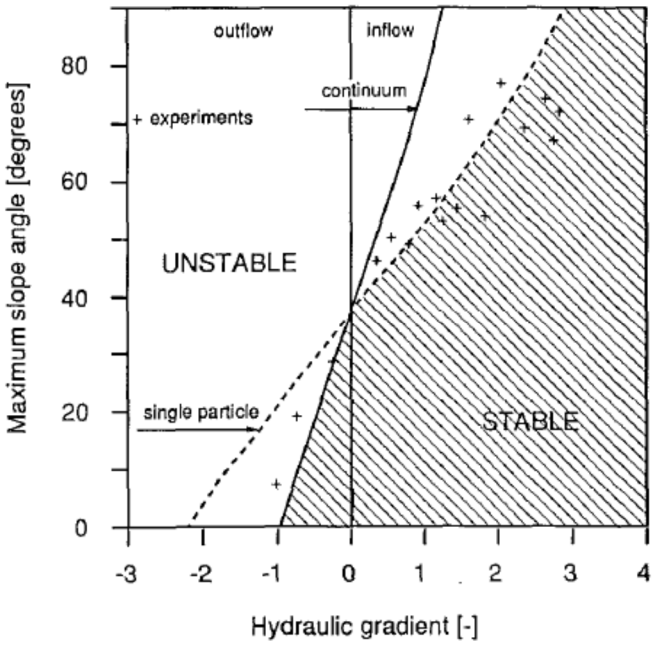

Figure 74 - Relation between maximum slope angle and hydraulic gradient (Van Rhee & Bezuijen, 1992)

Previous research ((Martin, 1970), (Moust-Jacobsen & Magda, 1988)) into the effect on the stability of sand grains influenced by seepage and currents, shows that the critical shear velocity increases with increasing seepage. This is due to the fact that that the seepage flow exerts a force onto the grains in the direction of the bed, increasing its resistance against motion and therefore increasing the critical shear velocity of the grains. However, another research found the opposite effect (Rao & Sitaram, 1999), stating that seepage into the bed decreases the bed stability and flow out of the bed increases bed stability. This is because the flow into the bed pushes the velocity profile of the parallel current down, increasing the shear velocity at the bed. Flow out of the bed pushes the velocity profile away from the bed, decreasing the shear velocity at the bed. Figure 75 provides a schematic overview of this principle.

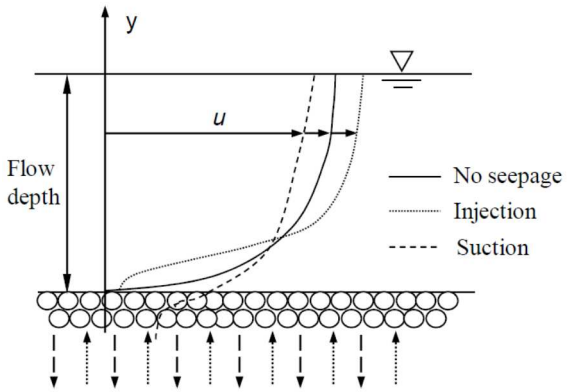

Figure 75 - Schematic diagram of velocity profile subjected to seepage (Liu & Chiew, 2012)

As long as the shear velocity is lower than the critical shear velocity, the grains are stable, but if the shear velocity becomes larger than the critical shear velocity, the grains start to move. The magnitude of the transport depends on the difference between the shear velocity and the critical shear velocity.

The differences in the conclusions of the different researches can be explained with the above relation. Seepage increases the critical shear velocity as well as the shear velocity, while flow out of the bed decreases the critical shear velocity as well as the shear velocity. Whether seepage decreases or increases the erosion rate, depends on which of these effects is more dominant, i.e. which shear velocity increases the most (Liu & Chiew, 2012). Figure 76 illustrates the above explanation using a quadrant analysis, in which quadrant 1 represents the increase of both velocities and quadrant 2 the decrease of both velocities. The diagonal line in the quadrants separates the areas of the dominant effects, determining whether the erosion rate increase of decreases.

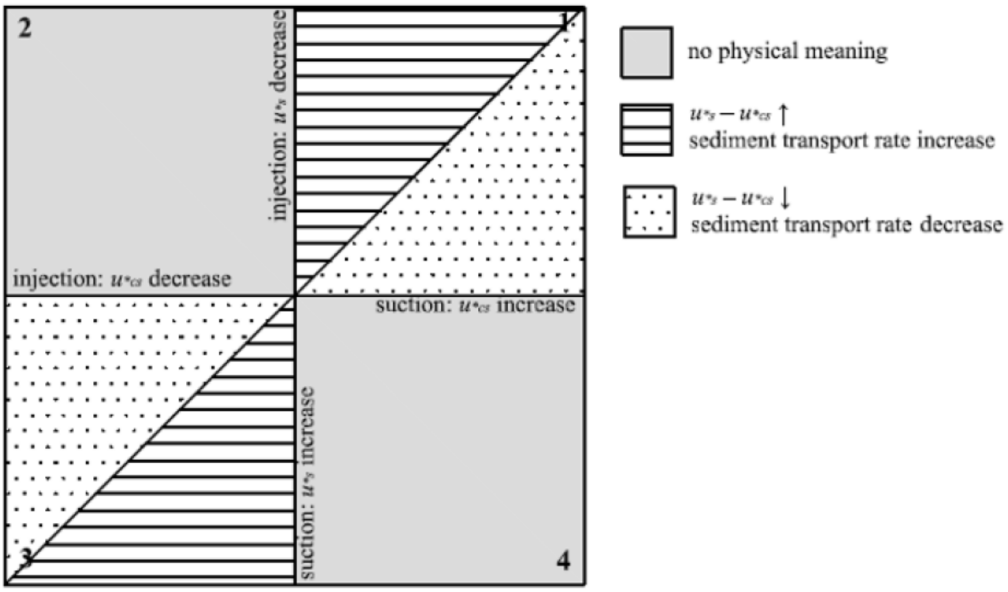

Figure 76 - Quadrant analysis of bed particle stability due to seepage (Liu & Chiew, 2012)

By controlling the flow in or out of the bed, the shear velocities can be influenced and the erosion rate can be decreased or increased.

Practical implementation

For the experiments found in literature is was necessary to create flow into or out of the bed. Generally this was achieved with pumps, which extracted water from underneath the bed or injected it into the bed. Those pumping systems were small scale, but it could be possible to scale up and construct a water extraction of injection system in dikes. Such a pumping system could be used to lower the erosion rate in case of a breach.

There is, however, no literature or trial project of such a system and thus it is not known if it would work in practice. It is possible to model the principle, but quite difficult to determine if it is a practical option.

Construction of a highly erosion resistant core

All the above options affect the whole dike body, increasing the erosion resistance of the whole dike. A different method is to allow erosion of a part of the dike, but stop it at a certain point, which is explained in this section.

Principle

It is not uncommon for dikes or dams to have a core of a different material than the rest of the embankment. Usually these cores are impermeable and have to prevent seepage and piping. A sketch of this principle can be seen in Figure 77.

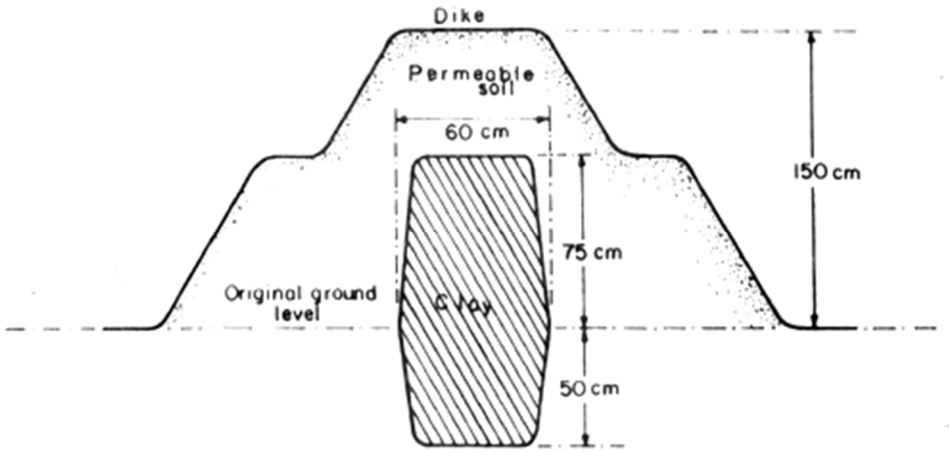

Figure 77 - Sketch of a dike with an erosion resistant core

In principle the erosion of the inner slope will stop when it reaches the core and thus further breaching of the dike is prevented. At the same time, the core will reduce the flow through the breach. If such a core is build, the choice could be made to allow water to flow through the breach, but at a predetermined rate, depending on the dimensions of the core. In this way the flow velocities and rise rate in the polder can be controlled. Whether water is or is not allowed to enter the polder depends on, among others, the retaining capacity of the polder and the stability of the core at different water levels below the dike crest. If the core cannot resist the water level in front of it, without support from the inner slope, it is of no use. It could, however, be difficult or impractical for the core to withstand the maximum outside

water level and it could therefore be allowed to have a water flow into the polder. It should be determined for each case what the maximum water flow into the polder can be and what appropriate dimensions for the core are.

Practical implementation

The core can be constructed with several materials and techniques, as long as it creates an impermeable and erosion resistant core. It is possible to construct a core in an existing dike. Possible options are:

- *Sheet piling*
  This is used when dikes need to be reinforced and there is no space for expansion of the dike. This is an expensive option, since steel is expensive and it is not easy to construct a sheet piling wall in a dike. It is also questionable if the sheet piling can withstand (a part of) the outside water level without support from the inner slope.

- *Diaphragm wall*
  A well-known technique for construction of foundations and retaining walls for excavations. A diaphragm wall is a concrete wall in the soil, constructed in-situ. This is option faces the same difficulties as the sheet piling, it is expensive, difficult and uncertainty about the strength.

- *Grouting*
  Already described in another option, is could also be used to create a core in a dike. It is cheaper than the previous options, but could not be strong enough to meet the requirements.

- *Biological*
  Also described in another option and thus has the same issues as that option. It is also not certain whether the obtained cemented sand does not erode and meets the other requirements.

There are probably more options to create a core into an existing dike, these are only a few examples. The increase of safety because of this option does not depend on the effect on the erosion rate, but on the design of the core and allowable water inflow. To determine whether this could be a feasible option, a study into possible designs is recommended, which is not part of this thesis.

B Erosion formulas promising options

For the three promising options which were selected (sand-bentonite mixture, sand-fibre mixture and biological improvement) an erosion formula is determined. This is necessary to be able to model them using the BRES-model and compare them to each other. The determination of the erosion formulas is described in this section.

Erosion formula sand-bentonite mixture

In this section is explained how an erosion formula for a sand-bentonite mixture is determined. This is achieved by comparing different possible formulas to known erosion data.

Erosion velocities

In a study (Gailani, 2001) the erosion velocities of sand with different percentages of bentonite were determined. These were measured for a few shear stresses and a small variation in bulk density of the mixtures. Since there are only measurements of the erosion velocities at a few shear stresses, it is necessary to inter- and extrapolate this data for other shear stresses. To be able to do this, first the measurements for each mixture and shear stress were averaged over the bulk density. This way, an average erosion velocity at a certain shear stress is known for the different mixtures. For inter- and extrapolation, a trendline through these points is plotted for each mixture. The result of the averaging and trendline plot can be seen in Figure 78, which also shows the formulas of the trendlines. The corresponding R^2 value for these formulas is also given, which indicates how well the formula fits the data (R^2=1 is a perfect fit).

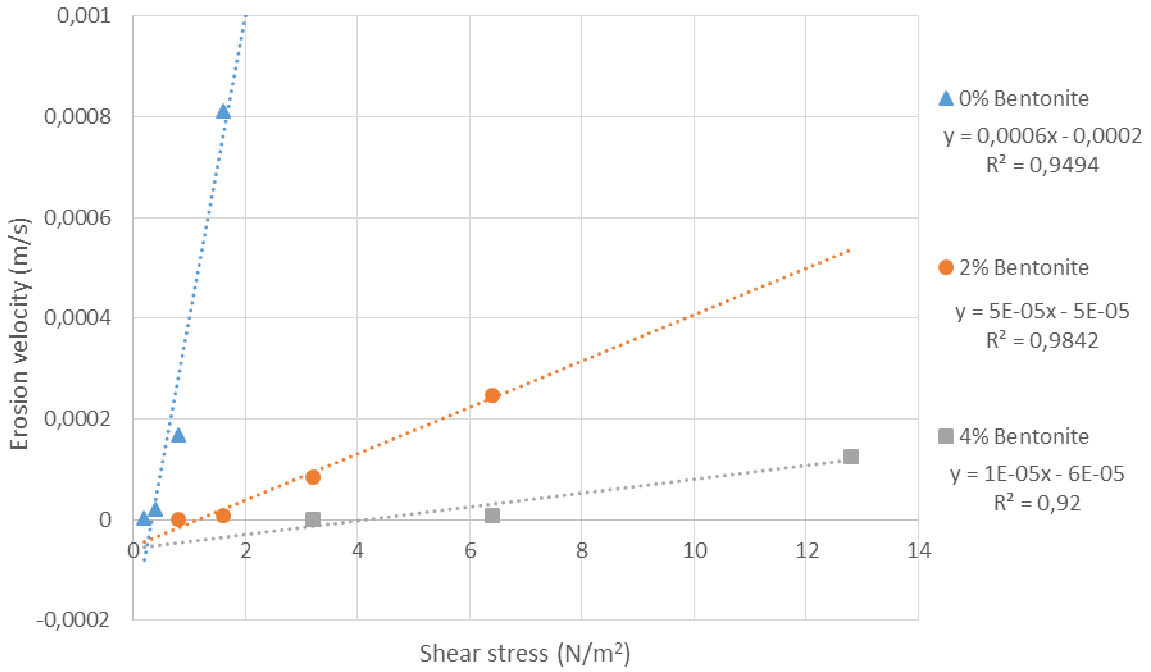

Figure 78 - Erosion velocities of sand with added bentonite as function of shear stress and bentonite percentage, including trendlines and their formulas (composed from (Gailani, 2001))

These trendline formulas are used to compare the outcome of possible erosion formulas to this data. Since there is a limited number of measurements, these formulas are only an approximation of these measurements.

Erosion formula of Lick, Jin and Gailani

A few years after Gailani did measurements of the erosion velocities of sand-bentonite mixtures (Gailani, 2001), Lick, Jin and Gailani derived a formula to calculate the erosion velocity of a sand-bentonite mixture (Lick, et al., 2007). This formula is already described in appendix A and is elaborated on in this section. The formula is (Lick, et al., 2007):

$$V_e = 10^{-4}\left(\frac{\tau-\tau_{cn}}{\tau_c-\tau_{cn}}\right)^n \tag{B.1}$$

$$\tau_{cn} = 0.414\cdot d \tag{B.2}$$

$$\tau_c = \left(1+\frac{a\exp(b\rho_b)}{d^2}+\frac{c_5}{c_3 d}\right)\tau_{cn} \tag{B.3}$$

$$c_3 = \frac{\pi(\rho_s-\rho_w)g}{6} \tag{B.4}$$

in which:

V_e	= erosion velocity [cm/s]
τ	= applied shear stress [N/m^2]
τ_c	= critical shear stress [N/m^2]
τ_{cn}	= critical shear stress for the erosion of non-cohesive particles [N/m^2]
d	= the particle diameter [mm]
ρ_b	= bulk density of sediment [g/cm^3]
ρ_s	= density of solids [g/cm^3]
ρ_w	= density of water [g/cm^3]
n, a, b, c_5	= parameters determined using Table 25

The parameters n, a, b, and c_5 can be found in Table 25, this table is a combination of several tables found in (Lick, et al., 2007). It gives the parameters for the formula in case 0%, 2% or 4% bentonite is added to the sand. The parameters are not known for every particle size, which makes it necessary to interpolate between different grain diameters to obtain the parameter values. It should be noted that the c_5 and n values for 4% added bentonite are derived from the values of 2% added bentonite. The ratio between these values is given by table 5 of the study (Lick, et al., 2007). This introduces some inaccuracy into the formula, which can be improved by doing more tests to obtain more values for the used parameters.

The erosion velocities calculated with this formula are given in Figure 79. The soil characteristics used to calculate the erosion velocities are given in Table 26.

	Sand with no added bentonite				*Sand with added bentonite*					
d	***a***	***b***	***n***	***c_5***	***a***	***b***	***c_5 2%***	***n 2%***	***c_5 4%***	***n 4%***
[mm]	***[N/mm^2]***	***[cm^3/g]***	***[-]***	***[N/m^2]***	***[N/mm^2]***	***[cm^3/g]***	***[N/m^2]***	***[-]***	***[N/m^2]***	***[-]***
0.0057	2.89E-09	8.43	1.87	0	-	-	-	-	-	-
0.0150	1.63E-08	7.23	2.17	0	1.01E-06	3.77	8.37	2.72	18.90	4.13
0.0183	1.72E-07	5.97	2.25	0	-	-	-	-	-	-
0.048	7.62E-07	5.52	2.14	0	2.20E-05	2.46	6.69	2.1	15.11	3.19
0.075	2.86E-07	6.08	1.94	0	-	-	-	-	-	-
0.125	7.48E-06	4.61	2.37	0	-	-	-	-	-	-
0.140	-	-	-	-	9.51E-04	1.33	6.19	3.28	13.98	4.98
0.170	-	-	-	-	1.59E-02	0	6.93	3.74	15.65	5.68
0.222	8.54E-02	0	2.46	0	-	-	-	-	-	-
0.280	-	-	-	-	1.57E-02	0	3.36	3.6	7.59	5.47
0.390	-	-	-	-	1.91E-02	0	4.22	3.54	9.53	5.38
0.432	7.11E-02	0	2.03	0	-	-	-	-	-	-
1.020	1.06E-01	0	1.84	0	-	-	-	-	-	-
1.350	8.19E-02	0	1.54	0	1.23E-01	0	0.83	3.94	1.87	5.99

Table 25 - Parameters from table 3, 4 & 5 of (Lick, et al., 2007)

Erosion formula of Van Rijn

The BRES-model can use the Van Rijn formula to calculate erosion (Visser, 1998). This makes it an interesting formula to calculate sand-bentonite erosion. This formula can be used under the assumption that with these low bentonite percentages the mixture still behaves as sand, albeit with slightly different properties (e.g. reduced permeability). For calculation of the erosion velocity of a sand-bentonite mixture, the formula needs to be adapted. The original Van Rijn formula is given by:

$$V_e = \frac{\alpha \rho_s (\Delta g D_{50})^{0.5} D_*^{0.3} T^{1.5}}{\rho_s (1 - n_0)} \quad \text{(B.5)}$$

$$\alpha = 0.00033 \quad \text{(B.6)}$$

$$\Delta = \frac{\rho_s - \rho_w}{\rho_w} \quad \text{(B.7)}$$

$$D_* = D_{50} \left(\frac{\Delta g}{\nu^2} \right)^{1/3} \quad \text{(B.8)}$$

$$T = \left(\frac{\tau - \tau_c}{\tau_c} \right) \quad \text{(B.9)}$$

in which:

V_e	= erosion velocity [m/s]
α	= deterministic factor [-]
ρ_s	= density of solids [kg/m^3]
ρ_w	= density of water [kg/m^3]
g	= gravitational acceleration [m/s^2]
Δ	= relative density ($(\rho_s-\rho)/\rho$) [-]
D_{50}	= median particle diameter [m]
n_0	= in-situ porosity [-]
D_*	= dimensionless particle diameter [-]
v	= kinematic viscosity of water [m^2/s]

In order to approximate the measurements (Gailani, 2001) this formula has to be adapted. In the original formula, the critical shear stress is calculated using the critical Shields parameter. This parameter is valid for sand, but cannot be used to for a sand-bentonite mixture. Therefore the critical shear stress of (Lick, et al., 2007) is used, which is calculated with (B.3). Besides this adaptation, the deterministic parameter α is adapted as well:

$$\alpha = 0.00033\frac{1}{10B_{\%}} \tag{B.10}$$

This adaptation reduces α using the added bentonite percentage ($B_{\%}$ in volume percentage). With this adaptation, the formula gives a reasonable approximation of the data, which can be seen in Figure 79. For the calculation of the erosion velocity for sand with no added bentonite, the original Van Rijn formula is used. This gives an overestimation of the data for only sand, but as already showed, the Van Rijn formula generally overestimates the erosion of sand (section 3.2). The soil characteristics used to calculate the erosion velocities are given in Table 26.

Erosion formula of Van Rhee

The hydraulic conductivity of sand decreases with increasing bentonite percentages (Sallfors & Oberg-Hogsta, 2002). This phenomenon can be used to calculate the erosion velocities. The Van Rhee-Bisschop formula (Bisschop, et al., 2010) has the porosity and hydraulic conductivity as parameters and is thus a possible formula to calculate the erosion velocities of sand-bentonite mixtures. This formula is adapted to approach the measured erosion velocities. The original formula is given by:

$$V_e^5 = \alpha^2 D_*^{0.6}\left(\frac{\tau-\tau_c}{\tau_c}\right)^3\left(\frac{k}{\delta}\right)^3 \tag{B.11}$$

$$\alpha = 0.00033\frac{\sqrt{\Delta g D_{50}}}{1-n_0} \tag{B.12}$$

$$D_* = D_{50}\left(\frac{\Delta g}{\nu^2}\right)^{1/3} \tag{B.13}$$

$$\delta = \frac{n_i - n_0}{1 - n_i} \frac{1}{\Delta(1 - n_0)} \tag{B.14}$$

in which:

V_e	= erosion velocity [m/s]
Δ	= relative density $((\rho_s-\rho)/\rho)$ [-]
D_{50}	= median particle diameter [m]
n_0	= in-situ porosity [-]
n_i	= porosity sheared layer [-]
D_*	= dimensionless particle diameter [-]
v	= kinematic viscosity of water [m^2/s]
τ	= shear stress [N/m^2]
τ_c	= critical shear stress [N/m^2]
k	= hydraulic conductivity, calculated with (B.15) [m/s]

The hydraulic conductivity is calculated with the Kozney-Carman formula (Chapuis & Aubertin, 2003):

$$k = 0.2 \frac{g}{\rho_w{}^2 \nu} \frac{e^3}{S^2 D_r{}^2 (1+e)} \tag{B.15}$$

in which:

k	= hydraulic conductivity [m/s]
S	= specific surface $(6/(D_{50}*\rho_s))$ [m^2/kg]
Dr	= relative density (ρ_s/ρ_w) [-]
e	= void ratio $(n_0/(1-n_0))$ [-]

To fit the measurements (Gailani, 2001), the original formula is adapted in two ways. The exponent of the shear stresses is multiplied with 2.5 and the alpha is multiplied with 0.1. Besides that, the formula is also adapted for the decreasing hydraulic conductivity. The porosity (n_0) decreases with increasing bentonite percentage ($B_{\%}$ in volume percentage):

$$n_{0B} = n_0 - B_{\%} \cdot 0.01 \tag{B.16}$$

The hydraulic conductivity decreases as well, which is given by:

$$k_B = k \cdot 10^{-B_{\%}} \tag{B.17}$$

These adaptions lead to an adapted Van Rhee-Bisschop formula:

$$V_e = \left(\left(0.00033 \frac{\sqrt{\Delta g D_{50}}}{1 - n_{0B}} \cdot 0.1 \right)^2 D_*{}^{0.6} \left(\frac{\tau - \tau_c}{\tau_c} \right)^{3 \cdot 2.5} \left(\frac{k_B}{\delta} \right)^3 \right)^{\frac{1}{5}} \tag{B.18}$$

$$k_B = 0.2\frac{g}{\rho_w{}^2 \nu}\frac{e^3}{S^2 D_r{}^2(1+e)}\cdot 10^{-B_{\%}} \tag{B.19}$$

$$\delta = \frac{n_i - n_{0B}}{1-n_i}\frac{1}{\Delta(1-n_{0B})} \tag{B.20}$$

Comparison of formulas

In Figure 79 the erosion velocities of the described formulas and measurements as function of the shear stress are given. The parameters necessary to calculate the erosion velocities with the different formulas are given in Table 26.

Parameter	*Value*
D_{50} *[m]*	$214\cdot10^{-6}$
ρ_w *[kg/m³]*	1000
ρ_s *[kg/m³]*	2650
ρ_b *[kg/m³]*	2089
n_0 *[-]*	0.21
v $[m^2/s]$	$1\cdot10^{-6}$

Table 26 – Parameters for calculation

As can be seen in Figure 79, the adapted Van Rijn formula and adapted Van Rhee-Bisschop formula give the best approximations of the data (measurements). This partly due to 'fitting' of the formulas to the data and partly because the changes of the soil parameters are taken into account. Due to the better support from literature and a slightly better fit than the adapted Van Rhee-Bisschop formula, the adapted Van Rijn formula is used in the BRES-model. The Lick et al. formula is not used or adapted to fit the data since it gives unrealistic results (i.e. the erosion velocity of sand-bentonite is higher than the erosion velocity of sand).

Although the adapted Van Rijn formula gives a reasonable approximation of the data, there is an obvious deviation between the formula and the data. This can be due to a too low or high critical shear stress, which is partly deterministically determined, or the assumption that the mixture behaves as sand is incorrect. Their might also be other causes. To come to a better formula and find the causes for the deviation, more laboratory tests need to be executed. With these test the critical shear stress could be determined, which can be used to improve the formula. These test might also expose other parameters on which the erosion velocity of a sand-bentonite mixture depends. Still, with the available data and knowledge, this is the best approximation, so this formula is used in the BRES-model.

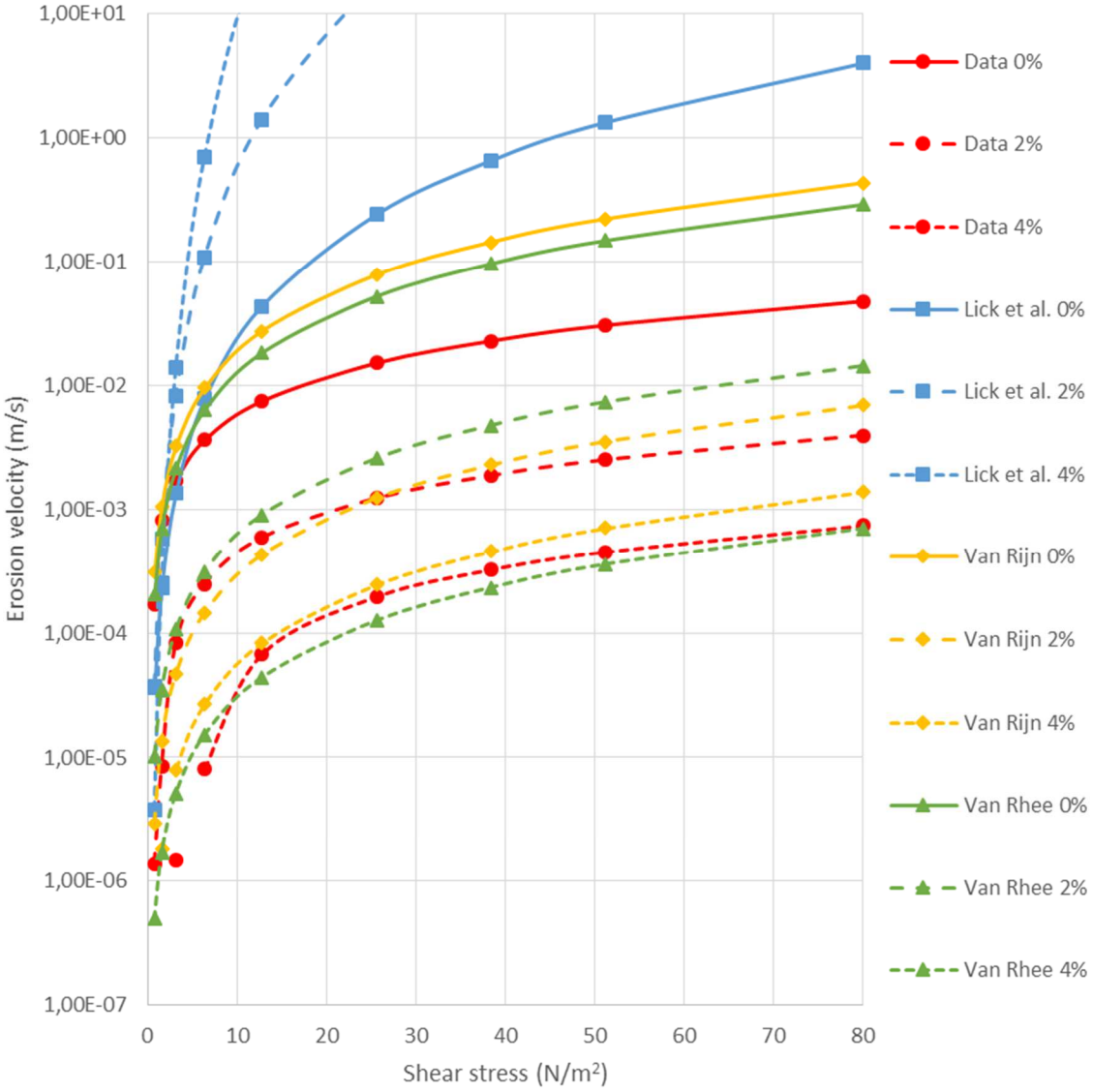

Figure 79 - Erosion velocity as function of shear stress for sand with added bentonite, approximated with different formulas (Lick et al., Van Rijn and Van Rhee) and compared with measured data (Gailani, 2001)

Erosion formula biological improvement

For the biological improvement option an erosion formula is necessary. Unfortunately there are no known erosion formulas or erosion measurements for bacterial cemented sand. In this section the attempt to develop an erosion formula using the material properties of cemented sand is described.

Material properties

The cementation of sand with bacteria was studied by several researchers. The most relevant research included a large scale test of cementing of sand and testing of the material properties (Van Paassen, et al., 2010). The results of this study are used to determine the material properties. These properties are the basis for the erosion formula. During this study a volume of 100 m^3 of sand was cemented using a *Sporosarcina pasteurii* bacteria suspension and a $CaCl_2$ solution. After 16 days the process was finished and laboratory tests of the obtained material were executed.

The material properties depend on the amount of calcite ($CaCO_3$, as percentage of dry weight) in the sand. This percentage can be seen in Figure 80, as well as a picture of the end result of the experiment.

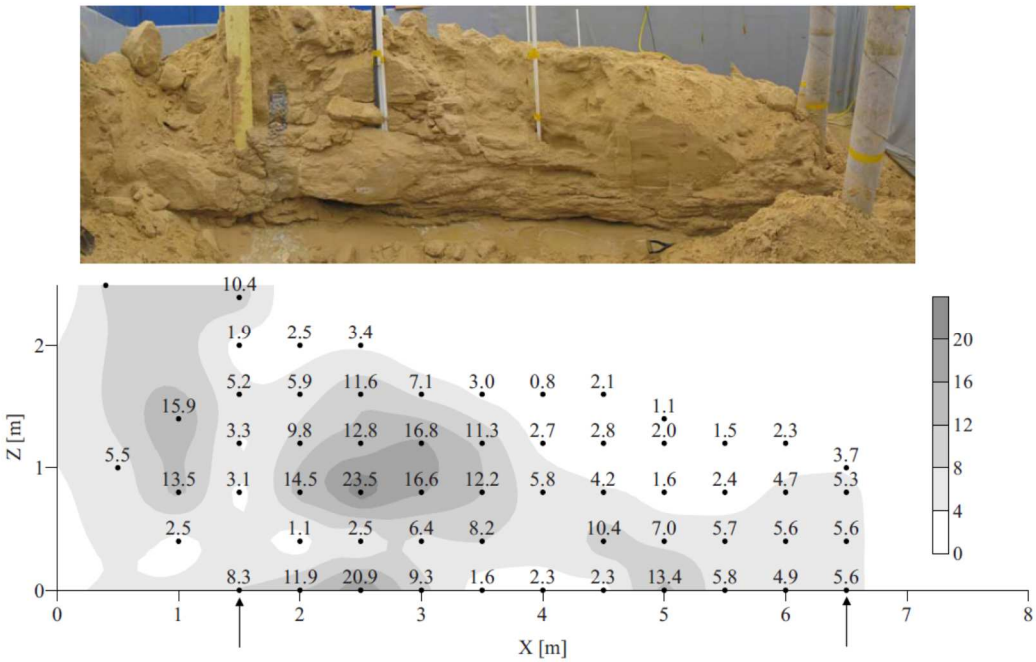

Figure 80 - $CaCO_3$ amount as percentage of dry weight of a vertical cross section through the sandbox (Van Paassen, et al., 2010)

The average content of $CaCO_3$ in the cross section was about 6.5%. The differences in $CaCO_3$ content are due to the influence of the flow velocities in the sand and the distance from the injection well. Samples of the material were taken and tested in the laboratory. Of each sample the $CaCO_3$ percentage, bulk density (ρ_b), Unconfined Compressive Strength (UCS), E-modulus (E_{50} and E_{ur}), axial strain at UCS, Poisson's ratio at UCS, and Poisson's ratio at 50% of UCS were determined. The results of these tests are given in table 2 of (Van Paassen, et al., 2010). The dry weight and UCS test results are approximated by fitting formulas, as shown in Figure 81. The R^2 value of these formulas indicates they are a reasonable fit to the data. These formulas are used to calculate the bulk density and UCS for different percentages of $CaCO_3$.

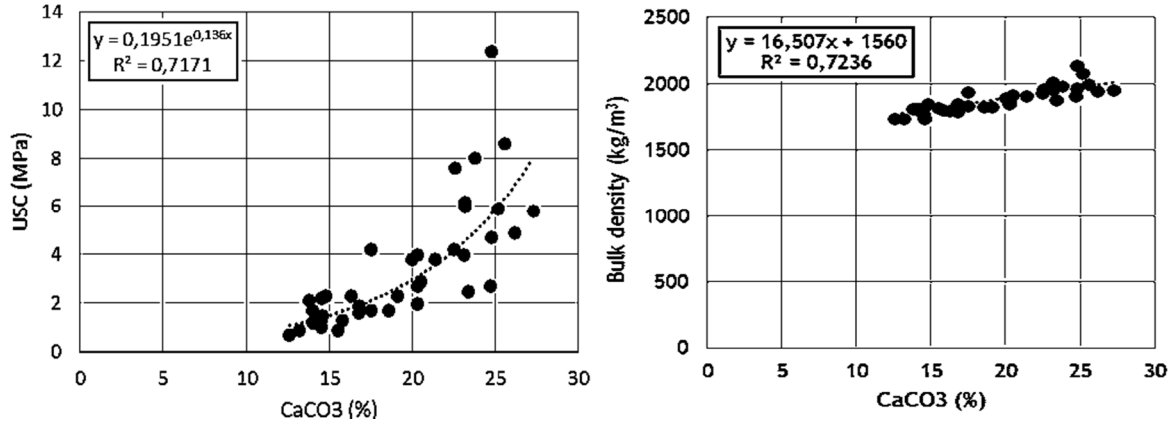

Figure 81 - Unconfined compressive strength (USC) and bulk density (ρ_b) as function of the $CaCO_3$ percentage (after (Van Paassen, et al., 2010))

The UCS is converted to a shear strength, friction angle and apparent cohesion (or shear strength at zero confining pressure) using the Hoek-Brown and Mohr-Coulomb failure criterion (Hoek, 1990):

$$c'_i = \tau_s - \sigma'_n \tan(\phi'_i) \quad \text{(B.21)}$$

$$\tau_s = \sigma'_n \sqrt{1 + \frac{m}{2\sqrt{s}}} \quad \text{(B.22)}$$

$$\sigma'_n = \frac{2s\sigma_c}{4\sqrt{s} + m} \quad \text{(B.23)}$$

$$\phi'_i = 90 - \arcsin\left(\frac{2\tau_s}{\sqrt{s}\sigma_c}\right) \quad \text{(B.24)}$$

$$m = \exp\left(\frac{RMR - 100}{14}\right) m_i \quad \text{(B.25)}$$

$$s = \exp\left(\frac{RMR - 100}{6}\right) \quad \text{(B.26)}$$

in which:

c'_i	= apparent cohesion [MPa]
τ_s	= effective shear strength [MPa]
σ'_n	= effective normal stress [MPa]
ϕ'_i	= friction angle [°]
σ_c	= unconfined compressive strength [MPa]
m,s	= constants [-]
m_i	= 7 [-] (according to table 1 of (Hoek, 1990))
RMR	= Rock Mass Rating [-] (estimated to be 80)

The effective shear strength which results from these formulas, is converted to a critical shear stress, which is used in erosion formulas. The relation between the shear strength and critical shear stress was studied (Léonard & Richard, 2004). In this study measurements of other researchers were combined to find a relation between the shear strength and the critical shear stress, which is given in Figure 82.

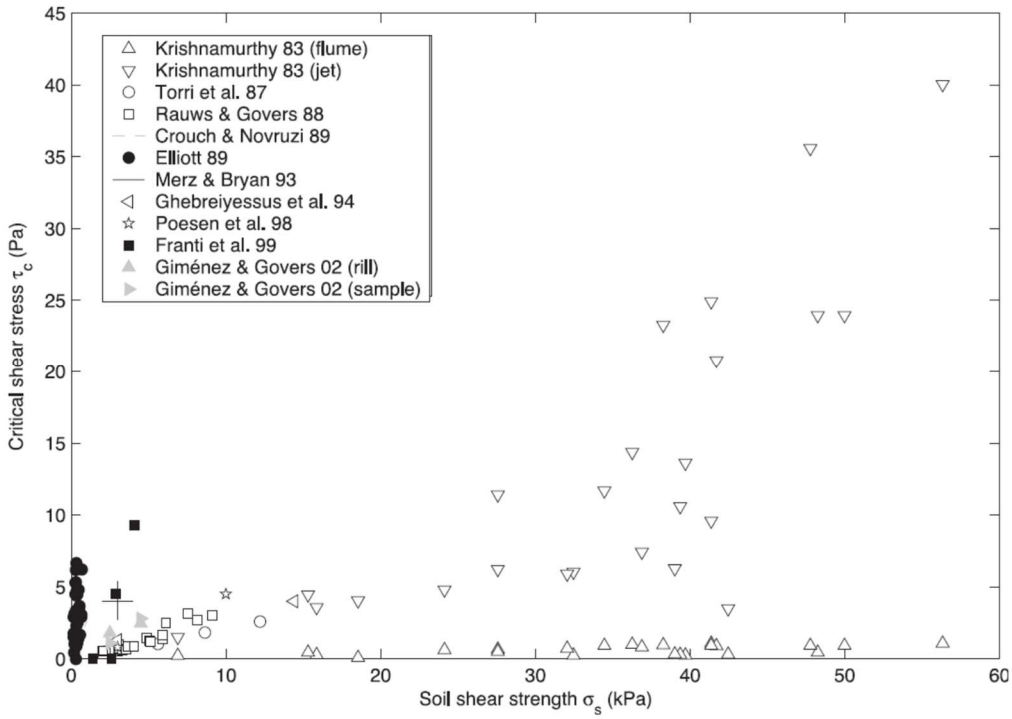

Figure 82 - Critical shear stress as function of soil shear strength (Léonard & Richard, 2004)

Based on this data an empirical relation is defined:

$$\tau_c = \beta \tau_s \tag{B.27}$$

In which:

τ_c = critical shear stress [Pa]
τ_s = soil shear strength [Pa]
ß = $2.60 \cdot 10^{-4}$ [-] (Léonard & Richard, 2004)

The erosion formula is based on these soil parameters. For calculation and comparison to other options, the average $CaCO_3$ percentage (6.5%) was used. The soil parameters for this $CaCO_3$ percentage are given in Table 27.

Parameter	***Value***
$CaCO_3$ [%]	6.5
Dry density [kg/m^3]	1667
USC (σ_c) [kPa]	470
σ'_n [kPa]	14
τ_s [kPa]	32
c'_i [kPa]	19
ϕ'_i [°]	44
RMR [-]	80
m_i [-]	7
m [-]	1.68
s [-]	0.04
τ_c [Pa]	**8.4**

Table 27 - Parameters for erosion formula

Erosion formula of Van Rijn

For the same reasons as described for the erosion formula of sand-bentonite mixtures, the Van Rijn formula is adapted for erosion of biological reinforced sand. Only two adaptations are made to the Van Rijn formula. Instead of using the critical shear stress of sand, the critical shear stress of the cemented sand is used. The second adaptation is the use of the dry density of the cemented sand (ρ_d) instead of the density of sand (ρ_s). The result of this adapted formula can be seen in Figure 83.

Erosion formula of Zhu

Research about breaching of clay dikes (Zhu, 2006) describes an erosion formula for cohesive sediment. This is given by (B.28) to (B.30). The formula for M (B.29) is based on research of Winterwerp and Van Kesteren (Zhu, 2006).

$$V_e = \frac{M(\tau - \tau_c)^a}{\rho_d} \tag{B.28}$$

$$M = \frac{c_v \phi_{s,0} \rho_d}{10 D_{50} \tau_s} \tag{B.29}$$

$$\phi_{s,0} = \frac{1}{1 + \omega \rho_s / \rho_w} \tag{B.30}$$

in which:

V_e	= erosion velocity [m/s]
a	= 1 [-] (Zhu, 2006)
M	= soil erodibility coefficient [s/m]
c_v	= consolidation coefficient [m^2/s]
ω	= water content [-]

In this formula there are still two unknowns, the water content and the consolidation coefficient. The water content is assumed to be equal to the porosity in saturated conditions, which is likely in case of a dike breach, and is given by:

$$\omega = n_0 = 1 - \frac{\rho_d}{\rho_s} \tag{B.31}$$

The consolidation coefficient can be calculated with (Cornell University, 1990):

$$c_v = \frac{k}{\gamma_w m_v} \tag{B.32}$$

in which:

γ_w	= unit weight of water [kN/m^3]
m_v	= coefficient of volume compressibility [m^2/N]
k	= hydraulic conductivity [m/s] (given by Kozeny-Carman (B.15))

The coefficient of volume compressibility is estimated to be 0.05. This is a value for heavy over-consolidated boulder clays, stiff weathered rocks and hard clays with a very low compressibility (Carter & Bentley, 1991). This description comes the closest to biological cemented sand and is therefore used in the formula.

Using these coefficients and parameters, the erosion velocity is calculated for different shear stresses, of which the result can be seen in Figure 83.

Erosion formula of De Boer

Another formula to calculate the erosion velocity of cohesive sediment is given by De Boer (De Boer, 2002). In this study the erosion formula of Van Kesteren is given:

$$V_e = \rho_d \frac{c_v}{10 D_{50} e_{cr}} \cdot \frac{\tau_c}{\tau_s - \tau_c} \cdot \frac{\tau - \tau_c}{\tau_c} \cdot \frac{1}{\rho_d} \tag{B.33}$$

The erosion velocity is in (m/s) and all parameters are already described. In this formula e_{cr} is the same as the water content ω. The erosion velocities calculated with this formula are also given in Figure 83.

Erosion formula of Van Rhee

Another formula to calculate the erosion velocities is the simplified Van Rhee formula (Van Rhee-Bisschop). This formula is not adapted, but the input for the critical shear stress, hydraulic conductivity and initial porosity is changed to the values calculated for the cemented sand. The results of this formula are given in Figure 83 as well.

Comparison of formulas

The erosion velocities for different shear stresses are calculated for all formulas, as can be seen in Figure 83. Also the erosion velocities of unimproved sand with the same particle size (D_{50}=214 μm), solid density (ρ_s=2650 kg/m^3) and initial porosity (n_0=0.41) are calculated. The erosion velocities of unimproved sand are calculated with the Van Rhee-Bisschop formula (see section 3.2). For comparison, also two graphs of erosion velocities of clay are included. These erosion velocities are calculated with the formula of Zhu and the soil properties of the 1st and 2nd clay dike experiment of Zhu (T1 and T2) (Zhu, 2006).

Figure 83 shows that the calculated erosion velocities are closer to the values of sand than of clay for all formulas. It can also be observed that the formula of De Boer and Van Rhee give similar results. The formula of Zhu gives lower erosion velocities than those formulas, while the adapted Van Rijn formula is somewhere in between. It also shows that there is a threshold shear stress for erosion, at approximately 10 N/m^2.

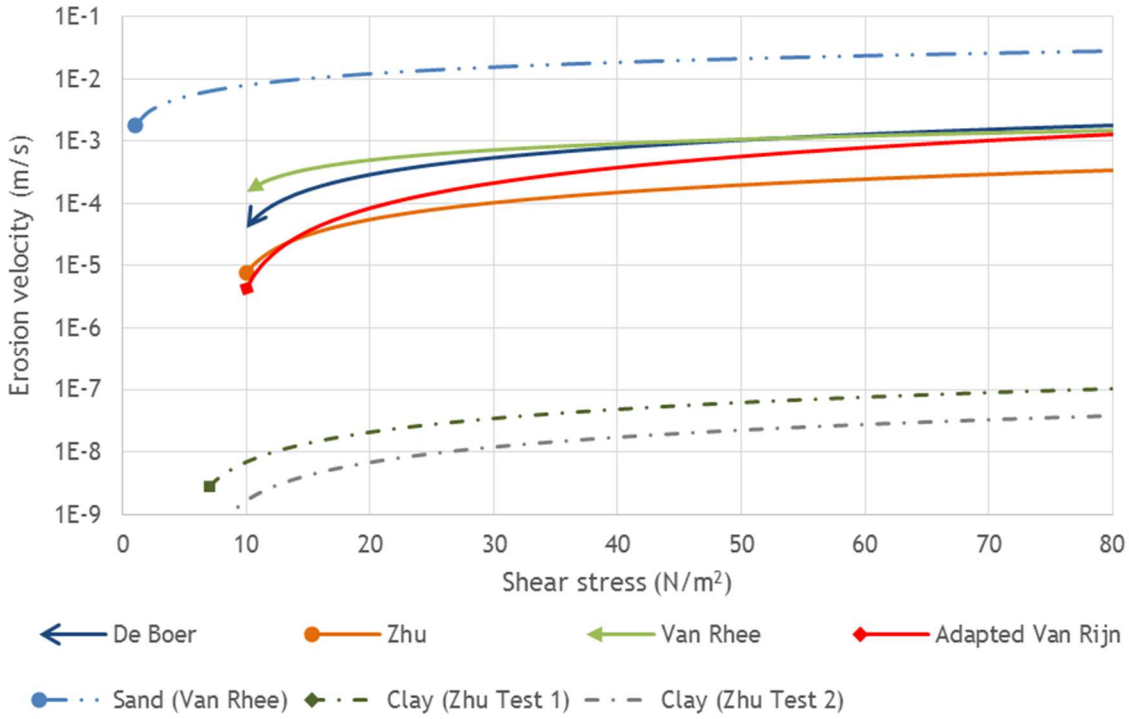

Figure 83 - Erosion velocities as function of shear stress for the formulas of De Boer, Zhu, Van Rhee and adapted Van Rijn, as well as the theoretical erosion velocities for sand and clay

The adapted Van Rijn formula is primarily based on the difference in critical shear stress and does not take the other difference in soil properties into account. This might give unrealistic results and therefore this formula s not used in the BRES-model. The Van Rhee formula takes, besides the difference in critical shear stress, also the difference in porosity and hydraulic conductivity into account. However, it does not include the density difference caused by the cementation and it is a formula for non-cohesive sediment. Based on these arguments, this formula is also not used in the BRES-model.

This leaves the formula of De Boer and of Zhu. These formulas take into account the same soil characteristics. The main differences between the formulas is the way the critical shear stress is incorporated into the formulas. Without data to compare the erosion rates to, it is difficult to determine which of these formulas gives better results. Due to the uncertainties in the parameters, the formula with the higher erosion velocities is used in the BRES-model, which is the formula of De Boer.

It should be noted that the results of these formulas are based on the soil properties and some estimated parameters. Due to this, it is not possible to say that these are accurate erosion velocities for biological improved sands. To verify this, the erosion velocity of the material should be measured and compared to these formulas. Since no such measurements are available, the outcome of these formulas is the best estimate available for the erosion velocities.

Erosion formula sand-fibre mixture

In this section the influence of fibres on the erosion rate of sand is described.

Types of fibres

The types of fibres for researching the influence of fibres on the erosion rate of sand are those which are used to weave geotextiles. Geotextile can be used for protecting slopes from surface erosion or as a filter in a revetment. Geotextiles are normally made from polypropylene (PP) or polyester (PET) fibres, but can also be made from glass fibres. The properties of these fibres are given in Table 28 (Hejazi, et al., 2012). These fibres were chosen because of their durability and known use in practice.

	Glass	*Polypropylene*	*Polyester*
Length, L_f [mm]	25	50	64
Average diameter, D_f [μm]	11	86.5	35
Density, ρ_f [kg/m^3]	2550	920	1350
Mass, M_f [mg]	0.006	0.270	0.083

Table 28 - Fibre properties (from (Hejazi, et al., 2012))

Reduction of erosion

It is expected that sand mixed with fibres reduces the erosion rate of sand. In literature there are no known formulas for calculation of this reduction by fibres. However, randomly distributed fibres resemble a fibrous root system, as described in appendix A. For the erosion reducing effect of fibrous root systems empirical formulas are available (De Baets, et al., 2005), (De Baets & Poesen, 2010):

- Composed formula:

$$RSD = \exp(-2.45RD + 0.03RD \cdot (1 - f_{\%})) \quad \text{(B.34)}$$

- Hill formulas:

$$RSD = \frac{RD^{-1.76}}{1.59 + RD^{-1.76}} \quad \text{(B.35)}$$

$$RSD = \frac{RLD^{-2.22}}{0.000026 + RLD^{-2.22}} \quad \text{(B.36)}$$

- Exponential formulas:

$$RSD = \exp(-1.14RD) \quad \text{(B.37)}$$

$$RSD = \exp(-0.0062\,\mathrm{RLD}) \quad \text{(B.38)}$$

- Power formulas:

$$RSD = 0.35RD^{-0.71} \quad \text{(B.39)}$$

$$RSD = 16.38RLD^{-0.78} \quad \text{(B.40)}$$

These formulas calculate an erosion reduction factor, RSD (Relative Soil Detachment rate). This factor multiplied with the erosion rate of unimproved sand, gives the erosion rate of sand mixed with fibres. These formulas are either a function of the Root mass Density (RD) or the Root Length Density (RLD). The RD is the mass of roots or fibres (in kg) divided by the soil volume (in m^3) and the RLD is the total length of roots or fibres (in km) divided by the soil volume (in m^3):

$$RD = \frac{f_{\%} \cdot \rho_f \cdot V_{soil}}{V_{soil}} = f_{\%} \cdot \rho_f \quad \text{(B.41)}$$

$$RLD = \frac{f_{\%} \cdot \rho_f \cdot V_{soil}}{M_f} \cdot \frac{L_f}{1000} \cdot \frac{1}{V_{soil}} = \frac{f_{\%} \cdot \rho_f}{M_f} \cdot \frac{L_f}{1000} \quad \text{(B.42)}$$

in which:

RD	= Root (or fibre) mass Density [kg/m^3]
RLD	= Root (or fibre) Length Density [km/m^3]
$f_{\%}$	= volume percentage of fibres [-]
ρ_f	= fibre density [kg/m^3]
V_{soil}	= soil volume [m^3]
M_f	= fibre mass [kg]
L_f	= fibre length [m]

These seven formulas can be used to determine the erosion reduction. It should be noted that these formulas are determined using experiments on grass root systems in loamy soil and are thus not tested for fibres in sand. However, it is the best available approximation and experiments should be executed to determine the validity of the formulas or to improve them.

To compare the formulas, for each formula and fibre type the fibre percentages to achieve different reduction rates were determined, as can be seen in Table 29.

Formula:	***(B.34)***	***(B.35)***	***(B.36)***	***(B.37)***	***(B.38)***	***(B.39)***	***(B.40)***
Glass fibre							
$f_{\%}$ (100x reduction)	0.07%	0.41%	0.01%	0.16%	0.01%	5.86%	0.13%
$f_{\%}$ (10x reduction)	0.04%	0.11%	0.00%	0.08%	0.00%	0.23%	0.01%
Polypropylene fibre							
$f_{\%}$ (100x reduction)	0.21%	1.14%	0.54%	0.44%	0.44%	16.3%	7.76%
$f_{\%}$ (10x reduction)	0.10%	0.29%	0.18%	0.22%	0.22%	0.63%	0.41%
Polyester fibre							
$f_{\%}$ (100x reduction)	0.14%	0.77%	0.09%	0.30%	0.07%	11.1%	1.27%
$f_{\%}$ (10x reduction)	0.07%	0.19%	0.03%	0.15%	0.04%	0.43%	0.07%

Table 29 - Comparison of formulas

It is difficult to determine which formula to use, when no erosion measurements are available for synthetic fibres. When looking at the outcome of the formulas, it can be seen that the outcome of the exponential formulas for polypropylene ((B.37) and (B.38)) are the same. This might indicate that these formulas for polypropylene fibres give the most consistent results. However, this can only be proven by comparing the formula outcomes to measurements. Since there are no measurements, one of these exponential formulas is used to compare the fibre types to each other. It is less elaborate to determine RD, so formula (B.37) is used. Using this formula, for all three fibre types the erosion rate was calculated for different fibre percentages, which can be seen in Figure 84.

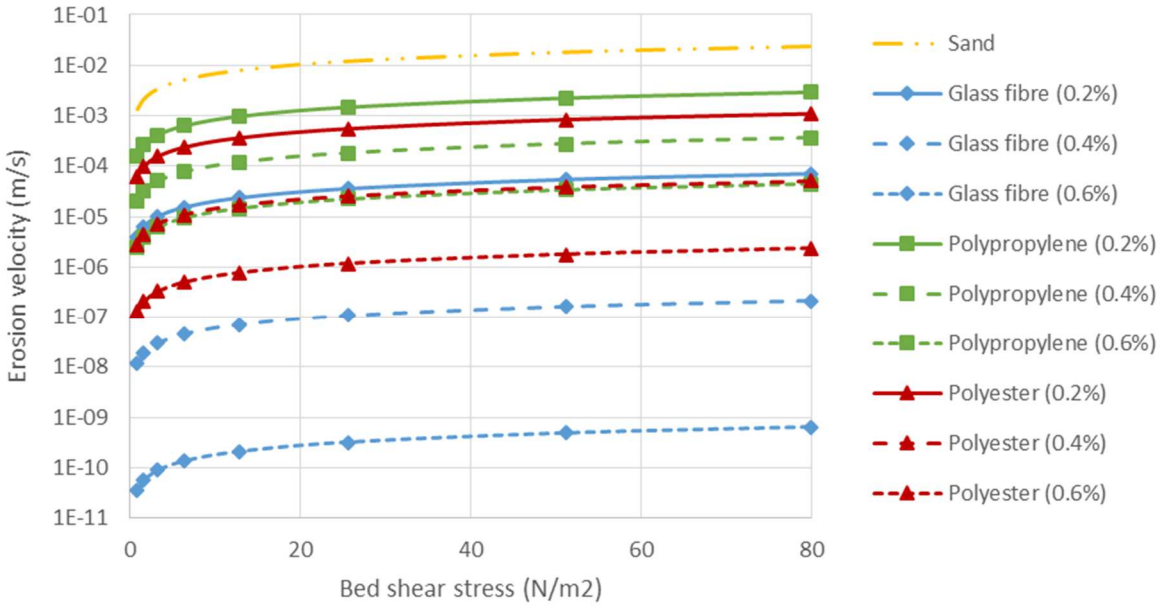

Figure 84 - Erosion velocities as function of bed shear stress for various fibre types and percentages

It can be seen that glass fibres give the greatest reduction using this formula and polypropylene fibres give the least reduction. Since there are a lot of uncertainties in calculating this erosion velocity, the fibre type with the least reduction is used, the polypropylene fibres. As already mentioned, this fibre type in combination with the used formula seems to give the most consistent results.

Because of the uncertainties, it is recommended to conduct more research into the behaviour and modelling of the erosion rate of sand mixed with fibres.

The conclusion of the above reasoning leads to an erosion formula for sand mixed with fibres, given by:

$$V_{e\_sand-fibres} = V_{e\_sand} \cdot RSD \tag{B.43}$$

$$RSD = \exp(-1.14RD) \tag{B.44}$$

in which:

$V_{e\_sand-fibres}$ = erosion velocity of sand-fibre mixture [m/s]
V_{e_sand} = erosion velocity of sand [m/s]
RSD = relative soil detachment rate [-]
RD = fibre density in mixture [kg/m^3]

Generally the weight content of the fibres in the mixture is between 0-1% (Hejazi, et al., 2012). The study that determined the formula (De Baets, et al., 2005), stated that a RD above 4 kg/m^3 does not reduce erosion further. For the chosen fibre type that is approximately 0.44% fibres. The fibre percentage which will be used, will have to be determined for each situation. With increasing fibre percentage, it gets more difficult to achieve a homogeneous mixture, so it is favourable to choose the lowest fibre percentage which achieves the necessary erosion reduction.

C Model results promising options

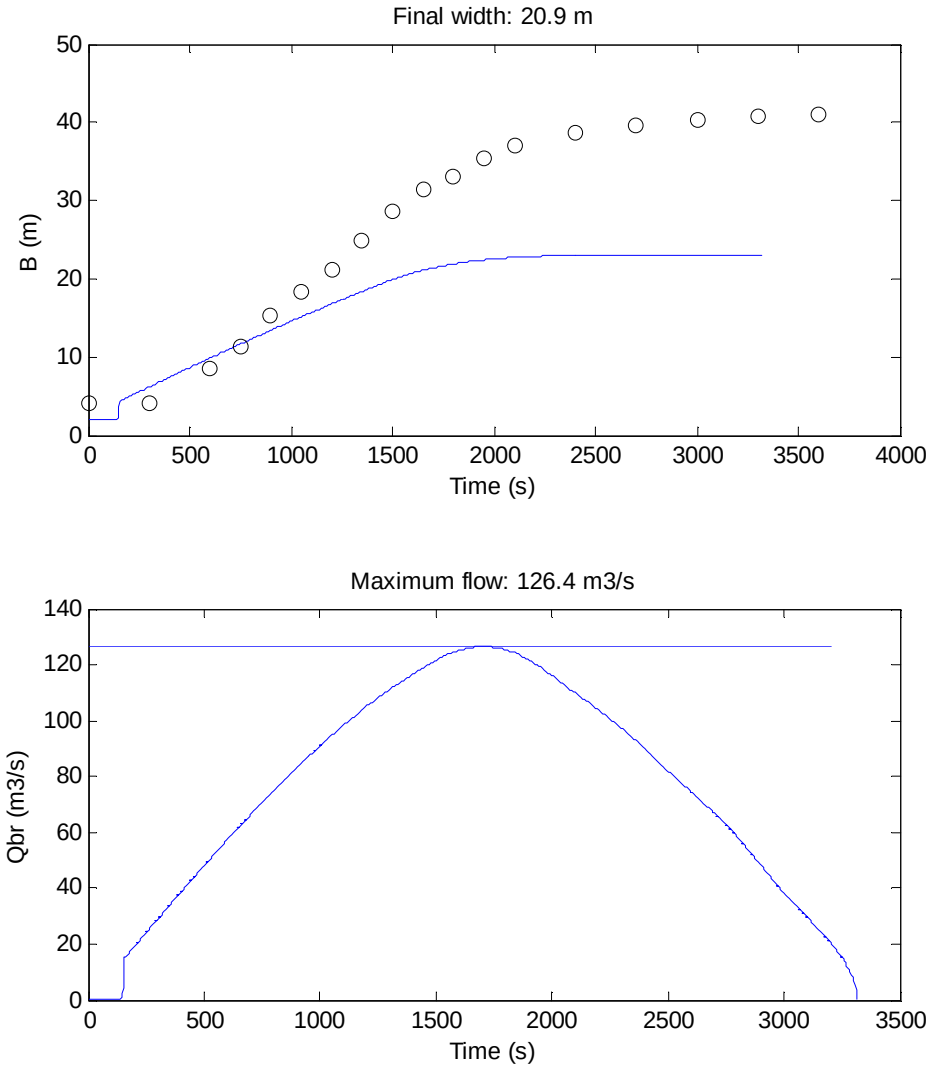

Figure 85 - Breach width (B) and flow rate (Qbr) as function of time for 2% added bentonite (t≈3300 s), circles are ZWIN'94 experiment results

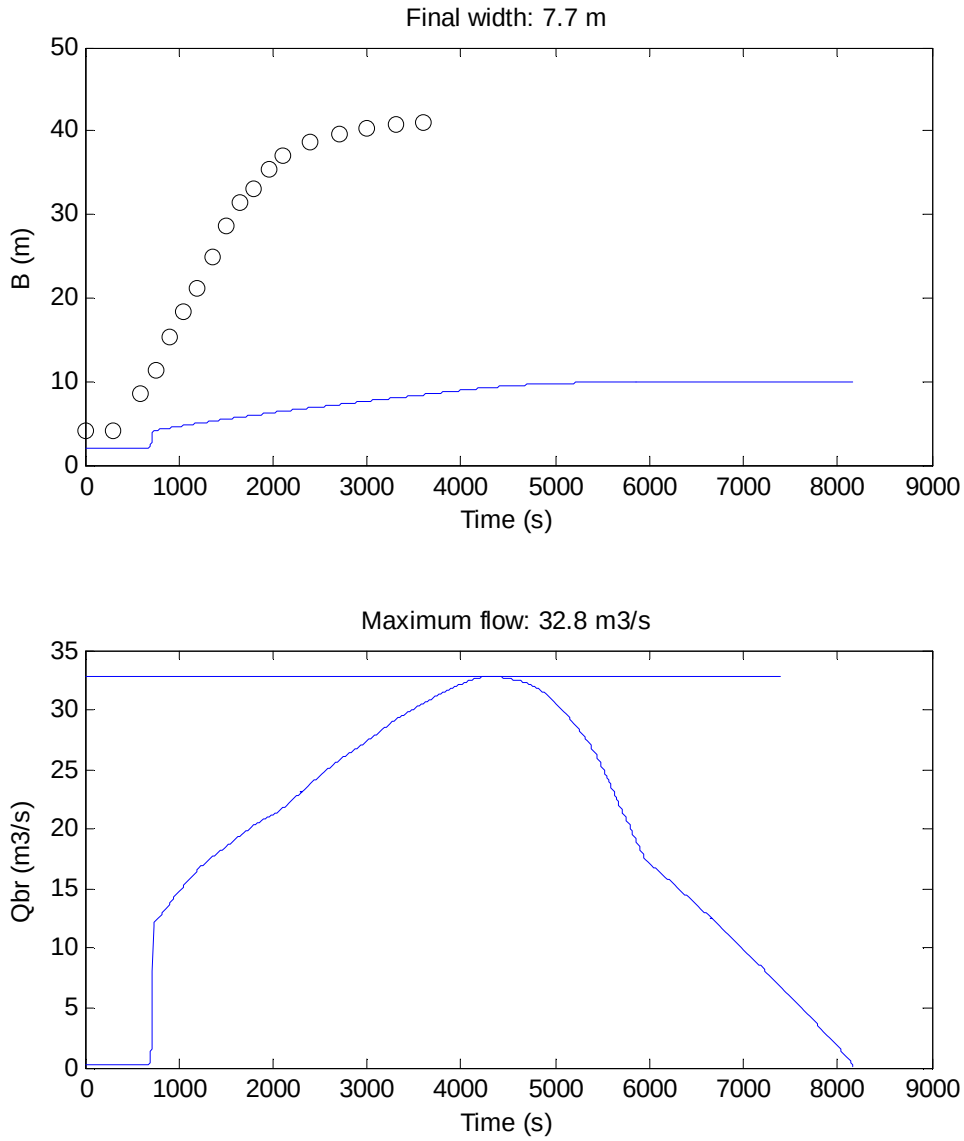

Figure 86 - Breach width (B) and flow rate (Q_{br}) as function of time for 4% added bentonite (t≈8200 s), circles are ZWIN'94 experiment results

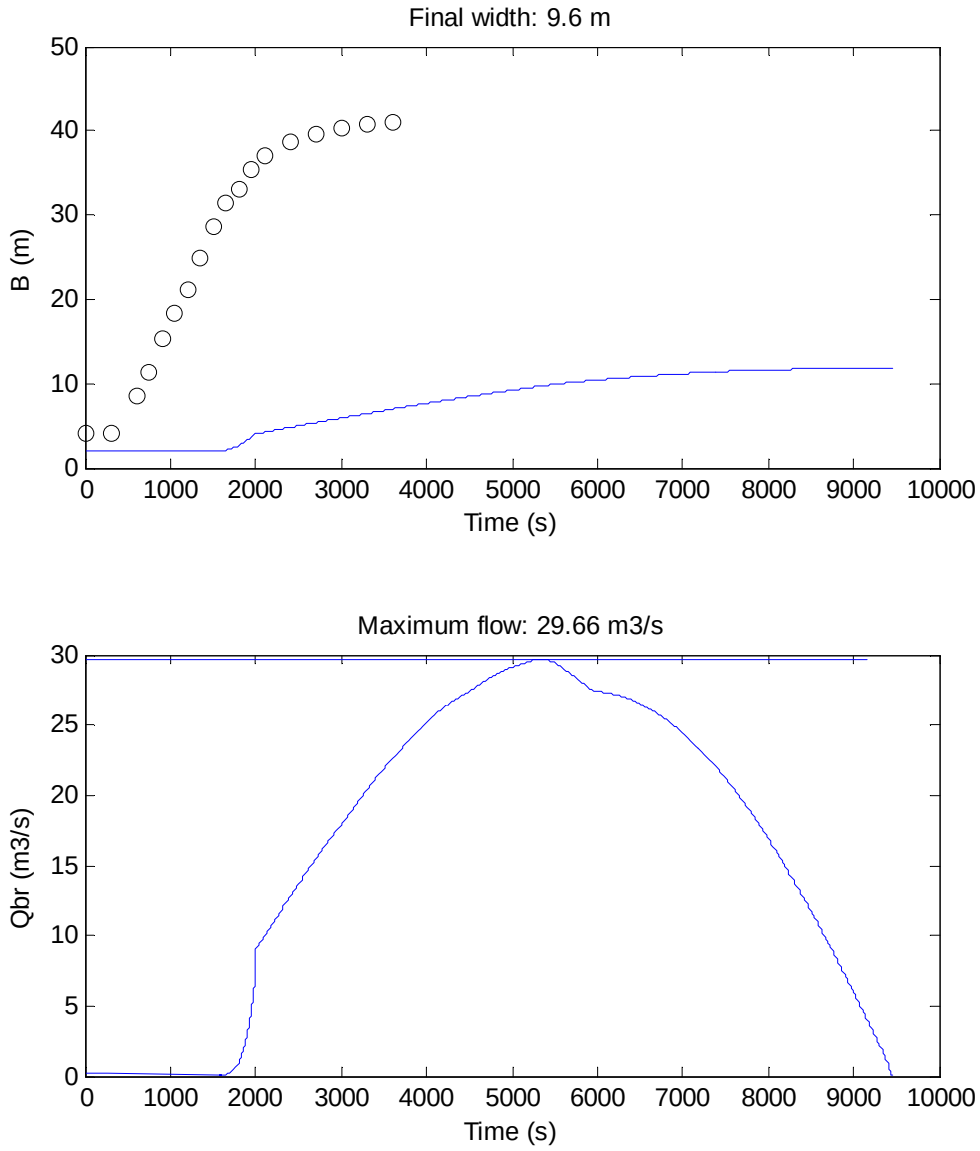

Figure 87 - Breach width (B) and flow rate (Q_{br}) as function of time for sand-fibre dike (t≈9400 s), circles are ZWIN'94 experiment results

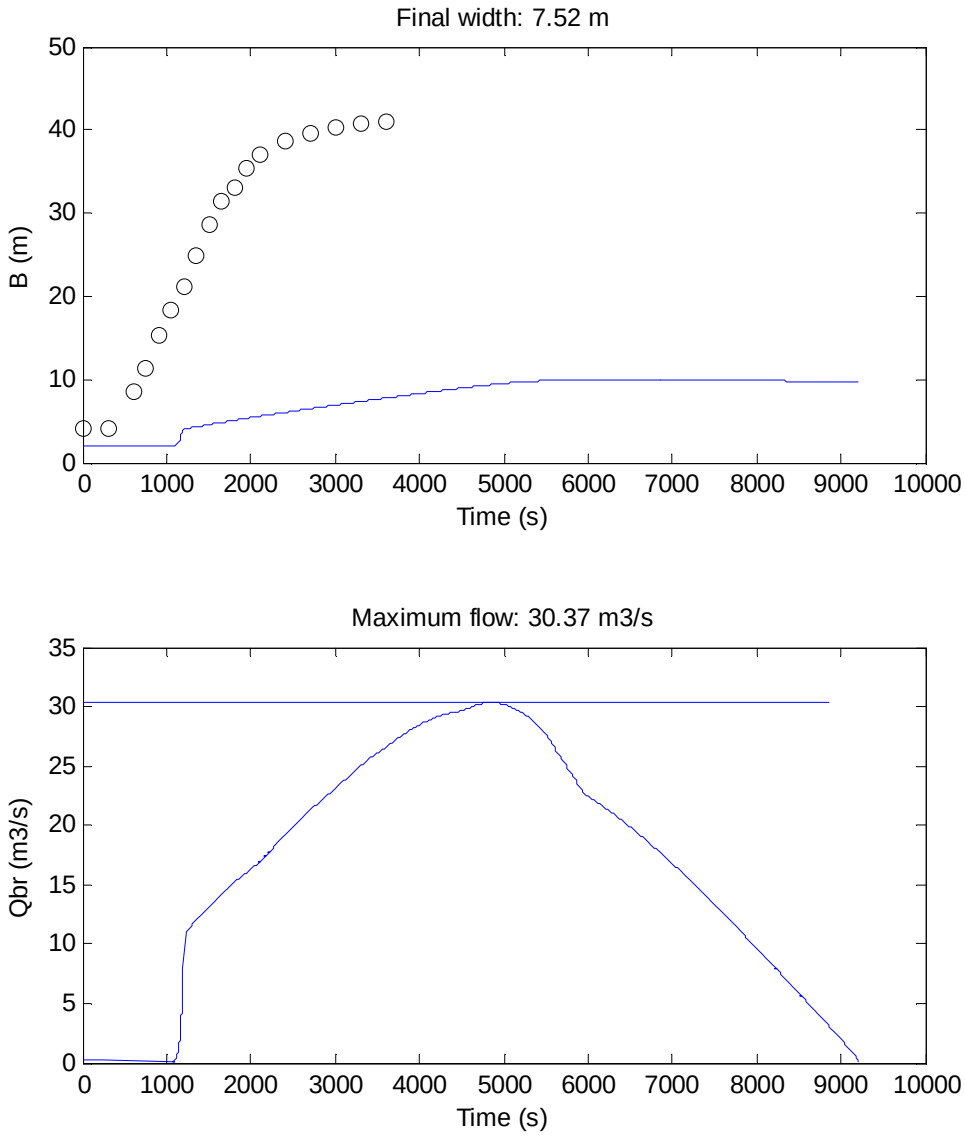

Figure 88 - Breach width (B) and flow rate (Q_{br}) as function of time for cemented sand (t≈9200 s), circles are ZWIN'94 experiment results

D Results direct shear experiment

In this appendix the results of all the direct shear tests can be found. For each mixture a graph of the shear stress versus the strain rate at three different normal stresses is given. Also a graph of the maximum shear stress at each normal stress is given. A linear fit line is plotted through these points to calculate the friction angle and (apparent) cohesion. These results are summarized per mixture in a table.

Type of tests

Two type of direct shear tests were performed. For sand and the sand-bentonite mixtures continues shear tests were executed, while for sand-fibres mixture single shear tests were executed. During a continuous test the sample is displaced until it has failed. After the failure, the sample stays untouched and is kept under the same stresses and displacements. Only weights are added to increase the normal stress on the sample. After that, the displacement continues until the sample fails again. A single shear test does only test the sample at one normal stress. After failure a new sample is prepared and the test starts over at a higher normal stress. Continuous tests are faster to perform and the exact same sample is used for tests at different normal stresses. The single test was only used on the sand-fibre mixtures because it could be possible fibres broke during a test. If such a same sample would have been used for a next test, it could give incorrect results.

Sample area correction

The lower part of the sample slides under the top part, thus the area on which the shear force works gets smaller during the test. This influences the calculation of the shear stress. To correct this, the sample area is recalculated at each step, corrected for the displacement. This corrected area is then used to calculate the shear stress. For the continuous tests also the displacement of lower normal stress tests has to be taken into account. This is due to the fact the sample area has gotten smaller during a test until it failed. The next test at a higher normal stress tests the same sample, while it is already displaced in the previous test. Beside the displacement during the actual test, also this initial displacement is used to correct the sample area.

Results sand-fibre mixture

Figure 97 shows the stress-strain curves for a 0.88% mixture. In this graph it can be seen that at higher normal stresses a bump in the curve is visible. This bump occurs at a high shear strain. This could possibly be explained with regard to the behaviour of fibres in sand. The fibres in the sand are randomly orientated and can initially not be in an orientation to increase the shear strength of the sand. As the shear strain increases, the orientation of the fibres might change. This might result into a better orientation for resisting the shear force and thus give a bump in the curves. Another explanation might be that the friction between the fibres and sand increases as the shear strain increases. This could lead to a delayed mobilization of the fibres to resist the shear force, resulting in the bump in the curves. Judging on the difference between the lower and higher fibre content, these effects only play a role at higher fibre content. This hypothesis was tested by redoing the F_n=296 N direct shear test for the sand-fibres (0.44%) sample, till an equally large shear strain was reached. This test showed no bump in the measurement. Since it cannot be concluded with certainty that the results with the bumps is correct, the bumps are ignored.

Direct shear results sand

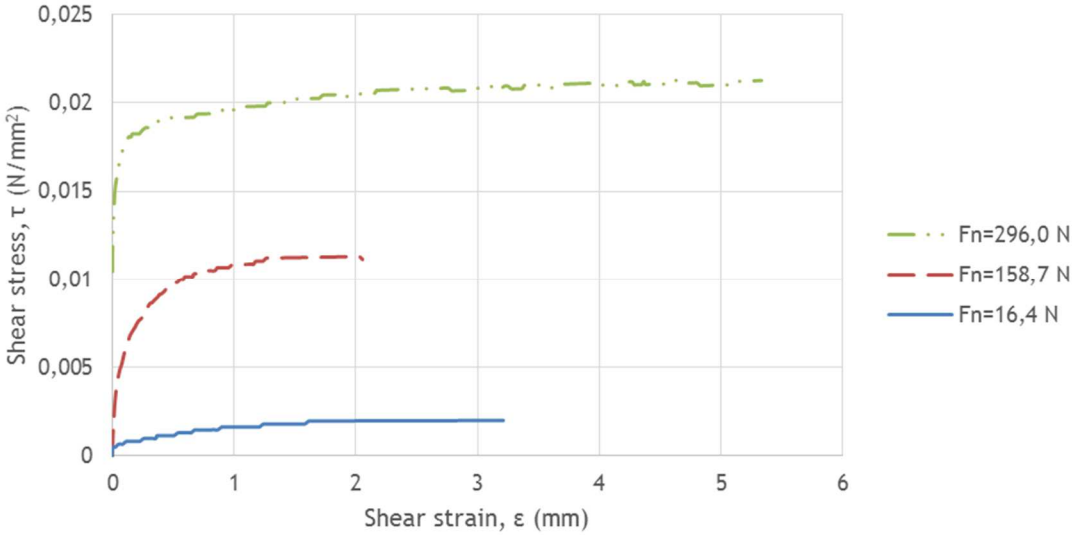

Figure 89 - Stress-strain graph sand

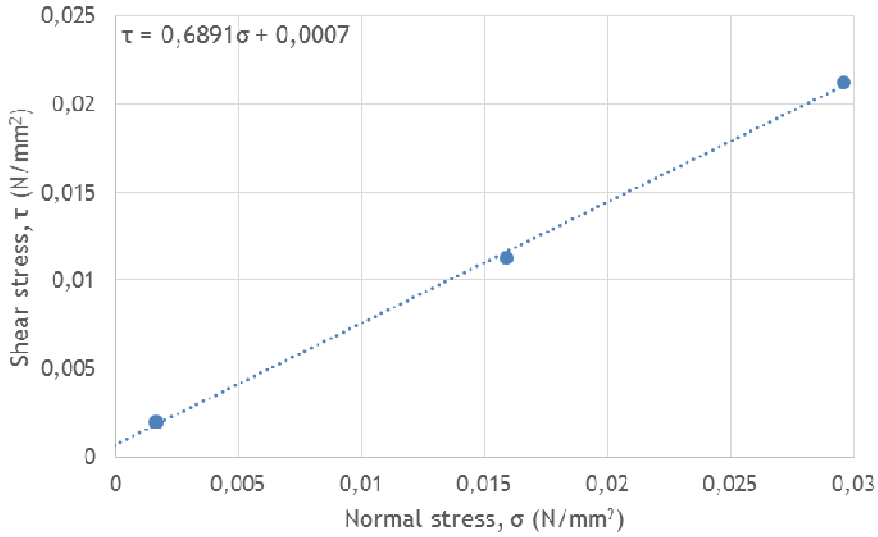

Figure 90 - Results direct shear test sand

Fn [N]	*σ [N/mm²]*	*τ [N/mm²]*
16.4	0.0016	0.0020
158.7	0.0159	0.0113
296.0	0.0296	0.0212
	φ [°]	*c [N/mm²]*
	34.6	7.00E-04
	$\rho_{b\text{-}sand}$ [kg/m³]	*p_{sand} [-]*
	1481	0.44

Table 30 - Results direct shear test sand

Direct shear results sand-bentonite (2%)

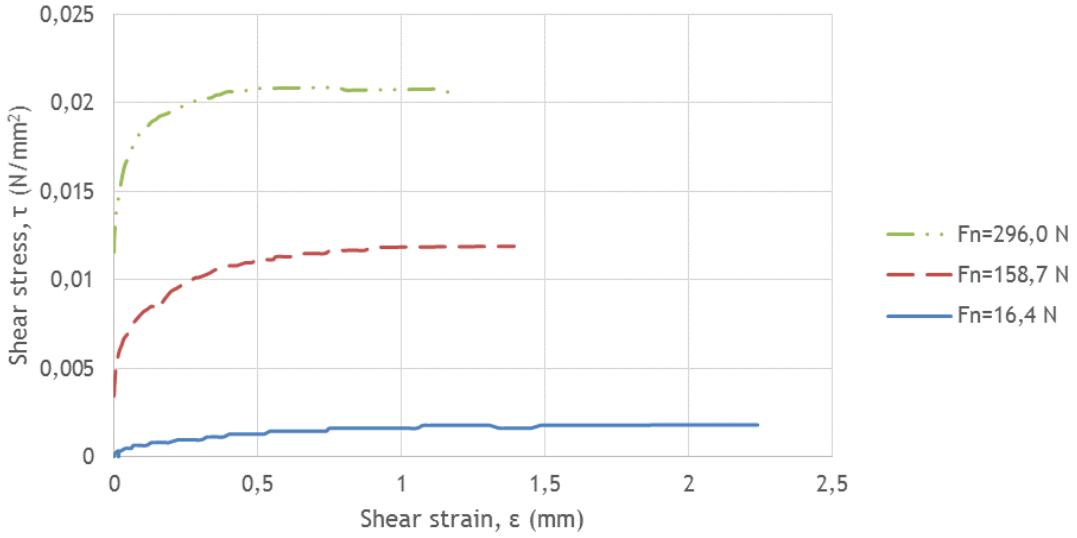

Figure 91 - Stress-strain graph sand-bentonite (2%)

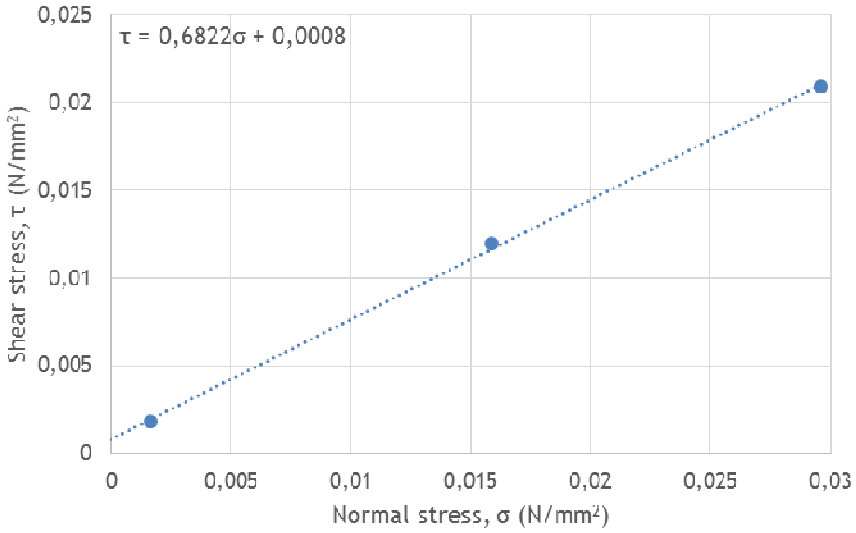

Figure 92 - Results direct shear test sand-bentonite (2%)

Fn [N]	*σ [N/mm²]*	*τ [N/mm²]*
16.4	0.0016	0.0018
158.7	0.0159	0.0119
296.0	0.0296	0.0209
	φ [°]	*c [N/mm²]*
	34.3	8.00E-04
	$\rho_{b\text{-}sand}$ [kg/m³]	*p_{sand} [-]*
	1464	0.45

Table 31 - Results direct shear test sand-bentonite (2%)

Direct shear results sand-bentonite (4%)

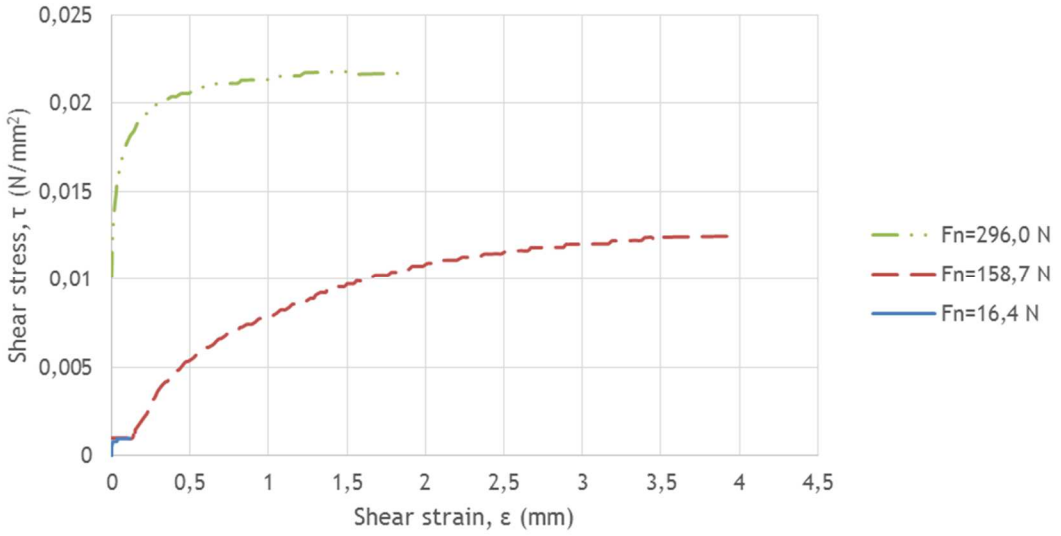

Figure 93 - Stress-strain graph sand-bentonite (4%)

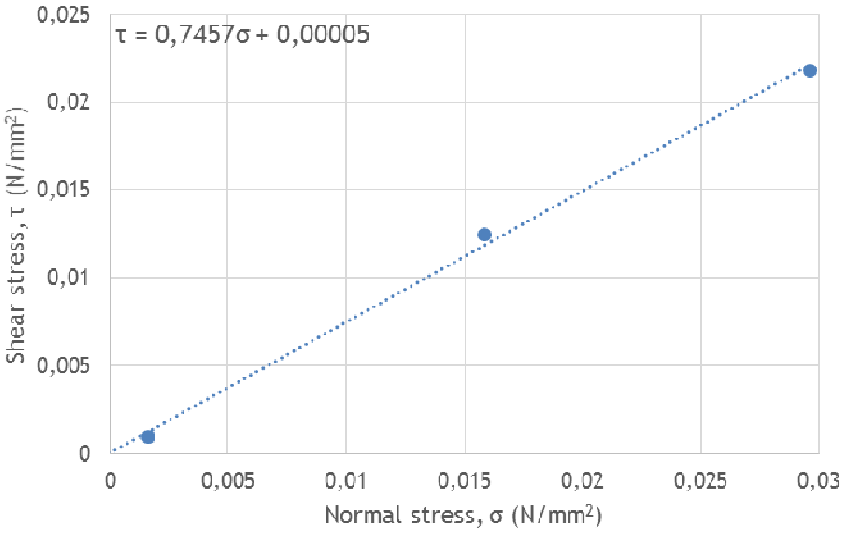

Figure 94 - Results direct shear test sand-bentonite (4%)

Fn [N]	*σ [N/mm²]*	*τ [N/mm²]*
16.4	0.0016	0.0010
158.7	0.0159	0.0125
296.0	0.0296	0.0218
	φ [°]	*c [N/mm²]*
	36.7	3.00E-05
	$\rho_{b\text{-}sand}$ [kg/m³]	*p_{sand} [-]*
	1446	0.45

Table 32 - Results direct shear test sand-bentonite (4%)

Direct shear results sand-fibres (0.44%)

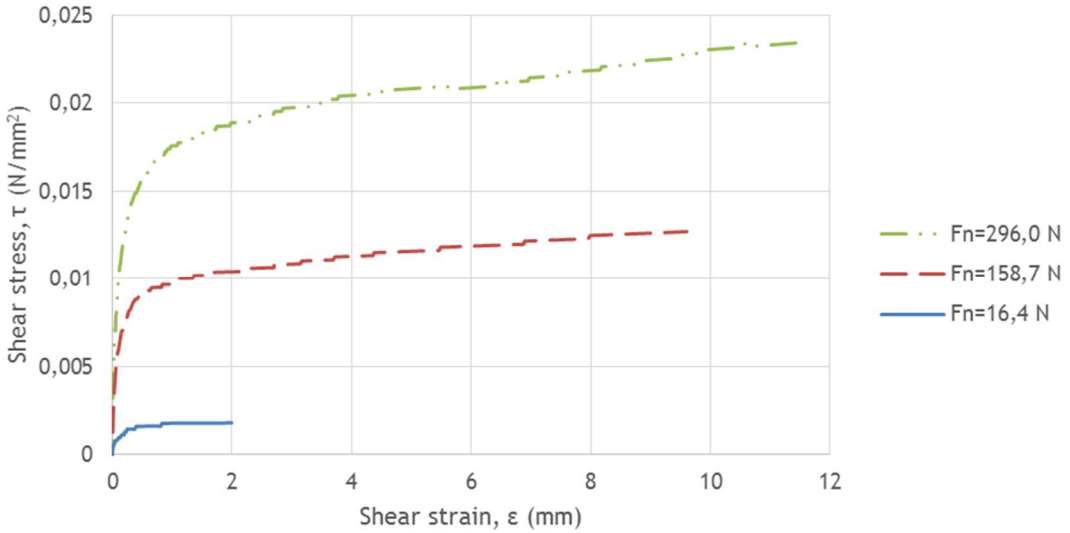

Figure 95 - Stress-strain graph sand-fibres (0.44%)

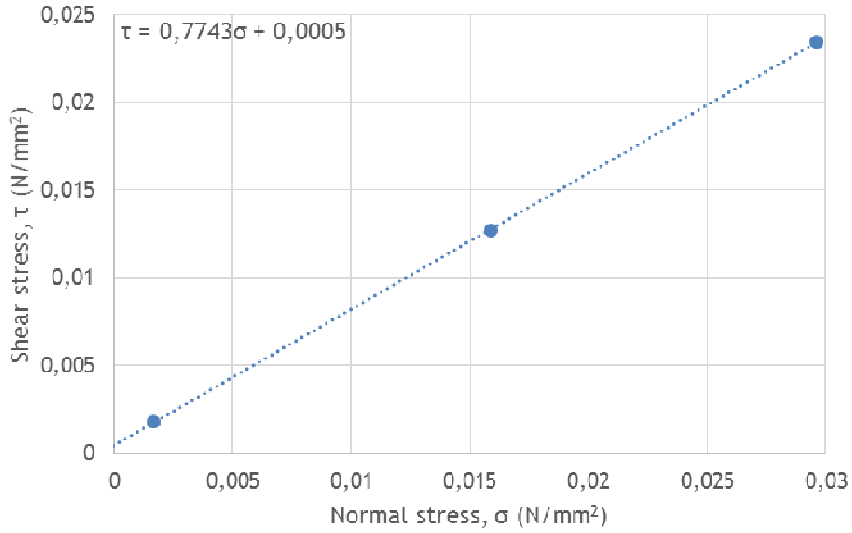

Figure 96 - Results direct shear test sand-fibres (0.44%)

Fn [N]	*σ [N/mm²]*	*τ [N/mm²]*
16.4	0.0016	0.0018
158.7	0.0159	0.0127
296.0	0.0296	0.0234
	φ [°]	*c [N/mm²]*
	37.8	5.00E-04
	$\rho_{b\text{-}sand}$ [kg/m³]	*p_{sand} [-]*
	1478	0.44

Table 33 - Results direct shear test sand-fibres (0.44%)

Direct shear results sand-fibres (0.88%)

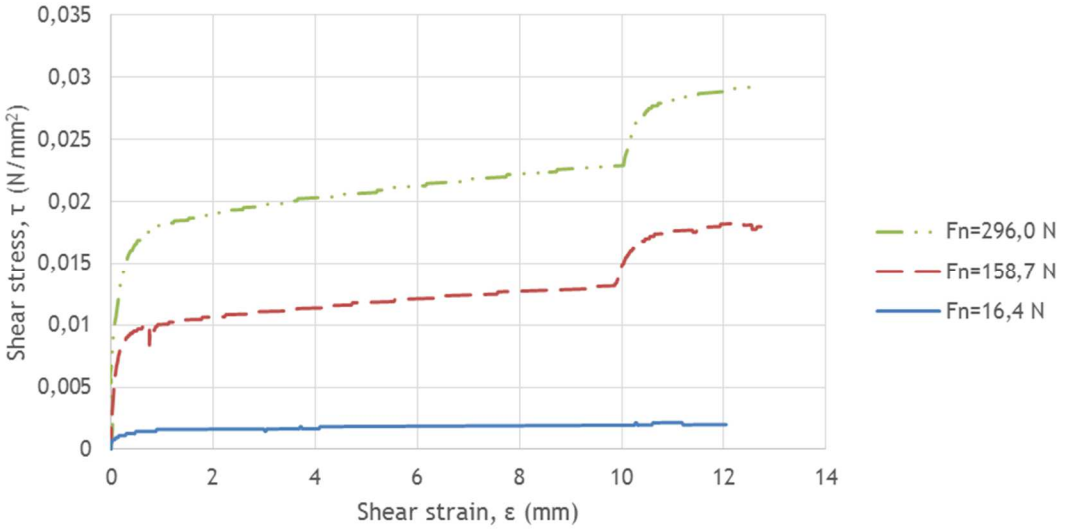

Figure 97 - Stress-strain graph sand-fibres (0.88%)

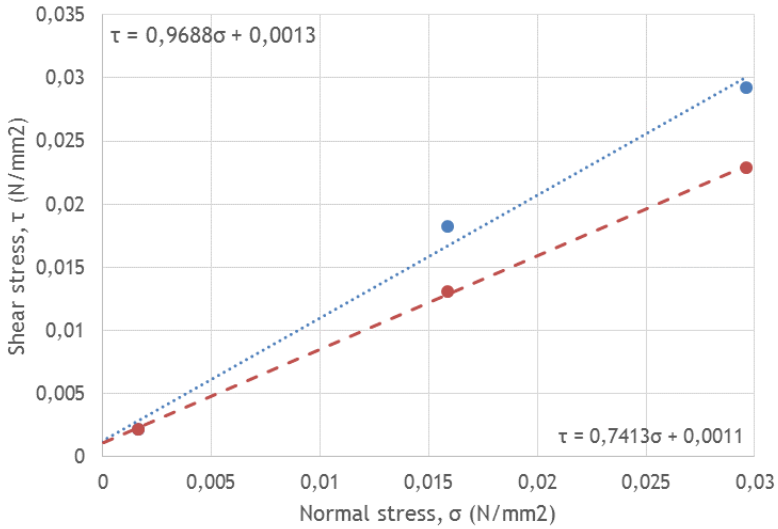

Figure 98 - Results direct shear test sand-fibres (0.88%), with (top line) and without (bottom line) taking the sudden shear strength increase (bumps in Figure 97) into account

Fn [N]	*σ [N/mm²]*	*τ [N/mm²] (top)*	*τ [N/mm²] (bottom)*
16.4	0.0016	0.0022	0.0022
158.7	0.0159	0.0182	0.0131
296.0	0.0296	0.0292	0.0229
	φ [°]	*c [N/mm²]*	
Top line	44.1	1.30E-03	
Bottom line	36.5	1.10E-03	*(used in Figure 33)*
	$\rho_{b\text{-}sand}$ [kg/m³]	*p_{sand} [-]*	
	1474	0.44	

Table 34 - Results direct shear test sand-fibres (0.88%)

E Results permeability experiment

In Figure 99 for each mixture the water level above the sample over time is plotted.

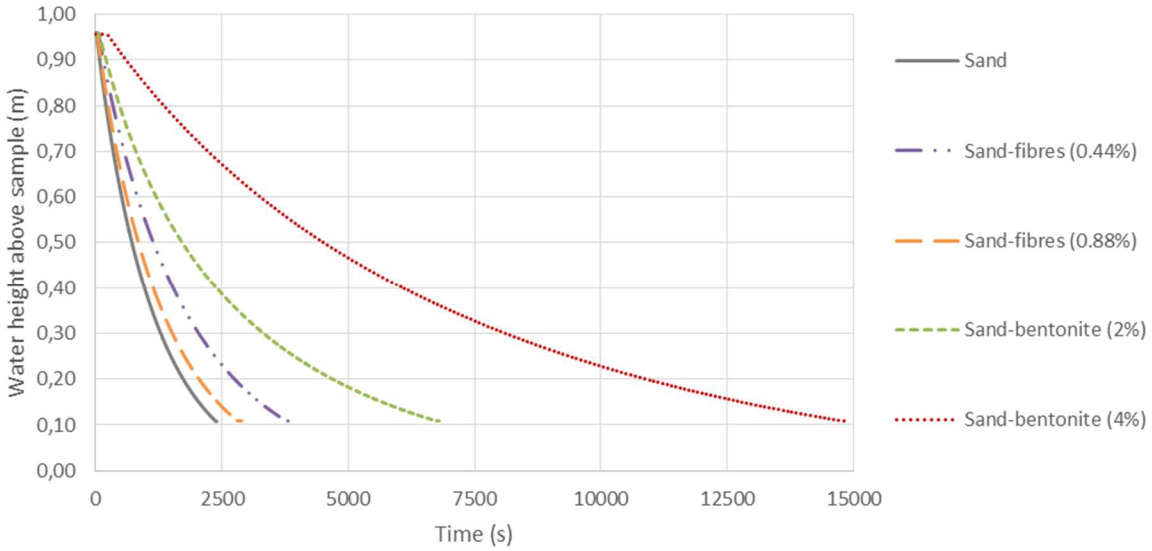

Figure 99 - Measurements falling head tests

These curves are used to calculate the hydraulic conductivity coefficient, using (Geotechdata.info, 2013):

$$K = \frac{a \cdot L}{A \cdot \Delta t} \ln\left(\frac{h_1}{h_2}\right) \qquad \text{(E.1)}$$

In which:

K	= hydraulic conductivity coefficient [m/s]
A, a	= area of column/mixture sample [m^2] (=0.040602 m^2)
L	= length of the mixture sample [m] (=0.21 m)
h1, h2	= higher and lower water level above sample [m]
Δt	= time between higher and lower water level [s]

Using this formula (E.1) and these curves, the hydraulic conductivity coefficients for the different mixtures were calculated, as shown in Table 35.

	Sand	*Sand-fibres (0.44%)*	*Sand-fibres (0.88%)*	*Sand-bentonite (2%)*	*Sand-bentonite (4%)*
h_1 *[m]*	0.900	0.900	0.900	0.900	0.900
h_2 *[m]*	0.200	0.200	0.200	0.200	0.200
t_1 *[s]*	83	159	115	219	622
t_2 *[s]*	1737	2748	2056	4693	10884
Δt [s]	1654	2589	1941	4474	10262
K [m/s]	**1.91E-04**	**1.22E-04**	**1.63E-04**	**7.07E-05**	**3.08E-05**
$\rho_{b\text{-}sand}$ *[kg/m^3]*	1513	1509	1505	1495	1477
p_{sand} *[-]*	0.43	0.43	0.43	0.44	0.44

Table 35 - Results falling head test and determination of hydraulic conductivity coefficient (K)

F Results erosion experiment

This appendix contains the results of the erosion tests. For each mixture the conditions for the Q=10 L/s and Q=20 L/s test are given. For each test the water levels and bed levels are plotted over time versus the measurements points. Each line represents the levels at a point in time, the time interval between two lines is noted above the figures. Using these measurements a graph was made of the results of both tests per mixture. This graph contains data points which represent the time averaged erosion velocities and time averaged flow velocities per measurement point per test. The values of these data points are given in the table below this graph. Through these data points a linear fit line is plotted to obtain an empirical function for the erosion velocity as function of the flow velocity. For this linear fit line the norm of residuals and R^2-value is calculated. The graph also shows the 95% confidence intervals to show the amount of spread in the data. For both tests the bed shear stresses were calculated, as explained in section 7.4. The results of these calculations are given in the tables at the end of each mixture section.

Calculation of flow velocities

Of each test the water levels above the bed for each measurement point are known over time. Furthermore, the width of the flow and flow rate per test are known. Using this data, the flow velocities for each measurement point at each time step are calculated:

$$U = \frac{Q \cdot 10^{-3}}{W_f \cdot (h_w - h_b)} \tag{F.1}$$

in which:

U	= flow velocity [m/s]
Q	= flow rate [L/s]
W_f	= width of flow [m] (=0.105 m)
h_w	= water level above flume bottom [m]
h_b	= bed level above flume bottom [m]

Calculation of erosion velocities

The bed levels above the flume bottom of each measurement point over time are known. These bed levels are used to calculate the erosion velocities of the tests. This is calculated using the difference in bed level between two measurements:

$$V_e = \frac{h_{b(n)} - h_{b(n+1)}}{t_{n+1} - t_n} = \frac{\Delta h_b}{\Delta t} \tag{F.2}$$

in which:

V_e	= erosion velocity [m/s]
h_b	= bed level [m]
t	= time of measurement [s]
Δh_b	= difference in bed level or eroded bed [m]
Δt	= time between measurements [s]

Used measurement points

To make the graphs containing the linear fit lines, only data from the last six measurement points (4 to 9) was used, because the first three gave unreliable results. This was partly due to a bit of turbulence above these points. Another reason was the horizontal movement of the initial bed slope into the measurement area, as can be seen in Figure 100. The water and bed levels were measured, until the bed slope became of too much influence on the measurements. Before that time the influence of the slope was notable in the results of the first three measurement points. This is the main reason the measurements from these points were discarded.

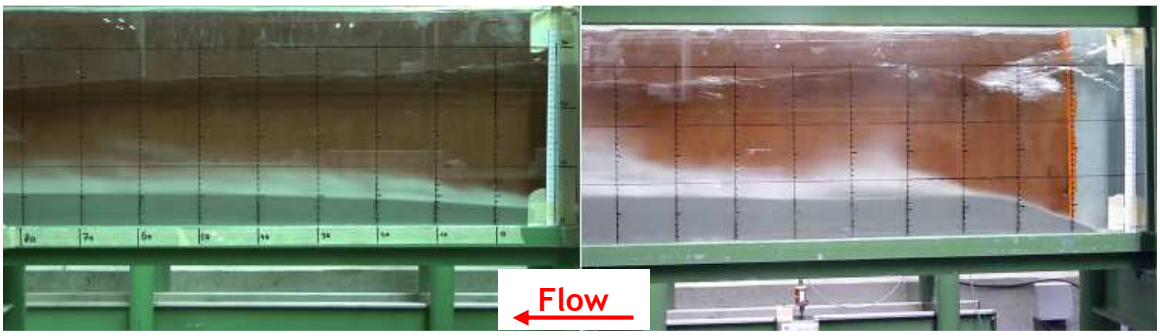

Figure 100 - Horizontal movement of initial bed slope. The picture on the right is at the start of the test. The picture on the left shows the slope entering the measurement area.

Calculation of soil parameters

For each test the bed volume, dry bulk density and porosity are calculated. The porosity and dry bulk density are calculated for just the sand, without an additive. The weight of the sand or mixture for each tests is known. The formulas used to calculate these parameters are given by:

$$V_b = (L_b \cdot h_b + 0.5 \cdot L_{bs} \cdot h_b) \cdot W_f \qquad \text{(F.3)}$$

$$\rho_{db-sand} = \frac{M_b - M_a}{V_b} \qquad \text{(F.4)}$$

$$p_{sand} = 1 - \frac{\rho_{db}}{\rho_s} \qquad \text{(F.5)}$$

in which:

V_b	= volume of bed [m^3]
L_b	= length of bed [m] (=3.37 m)
L_{bs}	= length of bed slope [m] (=0.4 m)
h_b	= initial height of bed [m]
W_f	= width of bed [m] (=0.105 m)
$\rho_{db-sand}$	= dry bulk density of the sand [kg/m^3]
M_b	= weight of the bed material [kg]
M_a	= weight of the additive [kg]
p_{sand}	= porosity of the sand [-]
ρ_s	= density of sand [kg/m^3] (=2650 kg/m^3)

Results clear water tests

Point	*x [m]*	*h [m]*	*U [m/s]*	*U^2 [m^2/s^2]*	*R [m]*	*H [m]*	*p [Pa]*
4	0.30	0.131	0.733	0.537	0.0375	0.1587	1288.2
5	0.40	0.130	0.738	0.545	0.0374	0.1581	1278.2
6	0.50	0.130	0.738	0.545	0.0374	0.1581	1278.2
7	0.60	0.127	0.756	0.571	0.0372	0.1564	1248.5
8	0.70	0.130	0.738	0.545	0.0374	0.1581	1278.2
9	0.80	0.127	0.756	0.571	0.0372	0.1564	1248.5
Mean	0.55	0.129	0.743	0.552	0.0374	0.1576	1270.0

dx [m]	*dh/dx [m/m]*	*dU/dx [m/s/m]*	*dU^2/dx [$m^2/s^2/m$]*	*dH/dx [m/m]*	*dp/dx [Pa/m]*	*corrected dp/dx [Pa/m]*	*$\tau_a=\tau_w$ [Pa]*
0.5	-0.008	0.047	0.069	-0.0046	-79.3	-148.5	5.55

Table 36 - Calculation wall shear stress for Q=10 L/s

Point	*x [m]*	*h [m]*	*U [m/s]*	*U^2 [m^2/s^2]*	*R [m]*	*H [m]*	*p [Pa]*
4	0.30	0.212	0.903	0.816	0.0421	0.2535	2079.4
5	0.40	0.215	0.890	0.792	0.0422	0.2554	2109.6
6	0.50	0.214	0.896	0.803	0.0421	0.2546	2095.9
7	0.60	0.212	0.904	0.816	0.0421	0.2535	2078.4
8	0.70	0.209	0.915	0.837	0.0420	0.2519	2053.0
9	0.80	0.206	0.929	0.863	0.0418	0.2501	2022.0
Mean	0.55	0.211	0.906	0.821	0.0421	0.2532	2073.0

dx [m]	*dh/dx [m/m]*	*dU/dx [m/s/m]*	*dU^2/dx [$m^2/s^2/m$]*	*dH/dx [m/m]*	*dp/dx [Pa/m]*	*corrected dp/dx [Pa/m]*	*$\tau_a=\tau_w$ [Pa]*
0.5	-0.012	0.051	0.094	-0.0069	-114.9	-208.8	8.78

Table 37 - Calculation wall shear stress for Q=20 L/s

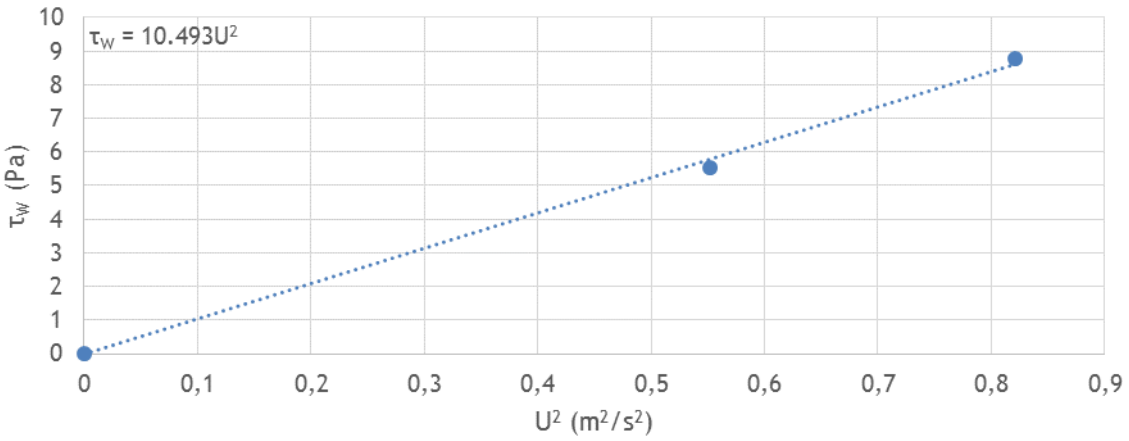

Figure 101 - Wall shear stress as function of U^2

Results erosion tests sand

Parameter	*Value*
Flow rate, Q [L/s]	10.1
Bed height, h_b [m]	0.080
Volume bed, V_b [m^3]	0.02999
Mass bed, M_b [kg]	50
Dry bulk density sand, $\rho_{db\text{-}sand}$ [kg/m^3]	1667
Porosity sand, p_{sand} [-]	0.37
Saturation time [h]	3
Test duration [s]	796

Table 38 - Test conditions sand for Q=10 L/s

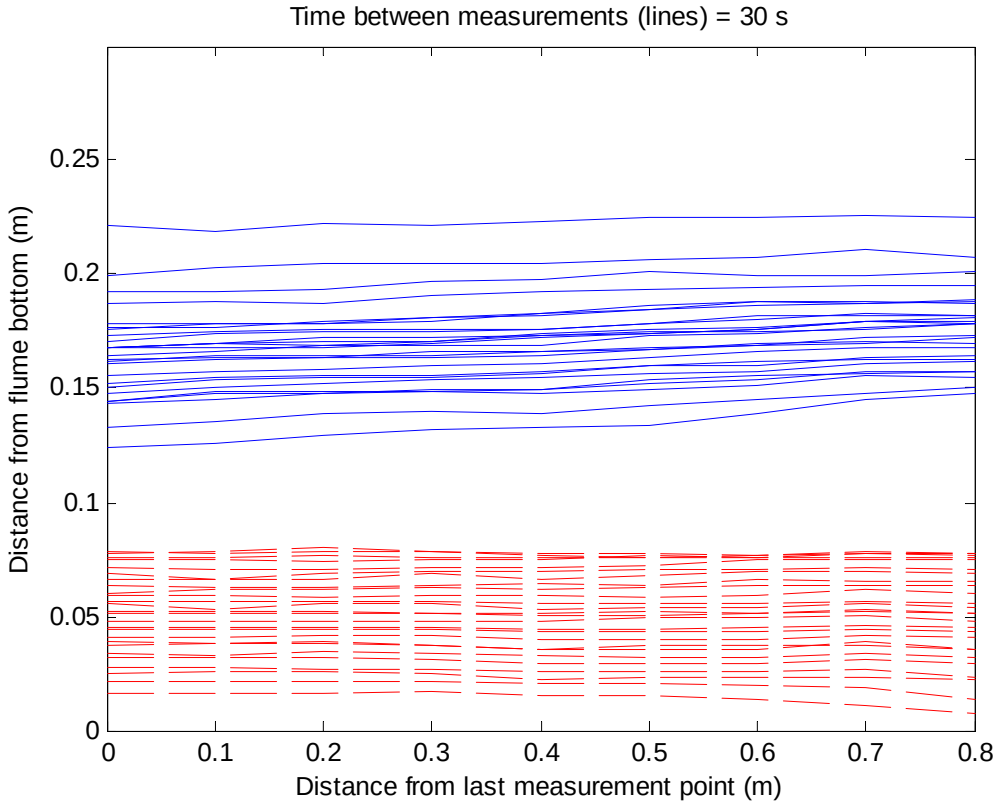

Figure 102 – Water (upper) and sand bed (lower) level measurements for Q=10 L/s

Parameter	*Value*
Flow rate, Q [L/s]	20.1
Bed height, h_b [m]	0.083
Volume bed, V_b [m^3]	0.03111
Mass bed, M_b [kg]	50
Dry bulk density sand, $\rho_{db\text{-}sand}$ [kg/m^3]	1607
Porosity sand, p_{sand} [-]	0.39
Saturation time [h]	4
Test duration [s]	224

Table 39 - Test conditions sand for Q=20 L/s

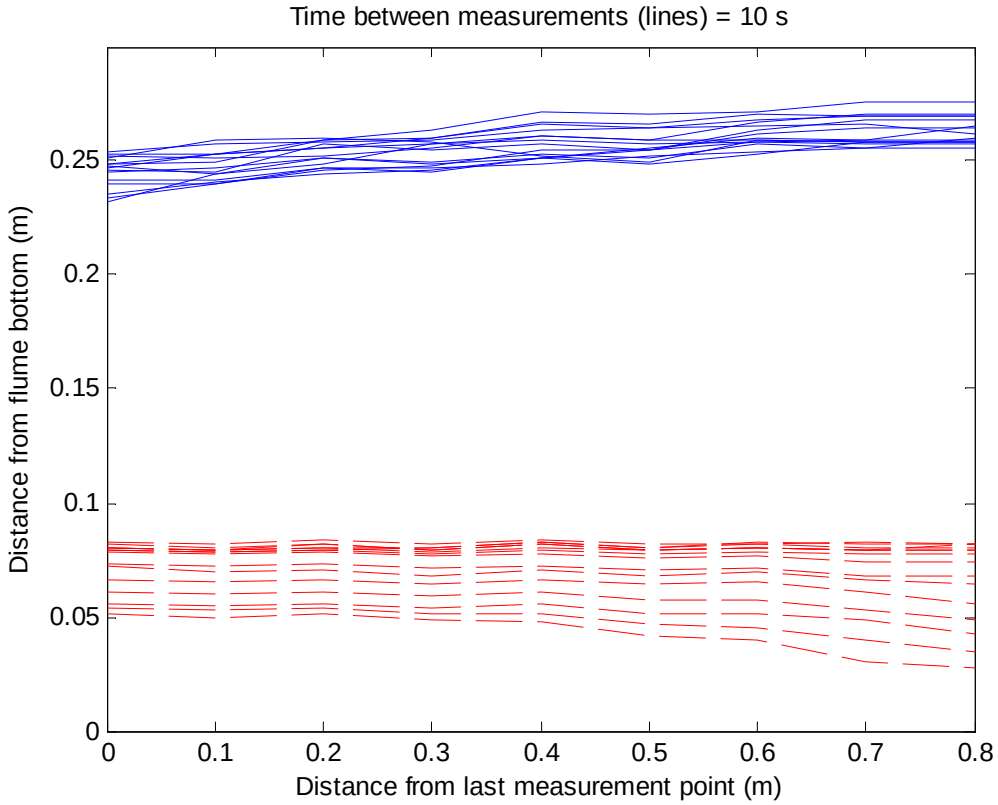

Figure 103 - Water (upper) and sand bed (lower) level measurements for Q=20 L/s

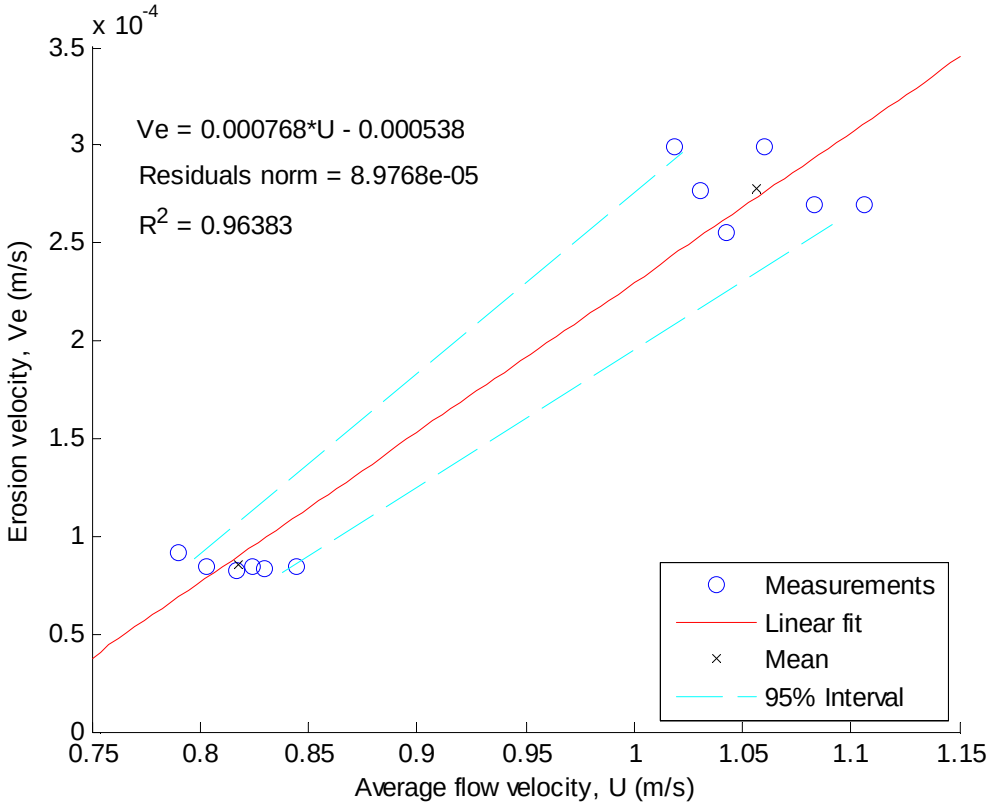

Figure 104 - Figure of average erosion velocity and flow velocities of measurement point 4 to 9 of Q=10 & 20 L/s sand tests; linear fit line plotted through data points, including the 95% confidence interval, formula, norm of residuals and R^2

Measurement point	*U [m/s]*	*V_e [m/s]*
Q=10 L/s		
4	0.790	9.15E-05
5	0.803	8.46E-05
6	0.817	8.19E-05
7	0.824	8.46E-05
8	0.830	8.33E-05
9	0.844	8.46E-05
Mean	**0.818**	**8.51E-05**
Q=20 L/s		
4	1.019	2.99E-04
5	1.030	2.77E-04
6	1.042	2.55E-04
7	1.060	2.99E-04
8	1.083	2.70E-04
9	1.106	2.70E-04
Mean	**1.057**	**2.78E-04**

Table 40 - Flow and erosion velocities sand

Point	*x [m]*	*h [m]*	*U [m/s]*	*U^2 [m^2/s^2]*	*R [m]*	*H [m]*	*p [Pa]*
4	0.30	0.122	0.790	0.624	0.0367	0.1539	1198.3
5	0.40	0.120	0.803	0.644	0.0365	0.1530	1178.6
6	0.50	0.118	0.817	0.667	0.0363	0.1521	1158.5
7	0.60	0.117	0.824	0.679	0.0362	0.1517	1148.5
8	0.70	0.116	0.830	0.688	0.0362	0.1513	1140.4
9	0.80	0.114	0.844	0.713	0.0360	0.1506	1121.0
Mean	0.55	0.118	0.818	0.669	0.0363	0.1521	1157.6

dx [m]	*dh/dx [m/m]*	*dU/dx [m/s/m]*	*dU^2/dx [$m^2/s^2/m$]*	*dH/dx [m/m]*	*dp/dx [Pa/m]*
0.5	-0.016	0.109	0.178	-0.0067	-154.5

τ_a [Pa]	*τ_w [Pa]*	*τ_a-τ_w [Pa]*	*τ_b (Vanoni & Brooks) [Pa]*	*corrected dp/dx [Pa/m]*
12.10	7.02	5.08	4.15	-333.0

Table 41 - Calculation bed shear stress sand for Q=10 L/s

Point	*x [m]*	*h [m]*	*U [m/s]*	*U^2 [m^2/s^2]*	*R [m]*	*H [m]*	*p [Pa]*
4	0.30	0.189	1.019	1.038	0.0411	0.2415	1850.5
5	0.40	0.186	1.030	1.062	0.0410	0.2404	1827.2
6	0.50	0.184	1.042	1.086	0.0408	0.2393	1804.5
7	0.60	0.181	1.060	1.124	0.0407	0.2382	1775.1
8	0.70	0.177	1.083	1.172	0.0405	0.2369	1737.8
9	0.80	0.173	1.106	1.224	0.0403	0.2356	1699.1
Mean	0.55	0.182	1.057	1.118	0.0407	0.2387	1782.4

dx [m]	*dh/dx [m/m]*	*dU/dx [m/s/m]*	*dU^2/dx [$m^2/s^2/m$]*	*dH/dx [m/m]*	*dp/dx [Pa/m]*
0.5	-0.031	0.175	0.372	-0.0119	-303.0

τ_a [Pa]	*τ_w [Pa]*	*τ_a-τ_w [Pa]*	*τ_b (Vanoni & Brooks) [Pa]*	*corrected dp/dx [Pa/m]*
27.50	11.73	15.77	12.38	-675.3

Table 42 - Calculation bed shear stress sand for Q=20 L/s

Results erosion tests sand-bentonite (2%)

Parameter	*Value*
Flow rate, Q [L/s]	10.1
Bed height, h_b [m]	0.085
Volume bed, V_b [m^3]	0.03186
Mass bed, M_b [kg]	50.6
Mass additive, M_a [kg]	0.6
Dry bulk density sand, $\rho_{db\text{-}sand}$ [kg/m^3]	1569
Porosity sand, p_{sand} [-]	0.41
Saturation time [h]	22
Test duration [s]	1252

Table 43 - Test conditions sand-bentonite (2%) for Q=10 L/s

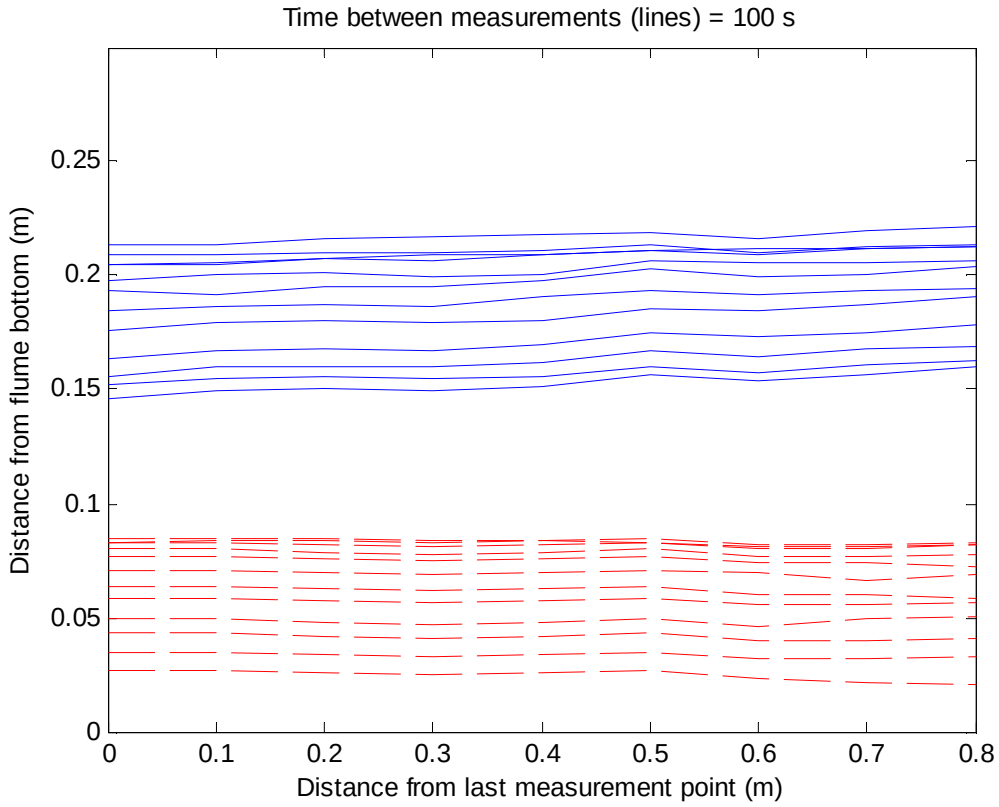

Figure 105 - Water (upper) and sand-bentonite (2%) bed (lower) level measurements for Q=10 L/s

Parameter	*Value*
Flow rate, Q [L/s]	20.2
Bed height, h_b [m]	0.087
Volume bed, V_b [m^3]	0.03261
Mass bed, M_b [kg]	50.6
Mass additive, M_a [kg]	0.6
Dry bulk density sand, $\rho_{db\text{-}sand}$ [kg/m^3]	1533
Porosity sand, p_{sand} [-]	0.42
Saturation time [h]	22
Test duration [s]	405

Table 44 - Test conditions sand-bentonite (2%) for Q=20 L/s

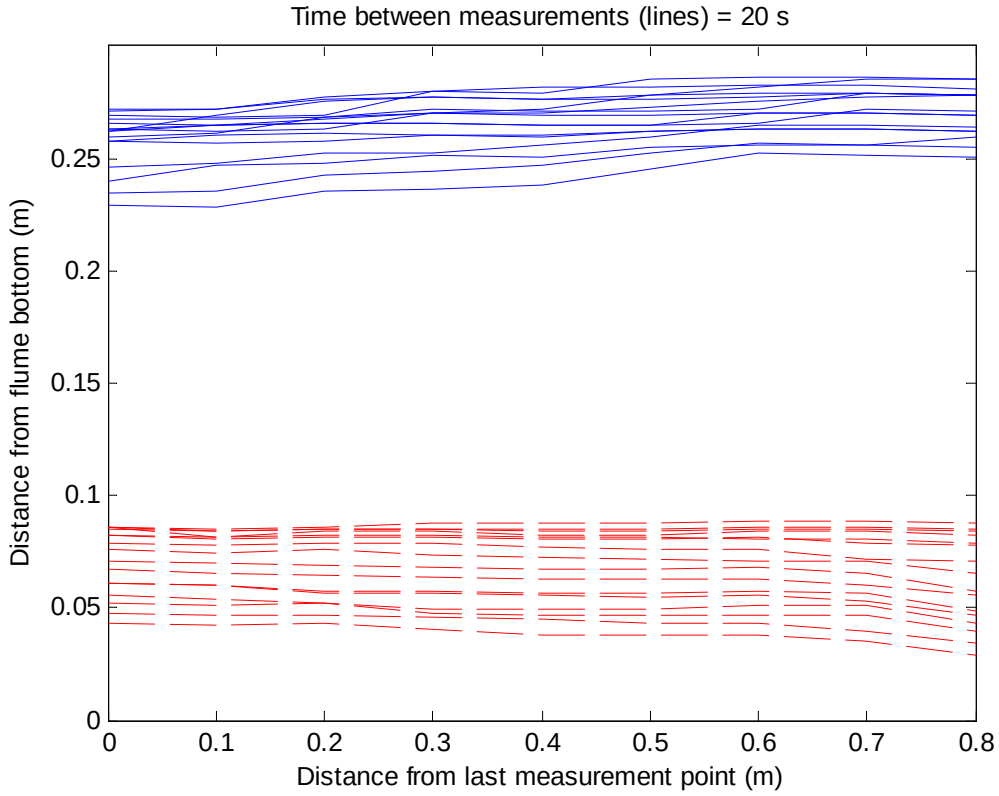

Figure 106 - Water (upper) and sand-bentonite (2%) bed (lower) level measurements for Q=20 L/s

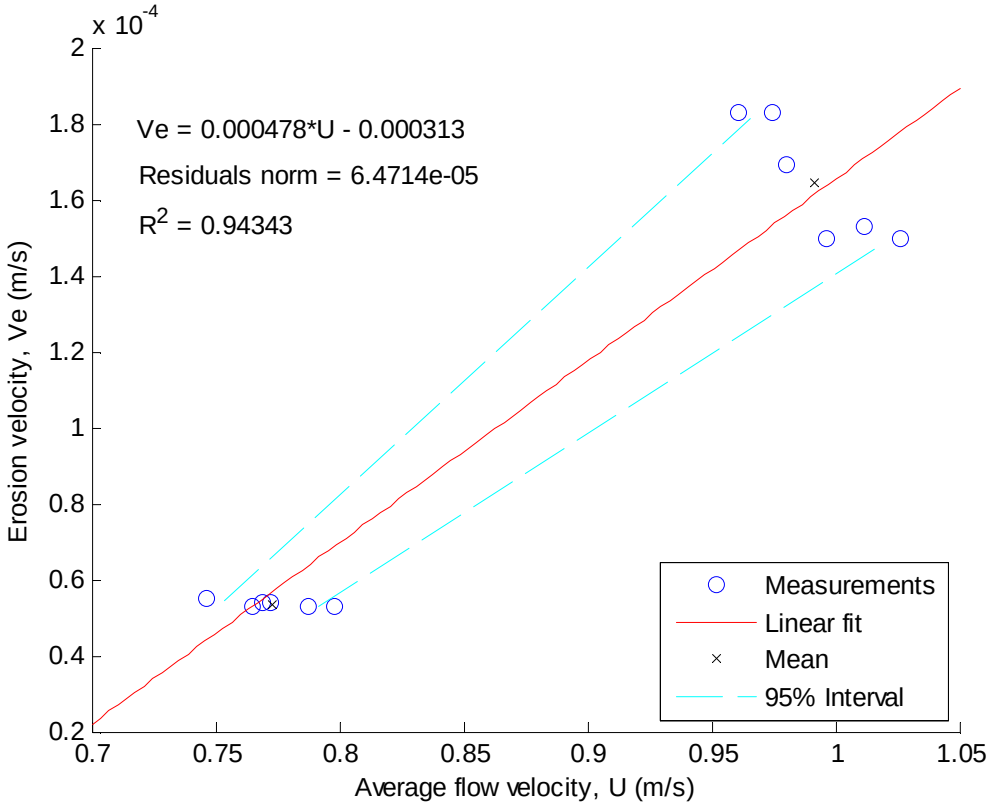

Figure 107 - Figure of average erosion velocity and flow velocities of measurement point 4 to 9 of Q=10 & 20 L/s sand-bentonite (2%) tests; linear fit line plotted through data points, including the 95% confidence interval, formula, norm of residuals and R^2

Measurement point	*U [m/s]*	*V_e [m/s]*
Q=10 L/s		
4	0.746	5.49E-05
5	0.765	5.31E-05
6	0.769	5.40E-05
7	0.772	5.40E-05
8	0.787	5.31E-05
9	0.798	5.31E-05
Mean	**0.773**	**5.73E-05**
Q=20 L/s		
4	0.961	1.83E-04
5	0.974	1.83E-04
6	0.980	1.69E-04
7	0.996	1.49E-04
8	1.012	1.53E-04
9	1.026	1.49E-04
Mean	**0.992**	**1.64E-04**

Table 45 - Flow and erosion velocities sand-bentonite (2%)

Point	*x [m]*	*h [m]*	*U [m/s]*	*U^2 [m^2/s^2]*	*R [m]*	*H [m]*	*p [Pa]*
4	0.30	0.129	0.746	0.557	0.0373	0.1574	1265.5
5	0.40	0.126	0.765	0.585	0.0371	0.1557	1235.4
6	0.50	0.125	0.769	0.592	0.0370	0.1553	1227.9
7	0.60	0.125	0.772	0.596	0.0369	0.1551	1222.8
8	0.70	0.122	0.787	0.620	0.0367	0.1539	1199.4
9	0.80	0.121	0.798	0.637	0.0366	0.1532	1184.3
Mean	0.55	0.125	0.773	0.598	0.0369	0.1551	1222.6

dx [m]	*dh/dx [m/m]*	*dU/dx [m/s/m]*	*dU^2/dx [$m^2/s^2/m$]*	*dH/dx [m/m]*	*dp/dx [Pa/m]*
0.5	-0.017	0.103	0.160	-0.0084	-162.4

τ_a [Pa]	*τ_w [Pa]*	*τ_a-τ_w [Pa]*	*τ_b (Vanoni & Brooks) [Pa]*	*corrected dp/dx [Pa/m]*
11.90	6.27	5.63	6.68	-322.2

Table 46 - Calculation bed shear stress sand-bentonite (2%) for Q=10 L/s

Point	*x [m]*	*h [m]*	*U [m/s]*	*U^2 [m^2/s^2]*	*R [m]*	*H [m]*	*p [Pa]*
4	0.30	0.201	0.961	0.923	0.0416	0.2478	1968.9
5	0.40	0.198	0.974	0.949	0.0415	0.2462	1940.2
6	0.50	0.197	0.980	0.961	0.0414	0.2455	1927.9
7	0.60	0.193	0.996	0.993	0.0413	0.2440	1896.8
8	0.70	0.190	1.012	1.024	0.0412	0.2425	1867.4
9	0.80	0.188	1.026	1.054	0.0410	0.2413	1840.6
Mean	0.55	0.194	0.992	0.984	0.0413	0.2445	1907.0

dx [m]	*dh/dx [m/m]*	*dU/dx [m/s/m]*	*dU^2/dx [$m^2/s^2/m$]*	*dH/dx [m/m]*	*dp/dx [Pa/m]*
0.5	-0.026	0.131	0.260	-0.0129	-256.7

τ_a [Pa]	*τ_w [Pa]*	*τ_a-τ_w [Pa]*	*τ_b (Vanoni & Brooks) [Pa]*	*corrected dp/dx [Pa/m]*
21.37	10.32	11.05	15.84	-517.1

Table 47 - Calculation bed shear stress sand-bentonite (2%) for Q=20 L/s

Results erosion tests sand-bentonite (4%)

Parameter	*Value*
Flow rate, Q [L/s]	10.1
Bed height, h_b [m]	0.090
Volume bed, V_b [m^3]	0.03374
Mass bed, M_b [kg]	51.2
Mass additive, M_a [kg]	1.2
Dry bulk density sand, $\rho_{db\text{-}sand}$ [kg/m^3]	1482
Porosity sand, p_{sand} [-]	0.44
Saturation time [h]	22
Test duration [s]	1635 *(test stopped after 2 cm erosion)*

Table 48 - Test conditions sand-bentonite (4%) for Q=10 L/s

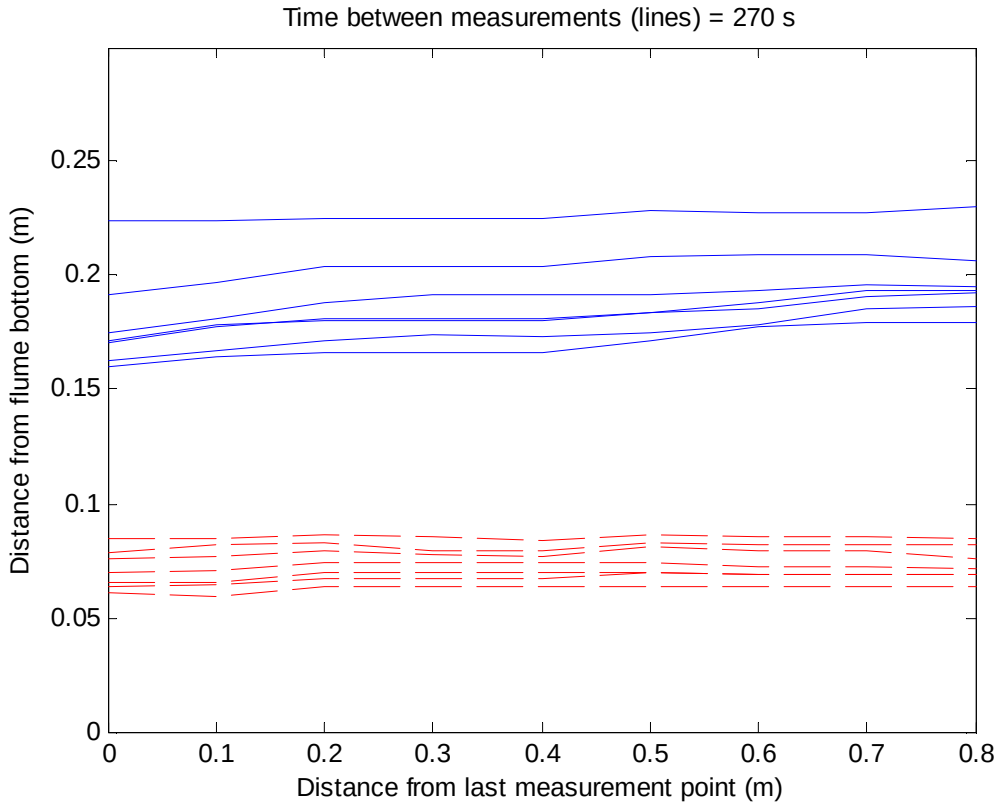

Figure 108 - Water (upper) and sand-bentonite (4%) bed (lower) level measurements for Q=10 L/s

Parameter	*Value*
Flow rate, Q [L/s]	20.1
Bed height, h_b [m]	0.090
Volume bed, V_b [m^3]	0.03374
Mass bed, M_b [kg]	51.2
Mass additive, M_a [kg]	1.2
Dry bulk density sand, $\rho_{db\text{-}sand}$ [kg/m^3]	1482
Porosity sand, p_{sand} [-]	0.44
Saturation time [h]	22
Test duration [s]	682 *(continued after Q=10 L/s test)*

Table 49 - Test conditions sand-bentonite (4%) for Q=20 L/s

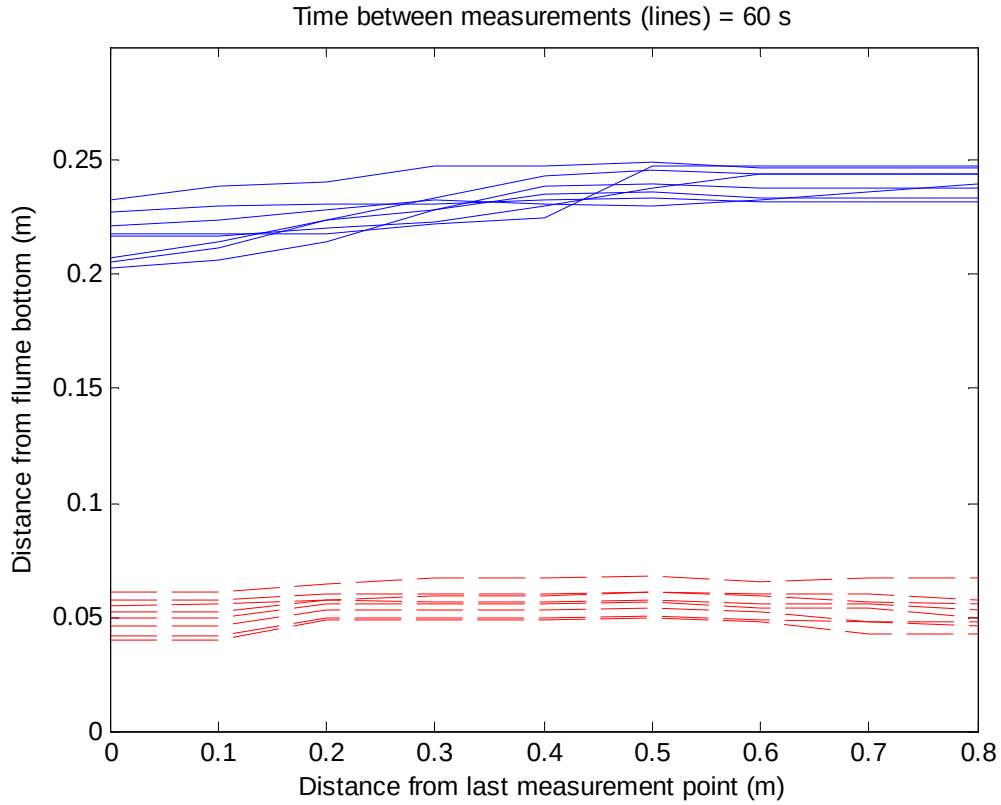

Figure 109 - Water (upper) and sand-bentonite (4%) bed (lower) level measurements for Q=20 L/s

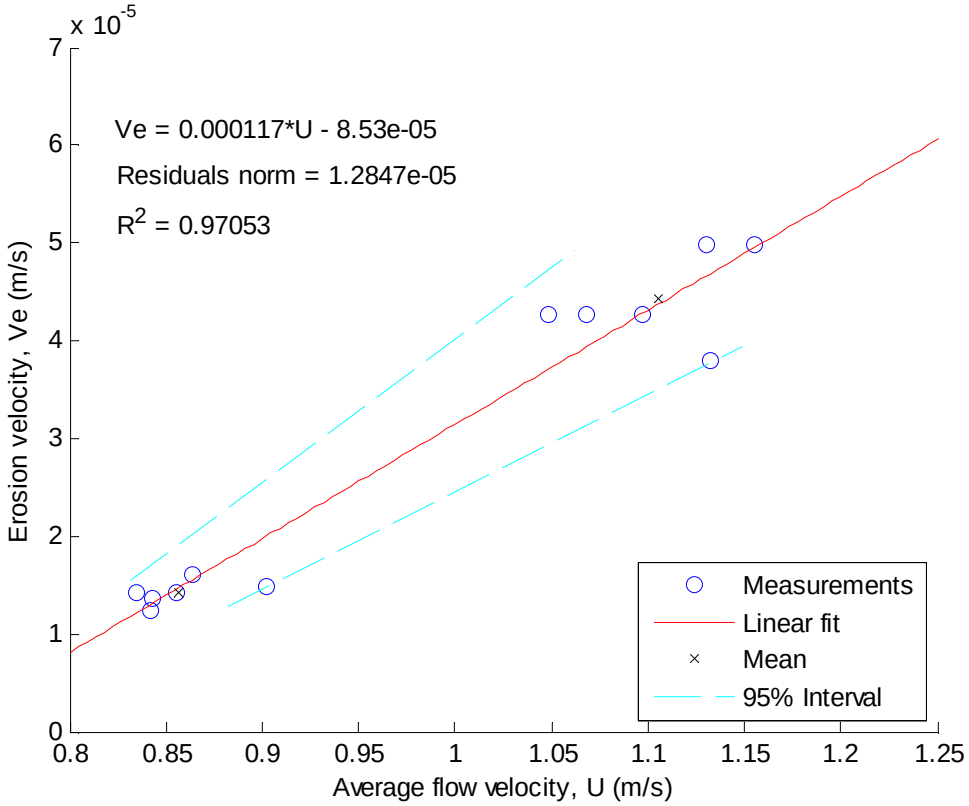

Figure 110 - Figure of average erosion velocity and flow velocities of measurement point 4 to 9 of Q=10 & 20 L/s sand-bentonite (4%) tests; linear fit line plotted through data points, including the 95% confidence interval, formula, norm of residuals and R^2

Measurement point	*U [m/s]*	*V_e [m/s]*
Q=10 L/s		
4	0.835	1.42E-05
5	0.842	1.23E-05
6	0.843	1.35E-05
7	0.856	1.42E-05
8	0.863	1.60E-05
9	0.902	1.48E-05
Mean	**0.857**	**1.42E-05**
Q=20 L/s		
4	1.048	4.27E-05
5	1.068	4.27E-05
6	1.097	4.27E-05
7	1.132	3.80E-05
8	1.130	4.98E-05
9	1.155	4.98E-05
Mean	**1.105**	**4.43E-05**

Table 50 - Flow and erosion velocities sand-bentonite (4%)

Point	*x [m]*	*h [m]*	*U [m/s]*	*U^2 [m^2/s^2]*	*R [m]*	*H [m]*	*p [Pa]*
4	0.30	0.116	0.835	0.697	0.0362	0.1518	1141.1
5	0.40	0.115	0.842	0.709	0.0361	0.1516	1132.8
6	0.50	0.115	0.843	0.711	0.0361	0.1514	1130.0
7	0.60	0.113	0.856	0.732	0.0359	0.1508	1113.2
8	0.70	0.112	0.863	0.746	0.0358	0.1505	1103.4
9	0.80	0.108	0.902	0.814	0.0353	0.1495	1060.1
Mean	0.55	0.114	0.857	0.735	0.0359	0.1509	1113.4

dx [m]	*dh/dx [m/m]*	*dU/dx [m/s/m]*	*dU^2/dx [$m^2/s^2/m$]*	*dH/dx [m/m]*	*dp/dx [Pa/m]*
0.5	-0.017	0.135	0.234	-0.0046	-162.0

τ_a [Pa]	*τ_w [Pa]*	*τ_a-τ_w [Pa]*	*τ_b (Vanoni & Brooks) [Pa]*	*corrected dp/dx [Pa/m]*
14.21	7.71	6.50	1.67	-396.0

Table 51 - Calculation bed shear stress sand-bentonite (4%) for Q=10 L/s

Point	*x [m]*	*h [m]*	*U [m/s]*	*U^2 [m^2/s^2]*	*R [m]*	*H [m]*	*p [Pa]*
4	0.30	0.183	1.048	1.099	0.0408	0.2390	1795.2
5	0.40	0.180	1.068	1.141	0.0406	0.2377	1761.0
6	0.50	0.175	1.097	1.203	0.0404	0.2362	1715.8
7	0.60	0.169	1.132	1.282	0.0401	0.2347	1660.8
8	0.70	0.170	1.130	1.278	0.0401	0.2349	1665.7
9	0.80	0.166	1.155	1.334	0.0399	0.2343	1631.5
Mean	0.55	0.174	1.105	1.223	0.0403	0.2361	1705.0

dx [m]	*dh/dx [m/m]*	*dU/dx [m/s/m]*	*dU^2/dx [$m^2/s^2/m$]*	*dH/dx [m/m]*	*dp/dx [Pa/m]*
0.5	-0.033	0.213	0.469	-0.0095	-327.5

τ_a [Pa]	*τ_w [Pa]*	*τ_a-τ_w [Pa]*	*τ_b (Vanoni & Brooks) [Pa]*	*corrected dp/dx [Pa/m]*
32.09	12.83	19.26	7.50	-796.1

Table 52 - Calculation bed shear stress sand-bentonite (4%) for Q=20 L/s

Results erosion tests sand-fibres (0.44%)

Parameter	*Value*
Flow rate, Q [L/s]	10.1
Bed height, h_b [m]	0.087
Volume bed, V_b [m^3]	0.03261
Mass bed, M_b [kg]	50.1
Mass additive, M_a [kg]	0.128
Dry bulk density sand, $\rho_{db\text{-}sand}$ [kg/m^3]	1533
Porosity sand, p_{sand} [-]	0.42
Saturation time [h]	4.5
Test duration [s]	1463

Table 53 - Test conditions sand-fibres (0.44%) for Q=10 L/s

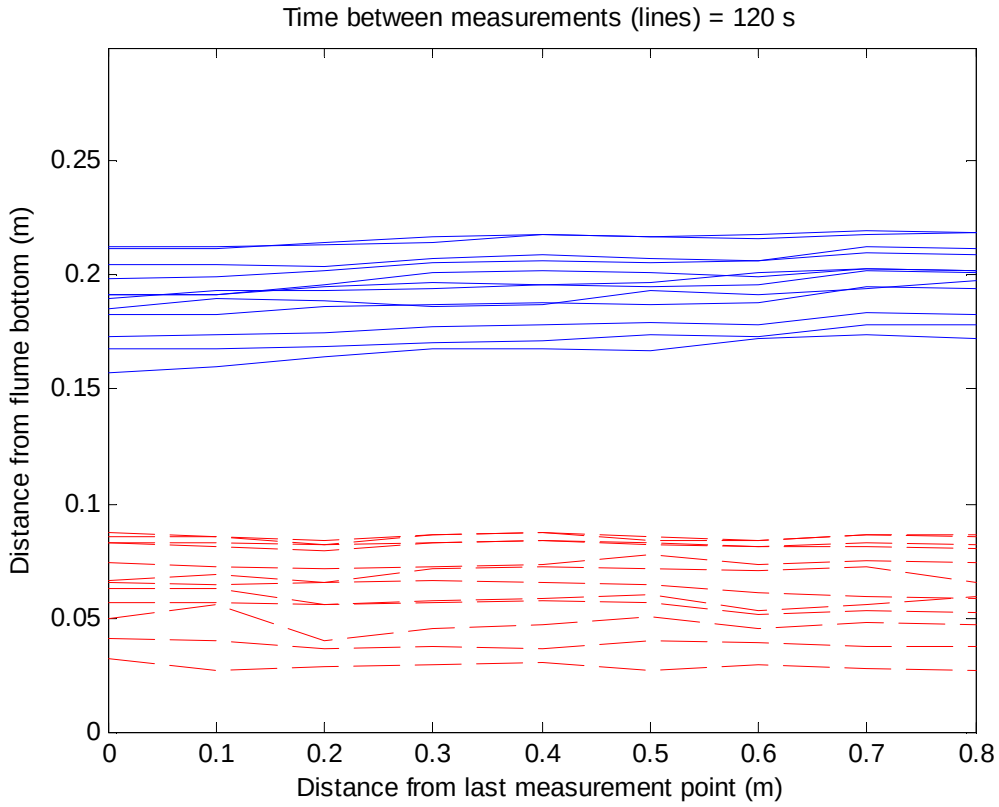

Figure 111 - Water (upper) and sand-fibres (0.44%) bed (lower) level measurements for Q=10 L/s

Parameter	*Value*
Flow rate, Q [L/s]	20.1
Bed height, h_b [m]	0.085
Volume bed, V_b [m^3]	0.03286
Mass bed, M_b [kg]	50.1
Mass additive, M_a [kg]	0.128
Dry bulk density sand, $\rho_{db\text{-}sand}$ [kg/m^3]	1522
Porosity sand, p_{sand} [-]	0.43
Saturation time [h]	16.5
Test duration [s]	249

Table 54 - Test conditions sand-fibres (0.44%) for Q=20 L/s

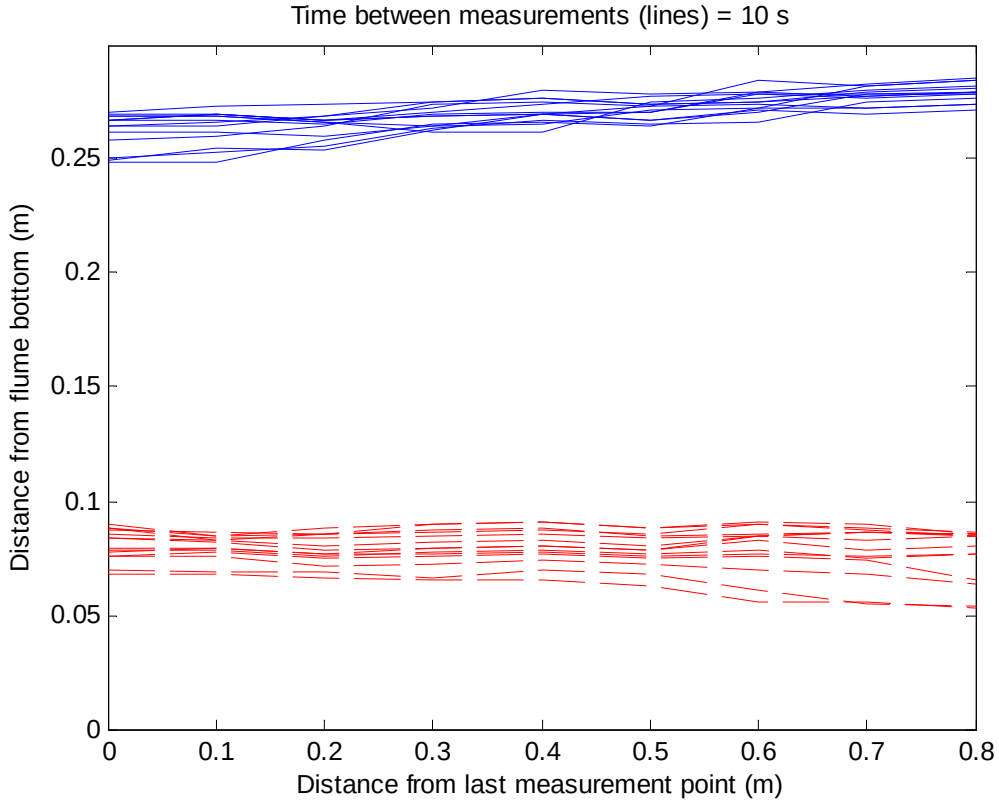

Figure 112 - Water (upper) and sand-fibres (0.44%) bed (lower) level measurements for Q=20 L/s

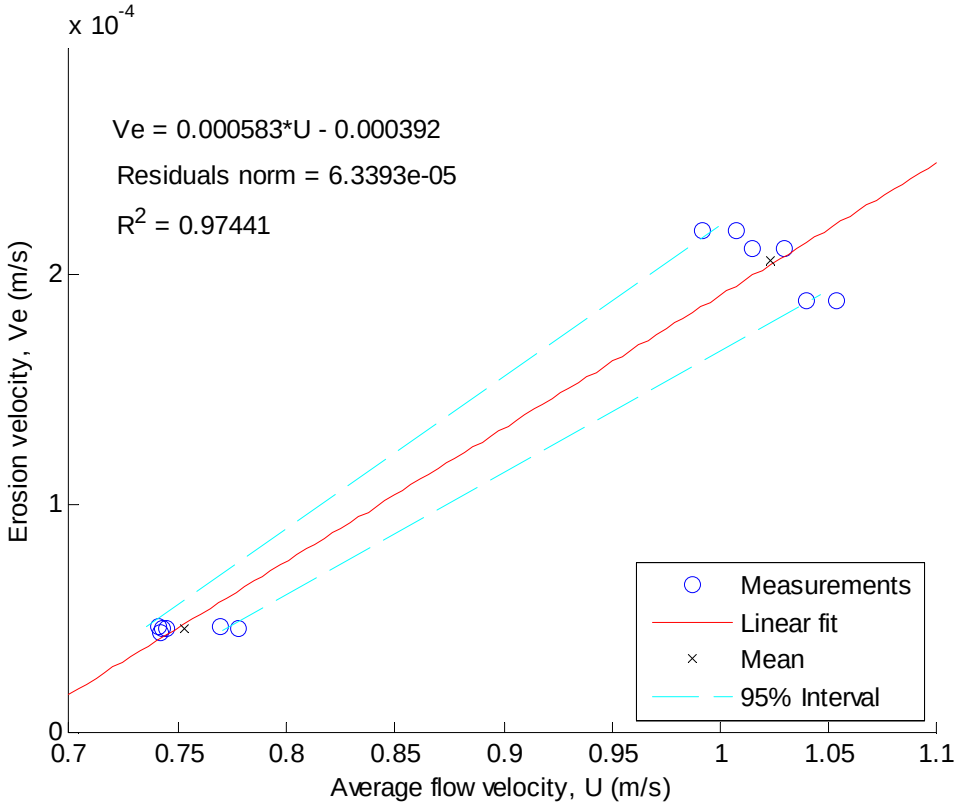

Figure 113 - Figure of average erosion velocity and flow velocities of measurement point 4 to 9 of Q=10 & 20 L/s sand-fibres (0.44%) tests; linear fit line plotted through data points, including the 95% confidence interval, formula, norm of residuals and R^2

Measurement point	*U [m/s]*	*V_e [m/s]*
Q=10 L/s		
4	0.741	4.57E-05
5	0.743	4.50E-05
6	0.745	4.50E-05
7	0.742	4.35E-05
8	0.770	4.57E-05
9	0.778	4.50E-05
Mean	**0.753**	**4.50E-05**
Q=20 L/s		
4	0.992	2.19E-04
5	1.007	2.19E-04
6	1.014	2.12E-04
7	1.029	2.12E-04
8	1.039	1.89E-04
9	1.054	1.89E-04
Mean	**1.023**	**2.07E-04**

Table 55 - Flow and erosion velocities sand-fibres (0.44%)

Point	*x [m]*	*h [m]*	*U [m/s]*	*U^2 [m^2/s^2]*	*R [m]*	*H [m]*	*p [Pa]*
4	0.30	0.130	0.741	0.549	0.0374	0.1580	1275.5
5	0.40	0.130	0.743	0.552	0.0374	0.1577	1271.4
6	0.50	0.129	0.745	0.555	0.0373	0.1575	1268.2
7	0.60	0.130	0.742	0.551	0.0374	0.1578	1273.0
8	0.70	0.125	0.770	0.592	0.0370	0.1553	1227.7
9	0.80	0.124	0.778	0.605	0.0369	0.1546	1213.9
Mean	0.55	0.128	0.753	0.567	0.0372	0.1568	1254.9

dx [m]	*dh/dx [m/m]*	*dU/dx [m/s/m]*	*dU^2/dx [$m^2/s^2/m$]*	*dH/dx [m/m]*	*dp/dx [Pa/m]*
0.5	-0.013	0.074	0.113	-0.0068	-123.0

τ_a [Pa]	*τ_w [Pa]*	*τ_a-τ_w [Pa]*	*τ_b (Vanoni & Brooks) [Pa]*	*corrected dp/dx [Pa/m]*
8.77	5.95	2.81	5.11	-235.6

Table 56 - Calculation bed shear stress sand-fibres (0.44%) for Q=10 L/s

Point	*x [m]*	*h [m]*	*U [m/s]*	*U^2 [m^2/s^2]*	*R [m]*	*H [m]*	*p [Pa]*
4	0.30	0.193	0.992	0.984	0.0413	0.2434	1895.3
5	0.40	0.190	1.007	1.014	0.0411	0.2420	1867.0
6	0.50	0.189	1.014	1.029	0.0411	0.2414	1853.2
7	0.60	0.186	1.029	1.059	0.0410	0.2402	1826.4
8	0.70	0.184	1.039	1.080	0.0409	0.2394	1808.4
9	0.80	0.182	1.054	1.110	0.0407	0.2385	1784.3
Mean	0.55	0.187	1.023	1.046	0.0410	0.2408	1839.1

dx [m]	*dh/dx [m/m]*	*dU/dx [m/s/m]*	*dU^2/dx [$m^2/s^2/m$]*	*dH/dx [m/m]*	*dp/dx [Pa/m]*
0.5	-0.023	0.124	0.253	-0.0097	-221.9

τ_a [Pa]	*τ_w [Pa]*	*τ_a-τ_w [Pa]*	*τ_b (Vanoni & Brooks) [Pa]*	*corrected dp/dx [Pa/m]*
19.46	10.98	8.49	9.52	-474.6

Table 57 - Calculation bed shear stress sand-fibres (0.44%) for Q=20 L/s

Results erosion tests sand-fibres (0.88%)

Parameter	*Value*
Flow rate, Q [L/s]	10.2
Bed height, h_b [m]	0.089
Volume bed, V_b [m^3]	0.03336
Mass bed, M_b [kg]	50.3
Mass additive, M_a [kg]	0.256
Dry bulk density sand, $\rho_{db\text{-}sand}$ [kg/m^3]	1499
Porosity sand, p_{sand} [-]	0.43
Saturation time [h]	18.5
Test duration [s]	1125

Table 58 - Test conditions sand-fibres (0.88%) for Q=10 L/s

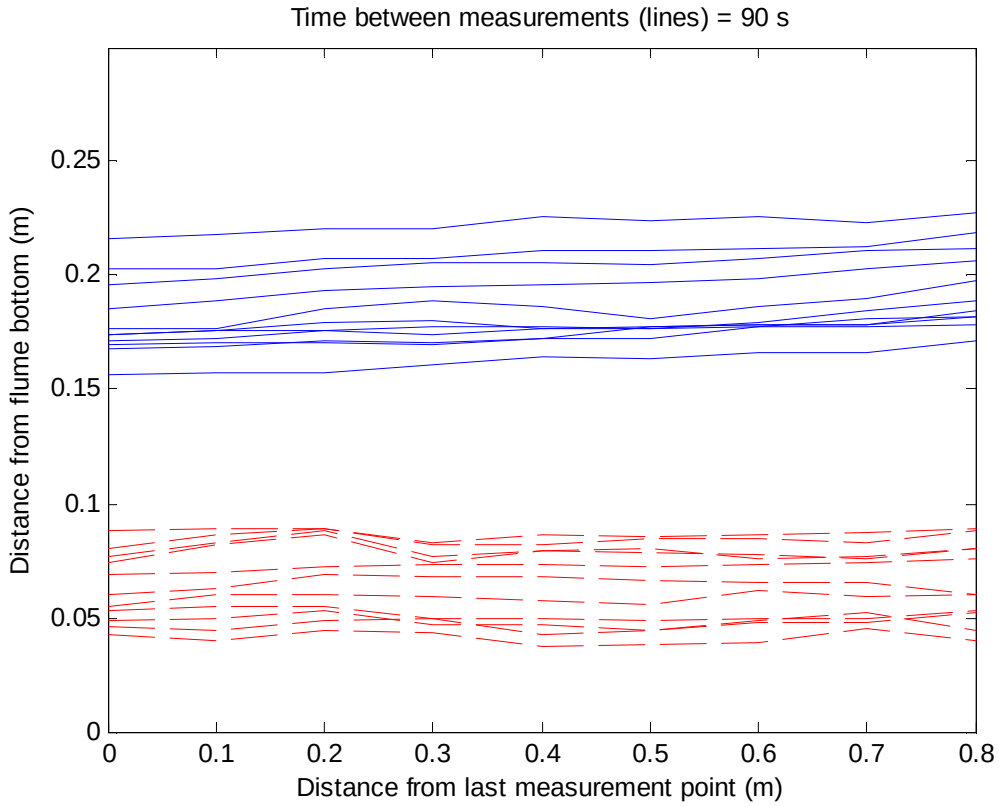

Figure 114 - Water (upper) and sand-fibres (0.88%) bed (lower) level measurements for Q=10 L/s

Parameter	*Value*
Flow rate, Q [L/s]	20.1
Bed height, h_b [m]	0.089
Volume bed, V_b [m^3]	0.03336
Mass bed, M_b [kg]	50.3
Mass additive, M_a [kg]	0.256
Dry bulk density sand, $\rho_{db\text{-}sand}$ [kg/m^3]	1499
Porosity sand, p_{sand} [-]	0.43
Saturation time [h]	18.5
Test duration [s]	315

Table 59 - Test conditions sand-fibres (0.88%) for Q=20 L/s

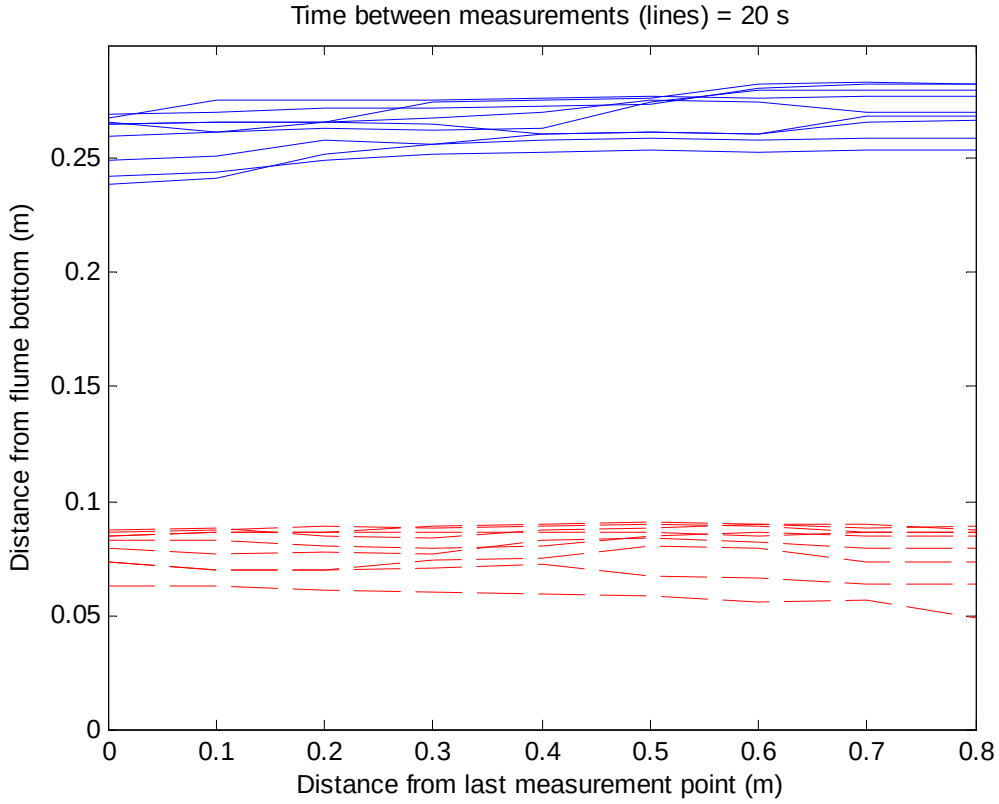

Figure 115 - Water (upper) and sand-fibres (0.88%) bed (lower) level measurements for Q=20 L/s

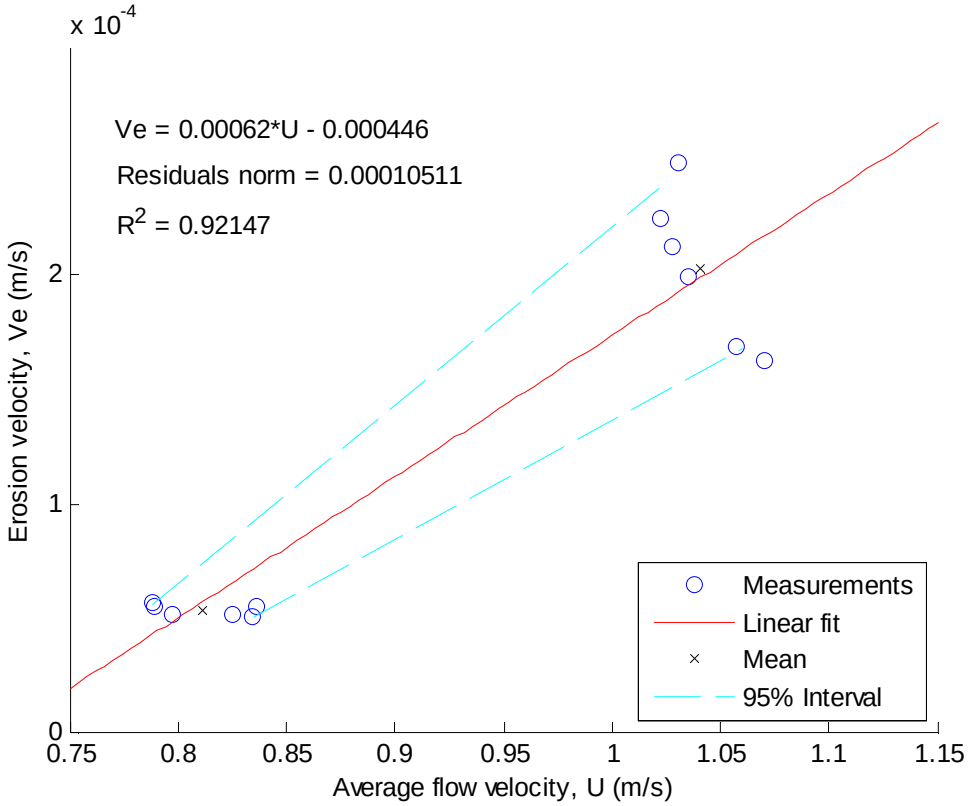

Figure 116 - Figure of average erosion velocity and flow velocities of measurement point 4 to 9 of Q=10 & 20 L/s sand-fibres (0.88%) tests; linear fit line plotted through data points, including the 95% confidence interval, formula, norm of residuals and R^2

Measurement point	*U [m/s]*	*V_e [m/s]*
Q=10 L/s		
4	0.788	5.66E-05
5	0.789	5.45E-05
6	0.798	5.12E-05
7	0.834	5.01E-05
8	0.836	5.45E-05
9	0.825	5.12E-05
Mean	**0.812**	**5.30E-05**
Q=20 L/s		
4	1.022	2.25E-04
5	1.031	2.50E-04
6	1.028	2.12E-04
7	1.035	2.00E-04
8	1.058	1.69E-04
9	1.070	1.62E-04
Mean	**1.041**	**2.03E-04**

Table 60 - Flow and erosion velocities sand-fibres (0.88%)

Point	*x [m]*	*h [m]*	*U [m/s]*	*U^2 [m^2/s^2]*	*R [m]*	*H [m]*	*p [Pa]*
4	0.30	0.124	0.788	0.621	0.0369	0.1556	1216.1
5	0.40	0.124	0.789	0.623	0.0369	0.1555	1214.3
6	0.50	0.122	0.798	0.636	0.0367	0.1547	1199.5
7	0.60	0.117	0.834	0.696	0.0362	0.1523	1146.2
8	0.70	0.117	0.836	0.699	0.0362	0.1523	1144.4
9	0.80	0.118	0.825	0.681	0.0363	0.1528	1158.4
Mean	0.55	0.120	0.812	0.659	0.0365	0.1539	1179.8

dx [m]	*dh/dx [m/m]*	*dU/dx [m/s/m]*	*dU^2/dx [$m^2/s^2/m$]*	*dH/dx [m/m]*	*dp/dx [Pa/m]*
0.5	-0.012	0.074	0.120	-0.0057	-115.4

τ_a [Pa]	*τ_w [Pa]*	*τ_a-τ_w [Pa]*	*τ_b (Vanoni & Brooks) [Pa]*	*corrected dp/dx [Pa/m]*
8.59	6.92	1.68	3.19	-235.2

Table 61 - Calculation bed shear stress sand-fibres (0.88%) for Q=10 L/s

Point	*x [m]*	*h [m]*	*U [m/s]*	*U^2 [m^2/s^2]*	*R [m]*	*H [m]*	*p [Pa]*
4	0.30	0.188	1.022	1.045	0.0410	0.2408	1839.7
5	0.40	0.186	1.031	1.063	0.0409	0.2400	1823.3
6	0.50	0.186	1.028	1.057	0.0410	0.2402	1827.7
7	0.60	0.185	1.035	1.072	0.0409	0.2396	1814.6
8	0.70	0.181	1.058	1.119	0.0407	0.2381	1776.5
9	0.80	0.179	1.070	1.145	0.0406	0.2374	1756.8
Mean	0.55	0.184	1.041	1.083	0.0409	0.2394	1806.4

dx [m]	*dh/dx [m/m]*	*dU/dx [m/s/m]*	*dU^2/dx [$m^2/s^2/m$]*	*dH/dx [m/m]*	*dp/dx [Pa/m]*
0.5	-0.017	0.095	0.198	-0.0068	-165.7

τ_a [Pa]	*τ_w [Pa]*	*τ_a-τ_w [Pa]*	*τ_b (Vanoni & Brooks) [Pa]*	*corrected dp/dx [Pa/m]*
14.86	11.37	3.50	4.28	-363.9

Table 62 - Calculation bed shear stress sand-fibres (0.88%) for Q=20 L/s

G Specifications additives experiments

In this appendix the specifications of the used bentonite and fibres can be found, as provided by the suppliers of the materials.

Polypropylene fibres (S200)

Provided by (Finish Beton Groep, 2014).

SYNTEC S200 macro synthetic fibres specification

Parameter	Units	Result
Material		**Polypropylene (PP)**
Tape width	mm	**1.4**
Length	mm	**45**
Thickness	micron	**180 -200**
Titer	dtex	**2100**
Tenacity	CN/dtex ^{2}	**55**
E –modulus (0 -10 %)	N/mm^2	**4584**
Tenacity	N/mm^2	**473**
Elongation	%	**14.13**
Density polypropylene	kg/m^3	**920**

Cebogel Sealfix bentonite (in Dutch)

Provided by (Cebo Holland B.V., 2014).

PRODUCT DATA

Cebo Holland

CEBOGEL SEALFIX

Toepassing
- In een mengsel met zand voor bodemafdichtingen.
- In boorvloeistof voor grondboringen.

Omschrijving
De basis voor CEBOGEL SEALFIX is een geactiveerde natrium bentoniet. CEBOGEL SEALFIX voldoet aan de CUR aanbeveling 33, die eisen stelt aan bentoniet voor granulaire afdichtingslagen.

Voordelen
- Het grote zwelvermogen maakt een kwalitatief zeer hoogwaardige zandbentoniet afdichting mogelijk.
- Beproefd materiaal voor zandbentoniet afdichtingen: met CEBOGEL SEALFIX is al meer dan 4 miljoen m^2 afgedicht.
- Een spoeling op basis van CEBOGEL SEALFIX is makkelijk te verpompen en zorgt voor een stabiel boorgat.

Specificatie
Voldoet aan de eisen voor bentoniet zoals gesteld in de CUR aanbeveling 33.

Parameter	Methode	CUR 33 Aanbeveling	Typische Waarde
Wateropnemend vermogen na 24 uur	Proef A CUR 33	≥ 700 %	840 %
Methyleenblauw absorptie	Proef B CUR 33	≥ 250 mg MB/gram	330 mg MB/gram
Droge zeefanalyse door 125 µm	Ontw. NEN 33976	≥ 95 %	98 %
Montmorillonietgehalte	Röntgendiffractie	≥ 70 %	80 %
Vochtgehalte (op droog)	NEN 5934	≤ 13,0 % m/m	11,5 % m/m

Cebo Holland BV
Westerduinweg 1
NL-1976 BV IJMUIDEN
P.O. Box 70
NL-1970 AB IJMUIDEN

Tel.: +31 255546262
Fax: +31 255546202
e-mail : sales@ceboholland.com
www.ceboholland.com

PRODUCT DATA

Cebo Holland

Chemische en fysische eigenschappen

Samenstelling	Hoogwaardige geactiveerde natrium bentoniet
Kleur	Beige
Vorm	Zacht poeder

Eigenschappen van de suspensie
Bij verschillende concentraties CEBOGEL SEALFIX aangemaakt in gedestilleerd water.

Parameter	Methode	30 kg/m^3	40 kg/m^3	50 kg/m^3	60 kg/m^3
Vloeigrens kogelnummer	Kugelharfengerät DIN 4126	1	1	2	3
Dichtheid	Mudbalans	1,02 g/ml	1,03 g/ml	1,03 g/ml	1,04 g/ml
Filtraatwaterverlies	DIN 4127	12 ml	10 ml	9 ml	8,5 ml
Marshfunnel API	API RP 13B section 2 (1 liter uit)	30 s	32 s	35 s	38 s

Verpakking
- 25 kg zakken per 1000 kg verpakt op een pallet met krimpfolie
- big bags van 1000 kg
- bulk

Cebo Holland BV
Westerduinweg 1
NL-1976 BV IJMUIDEN
P.O. Box 70
NL-1970 AB IJMUIDEN

Tel.: +31 255546262
Fax: +31 255546202
e-mail : sales@ceboholland.com
www.ceboholland.com

Revisiedatum : 18.03.2009
Document nr. : SF01IP

H Model results solution

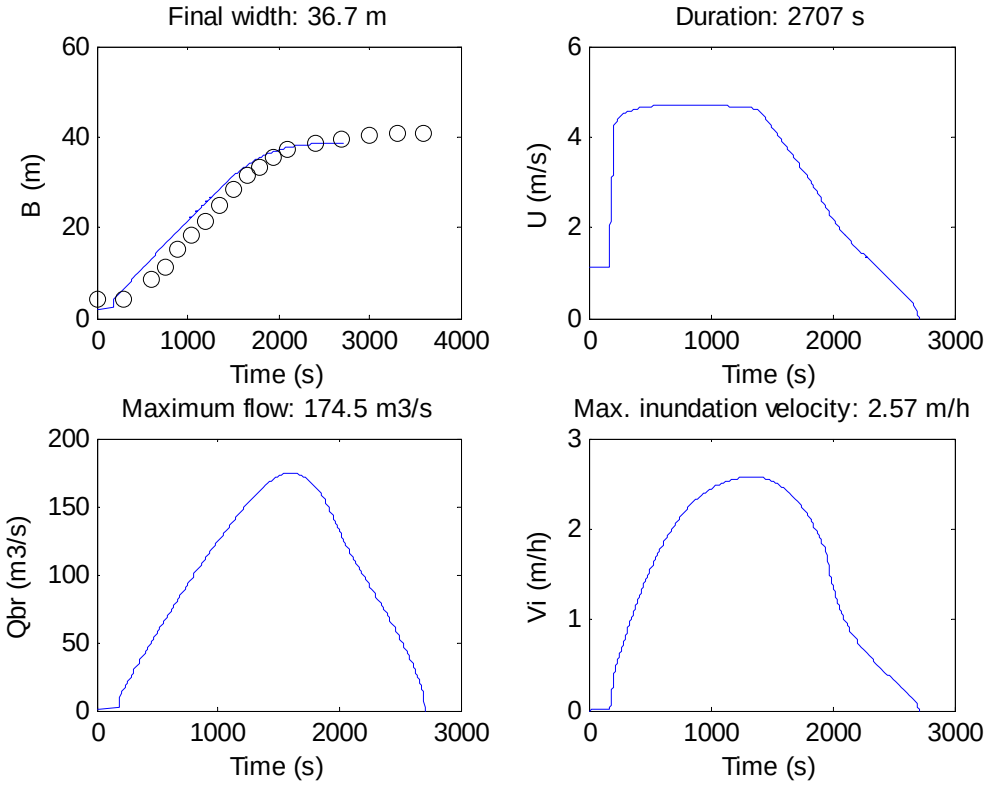

Figure 117 - Results BRES-model ZWIN'94 dike, sand
B=breach width, U=flow velocity, Qbr=flow rate, Vi=inundation velocity

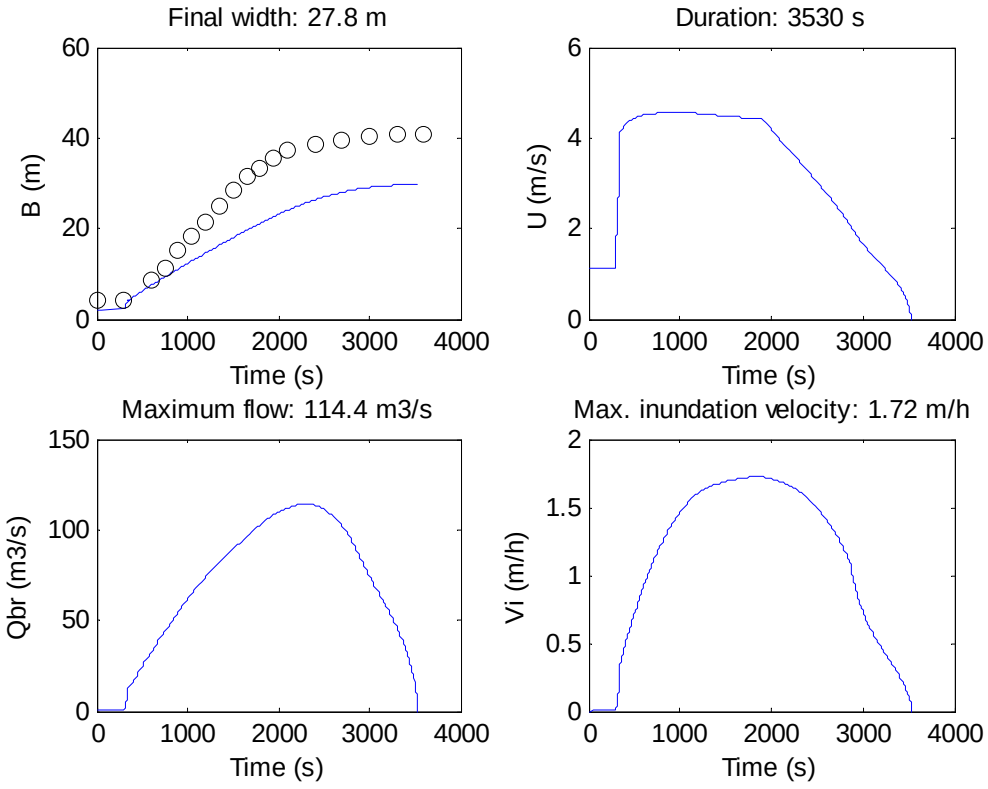

Figure 118 - Results BRES-model ZWIN'94 dike, sand-bentonite 1.2 weight-%
B=breach width, U=flow velocity, Qbr=flow rate, Vi=inundation velocity

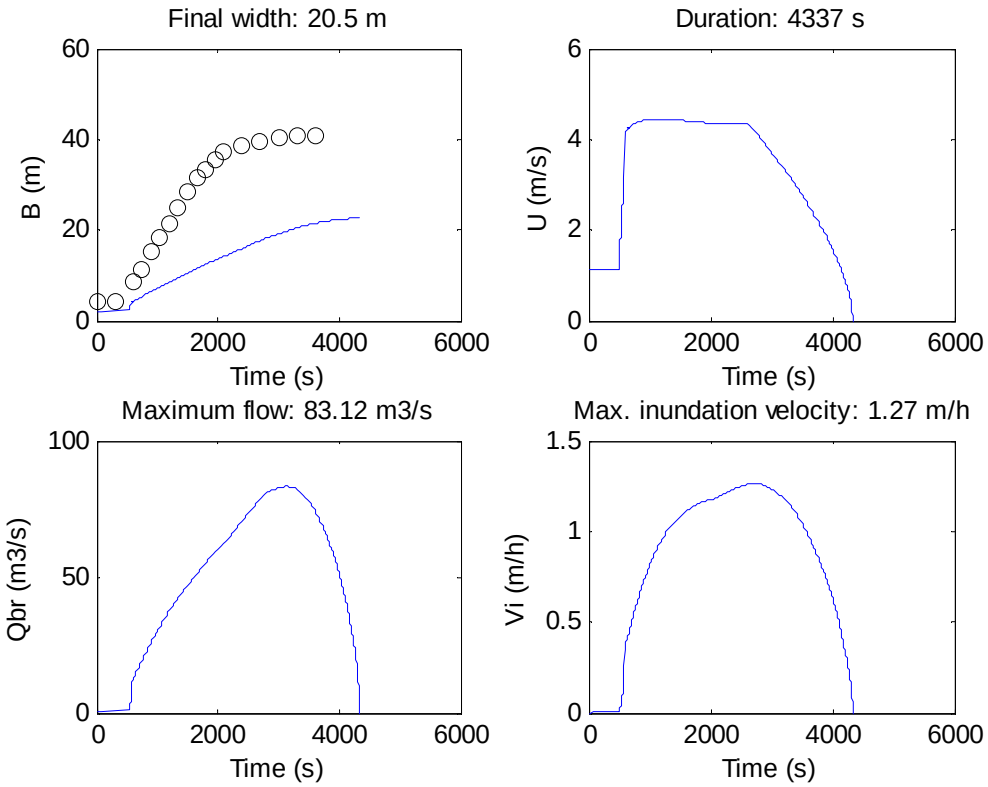

Figure 119 – Results BRES-model ZWIN'94 dike, sand-bentonite 2.4 weight-%
B=breach width, U=flow velocity, Qbr=flow rate, Vi=inundation velocity

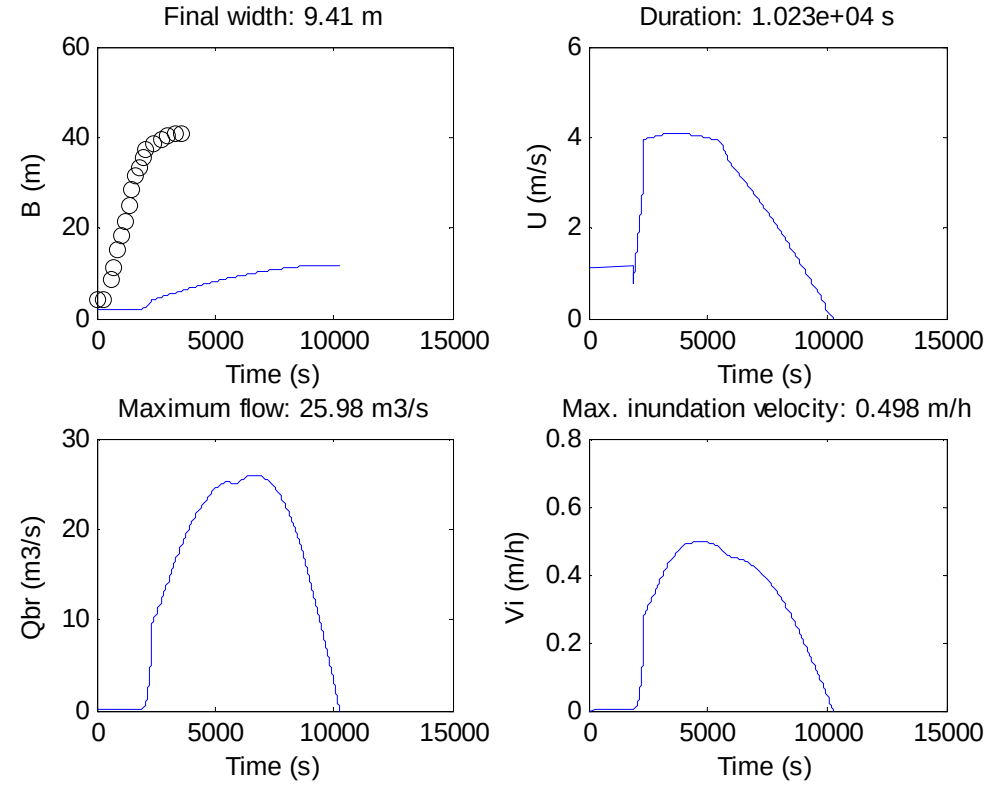

Figure 120 - Results BRES-model ZWIN'94 dike, sand-bentonite 5.4 weight-%
B=breach width, U=flow velocity, Qbr=flow rate, Vi=inundation velocity

I Cases VNK2

Case	Dike ring	Water	Breach	Scenario 1 (B)	Scenario 2 (B+5%)
1	5	Waddenzee	IJsdijk_1,5	TP plus 2 maal decimeringshoogte	TP plus 2 maal decimeringhoogte met 5% breedte
2	5	Waddenzee	IJsdijk_1,5	TP plus decimeringshoogte (wv21)	TP plus decimeringshoogte met dijkdoorbraak van 5% breedte
3	5	Waddenzee	Inlaagdijk van 1938_0	TP plus 2 maal decimeringshoogte	TP plus 2 maal decimeringhoogte met 5% breedte
4	5	Waddenzee	Inlaagdijk van 1938_0	TP plus decimeringshoogte (wv21)	TP plus decimeringshoogte met dijkdoorbraak van 5% breedte
5	5	Waddenzee	Inlaagdijk van 1977_0,5	TP plus decimeringshoogte	TP plus decimeringshoogte met dijkdoorbraak van 5% breedte
6	5	Waddenzee	Inlaagdijk van 1977_0,5	TP plus 2 maal decimeringshoogte	TP plus 2 maal decimeringhoogte met 5% breedte
7	5	Waddenzee	Oostdijk_0,5	TP plus decimeringshoogte	TP plus decimeringshoogte met dijkdoorbraak van 5% breedte
8	5	Waddenzee	Oostdijk_0,5	TP plus 2 maal decimeringshoogte	TP plus 2 maal decimeringhoogte met 5% breedte
9	5	Waddenzee	Oostdijk_2,5	TP plus 2 maal decimeringshoogte	TP plus 2 maal decimeringhoogte met 5% breedte
10	5	Waddenzee	Oostdijk_2,5	TP plus decimeringshoogte (wv21)	TP plus decimeringshoogte met dijkdoorbraak van 5% breedte
11	5	Waddenzee	Rijkszeewering Bolwerk_0,5	TP plus 2 maal decimeringshoogte	TP plus 2 maal decimeringhoogte met 5% breedte
12	5	Waddenzee	Rijkszeewering Bolwerk_0,5	TP plus decimeringshoogte (wv21)	TP plus decimeringshoogte met dijkdoorbraak van 5% breedte
13	5	Waddenzee	Zeedijk Prins Henderikpolder_0	TP plus decimeringshoogte	TP plus decimeringshoogte met dijkdoorbraak van 5% breedte
14	5	Waddenzee	Zeedijk Prins Henderikpolder_0	TP plus 2 maal decimeringshoogte	TP plus 2 maal decimeringhoogte met 5% breedte
15	5	Waddenzee	Zeedijk Prins Henderikpolder_2	TP plus 2 maal decimeringshoogte	TP plus 2 maal decimeringhoogte met 5% breedte
16	5	Waddenzee	Zeedijk Prins Henderikpolder_2	TP plus decimeringshoogte (wv21)	TP plus decimeringshoogte met dijkdoorbraak van 5% breedte
17	5	Waddenzee	Zeedijk van Oudeschild_0,5	TP plus 2 maal decimeringshoogte	TP plus 2 maal decimeringhoogte met 5% breedte
18	5	Waddenzee	Zeedijk van Oudeschild_0,5	TP plus decimeringshoogte (wv21)	TP plus decimeringshoogte met dijkdoorbraak van 5% breedte
19	13	Noordzee	Helderse Zeewering_1,5	TP plus 2 maal decimeringshoogte	TP plus 2 maal decimeringhoogte met 5% breedte
20	13	Noordzee	Helderse Zeewering_1,5	TP plus decimeringshoogte (wv21)	TP plus decimeringshoogte met dijkdoorbraak van 5% breedte
21	13	Noordzee	Helderse Zeewering_4	TP plus 2 maal decimeringshoogte	TP plus 2 maal decimeringhoogte met 5% breedte
22	13	Noordzee	Helderse Zeewering_4	TP plus decimeringshoogte (wv21)	TP plus decimeringshoogte met dijkdoorbraak van 5% breedte
23	13	Noordzee	Hondsbossche Zeewering_0,5	TP plus 2 maal decimeringshoogte	TP plus 2 maal decimeringhoogte met 5% breedte
24	13	Noordzee	Hondsbossche Zeewering_0,5	TP plus decimeringshoogte (wv21)	TP plus decimeringshoogte met dijkdoorbraak van 5% breedte
25	13	Waddenzee	Balgzanddijk_3	TP plus 2 maal decimeringshoogte	TP plus 2 maal decimeringhoogte met 5% breedte
26	13	Waddenzee	Balgzanddijk_3	TP plus decimeringshoogte (wv21)	TP plus decimeringshoogte met dijkdoorbraak van 5% breedte
27	13	Waddenzee	Balgzanddijk_7	TP plus decimeringshoogte	TP plus decimeringshoogte met dijkdoorbraak van 5% breedte
28	13	Waddenzee	Balgzanddijk_7	TP plus 2 maal decimeringshoogte	TP plus 2 maal decimeringhoogte met 5% breedte

(TP=Toetspeil) Source: (VNK2, 2014)

Case	Exceedance frequency [y]	People in flooded area		Casualties			Mortality [-]				Damage [million €]		
		B	B+5%	B	B+5%	B/B+5%	B	B+5%	B/B+5%	ΔM (B-B+5%)	B	B+5%	B/B+5%
1	400000	7889	7606	32	28	1.14	4.06E-03	3.68E-03	1.10	3.75E-04	311.5	286.8	1.09
2	40000	6085	7171	15	26	0.58	2.47E-03	3.63E-03	0.68	-1.16E-03	179.2	265.2	0.68
3	400000	596	1103	2	5	0.40	3.36E-03	4.53E-03	0.74	-1.18E-03	48.9	166.9	0.29
4	40000	1037	1103	3	4	0.75	2.89E-03	3.63E-03	0.80	-7.34E-04	127.9	150.9	0.85
5		5321	10257	11	59	0.19	2.07E-03	5.75E-03	0.36	-3.68E-03	151.7	461.1	0.33
6		5349	11426	12	80	0.15	2.24E-03	7.00E-03	0.32	-4.76E-03	160.5	526.8	0.30
7		3074	5461	3	10	0.30	9.76E-04	1.83E-03	0.53	-8.55E-04	75.8	150	0.51
8		3871	6637	6	21	0.29	1.55E-03	3.16E-03	0.49	-1.61E-03	105.1	231.3	0.45
9	400000	5376	11470	13	98	0.13	2.42E-03	8.54E-03	0.28	-6.13E-03	165.7	532.9	0.31
10	40000	5342	10096	12	61	0.20	2.25E-03	6.04E-03	0.37	-3.80E-03	157.2	462.7	0.34
11	400000	5401	8364	13	36	0.36	2.41E-03	4.30E-03	0.56	-1.90E-03	161.1	338.7	0.48
12	40000	5366	7858	12	31	0.39	2.24E-03	3.95E-03	0.57	-1.71E-03	152.8	307.9	0.50
13		359	713	3	5	0.60	8.36E-03	7.01E-03	1.19	1.34E-03	52.4	65.7	0.80
14		480	2100	3	8	0.38	6.25E-03	3.81E-03	1.64	2.44E-03	59.2	110.7	0.53
15	400000	694	11054	3	69	0.04	4.32E-03	6.24E-03	0.69	-1.92E-03	65.8	520.1	0.13
16	40000	502	9603	3	45	0.07	5.98E-03	4.69E-03	1.28	1.29E-03	59.8	413.1	0.14
17	400000	5276	5445	10	13	0.77	1.90E-03	2.39E-03	0.79	-4.92E-04	147.1	166.8	0.88
18	40000	4615	5239	9	10	0.90	1.95E-03	1.91E-03	1.02	4.14E-05	131.9	141.4	0.93
19	1000000	31763	60471	76	924	0.08	2.39E-03	1.53E-02	0.16	-1.29E-02	701.6	2269.9	0.31
20	100000	28483	57612	58	435	0.13	2.04E-03	7.55E-03	0.27	-5.51E-03	572.2	1831.6	0.31
21	1000000	51368	60590	239	1666	0.14	4.65E-03	2.75E-02	0.17	-2.28E-02	1468.7	2686	0.55
22	100000	40210	60357	135	995	0.14	3.36E-03	1.65E-02	0.20	-1.31E-02	1013.5	2262.8	0.45
23	1000000	340	6729	3	53	0.06	8.82E-03	7.88E-03	1.12	9.47E-04	27.4	247.4	0.11
24	100000	314	3671	1	26	0.04	3.18E-03	7.08E-03	0.45	-3.90E-03	21.5	141.4	0.15
25	1000000	10302	44541	32	842	0.04	3.11E-03	1.89E-02	0.16	-1.58E-02	305.7	1624.8	0.19
26	100000	10271	31563	28	439	0.06	2.73E-03	1.39E-02	0.20	-1.12E-02	282.4	1149.2	0.25
27	1000000	10286	10640	32	36	0.89	3.11E-03	3.38E-03	0.92	-2.72E-04	306	332.6	0.92
28	100000	10735	11051	36	59	0.61	3.35E-03	5.34E-03	0.63	-1.99E-03	335.9	451	0.74

Source: (VNK2, 2014)